



Project Report

Confidential

P511

YILGARN ATLAS

VOLUME III: UWA Gold Module

June 2002

CSIRO – Exploration & Mining
Centre for Global Metallogeny - UWA
CODES - University of Tasmania



YILGARN ATLAS

VOLUME III: UWA Gold Module

Part 1 – Structural Evolution and Controls on Gold Mineralization in the
Norseman-Wiluna Belt

Part 2 – A Generic Assessment of Orogenic Gold Provinces:
Factors Controlling the Formation of World-Class and Giant Deposits

Hydrothermal Systems, Giant Ore Deposits & A New Paradigm for Predictive Mineral Exploration

AMIRA Project P511

Authors:

David I Groves, Centre for Global Metallogeny, UWA
Roberto F Weinberg, Centre for Global Metallogeny, UWA
Paul Hodkiewicz, Centre for Global Metallogeny, UWA
Peter van der Borgh, Centre for Global Metallogeny, UWA

CONFIDENTIAL TO SPONSORS
June 2002

PART I

Structural Evolution and Controls on Gold Mineralization in the Norseman-Wiluna Belt

AMIRA Project P511

Authors: Roberto Weinberg, David Groves, Paul Hodkiewicz, Peter van der Borgh

Executive Summary

The SPIRT/LINKAGE segment of the gold module of project P511 is divided into two independent parts: the first focuses on the Yilgarn Craton, and the second on global characteristics of orogenic gold deposits. This project has derived a new and self-consistent structural history for the Norseman-Wiluna Belt, Yilgarn Craton, and provided new insights into the controls on gold mineralization. Essentially, the findings are that the belt underwent a late-Archean orogeny to produce the Kalgoorlie Orogen, which includes structures that reflect the regional deformation phases known as D_2 - D_4 . Deformation was in response to pure shear, and not sinistral transpression as previously proposed, and resulted from continuous ENE-WSW directed shortening. The orogen proceeded from a thickening phase D_2 , to a lateral extension phase characterized by strike slip shear zones D_3 , which became increasingly brittle as the crust cooled (D_4). During straining, the presence of competent granitoid bodies caused intense shearing and lateral escape of surrounding weaker greenstone sequences. Escape process was controlled by the interaction between the orientation of granitoid boundary and external stresses.

The orogeny was accompanied by low-Ca granitoid intrusion, metamorphism and gold mineralization. Mineralization took place in the later part of the history, except possibly for the Golden Mile, which had a prolonged history of mineralization. Zones of high straining, such as crustal scale shear zones, and rock competency contrast are the two key controls in the siting of mineralization. This is because shearing of rocks of contrasting strength lead to rock flow heterogeneities and dilation zones that focus fluid flow. Competency contrast is highest at greenschist facies temperatures, thus explaining, at least in part, why greenschist facies terranes tend to be more endowed with gold than other terranes. In this context, weak ultramafic rocks or shales and strong granitoid or doleritic intrusions play a key role in mineralization by providing very marked competency contrast with other rock types.

Sulphur isotope ratios of a number of deposits were investigated in order to determine their relationship to gold endowment. There is a tendency for large gold deposits to be associated with large variation $\delta^{34}\text{S}_{(\text{py})}$ values, but this is not universal. Another indicator for the location of potentially large gold deposits is complexity in the distribution of lithological contacts and structures, as quantified by fractal dimensions. Complex zones generally host the large gold deposits, because these zones provide a number of possible hosts and increased likelihood for

fluid focusing and traps. Surprisingly, the largest deposits are sited, not in the zones of highest complexity, but in zones of strong lateral gradient in complexity.

Gold exploration should focus on regions of lithological and structural complexity within greenschist facies belts, close to crustal-scale permeable shear zones. Within these areas, large deposits will be sited where there is strong lateral variation in complexity, as measured by variation in fractal dimensions. This project derived these conclusions by detailed comparisons of the evolution of the Boulder-Lefroy, Zuleika and Ida Shear Zones. The main results are listed below in point format, further summarized at the beginning of each major section of this report, and discussed in *Section 5*.

Point Summary

Timing of deformation (Section 2.3):

- Relative timing of deformation phases previously established based on structures relative to granitoid intrusions is flawed.
- Timing of D_2 - D_4 regional deformation phases is later and of shorter duration than previously considered. It is now estimated to have taken place between 2650-2630 Ma instead of 20 Ma earlier. A new time chart for the structural evolution of the Norseman-Wiluna Belt is developed.
- A major late tectono-thermal event is defined by the regional deformation phases D_2 - D_4 , low-Ca granite intrusion, and gold mineralization.

Boulder-Lefroy Shear Zone (Section 2.4):

- The shear zone developed in two stages: a) D_2 reverse faulting and folding; b) D_3 sinistral shearing.
- There is no evidence for late important dextral shearing, commonly reported as significant in previous studies.
- Early structures developed at Kalgoorlie (Golden Mile Fault and Kalgoorlie Anticline), interpreted as abandoned early D_2 , are cross cut and refolded by later active structures.
- Weaker D_2 strain at Kambalda preserved early regional D_1 thrusts, and also led to further crustal shortening as well as sinistral movement during D_3 .
- The D_3 dextral, sinuous, N-S striking, *en-echelon* Charlotte set of shear zones formed as a result of NNW-sinistral shear.

- D_4 is represented by later, brittle structures, which also reactivated earlier formed structures.
- Small total D_3 sinistral displacement on the shear zone is confirmed.
- Gold, with the exception of the Golden Mile, was deposited late in the tectonic history of the shear zone, either during D_3 or D_4 .
- Gold at the Golden Mile was deposited earlier, possibly during the early stages of D_2 .
- General thermal arguments based on the depositional, magmatic and deformation history of the Kalgoorlie Terrane suggests that two broad metamorphic, and consequently mineralization, events took place: the first during crustal extension and extrusion of the mafic-ultramafic sequence and high-Ca magmatism; the second during the Kalgoorlie Orogen and low-Ca magmatism.

Zuleika and Ida Shear Zones (Section 2.5):

- The Zuleika Shear Zone has complex kinematics, with significant eastward thrusting at Kundana, and sinistral strike slip movement further north at Ant Hill/Bullant.
- Complexity results from internal deformation of the shear-zone bounded blocks and possibly an evolving deformation history.
- The Zuleika-Kunanalling Corridor, between the Kundana area and the Bali granite/Kunanalling area, is a pop-up structure, with fold tightening towards the two bounding thrust zones: the Zuleika and Kunanalling Shear Zones.
- The Ida Shear Zone is enclosed within a narrow, amphibolite facies greenstone sequence, intensely flattened and attenuated by impinging granitoid bodies.
- Stretching direction along the corridor is sub-horizontal on a sub-vertical foliation and shear sense indicators are poorly defined due to predominant pure-shear deformation. There is no evidence for late normal faulting.
- Gently-dipping seismic reflectors at depth are not obviously related to the surface expression of the Ida Shear Zone.

Contrasting Shear Zones and Gold Endowment (Section 2.6):

- Irregular margins of competent granite batholiths cause an added degree of complexity on the kinematics of neighbouring shear zones.
- Different endowment along shear zones is related to variety in rock types along the shear zone, metamorphic facies, and geometry (tight/gentle antiforms/synforms).

- Competency contrasts play a key role in localizing fluid flow within the crust by creating regions of dilation (strain incompatibility).
- Competency contrast is high in greenschist facies rocks (ductile talc- or chlorite-schist versus brittle dolerite or granitoid) and low in amphibolite facies rocks (ductile amphibole- or quartz dominated rocks). Amphibolite facies rocks retain low competence contrasts as they cool to greenschist facies conditions, as long as they are not strongly retrogressed.
- Homogeneous rock deformation leads to unfocused fluid flow and poor mineralization, as opposed to heterogeneous rock deformation.
- The giant gold deposit (Fimiston lodes) is the only one to have possibly been deposited either before or during early D_2 .

Kalgoorlie Orogen (Section 2.7):

- A late-Archean Kalgoorlie Orogen is proposed. There was an ENE-WSW continuum of shortening during orogen evolution, from D_2 crustal thickening to D_3 - D_4 lateral escape. Granitoid bodies control local rock flow and stress distribution.
- The pattern of deformation and distribution of regional shear zones resulted from the interaction between these external forces and the presence of large, competent granitoid bodies which impinged upon the weaker greenstone sequences, causing them to escape in the direction of least pressure.
- External stresses and the escape from impinging granitoids led to the development, at the scale of the Norseman-Wiluna Belt, of a conjugate pair of NW-striking sinistral shear zones and NE-striking dextral shear zones.
- D_2 - D_4 deformation resulted from pure shear due to ENE-WSW shortening, and not as a result of sinistral transpression.

Gold Distribution and Fractal Dimensions (Section 3.1):

- Gold distribution along the Boulder-Lefroy Shear Zone follows a very well determined pattern, with four peaks in gold endowment, corresponding to the major mining camps, spaced systematically every 30-40 km, and each peak followed by an area of very low gold endowment.

- Interestingly, the highest endowed area (the Golden Mile) is followed to the north and to the south along the BLSZ by the poorest areas, suggesting that either gold or fluids were focused towards the Golden Mile, depleting the immediate surroundings.
- Fractal dimension can be used to quantify complexity of lithological contacts and major structures. The largest gold deposits are sited, not at regions of maximum complexity (highest fractal dimensions), but in regions of greatest complexity gradients (fractal dimension gradients), representing tectonic/structural domain boundaries.
- Fractal dimension is proposed as a relatively simple and low-cost method to focus exploration studies.

Sulphur Isotopes (Section 3.2):

- Large variations in gold-related pyrite sulphur-isotope compositions (>10‰) in larger gold deposits (>1Moz) are typically related to specific structural settings, hydrothermal alteration assemblages and host rocks.
- Anomalous $\delta^{34}\text{S}_{(\text{py})}$ values and large variations are related to a sensitivity to ore depositional processes, which relate to local scale physical and chemical controls. Thus, variation in sulphur isotope ratios could be accounted for by local processes rather than specific fluid sources.
- A further source of sulphur isotope variation could be related to pyrites from unmineralized sedimentary rocks, which were found to have large variations in sulphur isotope composition, in contrast to previous studies. These are a potential sulphur source to deep-seated hydrothermal fluids.

Gold Endowment Analysis (Section 4):

- Parameters critical to the control of world-class gold deposits are defined through a combination of genetic studies and empirical analyses within a GIS environment.
- These are summarized in Table 4.1 in terms of a mineral system analysis. They can form the basis of endowment analyses, either semi-quantitative in nature or involving more sophisticated integration using fuzzy logic or artificial neural network methodologies.

Table of Contents

PART I: STRUCTURAL DEVELOPMENT AND CONTROLS ON GOLD MINERALIZATION IN THE KALGOORLIE TERRANE

1. Introduction	1
2. Structural Evolution and Gold in the Norseman-Wiluna Belt	3
Abstract	3
2.1. Introduction	6
2.2. Previous Studies	7
<i>Deformation</i>	7
<i>Timing of Gold Mineralization</i>	10
2.3. New Deformation Time Chart for the Norseman-Wiluna Belt	11
<i>Summary</i>	11
<i>Relative Timing of Granite Intrusion: The Established View</i>	11
<i>Strain Intensity and Granite Age</i>	14
<i>Folding and Deflection: Timing of D₂</i>	15
<i>Relation between D₂ and D₃</i>	17
<i>D_{2e}: the Pre- D₂ Extension Phase</i>	19
<i>D₁ and D_{1e}</i>	20
<i>Numerical Models of Folding and Rigid Bodies</i>	21
<i>Discussion</i>	23
<i>Gold Mineralization, Metamorphism and Magmatism</i>	25
<i>Third Tectono-thermal Event: the Late Archean Kalgoorlie Orogen</i>	30
<i>Conclusions</i>	31
2.4. Boulder-Lefroy Shear Zone: Kinematic History and Gold Mineralization	32
<i>Summary</i>	32
<i>Introduction</i>	32
<i>Gold Distribution</i>	34
<i>New Celebration District</i>	35
<i>Kalgoorlie District</i>	47
<i>Kambalda-Saint Ives Goldfield</i>	52
<i>Discussion and Conclusions</i>	58
2.5. Ida and Zuleika Shear Zones: Kinematic History and Gold Mineralization	62
<i>Summary</i>	62
2.5.1. <i>The Ida Shear Zone</i>	63
<i>Introduction</i>	63
<i>Previous Work</i>	64

<i>Stratigraphy</i>	65
<i>Regional Metamorphism</i>	67
<i>Geochemistry</i>	68
<i>Structure and Shearing-Related Metamorphism</i>	69
<i>Gold Deposits along the Ida Structural Corridor</i>	76
<i>Discussion</i>	79
2.5.2. The Zuleika Shear Zone	82
<i>Introduction</i>	82
<i>Previous Work</i>	82
<i>Stratigraphy and Metamorphism</i>	84
<i>Regional Folds</i>	85
<i>Late Brittle-Ductile Structures</i>	86
<i>Field Observations</i>	86
<i>Discussion</i>	93
<i>Escape Tectonics and Deformation of the Kalgoorlie Terrane</i>	98
2.6. Controls on Gold Endowment: Shear Zone Comparison	101
<i>Summary</i>	101
<i>Introduction</i>	102
<i>Competency Contrast</i>	103
<i>Lithological Complexity</i>	104
<i>Metamorphic facies</i>	105
<i>Ultramafic Rocks</i>	105
<i>Role of Folds</i>	106
<i>Shear Zone Orientation</i>	106
<i>Conclusions</i>	108
2.7. Kalgoorlie Orogen	110
<i>Summary</i>	110
<i>Introduction</i>	110
<i>Shear Zones of the Central Kalgoorlie Terrane: Linking Local to Regional</i>	
<i> Deformation</i>	111
<i> Indentation Tectonics: the Role of Granitoids</i>	112
<i> Regional Deformation</i>	113
<i> Nature of the Kalgoorlie Orogen</i>	116

3. Fractal Dimensions and Sulfur Isotopes: Significance of Physical and Chemical Complexity Gradients	117
Summary	117
Introduction	118
3.1. Fractal Dimensions	120
<i>Objectives</i>	120
<i>Methodology</i>	121
<i>Results – GIS Methods</i>	128
<i>Results – Fractal Dimensions</i>	133
<i>Discussion and Conclusions</i>	137
3.2. Sulfur Isotopes	140
<i>Objectives</i>	140
<i>Methodology</i>	142
<i>Results</i>	144
<i>Discussion and Conclusions</i>	167
4. GIS and Gold Endowment	171
4.1. Introduction	171
4.2. Major Factors Controlling World-Class Gold Deposits	171
Table 4.1	172
5. Final Remarks	175
5.1. Structural Evolution: the late Archean Kalgoorlie Orogen	175
5.2. Gold Mineralization	177
5.3. Sulphur Isotopes	178
Acknowledgments	179
References	179

**PART II: A GENERIC ASSESSMENT OF OROGENIC GOLD PROVINCES:
FACTORS CONTROLLING THE FORMATION OF WORLD-CLASS AND
GIANT DEPOSITS**

Preamble	2
1. What is the Size and Structural-Lithological Architecture of World-Class Giant Orogenic Gold Systems?	4
1.1. Constraints	4
1.2. Interpretation	5
1.3. Outstanding Problems	5
1.4. Exploration Criteria	5
2. What is the Geodynamic History of World-Class/Giant Orogenic Gold Systems?	7
2.1. Constraints	7

2.2. Interpretation	7
2.3. Outstanding Problems	8
2.4. Exploration Criteria	9
3. What is the Nature of Fluid Reservoirs?	10
3.1. Constraints	10
3.2. Interpretation	11
3.3. Outstanding Problems	13
3.4. Exploration Criteria	13
4. What is the Method of Fluid Advection/Convection?	14
4.1. Constraints	14
4.2. Interpretation	14
4.3. Outstanding Problems	14
4.4. Exploration Criteria	15
5. Mechanisms of Metal Transport and Deposition	16
5.1. Constraints	16
5.2. Interpretation	17
5.3. Exploration Criteria	17
6. Executive Summary of Positive Geological Exploration Criteria for Giant to World-Class Deposits	18
6.1. Terrane or Province Selection Scale	18
6.2. Goldfield or Camp Selection Scale	18
6.3. Indicative Target-Scale Geological Guides (Not Exclusive to Large Deposits)	19
References	19

Introduction

Arguably, the most important control on the distribution of orogenic “lode” gold deposits in the Yilgarn Craton is structure. Understanding the structural evolution of the Craton and the relative timing of mineralization is therefore essential in determining the processes that lead to giant to world-class gold deposits. Early in the project, a consensus was reached via discussion with sponsors that researchers at UWA, largely funded by a SPIRT/Linkage Grant attached to the AMIRA Grant, would focus on the structure/gold relationships, and provide constraints for modeling mineralization processes at the gold module within CSIRO, supported by the AMIRA Grant. Structural knowledge would also complement results from other AMIRA projects on the Norseman-Wiluna Belt, in which structure was a secondary consideration, and yield a broad view of the tectonic and temporal development of the belt between 2.7-2.6 Ga. In this process, a strategy was required that took into account the limited access to the Golden Mile, the only giant deposit in the Craton. Thus, in agreement with sponsors wishes, the project focused on a broad region of the Kalgoorlie Terrane, around the Golden Mile, seeking to understand the patterns of gold distribution in terms of its structural evolution, and seeking to compare well-endowed and poorly-endowed regional shear zones. These studies were accompanied by GIS-based studies designed to test models and generate more quantitative relationships between parameters visible on maps and the distribution of large gold deposits. Fractal analysis methodologies were developed as part of the Project, whereas other data were contributed to the project but are not proprietary to it. Due to the perceived importance of the composition of the sulphur isotope ratios in sulphides as an indicator of large gold deposits, this module carried out also documentation of the variability of sulphur isotopes in gold-related pyrites.

Research was undertaken between 1999 and 2002 by a team based at the Centre for Global Metallogeny at UWA. The team comprised Prof. David Groves, Dr. Derek Wyman (1999), Dr. Roberto Weinberg (2000-2002), and PhD students Peter van der Borgh and Paul Hodkiewicz. In this report, the main findings of the module are described. Most of the main findings have been reported in the six-monthly meetings with sponsors, and more detailed work will be provided to the sponsors upon completion of the two PhD theses.

Research involved detailing the structural evolution of major shear zones in the Kalgoorlie Terrane, seeking to understand the broader kinematic history of the terrane (*Sections 2.4 to 2.6 and 2.8*), and how their differences controlled gold mineralization and their contrasting gold endowments (*Section 2.7*). Research involved also characterizing structural complexity and

comparing that to gold distribution. Many GIS-based methods were experimented with, and the use of fractal dimensions as a means to quantify complexity was particularly successful (*Section 3.1*). The sulphur isotope value of pyrite has been suggested as an indicator of fluid oxidation state, and therefore fluid origin, with the potential to constrain the gold endowment of individual deposits. In an attempt to clarify its significance, $\delta^{34}\text{S}$ values of pyrites from a number of different deposits were determined and the results are discussed in *Section 3.2*.

The underlying approach taken stems from the recognition that to ultimately understand the origin of giant gold deposits and to progress from a purely empirical approach to a process-based approach in gold exploration it is necessary to integrate empirical data and process-oriented thinking and modelling. The highly endowed Boulder-Lefroy Shear Zone was compared with less endowed shear zones in the Kalgoorlie Terrane, seeking to understand the role of deformation on mineralization, by detailing the relation between structural development and relative timing of gold mineralization. The results of this project contribute to a longer-term national cross-discipline effort to understand the tectonic setting and thermal evolution of the Kalgoorlie Terrane and Yilgarn Craton, one of the most endowed cratons worldwide. Despite very limited access to the Golden Mile deposit, it still remained the centre of attention throughout this module, as the ultimate exploration target.

The structural evolution of the Terrane was investigated across scales, starting from detailed descriptions of gold deposits and districts along shear zones, and then linking them along strike to determine shear zone history and the large-scale kinematic history of the Kalgoorlie Terrane and, with the help of aeromagnetic imagery, regional scale maps and literature descriptions, expand those conclusions to the entire Norseman-Wiluna Belt.

Finally, the results of a preliminary orogenic gold database are combined with results of ongoing GIS research to provide guidelines for distinction between giant to world-class gold provinces and deposits. These are presented in a format consistent with the five research questions that formed the basis for the GODs Project.

Structural Evolution and Gold in the Norseman-Wiluna Belt

Abstract

This section details the structural evolution and the timing of gold mineralization in the Norseman-Wiluna Belt, by focusing on the Kalgoorlie Terrane and some of its regional shear zones. First, the constraints on the absolute timing of deformation are discussed (*Section 2.3*), followed by a detailed description of the structural evolution of regional shear zones, their role in the evolution of the belt and the relative timing of mineralization.

Establishing relative and absolute time frameworks for the sedimentary, magmatic, tectonic and gold mineralization events in the Norseman-Wiluna Belt of the Archean Yilgarn Craton of Western Australia has long been the main aim of research efforts. Recently published constraints on the timing of sedimentation and absolute granite ages have emphasized the shortcomings of the established rationale used for interpreting the timing of deformation events. In this section the assumptions underlying this rationale are scrutinized, and it is shown that they are the source of significant misinterpretations. A revised time chart for the deformation events of the belt is established where the regional events D_2 - D_4 are given a significantly younger age, being broadly contemporaneous with gold mineralization. It is proposed that D_2 - D_4 define a tectono-thermal event which includes late-stage low-Ca granitoid magmatism and gold mineralization. Together these characterize the late Archean Kalgoorlie Orogen (*Section 2.7*).

Studies of several gold camps along the Boulder-Lefroy Shear Zone revealed that it developed in two main stages (*Section 2.4*). The first stage was related to the regional D_2 deformation phase of NNW-SSE trending folding and thrusting. The second phase was related to the regional D_3 regional deformation phase was dominantly expressed by sinistral shearing along the shear zone, and reactivated the pre-existing NNW-SSE trending network of steepened thrust planes. Whereas regionally, the maximum shortening axis remained constant during the change from D_2 to D_3 , locally there was a small clockwise rotation of this axis. Sinistral movement linked previously disconnected thrust planes along strike and accommodated relatively modest total displacement. D_4 is interpreted as a continuation of D_3 as the crust cooled, and deformation became partitioned to narrow brittle or semi-brittle planes. The changes from a crustal thickening D_2 event, characterized by intracrustal thrusting, creating an anastomosing NNW-striking

network of listric thrusts, to a lateral escape D_3 event, characterized by conjugate strike slip shear zones suggest that the crust may have reached its maximum sustainable thickness ending D_2 .

The Zuleika Shear Zone is a NW-striking curved zone, separating the Coolgardie Domain from the Ora Banda Domain (*Section 2.5*). Its history is complex, with reverse, east-directed thrusting (D_2) dominating in the Kundana District, while sinistral movement (possibly D_3) dominates further north in the Ant Hill area. North- or NNE-striking shear zones and brittle faults cut across the main trend and localize gold mineralization at Kundana. Like at the Boulder-Lefroy Shear Zone, these are interpreted to have been initiated during D_3 (possibly even D_2) and reactivated in the brittle D_4 stage, giving rise to multiply brecciated quartz veins.

The Ida Shear Zone (*Section 2.5*) lies within a narrow deformation corridor of dominantly amphibolite facies greenstone rocks trending NNW. Lineation is dominantly gently plunging, but kinematic indicators are commonly ambiguous, although locally a dextral shear sense may be depicted. Lack of asymmetries and strong attenuation of the rock sequence plus intensive deformation suggest that this greenstone corridor underwent intensive flattening with a sub-horizontal NNW-SSE direction of extension and perpendicular shortening. The main trend of the deformation corridor deviates around a granite batholith, suggesting they reacted to the indentation of the granite during shortening.

Mineralization along the Boulder-Lefroy Shear Zone took place late in the tectonic history of the terrane, either during D_3 or during a D_4 brittle faulting event. Fimiston-style mineralization at the Golden Mile is an exception, not only because it is by far the most endowed but also because it most likely took place during early D_2 or even earlier. Similarly, where the timing of gold deposition was constrained along the Zuleika and Ida Shear Zones, mineralization took place after shearing, in brittle structures which cross-cut the foliation (e.g. Igoana and Kundana).

Comparison between rock sequences sheared at greenschist and amphibolite facies conditions (*Section 2.6*) suggest that at higher temperature, shearing is more homogeneous due to generalized rock viscous flow, while at lower temperatures competency contrast is enhanced, with phyllosilicate rich rocks flowing viscously while quartz and feldspar dominated rocks deform in a brittle fashion. This difference in behaviour leads to efficient fluid focusing in rocks at greenschist facies because strain localizes to lithological contacts and heterogeneous flow due to competence contrasts leads to zones of dilation, high permeability and gold mineralization.

Discussion surrounding the timing of gold mineralization is deeply linked with our incomplete understanding of the sources of mineralizing fluids. Thermal considerations suggest that the Kalgoorlie Terrane must have undergone two phases of metamorphism: the first, related to mafic-ultramafic magmatism and crustal extension and the second, related to subsequent crustal shortening. If fluids liberated by crustal metamorphism played a role in leaching and transporting gold, an argument can be made for the possible existence of two distinct phases of mineralization related to the phases of metamorphism.

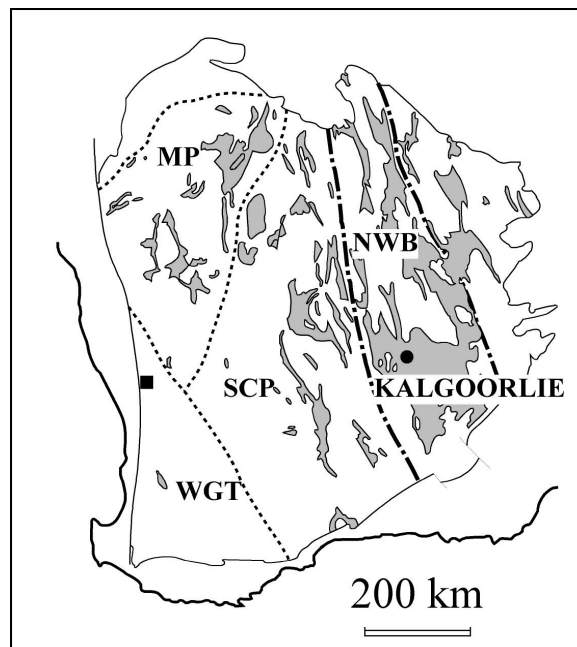
2.1 Introduction

The Archean Yilgarn Block of Western Australia is one of the major gold provinces on Earth, with the Kalgoorlie Golden Mile and Mount Charlotte gold deposits alone having produced 1% of the world's total gold production. Most gold deposits in this Archean craton are structurally controlled and as such implies that understanding its structural evolution and the timing of gold mineralization are fundamental for improving our understanding of the processes of mineralization and for prospectivity.

Several major gold deposits in the Yilgarn Block, including the Golden Mile, lie in the immediate vicinity of major regional shear zones, such as the Boulder-Lefroy Shear Zone (Fig. 2.4.1). Understanding the relationship between shear zones and gold mineralization has therefore been the subject of major scientific and exploration efforts in the Yilgarn, yielding many important exploration models which are today applied worldwide. This section focus on the timing and character of the regional deformation, and the relative timing of gold mineralization, aiming specifically at three regional shear zones of contrasting gold endowment: the richest Boulder-Lefroy Shear Zone, the Zuleika Shear Zone, and the poorest Ida Shear Zone. The approach was to detail deposit scale structural information and link that to regional scale structures as derived from geological maps and aeromagnetic imagery.

This section starts with a general review of the literature regarding both the regional structural development of the Norseman-Wiluna Belt, as well as the timing of gold mineralization. This review is followed by a re-evaluation of the timing of deformation, and its relation to granite intrusion. Then the three major shear zones in the Kalgoorlie Terrane are described: the Boulder-Lefroy, Zuleika and Ida Shear Zones.

Fig. 2.1.1. The Yilgarn Craton and its main division: Western Gneiss Terrane (WGT); Southern Cross Terrane (SCP), Norseman-Wiluna Belt (NWB) which includes the Kalgoorlie Terrane and is part of the Eastern Goldfields Province.



2.2 Previous Studies

Deformation

In the literature, the deformation history of the Norseman-Wiluna Belt is generally divided into four main shortening phases, D_1 - D_4 (e.g. Archibald et al. 1978; Platt 1978; Witt and Swager 1989; Swager et al. 1992; Swager 1997). D_1 comprises the earliest recognizable structures. In the region surrounding the BLSZ, D_1 is described as a major north-directed thrusting phase, recumbent folding and large-scale stratigraphic repetition (Archibald 1978; Martyn 1987; Vearncombe et al. 1989; Witt and Swager 1989; Swager and Griffin 1990; Swager et al. 1992, Knight et al. 1993). Archibald (1978) distinguished two stages of subhorizontal deformation: a) stratigraphic stacking through thrusting; and b) isolated recumbent to inclined folds. Swager and Griffin (1990) described a south-over-north thrust duplex in the Kambalda domain, including several D_1 fault bounded horses separated by three major thrust planes, associated with large-scale recumbent folds, some of which have been folded during D_1 into vertical attitudes (e.g. the Kalgoorlie Anticline). Repetition of the mafic-ultramafic sequence has also been mapped around the margins of granite domes (e.g. Dunnsville Dome, Swager 1989; Widgiemooltha Dome, Griffin 1990).

A major change in the stress system took place at ca. 2655-2650 Ma (this volume) and initiated a second major shortening event, defining a late Archean orogen in the Norseman-Wiluna Belt. This orogen has been divided in the literature into three distinctive phases. The first event, known as D_2 , is a crustal thickening event characterized by thrusting and folding, which gave rise to regional NNW-SSE trending fabric (Archibald 1978; Platt 1978; Witt and Swager 1989; Swager and Griffin. 1990). This phase was followed by D_3 and D_4 , dominantly strike slip events, overprinting D_2 and associated with en-echelon N-trending folds (Witt and Swager 1989; Swager and Griffin. 1990). D_3 - D_4 define a phase of lateral crustal extension (lateral escape) and the transition from D_2 to D_3 - D_4 was most likely continuous, and a result of the crust having reached its maximum sustainable thickness during D_2 .

The literature has focused mostly on the sinistral character of D_3 , probably as a result of over-focusing on the major NW- and NNW-trending shear zones of the Kalgoorlie region (e.g. Boulder-Lefroy, Zuleika and Kunanaling Shear Zones; Langsford 1989; Hunter 1993). It is clear, however, that D_3 comprises also important N- and NNE-trending dextral shear zones, as

exemplified north of the Kalgoorlie by the Waroonga Shear Zone (Platt 1978; Hammond and Nisbet 1992) and the N-trending part of the Mt. George Shear Zone (Skwarnecki 1987), in contrast to its sinistral NNW-trending part (Williams et al. 1989).

D_4 , the last deformation phase, is subject of some disagreement and much misunderstanding. Some authors used the term to include all N- or NNE-trending dextral shear zones, neglecting the possibility of them being conjugate to the sinistral NNW-trending shear zones. Mueller et al. (1988) on the other hand suggested that deformation patterns in the Kalgoorlie area resulted from a dextral wrenching event, which overprinted an earlier sinistral wrenching (D_3). Ridley and Mengler (2000) used the term to define continued regional shortening leading a brittle reactivation of dextral D_3 NNE-SSW and N-S shear zones (Kalgoorlie District). A more general definition of D_4 , and the one used here, is that it comprises a brittle and semi-brittle conjugate pair of faults: a dextral NNE-SSW and sinistral ESE-WNW. This pair developed as a result of the same straining as D_3 but in a cooler environment, where deformation is more strongly partitioned to well-defined planes. These faults are visible in aeromagnetic imagery in most areas, but are particularly well expressed in the more competent granite bodies.

Groves and Batt (1984) and Hallberg (1986) emphasized the importance of early extension in the evolution of the belt, since the accumulation of voluminous mafic-ultramafic volcanic rocks followed by felsic volcanoclastic and sedimentary rocks, must have taken place during an extension event. However, extensional related structures are less clearly defined than shortening phases. The difficulty lies partly in the overprinting by shortening structures, and partly in separating a regional phase of extension from local extensional structures developed during regional shortening phases. For example, Swager and Nelson (1997) suggested that the extension structures around the Eastern Gneiss Complex are due to doming during shortening, whereas Passchier (1994) interpreted the early extensional structures around the Raeside granite near Leonora to be a result of regional extension, unrelated to doming. Hammond and Nisbet (1992) determined movement direction on a number of shear zones and concluded that the earliest set of ductile shears records an extensional event, which Williams and Whitaker (1993) argued was contemporaneous with an early phase of gneiss and granite doming. There is general consensus that there was an extension phase before D_1 , which Hammond and Nisbet (1992) labeled D_e (see Swager 1997). Williams and Currie (1993), based on the N-S trend of early

granite domes, suggested an east-west extension axis for this phase. Passchier (1994) suggested that early extension structures in the north could be contemporaneous to thrusting in the south.

Witt (1994) inferred an extensional collapse stage following D_1 thrust stacking. The results of a regional east-west, deep crustal seismic reflection profile north of Kalgoorlie have indicated the presence of a prominent subhorizontal reflector interpreted as a detachment underlying the greenstone sequence (Drummond et al. 1993; Goleby et al. 1993). Goleby et al. (1993) and Williams (1993) suggested that major east-west extension above the detachment resulted in truncation of greenstones and thrusts. This extension was interpreted to have taken place after D_1 thrusting but before D_2 shortening (see also Swager 1997). According to Swager (1997) this extension accounts for the clastic deposits in basins folded during D_2 , such as the Kurrawang Sequence, at the core of the Kurrawang Syncline, and the Merougil Sequence. He estimated extension to have occurred at ca. 2675 Ma ago. This contrasts with the recent results of Krapez et al. (2000).

Krapez et al. (2000) studied the timing of deposition of a number of volcano-sedimentary sequences in the Norseman-Wiluna Belt and found a number of unconformities, indicating phases of uplift and erosion (shortening?), separating phases of subsidence. They found that the Kurrawang Sequence comprises a succession of quartzofeldspathic conglomerate, sandstone and mudrock representing high-density to low-density turbidites, deposited in a deep-marine environment. An erosional unconformity separates the Kurrawang Sequence from the underlying Kalgoorlie Sequence (formerly Black Flag Group). The deposition of the Kalgoorlie Sequence is divided into two tectonic stages with depositional ages of 2681-2670 Ma and 2661-2655 Ma (Fig. 2.3.1), as constrained by zircons ages (Krapez et al. 2000). These ages and the unconformity imply subaerial uplift and erosion of the Kalgoorlie Sequence followed by rapid drowning and deposition of the Kurrawang Sequence after 2655 Ma (Krapez et al. 2000). The deposition of the Kurrawang Sequence seems to require an important phase of subsidence after D_1 . The late deposition of the Kalgoorlie and Kurrawang Sequences implies that earlier interpretations of the timing of deformation based on their early deposition must be reassessed.

The new results of Krapez et al. (2000) demand a careful scrutiny of the assumptions behind the established view of the timing of deformation. It is the purpose of *Section 2.3* to discuss the limitations of these assumptions, and to propose alternative interpretations and a new time chart for the structural evolution of the Norseman-Wiluna Belt.

Timing of Gold Mineralization

Detailed mine studies, and our own observations, suggest that gold mineralization generally took place late in the tectonic evolution of the craton, either during D_3 or D_4 (Mueller et al. 1988; Vearncombe et al. 1989; Clout et al. 1990; Groves et al. 1990; Ridley and Mengler 2000; Groves et al. 2000). This is supported by age determinations, which constrain mineralization to between ca. 2640-2625 Ma (e.g. Groves et al. 1995, 2000; Yeats et al. 1999).

There is, nevertheless, evidence that gold mineralization may have been more protracted, with a number of gold deposits in the Norseman-Wiluna Belt demonstrably multiply deformed and arguably deposited during early folding and thrusting events (e.g. Knight et al. 2000; Tower Hill deposit, Witt 2001; Mulgarrie, Davis in press). Most importantly, the Kalgoorlie gold District, the largest of them all, has had multiple mineralizing events (e.g. the Golden Mile and Mt. Charlotte deposits at Kalgoorlie, e.g. Clout et al. 1990; Kent and McDougall 1995; Ridley and Mengler 2000) suggesting a protracted mineralization history (Bateman et al. 2001).

During mineralization temperature remained very close to those recorded by peak mineral assemblages (e.g. McNaughton et al. 1990; Groves et al. 2000; Knight et al. 2000) so that gold-related wall-rock alteration assemblages vary systematically with metamorphic grade, and high temperature alteration generally occurring around granitoids (Witt 1991).

2.3. New Deformation Time Chart for the Norseman-Wiluna Belt

Summary

In this section a *revised time chart* for the deformation events of the belt is established, based on several lines of evidence, and supported by the results of Krapez et al. (2000). It is proposed that a tectono-thermal event defined by D_2 - D_4 started at approximately 2650 Ma and ended at 2630 Ma (see also Davis 2002 in press). This event coincides with the third tectono-thermal event for the Yilgarn proposed by Smithies and Champion 1999), and includes relatively small volumes of the 2650-2630 Ma low-Ca and alkaline granites, as well as major gold mineralization.

The first shortening phase to affect the belt, D_1 , was preceded by an extensional event D_{1e} and accompanied by a change from volcanic-dominated to plutonic-dominated magmatism at ca. 2685-2675. Later extension (D_{2e}) controlled deposition of the ≤ 2655 Ma Kurrawang Sequence and was followed by D_2 , a major shortening event, which folded this sequence. D_2 must therefore have started after 2655 Ma - at least 20 Ma later than previously thought and later than the voluminous 2670-2655 Ma granite intrusion. Younger transcurrent deformation, D_3 - D_4 , waned at around 2630 Ma, suggesting that the crustal shortening deformation cycle D_2 - D_4 lasted ca. 20 Ma, contemporaneous with low-volume 2650-2630 Ma low-Ca granites and alkaline intrusions. Time constraints on gold deposits suggest a late mineralization event between 2640-2630 Ma. Thus, D_2 - D_4 deformation cycle and late felsic magmatism define a 20-30 Ma long tectono-thermal event, which culminated with gold mineralization.

The finding that D_2 folding took place after granite intrusion lead to research into the role of competent bodies during folding by means of numerical models. Results suggest that buoyancy-driven doming of pre-tectonic competent bodies trigger growth of antiforms, whereas non-buoyant, competent granite bodies trigger growth of synform. The conspicuous presence of pre-folding granites in the cores of anticlines may be a result from active buoyancy doming during folding.

Relative Timing of Granite Intrusion: the Established View

A large number of crystallization ages of felsic magmatic rocks of the Yilgarn Craton have been determined out over the last decade (e.g. Nelson 1997). Many granite gneisses previously interpreted as basement rocks have now been shown to be intrusive into the greenstone sequence (e.g. Swager and Nelson 1997). It has also been found that early granite intrusions in the Norseman-Wiluna Belt are contemporaneous with the youngest felsic volcanic rocks and were

intruded at ca. 2685-2675 Ma (e.g. Campbell and Hill 1988; Nelson 1997). The most voluminous intrusion occurred between 2675 and 2655 Ma (Nelson 1997). These absolute ages were used to constrain the timing of deformation by using Witt and Swager's (1989) tectonic/structural classification of granites of the Ora Banda-Coolgardie area (NNW and W of Kalgoorlie, respectively) (Table 2.3.1; e.g. Swager et al 1992; Nelson 1997; Witt and Davy 1997).

Witt and Swager (1989) defined a pre- to syn- D_2 group of granites characterized by ellipsoidal shapes at the cores of regional F_2 anticlines. These were followed by post- D_2 syn- D_3 granites, which form ovoid to circular bodies and display a well-defined, contact-parallel foliation. They occur as individual plutons or in clusters where single plutons are separated by narrow screens of poorly exposed greenstones (traced by their distinct aeromagnetic expression). In Witt and Swager's (1989) view, these plutons either pushed aside F_2 regional upright folds or were emplaced across them. They used the displaced axial trace of the Kurrawang Syncline in the vicinity of granites in the Siberia area as an example. Another example is the Bali Monzogranite, which was interpreted to displace and cross-cut an F_2 anticline (Witt and Swager 1989).

Several of these granites appear to be bounded by regional D_3 shear zones. Unlike F_2 folds, these shear zones are not locally deflected to any large extent by the granites and overprint contact foliation indicating that D_3 transcurrent faulting at least partly post-dated emplacement of these granites (Witt and Swager 1989). Late tectonic plutons (late- to post- D_3) are massive or only weakly sheared by D_3 shear zones and generally have ages ≤ 2640 Ma (Campbell and Hill 1988; Nelson 1997).

Assumptions. In order to understand the timing relationship between granite emplacement and structural evolution of the belt, and the origin of the discrepancies in the literature, it is necessary to fully explore the assumptions underlying Witt and Swager's (1989) rationale. These are: a) the degree of deformation of granites is related to the time of magma crystallization in relation to the time of deformation, e.g. weakly sheared granites are late-tectonic; b) pre- or syn- D_2 granites lie at the core of anticlines; and c) granite emplacement causes deviation of structures (e.g. folds) from their regional trend, i.e. granite post-dates structures. A fourth, more general assumption, often implicit in the literature, is that: d) the age of magma crystallization, as derived from SHRIMP zircon dating represents the age of granite emplacement. These assumptions are not necessarily incorrect, their problem is that they do not uniquely and tightly define the timing of granite intrusion in relation to deformation. Their use,

Table 2.3.1. Structural Evolution and Granite Intrusion Timing: the Established and New Views

Deformation Phases	Granite Intrusion	This report
<p><i>compiled after Swager (1997), Witt and Swager (1997), Nelson (1997), Ridley and Mengler (2000)</i></p>	<p><i>after Witt and Swager (1997) and Smithies and Champion (1999)</i></p>	
<p>D₄ dextral shearing on NNE-SSW trending zones (Mueller et al. 1988, Ridley and Mengler 2000).</p>	<p>Late- to post-tectonic granites: 2650-2630 Ma, equidimensional, relatively small, unfoliated. Include alkaline igneous rocks (Smithies and Champion 1999)</p>	<p>D₄ brittle dextral shearing Low-Ca granitoid intrusion throughout D₂-D₄</p>
<p>D₃ strike slip shear zones with both sinistral and dextral movement. Ca. 2663- 2632 Ma</p>	<p>Post- D₂ syn- D₃ granites, deflect D₂ folds and are cut by D₃ shear zones</p>	<p>D₃ sinistral and dextral (conjugate) shearing waning at 2640±8 Ma (intrusion of Clarke Well Granite). Contemporaneous to and outlasting D₂.</p>
<p>D₂ upright macroscopic to regional-scale folds, associated axial planar fabrics reflecting penetrative ENE-WSW shortening. Local extension around granite domes. Ca. 2675-2657 Ma</p>	<p>Pre- to syn- D₂ granites in cores of anticlines</p>	<p>D₂ shortening, syn- or late-deposition of the Kurrawang Seq. (≤2655 Ma). Folding and doming of granite bodies driven by granite buoyancy and regional stresses.</p>
<p>D_{2e} (Witt 1994; Swager 1997) east-west extension (Goleby et al. 1993)</p>		<p>D_{2e} follows D₁ at < 2672 to > 2655 Ma, pre-dates Kurrawang Seq. Doming of Eastern Gneiss Complex and intrusion of voluminous granites.</p>
<p>D₁ low angle shear zones, thrusts and stratigraphic repetition, ≥2675 Ma (Swager and Nelson 1997).</p>		<p>D₁ shortening starts at ca. 2683 Ma, active to < 2672 Ma. Unconformity between Spargoville Seq. and Kalgoorie Seq.? (Krapez et al. 2000) Overlap between felsic volcanism and plutonism. Intrusion of 2675 Ma Eastern Gneissic Complex</p>
<p>D_e low-angle shear zones along granite-greenstone contacts, top-to-SSE movement sense, polydirectional extension (Hammond and Nisbet 1992, Passchier 1994)</p>		<p>D_{1e}</p>

implicit or explicit, lies at the core of the discrepancies between absolute age of granites and their interpreted structural context. As previously published interpretations are interrogated below, a new time chart emerges.

Strain Intensity and Granite Age

The use of strain intensity recorded by granites to estimate the relative timing of granite intrusion - assumption (a) - is deeply rooted in the geological literature, despite numerous contributions outlining its pitfalls (e.g. Archibald et al. 1978; Paterson and Tobisch 1988). In the Yilgarn, early classification of granites was based on a combination of amount of strain combined with other structural characteristics (Archibald and Bettenay 1977) and has since permeated the literature. Champion and Sheraton (1997) avoided these pitfalls by using geochemistry to classify granite intrusions of the Leonora-Lenster area (Norseman-Wiluna Belt).

The strain intensity recorded by granites depends on a range of factors. Apart from the timing of intrusion relative to regional deformation, strain intensity depends also on deformation related to magma pressures (Paterson and Tobisch 1988; Weinberg and Podladchikov 1995), on the shape and size of the granite body, depth of emplacement, the location of the granite in relation to high strain zones in the country rock, as well as the competence contrast to country rocks. With the exception of coarse-grained pegmatites, narrow bodies such as granite dykes are relatively easily deformed. Large, ellipsoidal granite plutons surrounded by relatively incompetent rocks such as phyllosilicate-dominated rocks (Robin 1979; Wintsch et al. 1995) will behave rigidly and deflect deformation rather than record it. By contrast a similar pluton, at high temperature and surrounded by relatively competent amphibolites, may behave incompetently and deform during regional deformation. Furthermore, a cooling granite body may change from relatively incompetent to competent, and from recording deformation to deflecting it.

In the Norseman-Wiluna Belt, shear strain is partitioned to well-defined deformation corridors (e.g. the Bardoc and Zuleika-Kunanalling Shear Zones in Fig. 2 of Witt and Swager 1989) composed predominantly of phyllosilicate-rich greenschist facies rocks. These corridors deflect around large masses of granite suggesting a large-scale organization of deformation into corridors around the relatively competent granite cores.

The difficulty in relating strain intensity to time of magma intrusion is best exemplified in the Yilgarn by the Siberia Battery syenogranite (Nelson 1997). This body was interpreted by Witt and Swager (1989) as being post- D_3 because it is only weakly deformed where cut by D_3

shear zones. However, recent dating yielded a crystallization age of 2673 ± 3 Ma for the syenogranite (Nelson 1997, sample 98256), making it contemporaneous to complexly deformed gneisses interpreted to be pre- D_2 , such as the foliated Two Lids Soak granodiorite and the Barret Well orthogneiss (in Nelson 1997, samples 112153 and 112179, respectively). The differences in strain intensity could be simply due to emplacement depth or strain-rate partitioning across the belt (Davis et al. 2001).

Another key Yilgarn example is the weakly deformed 2640 ± 8 Ma old Clarke Well monzogranite, which cross-cuts the Ida Fault. It was used to constrain the minimum age of D_3 movement on the fault (Nelson 1997), but just as the granite may have intruded after D_3 , it may have intruded an inactive part of a wide fault zone.

Folding and Deflection: Timing of D_2

Assumption (b) above, that granites in the core of F_2 anticlines are pre- to syn- D_2 , and (c), that deflection of regional trends is caused by granite emplacement, are both flawed. Whether pre-, syn- or post-tectonic granites lie at the core of folds depends on the timing of deformation as well as on the mechanism of granite emplacement (Paterson and Tobisch 1988). Pre-tectonic rigid granites can control the sites of synclinal and anticlinal folds. Granites emplaced as diapirs may cause anticline growth contemporaneous to emplacement, conversely pre-existing or developing folds may control emplacement of granites as melt migrates to fold hinge zones (Allibone and Norris 1992; Davis 1993; Weinberg 1996).

The role of pre-existing granites during folding depends on the competence contrast to the country rocks and on the characteristic wavelength of the folds. Granites in the Norseman-Wiluna Belt have responded to deformation mainly as competent bodies. This is evidenced by strong shearing and shortening in the greenstones and at granite-greenstone contacts while granites away from the margins remained relatively weakly deformed. Granite dykes are commonly boudinaged, and importantly, regional structures are deflected around elliptical granite bodies, similar to the deflection of foliation around rigid porphyroblasts.

A competent granite body with a width much smaller than the wavelength of folds commonly fold with the entire package, while a competent body much wider than the fold wavelength, cause folds to develop on their margins, while the granite acts as a buttress. These folds wrap around the rigid body as a result of regional deformation and not as a result of magma emplacement efforts. Thus, contrary to assumption (c), early emplaced granites may cause

deflection of structures developed long after granite emplacement, (see also Paterson and Tobisch 1988). The role of granite bodies of sizes comparable to typical fold wavelengths of a rock sequence is explored below by means of numerical models (“*Numerical Models of Folding and Rigid Bodies*”).

An illustrative example of the problems related to assumption (c) is the deflection of the F_2 Kurrawang Syncline, which includes the Kurrawang Sequence, from its NNW-SSE regional trend. Witt and Swager (1989) estimated a deflection of approximately 15 km, as it approaches the 2660 ± 3 Snot Rocks monzogranite (Nelson 1997). Deflection was interpreted to have resulted from granite intrusion, implying that the 2660 ± 3 Ma intrusion post-dated deposition of the Kurrawang Sequence and F_2 folding (Witt and Swager 1989; Nelson 1997). By contrast, the Split Rock granodiorite, which crops out at the core of the Scotia-Kanowna Dome, a regional F_2 anticline 40 km SE of the Snot Rocks, was interpreted by Witt and Swager (1989) to be a pre- to syn- D_2 body. However, this pre- to syn- D_2 granite, when dated, yielded a crystallization age of 2657 ± 5 Ma (Nelson 1997, sample 93901), within error to the crystallization age of the post- D_2 Snot Rocks monzogranite. So here are two contemporaneous granites, one interpreted as pre- to syn- D_2 and the other as post- D_2 . Nelson (1997) rationalised this discrepancy by arguing that the Split Rock granodiorite must have intruded during the waning stages of D_2 , and the Snot Rocks soon after the end of D_2 .

Nelson’s (1997) interpretation is not particularly satisfactory because it attempts to fit the results of dating into a flawed granite classification. There are other, equally valid alternative interpretations consistent with available information. One alternative is that the Snot Rocks monzogranite crystallization age does not represent emplacement age (assumption (d) above) and that solid granite moved vertically after crystallization driven by its buoyancy (diapirism), thereby causing bending of regional trends. In this case the time of folding is unconstrained by granite crystallization age. Another possibility is that the sequence was folded against a pre-existing granite buttress emplaced at ca. 2660 Ma. In this case both folding and sedimentation are younger than the granitic rocks, and like the Split Rock, the Snot Rocks monzogranite is not post- D_2 but either pre- or syn- D_2 . This interpretation is considered here as more likely because it provides a straightforward explanation for the similar ages of the Snot Rocks and Split Rocks granites. Furthermore, it is fully consistent with the findings of (Krapez et al. 2000) that the Kurrawang Sequence is younger than 2655 Ma.

Relation between D_2 and D_3

Assumption (c) has implications beyond those discussed above. The view that granite emplacement is accompanied by deflection of surrounding rocks to accommodate volume increase has partly underlain the interpretation that sinistral shear zones must, in the main, postdate D_2 folding. This is because F_2 folds have apparently been deflected around granite bodies whereas many shear zones have not (Witt and Swager 1989). Like Swager et al. (1992), we note that N-S folds and NNW-SSE sinistral shear zones could develop simultaneously as a result of regional E-W shortening, where folding and shearing are partitioned (vorticity partitioning, see Passchier 1994). In this case, the different apparent behaviour of folds and shear zones may result from their different nature. Shear zones accommodate shortening by moving crustal blocks in relation to one another. If such a zone is deflected from its original orientation, it may stop moving and a new shear zone may develop with the original orientation. Evidence from shear zones cross-cutting folds suggests that movement on shear zones may have outlasted folding, but the different responses of shear zones and folds to the presence of granites are in themselves insufficient evidence to establish the relative timing of the two structural sets.

The timing of D_2 and D_3 as interpreted here is summarized in Fig. 2.3.1. It has been demonstrated that the Snot Rocks monzogranite does not constrain the minimum age of D_2 . Rather, the discussion above suggests that it is likely that the Snot Rocks and Split Rocks were intruded pre- or syn- D_2 and that their presence, and not their emplacement, caused the deflection in the Kurrawang Syncline during D_2 . In view of the findings of Krapez et al. (2000), it is suggested that folding (D_2) possibly associated with shear zones (normally assigned to the later phase D_3) started after 2655 Ma, post-dating the end of the deposition of the Kalgoorlie Sequence, and either contemporaneous with or post-dating the deposition of the Kurrawang Sequence.

There are no simple rules to assess the age of granites in the Norseman-Wiluna Belt based on structural relationships. Each granite body and its relationships to regional structures need to be understood individually. Having demonstrated that D_2 and D_3 most likely developed after 2655 Ma, and not before 2660 Ma as previously thought, it is now possible to reinterpret the timing of other events by working first backwards in time towards D_1 .

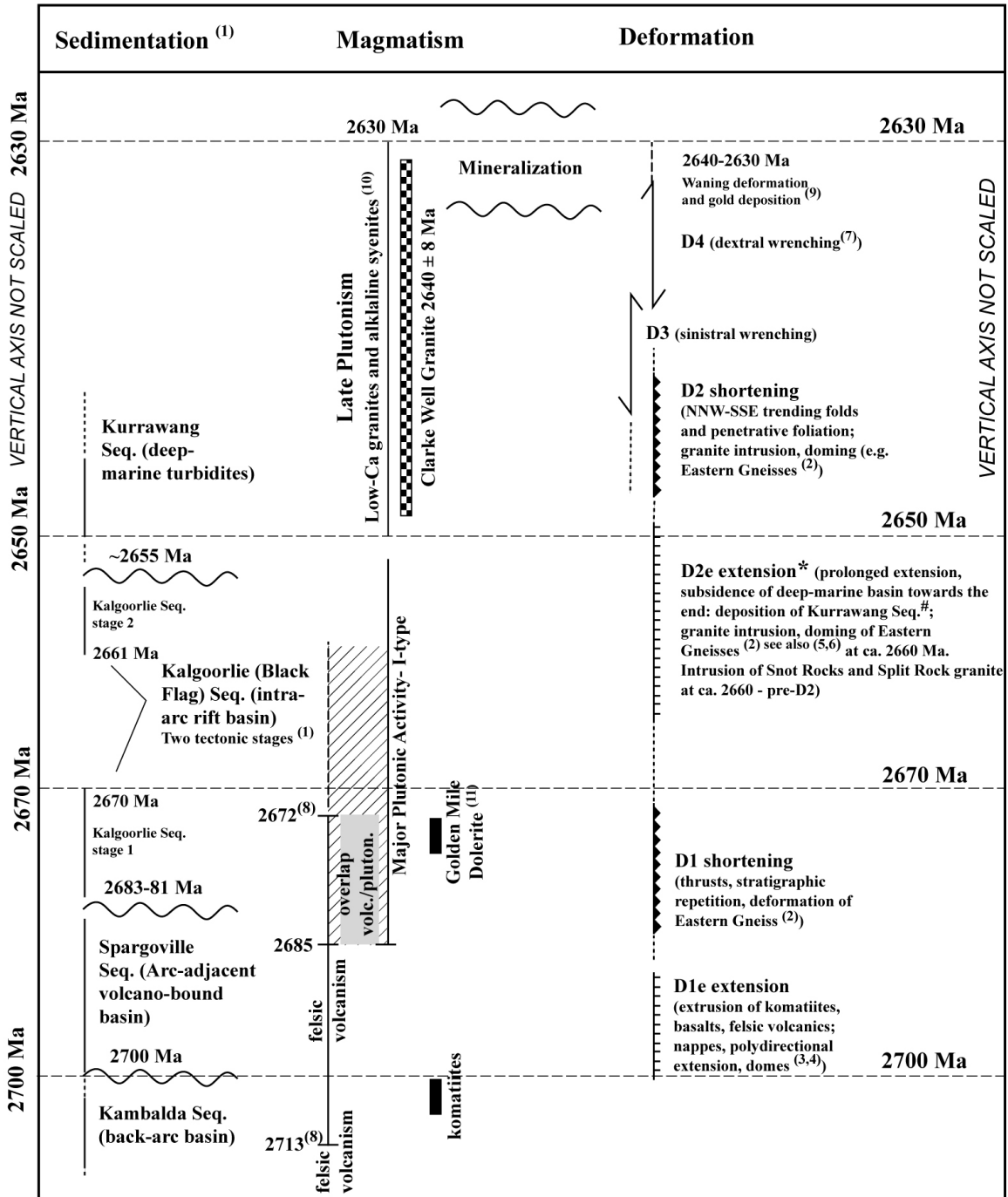
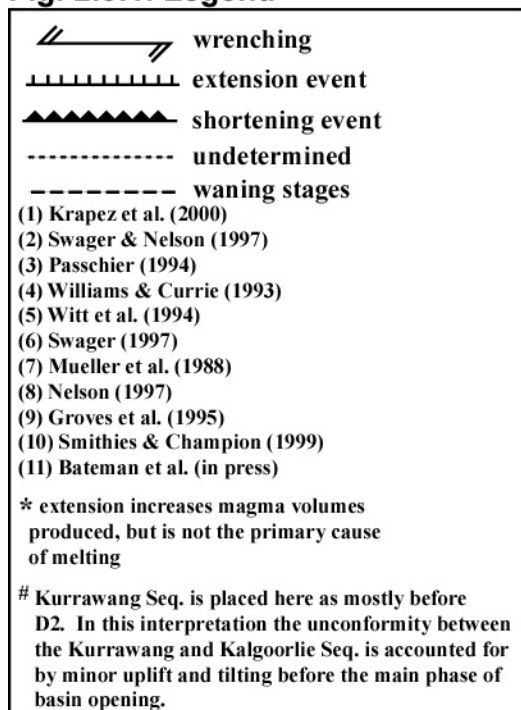


Fig. 2.3.1. Time chart summarizing sedimentation, magmatism and deformation of the Norseman-Wiluna Belt. Note that the vertical axis, corresponding to time evolution is not scaled for clarity. In contrast to previous interpretations, D₂-D₄ are all post-2655 Ma, since D₂ must have occurred after the initiation of sedimentation of the Kurrawang Sequence. This implies that most of the granite bodies were emplaced before D₃-D₄ transcurrent events.

Fig. 2.3.1. Legend***D_{2e}: the Pre-D₂ Extension Phase***

The need for a prolonged subsidence phase before D_2 has already been discussed above in relation to the deposition of the deep-marine Kurrawang Sequence. Although subsidence may not necessarily be associated with extension, there is evidence for a phase of extension preceding D_2 . This phase is here termed D_{2e} and it is suggested that granite doming could have occurred during this phase.

Eastern Granitic Gneiss Complex.

Swager and Nelson (1997) determined that the Barret Well granite gneiss and the foliated Two Lids Soak granodiorite crystallized at ca. 2675 Ma. These foliated rocks are intruded by

massive monzogranite plutons that cross-cut regional structures, such as the normal Pinjin Fault. Small sheets of monzogranite are also present along the fault plane. These are foliated and contain the same steep north-plunging mineral lineation with west-block down kinematic indicators as found along the fault. The Pinjin fault is interpreted as an extensional feature which accommodated the uplift of gneiss and monzogranite but is also intruded by the monzogranite magma (Swager and Nelson 1997). This younger monzogranite phase is presumed to be contemporaneous with the 2660 Ma intrusions of the Eastern Goldfields, and its deformation indicate that “some uplift, accommodated by normal fault movement, occurred during intrusion” (Swager and Nelson 1997). Because of the weak or absent foliation in the voluminous monzogranite plutons and their cross-cutting of the Pinjin Fault, the authors concluded that monzogranite intrusion at 2660 Ma dates the last stage of uplift of the granitic gneiss complex into the lower grade greenstone.

According to Swager and Nelson (1997), the evolution of the gneiss complex is characterized by three steps. The first step, deformation of the 2675 Ma gneisses occurred soon after their emplacement during D_1 and produced banding in zones of high strain. The uplift of this high-grade gneissic complex postdates early D_1 and was accompanied and/or followed by intrusion of the voluminous monzogranite. Because the 2660 Ma age assigned to the massive

monzogranite coincides with the established perception of the timing of D_2 shortening, the authors argue that doming took place in two further steps. First, an early dome developed during an extensional phase after D_1 , this was then further uplifted during D_2 shortening and possibly driven by monzogranite intrusion, representing extensional structures developed during a shortening event.

The younger timing for D_2 deduced here (≤ 2655 Ma) implies that the 2660 Ma granites were not contemporaneous with D_2 shortening. The structural evolution of the Eastern Gneiss Complex may thus be simplified to a two-stage process: a) granite intrusion at 2675 Ma and deformation during D_1 , followed by b) doming accompanied by the intrusion of monzogranites during an extensional phase at 2660 Ma, before D_2 shortening. Thus, rather than representing extensional structures during a shortening event, the Eastern Gneiss Complex define an extensional phase pre-dating D_2 shortening.

D₁ and D_{1e}

Moving further back in time, Krapez et al. (2000) constrained the unconformity marking the end of the Spargoville Sequence deposition and the start of the Kalgoorlie Sequence, to between 2683-2681 Ma based on zircon populations. This unconformity most likely represents an intrabasinal uplift (Krapez, pers. commun. 2000). It coincides temporally with the early intrusion of granites in the Norseman-Wiluna Belt, between 2685 and 2675 Ma ago (Nelson 1997), as well as layered gabbro sills in the Kalgoorlie area (Mount Pleasant sill, U-Pb age 2687 \pm 5 Ma, Kent and McDougall 1995); Golden Mile Dolerite 2675 \pm 2 Ma (Bateman et al., in press). These early granites mark a change from predominantly extrusive magmatism to an extrusive-intrusive magmatic event. Time constraints on D_1 suggest that it was active after 2684 Ma (thrusting of the Bulong Anticline; Swager 1997), during or soon after the emplacement of the ca. 2675 Ma Eastern Granitic Gneiss Complex (Fig. 2.3.1; Swager and Nelson 1997) and before or during the intrusion of the 2674 \pm 4 Ma felsic porphyry dyke, which crosscuts D_1 folds at Kalgoorlie (U-Pb age; Kent and McDougall 1995).

It was argued here that a subsidence phase, possibly associated with extension, D_{2e} , must have been active during deposition of the younger part of the Kalgoorlie Sequence and early Kurrawang Sequence. However, it is also known that D_1 must have been active during the deposition of the early part of the Kalgoorlie Sequence since the sequence is deformed and repeated by D_1 thrusts (Fig. 2.3.1; Archibald et al. 1981). Based on these independent

constraints, it is here proposed that the beginning of D_1 is marked by the initiation of plutonism at ca. 2685 Ma, and by the unconformity between the Spargoville and Kalgoorlie Sequences. D_1 was active during the deposition of the early part of the Kalgoorlie Sequence, which ended at ca. 2670 Ma, or alternatively there were two or more phases of D_1 , bracketing the deposition of the early Kalgoorlie Sequence. This phase is responsible for early thrusting and possibly also nappe/slumping of the volcano-sedimentary sequence (Martyn 1987, Passchier 1994).

Numerical Models of Folding and Rigid Bodies

The close relationship between granites and regional folds warrants a more detailed study of the interaction between rigid-body granites and folding. Numerical models were designed to determine the role of pre-existing rigid bodies on folding of purely viscous, layered sequences. The rigid “pluton” width was similar to the typical fold wavelength of the sequence. The code used is detailed in the appendix. The Eastern Goldfields gross regional geology and seismic reflection profile reveals the geometry of antiforms cored by granites. Both pre- to syn- D_2 or post- D_2 , granites have similar geometry (Swager et al. 1997; Swager 1997). They are imaged seismically as approximately rectangular massive bodies with vertical eastern and western margins, truncating gently dipping fold limbs, and a flat bottom below which greenstones are continuous (Fig. 2.3.2a).

The numerical models used a rectangular rigid body embedded in a horizontal layered sequence. The sequence may be shortened or extended by moving the right-hand side vertical wall (Fig. 2.3.2b). The model box width was three times its height for shortening models. The layer embedding the granite is overlain by material analogue to air (compressive and inviscid) and occupies half the height of the box for shortening models. The “granite” is embedded in a layer 100 times less viscous. This layer is underlain by a low viscosity layer at the base of the box (1000 times less viscous than the granite analogue). The narrow sub-layers in the embedding layer are competent, having the same viscosity as the granite. The “granite” was first modeled as having the same density as the country rocks (Fig. 2.3.3b), and made buoyant in later models (Fig. 2.3.3c).

Fig. 2.3.2. a) Seismic interpretation of the shape of granite bodies and relation to country rocks (after Swager et al. 1997, Fig. 10); b) initial geometry and set-up of the numerical models. The model box has three wide layers: the bottom layer (viscosity $n=1$) accommodates the folding of the middle layer ($n=10$ and 1000), which embeds the rigid granite analogue, modelled as a high viscosity rectangle ($n=1000$).

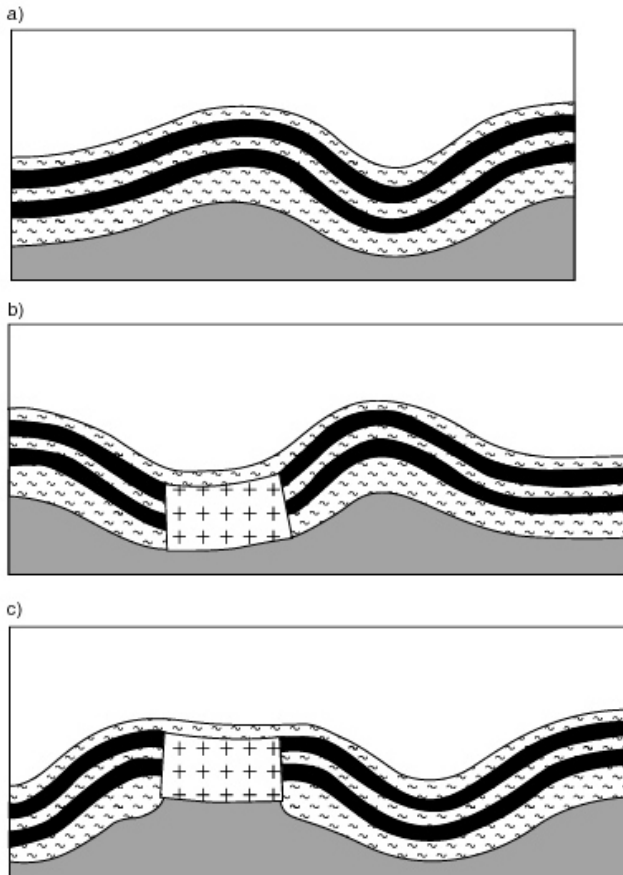
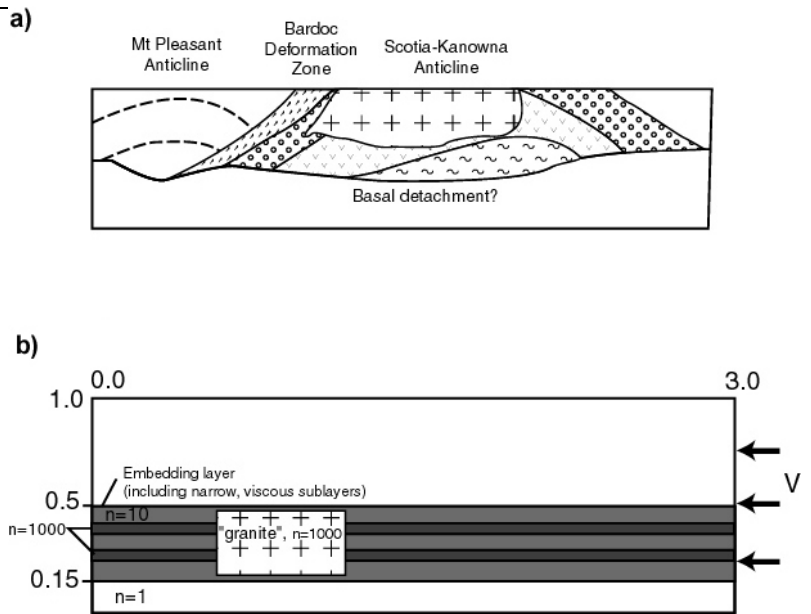


Fig. 2.3.3: Numerical models of folds developed in a layered sequence similar to Fig. 2.3.2. a) Folding of simple layers; b) “granite pluton” (rectangle) was placed at the position where the antiform developed in (a), and caused synclinal folding. In this case all materials have the same density. c) Same as (b) with the “granite” being less dense than the surrounding. Whereas in (b) the rigid rectangle triggered synclinal folding, buoyancy in (c) led to anticlinal folding. In this case, if shortening rate is increased, buoyancy-related doming will be dominated by the tendency of the rigid “granite” to trigger synclinal folding.

The role of a rigid body during shortening is depicted in Fig. 2.3.3. The pattern of folding caused by the presence of the two narrow competent layers alone is shown in Fig. 2.3.3a. Fold wavelength is controlled by the width and viscosity contrast of the folding layers. (In the absence

of the two narrow competent layers, layer shortening occurred without folding.) A rigid rectangle was introduced in Fig. 2.3.3b, in the position where the antiform formed in Fig. 2.3.3a. The rigid body, by inhibiting thickening of the embedding layer, triggered the down warping of the layer to form a synform where there was previously an antiform. Antiforms developed where the layer thickened, away from the granite. Figure 2.3.3c depicts the results where the rigid body was buoyant. In this example, the “granite” forms the core of an antiform because its buoyancy was sufficiently important to overpower its down warping into a synform. In the case of buoyant granites, whether a synform or an antiform develops depends on the relative velocities of shortening and buoyancy-driven doming. For the density contrast between granite and country rocks chosen for this calculation, the lateral shortening had to be reduced by an order of magnitude. Faster shortening inhibits doming and a synform develops. Folds in Fig. 2.3.3a attained the same amplitude as those in Figs. 2.3.3b, c only after considerably more shortening. This is because in the absence of the rigid “granite” shortening could more easily be taken up by homogeneous layer thickening.

The results are not particularly sensitive to the shape and size of the granite body. Runs with a narrower “granite” (height of 0.05 instead of 0.24 in Fig. 2.3.3) resulted in similar folding structures by slowing down shortening rate in order to match the slower deformation driven by smaller “granite” buoyancy. Only very small rigid bodies, in relation to the thickness of the embedding layer, will not play any major role during folding.

Summary and Implications. The results indicate that rigid granite bodies may trigger either growth of a synform or an antiform depending on the relative rates of shortening and buoyancy-driven doming. In nature, the presence of pre-deformation rigid plutons in the cores of antiforms commonly indicates that their buoyancy played an active part during folding. The results imply that, in the same orogen, low buoyancy granites determine the site of synformal folding, whereas large buoyancy plutons trigger antiform growth. The inverse is true for a low viscosity, dense, mass of ultramafic rock relatively localized (as opposed to an extensive, narrow layer): its low viscosity will speed up local layer shortening and antiform growth, whereas its high density may lead to the sinking of the region into a synform.

Discussion

The revised timing of events in the Norseman-Wiluna Belt is summarized in Fig. 2.3.1. As noted by Davis and Forde (1994) the effects of metamorphic grade, deformation partitioning,

diachroneity of deformation, successive deformations with common far-field stress directions, and the presence of pre-existing tectonic elements that influence the orientation of later formed ones, presents a formidable list of factors that must be considered when attempting to resolve the structural history of the belt. Here, only a few of these effects have been considered, and some, like diachroneity of deformation, have been left entirely out of the discussion due to lack of significant information.

There are a number of observations which suggest that D_1 was active at around 2675 Ma, and that it has deformed at least part of the Kalgoorlie Sequence. D_1 must therefore be at least partly contemporaneous with deposition of this sequence. In Fig. 2.3.1 the unconformity between the Spargoville and Kalgoorlie Sequences and the initiation of voluminous pluton emplacement are ascribed tentatively to a change in deformation marking the onset of D_1 . This was followed by a period of extension, D_{2e} , the pre- D_2 extensional phase of Witt (1994) and Swager (1997). This phase is related to subsidence that may have controlled deposition of the late stage of the Kalgoorlie Sequence and the deep marine deposition of the Kurrawang Sequence. Extension also accounts for granite doming such as the Eastern Gneiss Complex. D_{2e} could arguably account for the extensional structures around Leonora (Williams and Currie 1993; Williams and Whitaker 1993), although Passchier (1994) suggested that extension could be either immediately before or contemporaneous with D_1 shortening in the Kalgoorlie area. Folding experiments described above indicate also that doming is not limited to extensional phases, and that buoyant granites could trigger the developments of doming antiforms during shortening phases. It is possible that granite doming occurred throughout the evolution of the belt.

The unconformity between the Kalgoorlie Sequence and the deep-marine basin sediments represented by the Kurrawang Sequence is not accounted for by any major shortening event (Fig. 2.3.1). Although D_2 could potentially be the cause of the Kalgoorlie/Kurrawang Sequences unconformity, it is unlikely that subsidence and a deep marine succession would be contemporaneous with the intensive folding and shortening that characterizes D_2 . Thus, D_2 started after 2655 Ma either late or after sedimentation of the Kurrawang Sequence. It is most likely that the unconformity between the Kalgoorlie and Kurrawang Seqs. was a result of uplift and tilting related to changes in the extension regime.

Although the timing of D_2 is based on the late deposition of the Kurrawang Sequence determined by Krapez et al. (2000), the argument for a late D_2 (at least younger than 2660 Ma) stands independently. The argument is based on the contemporaneous intrusion of the ca. 2660

Ma Snot and Split Rocks (see above), and the role of granites in deflecting the Kurrawang Syncline during D_2 folding. The main conclusion reached here is that the bulk of deformation in the Norseman-Wiluna Belt ($D_2 - D_4$) took place between 2650-2630 Ma. This is broadly contemporaneous with gold mineralization and post-dates the main phase of granite intrusion.

Gold Mineralization, Metamorphism and Magmatism

Gold Mineralization. Age constraints of structurally controlled lode gold deposits in the Yilgarn Craton have recently been summarized by Yeats et al. (1999) and Groves et al. (2000). Timing of mineralization is generally regarded as late in the tectonic evolution of the granitoid-greenstone terrains, during D_3 or D_4 (Mueller et al. 1988; Vearncombe et al. 1989; Clout et al. 1990; Groves et al. 1990; Ridley; Groves et al. 2000; Mengler 2000). There are examples, however, where mineralization took place during D_2 (e.g. Knight et al. 2000). Direct dating of deposits and indirect constraints yielded gold deposition ages between ca. 2640-2625 Ma (e.g. Groves et al. 2000) supporting the view that mineralization is a late event. Groves et al. (2000) summarized the view held by several authors, that there has been a late Yilgarn-wide, gold mineralization event, between about 2660 and 2610 Ma with most voluminous and widespread deposition between 2640 and 2630 Ma. During this event metamorphic conditions (mostly temperature) remained very close to those recorded by peak mineral assemblages (McNaughton et al. 1990; Groves et al. 2000; Knight et al. 2000) so that gold-related wall-rock alteration assemblages vary systematically with metamorphic grade, with high temperature alteration and metamorphic assemblages occurring around granitoids (Witt 1991).

Thus, it seems that gold mineralization is closely related to the 2650-2630 Ma $D_2 - D_4$ deformation cycle, with pronounced mineralization concentrated towards the waning stages of the cycle.

Metamorphism. Considerations on the timing and heat source of regional metamorphism have led to the alternative view that mineralization occurred diachronously across the belt. Bickle and Archibald (1984) studied the metamorphic reactions of a sample collected two kilometres away from the Widgiemooltha Dome. The sample records a temperature 530-560 °C at ~4 kbar. These conditions represent peak regional metamorphic conditions, independent from granite intrusion, and broadly coincide with regional conditions determined further north, near Coolgardie (Knight et al. 2000). Bickle and Archibald (1984) studied the reactions of another sample collected 700m away from the margin of the Pioneer Dome. The sample records nearly

isobaric heating from the regional conditions (560 °C at 4 kbar), to 600-650 °C. The high peak temperatures attained close to the granite are demonstrably related to granite magma emplacement (Bickle and Archibald 1984). The dissipation of heat carried by granite magmas within a few million years of their emplacement, lead (Bickle and Archibald 1984) to conclude that D_2 - D_3 must have occurred soon after granite emplacement. However, the authors fail to describe the relationship between metamorphic minerals and structures, making it impossible to critically analyse this conclusion.

Mueller and McNaughton (2000) discussed in detail metamorphism in the Southern Cross area (west of the Norseman-Wiluna Belt), and though the ages in that area differ from those in the Norseman-Wiluna Belt, the controls on metamorphism are probably similar. They concluded from their geochronology study that gold deposition did not occur during peak metamorphism, as previously thought, but 150 Ma later at ca. 2620 Ma. They suggested that granite-centred metamorphic aureoles are related to granite magma emplacement, but due to different granite ages, peak temperatures in different aureoles were diachronous. The multi-pulse nature of the Ghooli Dome in the Southern Cross, where younger plutons intruded the core of the dome suggests that metamorphism could have been a protracted event, but as argued by Mueller and McNaughton (2000) regional temperature could have decreased to 400 °C in between major magmatic events. Mueller and McNaughton (2000) exemplify the difficulties in deriving the relative timing between gold mineralization and peak metamorphism from field and petrographic relationships.

There are few direct dating of metamorphism in the Norseman-Wiluna Belt. Works such as those by Bickle and Archibald (1984) and Mueller and McNaughton (2000) imply that although peak temperatures in granite contact aureoles are controlled by granite intrusions, temperature conditions away from granite margins are controlled by far field heat sources, independent of exposed granites. Regional thermal conditions away from granite margins are controlled by the total heat flux into the crust, crustal heat production and intracrustal magma and heat migration. The long magmatic and tectonic history of both the Southern Cross area and the Norseman-Wiluna Belt suggests that temperatures fluctuated over time, producing long-lasting and fluctuating low pressure-high temperature conditions through the middle and upper crust. The prevalent view that voluminous magmatism at 2660 Ma is responsible for regional metamorphism disregards the complex evolution of the belt, and must be proven rather than assumed.

Although high temperature (>600 °C), narrow aureoles at the margins of granite domes are most likely related to magma cooling, wider and lower temperature contact aureoles may have alternative origins. One possibility is differential vertical uplift centred at buoyant granites and exhuming deeper and hotter rocks. Bickle and Archibald (1984) concluded that this was probably not the case for the Pioneer and Widgiemooltha Domes (isobaric heating), but this could nevertheless be the case for other domes across the belt. Another possibility is that high temperatures result from fluid flow and heat advection along the strained granite margins. A final possibility is that the aureole results from a combination of higher granite conductivity and heat production, compared to greenstones. As illustrated by the Sybella Batholith in Mount Isa (McLaren et al. 1999; see also Sandiford and Hand 1998), a granite body a few kilometres deep with high heat production and blanketed by low conductivity rocks may be a long-term heat source capable of imposing considerable long-term temperature perturbation on their surrounding.

Calculations using the values of conductivity for greenstones and quartz-porphyry (assumed to be similar to that of granites) measured in Norseman (Howard and Sass 1964), and the average content of heat producing elements of the Bali Suite (granites near Coolgardie; Witt and Davy 1997), indicate that the long term horizontal thermal gradient around granites of vertical thickness of a few kilometers, is relatively weak (20-30 °C decay over 35 km) and can not account for an observable thermal aureole (Mike Sandiford, personal communication 2000). These experiments suggest that a large proportion of the temperature difference between rocks near Coolgardie and rocks near Kalgoorlie (250-300 °C at ~2 kbar) is related to the different burial depths and regional geothermal gradient and not to horizontal gradients imposed by different rates of heat production. It is important to point out that even a relatively small long-term, long-distance lateral temperature difference could be an important factor in controlling horizontal hydrothermal flow across the belt. (Average values used were $U=4$ ppm, $Th=22$ ppm and $K_2O=4.2$ % taken from Witt and Davy (1997) for the Bali Suite and excluding one anomalously high U sample. This suite includes several granites emplaced in a zone of amphibolite facies metamorphism around Coolgardie, including the Widgiemooltha granite. Heat production of Bali Suite granites would have been a reasonably high 5-6 $\mu\text{W}/\text{m}^3$ at 2.7 Ga, approximately double the heat production at present time. Low mantle heat flux into the base of the crust was used in the calculation.)

In view of the above results, it seems unlikely that aureoles in the Norseman-Wiluna Belt result from granite radioactive heat production and high conductivity. This supports the view held by several authors that the granite-centered isograds results from voluminous intrusion (e.g. Witt 1991). However, the other two possibilities to explain the aureoles (heat advection by fluid flow or differential exhumation around domes) remain viable alternatives.

Dating of high temperature gold mineralization on the grounds of their temperature being directly related to granite intrusion (e.g. Witt 1991; Knight et al. 2000) has to be tempered with the results presented by Mueller and McNaughton (2000) illustrating how difficult and misleading it can be to interpret the relative time of gold deposition in relation to peak metamorphism.

In summary, at present there is insufficient reliable information to understand the pattern and timing of peak metamorphism across the belt. There are difficulties in establishing the timing of metamorphism in relation to deformation phases and gold deposition, and there are few reliable ages of peak metamorphism in the Norseman-Wiluna Belt. It is clear, however, that granite intrusion produces a narrow high temperature aureole in its surroundings. Because of the variety of granite ages the aureoles are diachronous across the belt. There are also other processes that could give rise to the wider, lower temperature contact aureole, though calculations suggest that lateral thermal gradient caused by heat production and conductivity differences may be neglected. Timing of peak metamorphism away from the aureoles cannot be equated with the time of most voluminous magmatism, since it depends on the entire tectono-thermal evolution of the belt.

Magmatism and Deformation. Figure 2.3.4 summarizes the relationship between magma intrusion and deformation phase. Early granites (>2672 Ma) were intruded during shortening associated with D_1 , as demonstrated by Swager and Nelson (1997). Different from previous authors, Krapez et al. (2000) suggested that the most voluminous intrusive phase, comprising plutons crystallized between 2670 and 2655 Ma, were emplaced during D_{2e} extension. Relatively small volumes of 2650-2630 Ma low-Ca granites and alkaline granites are exposed (Smithies and Champion 1999) and were intruded during the D_2 - D_4 deformation cycle. The alkaline granites have an A-type affinity, but as pointed out by these authors, their anorogenic tectonic setting cannot be inferred from their chemistry.

The Clarke Well granite, emplaced within rocks deformed by the Ida Fault zone, is only weakly deformed. If it can be assumed that its deformation is related to the waning stages of regional deformation (Nelson 1997), an improvement of the error bar on its 2640 ± 8 Ma zircon (magma crystallization) age is required, since the present error bar covers most of the duration of the D_2 - D_4 deformation cycle (Fig. 2.3.1).

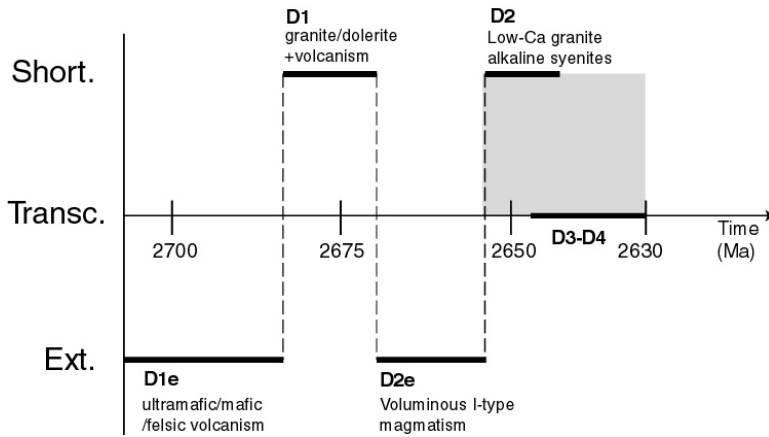


Fig. 2.3.4. Summarizing plot of the relationship between magmatism and inferred phase of deformation.

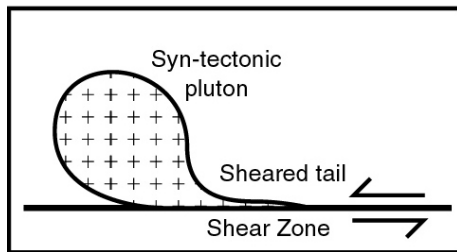


Fig. 2.3.5. Typical pluton shapes of regions where magma emplacement was contemporaneous to transcurrent shearing.

The conclusion that the voluminous granite intrusions are pre- D_3 , the transcurrent phase of deformation, is borne out also by the general shape of granite bodies throughout the belt. Even though shapes alone can not be used as indicators of timing in relation to deformation, the typically elliptical or spherical shape of plutons of the Norseman-Wiluna Belt (Witt and Swager 1989; see also maps in Hallberg 1986; Hammond and Nisbet 1992, Williams and Whitaker 1993; Swager and Nelson 1997; Witt and Davy 1997), are in stark contrast to shapes of granites intruded during transcurrent deformation. These are typically molded by active shear zones: plutons may grow within the shear zone as a complex of sheared sheets (Main Donegal granite; Hutton 1982); they may link two or more shear zones and exhibit magmatic foliation related to regional shearing (e.g. the Mortagne pluton Brittany, Guineberteau et al. 1987; and plutons of the

Borborema Province, Brazil, Neves et al. 1996; Jardim de Sá et al. 1999); or more characteristically, they may form elliptical plutons with sheared tails within shear zones (Fig. 2.3.5; the Ardara pluton, Pitcher and Berger 1972; plutons of the Borborema Province, Neves et al. 1996).

Third Tectono-thermal Event: the Late Archean Kalgoorlie Orogen

Smithies and Champion (1999) defined three tectono-thermal events in the Eastern Goldfields. The first one was marked by a major thermal anomaly at ca. 2705 Ma and the extrusion of komatiites and felsic volcanic rocks. The second event was marked by the main phase of regional magmatism, which according to them, started at ca. 2690 and peaked between 2670 and 2655 Ma. The third event spans the period between ca. 2650 and 2630 Ma, and is characterized by the intrusion of low-Ca granites and alkaline granites, and gold mineralization. Smithies and Champion (1999) argued, based on Kent et al. (1996), Qiu (1997) and Ridley (1993), that despite small exposures, these late granites may be voluminous at depth, as observed in more deeply eroded terranes of the Yilgarn Craton (e.g. Southern Cross and Murchison Terranes). Kent et al. (1996) related gold mineralization at 2640-2620 Ma and this late felsic magmatism to a period of lower-middle crustal reworking between 2650-2630 Ma, involving anatexis and granulite to amphibolite facies metamorphism (see also Ridley 1993).

This work changes the character of the third tectono-thermal event proposed by Smithies and Champion (1999). Rather than being characterized by extension and possibly driven by lithospheric delamination (Smithies and Champion 1999), this event is characterized by a shortening cycle ($D_2 - D_4$) defining what we term the late Archean Kalgoorlie Orogen. Gold mineralization may have taken place above contemporaneous and voluminous magma intrusion at depth. The requirement of higher temperatures to produce A-type magmas (ca. 850-950 °C; Clemens et al. 1986) indicates that temperatures underneath the Norseman-Wiluna Belt may have risen after the end of the earlier and voluminous I-type magmatic event (Smithies and Champion 1999). This could be a result of crustal thickening during D_2 thrusting and folding combined with the previous extraction of I-type melts, leaving a restitic lower crust (Clemens et al. 1986).

Conclusions

The new time constraints provided by the work of Krapez et al. (2000) and the scrutiny of implicit and explicit assumptions underlying earlier interpretations, have provided the basis for reinterpreting the timing of structural events in the Norseman-Wiluna Belt and for producing a self-consistent time chart. The main results presented here are:

- a) The onset of voluminous plutonism at ca. 2685 Ma, marks the onset of D_1 shortening after a period dominated by extension associated with volcanism (D_{1e}). This change accounts for the contemporaneous unconformity between the Spargoville and the early stage of Kalgoorlie Sequences (Krapez et al. 2000).
- b) D_{2e} is an extension event cotemporaneous to subsidence and deposition of the late stage of the Kalgoorlie Sequence and the Kurrawang Sequence.
- c) Doming of low-density granite masses may have occurred during D_{1e} (the Raeside Batholith; Williams and Whitaker 1993, Passchier 1994) or D_{2e} (the Eastern Gneiss Complex). Doming may also have occurred during shortening phases driven by granite buoyancy and leading to antiform growth.
- d) Pre-existing buoyant masses of rigid granite bodies trigger the nucleation and growth of antiforms.
- e) D_2 is younger than previously thought (≤ 2655 Ma) and shear zones, normally ascribed to D_3 , may have been contemporaneous with and outlasted D_2 (vorticity partitioning). The D_2 - D_4 deformation cycle took place between ca. 2650 - 2630 Ma after, and not during earlier, voluminous granite intrusion.
- g) Intrusion of low-Ca and alkaline granites, D_2 - D_4 crustal shortening cycle, and gold mineralization, define the third tectono-thermal event between 2650-2630 Ma. Shortening proposed here contrasts with the previous suggestion that this event was related with extension and possibly lithospheric delamination (Smithies and Champion 1999). Magmatism during this phase could be result of crustal thickening during D_2 leading to renewed melting.

The new time chart proposed here is consistent with the timing of sedimentation, as well as structural and magmatic events.

2.4. Boulder-Lefroy Shear Zone: Kinematic History and Gold Mineralization

Summary

Large gold mineralizations are concentrated along the immediate surroundings of the Boulder-Lefroy Shear Zone. Whereas a number of published and unpublished work detail parts of this shear zone, there is no recent published work systematically covering the structural information and controls on gold mineralization along its length. This section brings together literature descriptions and structural data from its different mining districts, in order to determine the structural evolution of the shear zone and its relation to gold mineralization.

Introduction

The NNW-trending BLSZ is a major shear zone, over 200 km in length, located within the greenstone sequence of the Kalgoorlie Terrane (Fig. 2.4.1), in the southern part of the 600-km long Norseman-Wiluna belt, one of four provinces of the Yilgarn (Gee 1979). This belt is characterized by abundant tholeiites and komatiites, overlain by felsic volcanic and sedimentary rocks, and intruded by granitic rocks, and the broad stratigraphy is constant across the terrane, and its main rock packages, as well as their different names are summarized in Table 2.4.1. The shear zone can be traced from Paddington, north of Kalgoorlie, to south of Kambalda (e.g. Gemuts and Theron 1975; Griffin 1990). Whereas its main trend is parallel to the main regional fabric, its main trace is relatively poorly defined because it is split into a number of strands and splays (e.g. Griffin 1990, and maps in Keats 1987). Many authors separate the Boulder, to the north, from the Lefroy Shear Zone to the south.

A wide range of movement senses have been reported in the literature, suggesting either a complex evolution or incomplete information. Swager (1989) interpreted the BLSZ as a major sinistral wrench structure. This is clear from both the apparent 12 km movement recorded by displacement of the Triumph-Mount Goddard gabbro near New Celebration (Langsford 1989), and N-trending en-echelon folds around the shear zone, and the sigmoidal, en-echelon distribution of N-trending dextral shear zones in the Kalgoorlie District. An important reverse sense of shear (discussed in detail below) has also been interpreted from seismic lines (Goleby et al. 2000) and confirmed by field observation (Copeland 1998; Boulter et al. 1987, Ridley and Mengler 2000). Other authors recognized oblique-sinistral movement (e.g. Swager 1989, 1991,

Swager et al. 1990 a, b, Witt 1990; see p. 1627 in Nguyen et al. 1998), as well as dextral (Mueller et al. 1988).

The shear zone and its immediate surroundings host four major gold districts with more than 100 t of total gold each. From north to south these are: Paddington, Kalgoorlie, New Celebration and Kambalda Districts. North of Paddington, the BLSZ merges with the Boorara Shear Zone, to form the Bardoc Tectonic Zone, where gold endowment of major districts are generally one order of magnitude less endowed than those along the BLSZ.

A major difficulty for research along the BLSZ is the very poor regional exposure, and consequent bias of geological descriptions towards open pits and underground mines. Because of the temporary nature of mines, many of the exposures described in the literature are commonly no longer available so that it is not always possible to confirm or expand on earlier studies.

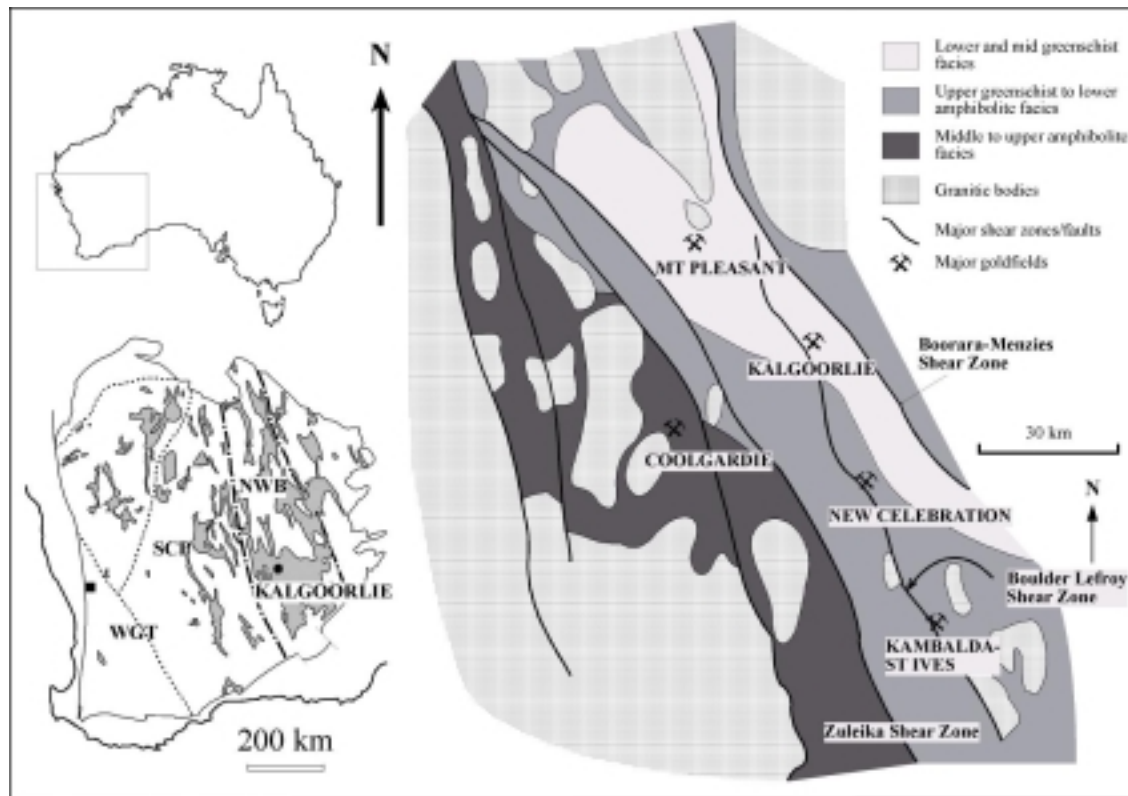


Fig. 2.4.1. Schematic map of the Kalgoorlie Terrane, depicting the main granite bodies, the greenstone belt where the grey tones indicate recorded metamorphic facies, the major shear zones and the main gold camps. Three important gold camps lie in the immediate vicinity of the Boulder-Lefroy Shear Zone. Inserts show the Yilgarn Craton where the Norseman-Wiluna Belt (NWB), which includes the Kalgoorlie Terrane, is a NNW-ESE trending belt bounded by the two thick dashed lines (redrawn from Phillips et al. 1996).

Table 2.4.1. Stratigraphy of the mining districts along the Boulder-Lefroy Shear Zone

Kalgoorlie (Swager 1989)	New Celebration (Langsford 1989)	Kambalda-Saint Ives (Watchorn 1998)
<p>Black Flag Group, felsic volcanic and sedimentary succession >1 km thick. Upward coarsening 2676±4 Ma</p> <p>Golden Mile Dolerites, differentiated into 10 units. Competent granophyric unit 8, with abundant plagioclase and quartz, hosts gold</p> <p>Kalgoorlie Group</p> <p>Paringa Basalt, 1000-1500 m, siliceous, high Mg basalt, variolitic and pillowed and numerous chert interflows, 2690±5 Ma</p> <p>Williamstown Dolerite, up to 300 m, in situ fractionation at the base of the Paringa Basalt</p> <p>Kapai Slate, persistent 5-25 m marker horizon varying from pyritic graphitic slate to magnetite-bearing laminated chert. 2692±4 Ma</p> <p>Devon Consols Basalt, 60-100 m, high-Mg variolitic basalt. 2693±30 Ma</p> <p>Hannan's Lake Serpentinite, 800-1200m, serpentinised ultramafic lavas, spinifex and cumulate textures. Nickel orebodies at lower contact. Grade upwards to high-Mg basalts 2709±4 Ma</p>	<p>Black Flag Group</p> <p>Triumph Gabbro, ~600m</p> <p>Kyarra Basalt</p> <p>Pernatty Dolerite, 300-500 m, basal cumulate pyroxenite</p> <p>Kapai Slate</p> <p>Mutooroo Basalt, 100-200 m</p> <p>Kambalda Komatiite</p>	<p>Black Flag Group</p> <p>Condenser and Junction Dolerites</p> <p>Paringa Basalt</p> <p>Defiance Dolerite</p> <p>Kapai Slate</p> <p>Devon Consols Basalt</p> <p>Kambalda Komatiite (also known as Tripod Hill Fm.)</p> <p>Lunnon Basalt, >2000m, thin flows of uncontaminated pillowed tholeiites, thin interflow sediments, 2720 Ma</p>

This section starts with a study of the pattern of gold distribution along the immediate surrounding of the shear zone. It then describes the structural evolution of the three major mining districts along the BLSZ: a) the Kalgoorlie District, in the north; b) the New Celebration District in the center; and c) the Kambalda-Saint Ives District in the south. For each of these districts, the literature is reviewed first followed by our own observations and interpretations. The literature review carried out here is in no way complete, and a large number of company reports include detailed work which we either did not have access to, or if we did, must remain confidential.

Gold Distribution

The distribution of gold along the BLSZ from Paddington to the north to SIG to the south is highly heterogeneous. Gold peaks corresponding to mining districts are followed by regions of very low gold endowment (Fig. 2.4.2). The regular spacing of the districts, and their systematic relation to gold-poor zones along shear zone strike suggest a systematic control on mineralization of some crustal scale process such as convection.

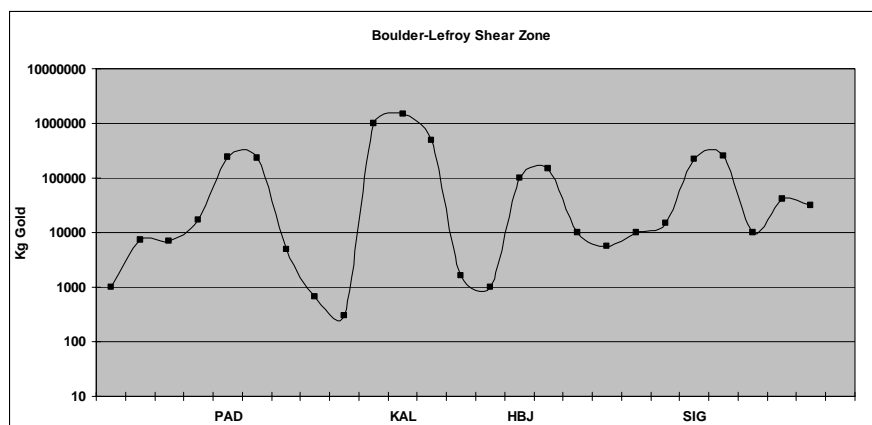


Fig. 2.4.2. Gold endowment (log-scale) along the BLSZ plotted from Paddington in the north to SIG in the south. Endowment includes all gold produced and reserves in a buffer zone of 5 km on either side of the shear zone. Gold peaks occur at regular intervals of approximately 35 ± 5 km. Each peak is followed by very significant gold troughs. The Golden Mile forms the highest peak is followed both to the north and south by the lowest troughs along the length of the shear zone.

We start our descriptions by the New Celebration District located in the central part of the shear zone because it is the most illustrative of our findings. We will then go on to describe the structural development of the Kalgoorlie District to the north and the Kambalda District to the south.

New Celebration District

This area, also known as Hampton-Boulder-White Hope District, was described by Griffin (1990) and by detailed studies carried out by mining companies (e.g. Langsford 1989) (Fig. 2.4.3). The greenstone sequence in the district is interpreted as having the same stratigraphy as the Kambalda sequence to the south and the Kalgoorlie sequence to the north (Table 2.4.1; Griffin 1990). The size and geometry of the main geological structure at New Celebration and Kalgoorlie Districts are strikingly similar. Similarly large folds, the Celebration and the Boomerang Anticlines, characterize both districts respectively, comprised essentially of similar rock types, including similar areas of differentiated intrusive dolerites. Furthermore, in both areas the BLSZ truncates the folds (compare Figs. 2.4.3 and 2.4.12).

Despite similarities, gold endowment and mineralization siting differ considerably between the two districts. Gold endowment at New Celebration, at more than 100 t is one order of magnitude less than the 1800 t total gold in the Kalgoorlie District. By contrast to other districts, the deposits at New Celebration (Hampton-Boulder, Jubilee, Celebration, Triumph, Pernatty), tend to occur within or immediately adjacent to the BLSZ (Copeland and al. 1998; Norris 1990). The largest deposit in the district, and the main focus of this section, is the Hampton-Boulder-Jubilee, sited at the margins of a thick porphyry emplaced within the shear zone (e.g. Griffin 1990).

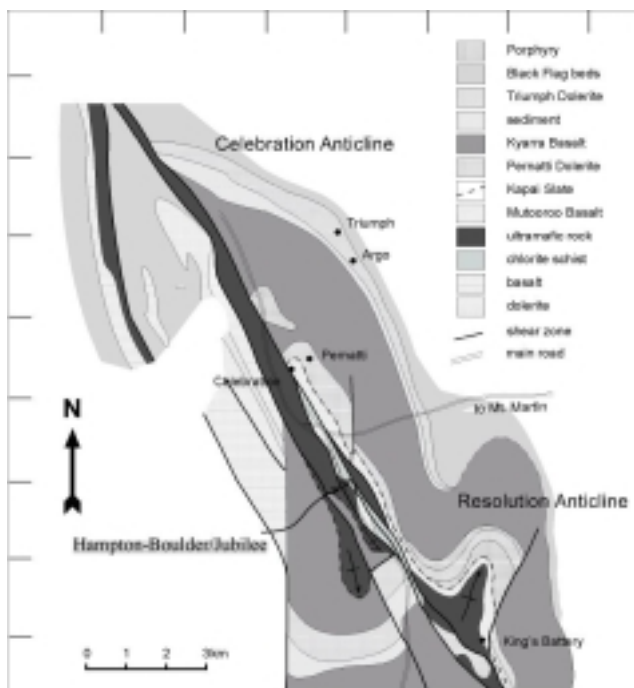


Fig. 2.4.3. Geological map of the New Celebration District. The Hampton-Boulder/Jubilee mines and the area around King's Battery are discussed in the text. The Celebration and Resolution Anticlines are depicted. Maximum displacement on this part of the BLSZ has been determined by the apparent displacement of the Triumph gabbro (south part of the map). Redrawn from Swager (1989).

Previous Studies. Hampton-Boulder and Jubilee form a contiguous open pit and are part of the same ore body and together have produced 45 t of Au and have 78 t remaining (above 0.5 g/t; S. Devlin 2001, pers. commun.). The main feature of these deposits is that they lie along the regional trace of the BLSZ (Norris 1990; Williams 1994; Copeland and al. 1998; Dielemans 2000), at the contact between schistose country rocks and a boudinaged granitic dyke (Fig. 2.4.4).

Mylonitic rocks exposed in the open-pits illustrate the kinematic development of the BLSZ. Intense shearing is up to 100 m wide, dipping steeply west, consisting of chlorite schists enclosing boudins and lenses of felsic granite dykes (Norris 1987). Mineralization is controlled by a boudinaged quartz-feldspar porphyry granite, more than 1 km long and up to 80 m wide, which dips steeply west and separates a mafic hanging wall from an ultramafic footwall (see Copeland 1998 for detailed description of the stratigraphy at Jubilee). Major mineralization is related to stockworks of quartz-carbonate-pyrite veinlets along both contacts of the fractured porphyry, producing a series of tabular, steeply west-dipping ore zones. Ultramafic schists and porphyry intrusions occupy the central part of the mineralization and contain the main trend of the BLSZ (Griffin 1990).

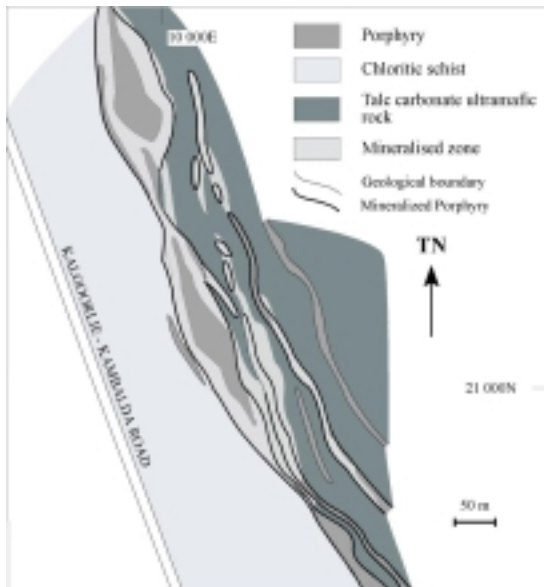


Fig. 2.4.4. The boudinaged, wide porphyry hosting the mineralization at Hampton-Boulder/Jubilee, as well as other mineralized porphyries in the area. Redrawn from Norris (1990).

Structural descriptions of these two pits have been carried out by a number of authors. Mueller et al. (1988) described the structures at Hampton-Boulder where pods of schist preserve

kinematic indicators showing sinistral sense, wrapped by an anastomosing shear fabric containing dextral sense kinematic indicators and mineral lineation plunging 20 SSE. This dextral sense was not further confirmed in our study. Detailed description of the structures in the underground workings at the *Southern Ore Zone (SOZ)* at Hampton-Boulder was carried out by Williams (1994) and Dielemans (2000). To the south, at Jubilee, a general structural description is given in Copeland (1998).

The most detailed structural study of the Hampton-Boulder focused on the Southern Ore Zone, SOZ (Dielemans 2000), a very rich ore zone at the southern end of Hampton-Boulder studied in detail by Dielemans (2000). He described a penetrative mylonitic foliation, which transposed original rock contacts and strikes on average N40W/ 82W. He noticed a gradual change in foliation orientation from northwesterly at SOZ (and Jubilee to the south), to nearly northerly in the northern end of the Hampton-Boulder pit, accompanied by a gradual rotation in orientation of the main porphyry boudins. This penetrative foliation is overprinted by what Dielemans (2000) described as anastomosing shear planes, with glistening surfaces, spaced >10 cm, and striking between N40W and N-S and dipping 70-90W.

A wide number of lineation types were determined by Dielemans (2000). These may be divided into three main groups: a) boudin axes commonly plunging gently south; b) a gently to moderately SE-plunging mineral and stretching lineation; and c) a steeply NW-plunging lineation (crenulation, mineral and stretching lineations).

The lack of kinematic indicators, suggested to Dielemans (2000) that straining must have been intense and destroyed all asymmetries. In the absence of indicators, he assumes that sinistral movement dominated (observed elsewhere, e.g. Langsford 1989) and interpreted the SE-plunging lineation (b) as the movement direction, and the almost perpendicular, steep NW-plunging crenulation lineation to represent the intermediate stress axis. He argued correctly that variations in lineation plunge are due to strain heterogeneities resulting from local anisotropies. A key finding in Dielemans (2000) was that of carbonate fibres growing perpendicular to pyrite grain margins in the ore, and parallel to the SE-plunging lineation (b), indicating that pyrite deposition, and possibly gold, took place either during of before the development of that lineation.

At Jubilee, like Hampton-Boulder, mineralization is centered upon a series of semi-concordant felsic porphyry dikes within the BLSZ dipping at around 85W (Copeland 1998). Gold grade in felsic porphyries is generally less than intermediate porphyries, where the highest grades are found. Dolerites are also mineralized. The main orebody at Jubilee has a strike length

of 800 m and an average width of approximately 40 m (Copeland 1998). Mineralization is controlled by anastomosing shear zones, which define the BLSZ, and is best developed where shear zones coalesce. Gold occurs as 2-20 μm grains in pyrite in quartz-carbonate veins. Copeland (1998) concludes that gold mineralization appears to be late in the metamorphic-structural sequence and is associated with retrogression assemblages and largely potassium-sulphur alteration.

With regards to the BLSZ, Copeland (1998) concludes that in Jubilee, it is a system of anastomosing shear zones with a strong vertical extension component as indicated by down-dip lineation, flat-lying quartz-veins and subhorizontal boudin axis. These shear zones have transected the hinge of a large-scale anticline (as determined from opposite younging orientations on either side of the shear zone). Strike slip shearing is late and associated with minor movement, and the NNE-trending Pisces shear zone, transect the main foliation trend and roughly separates Jubilee from Hampton-Boulder orebodies. Copeland (1998) concludes further that the structures are inconsistent with the interpretation that the BLSZ is a major wrench system and suggests that the structures represent either a reoriented thrust, which has been subsequently steepened, or it is a ramp interconnecting low-level thrusts.

Structural Study. The continuous Hampton-Boulder/Jubilee open pit is presently closed and most parts are inaccessible due to wall slides. Observations described here are limited to the northern and eastern walls of the Hampton-Boulder pit, and to the southern wall of the Jubilee pit. Structural information on the underground Southern Ore Zone (SOZ) of the Hampton-Boulder deposit (Williams 1994; Dielemans 2000) is reinterpreted here.

The northern wall of Hampton-Boulder is a zone of intense shearing with penetrative and steep mylonitic foliation (Fig. 2.4.5a) and approximately down dip mineral and stretching lineation, exposed over more than 50m across strike (Fig. 2.4.6a). Folding and thrusting structures (Fig. 2.4.7) associated with the observed lineation indicate horizontal shortening and vertical extension.

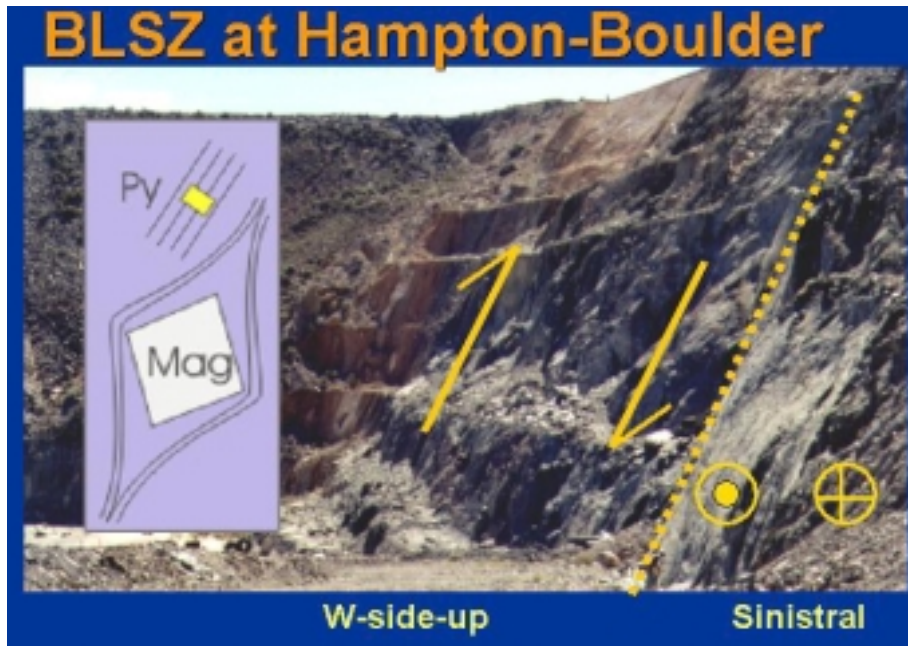


Fig. 2.4.5. a) The northern wall of Hampton-Boulder open pit. On the left-hand-side, intense foliation with roughly down dip lineation and a dominant west-side-up sense of shear. On the right-hand-side, a 3-meter wide sinistral shear zone crops out. Person for scale, on the footwall of the thrust. b) Foliation planes and stretching lineation and striae on sinistral shear zones on the eastern wall of Hampton-Boulder.

Lineations plunge SSE (see also Dielemans 2000). Sense of shear indicators suggest a sinistral movement with a W-side down component. Elongated “pebbles” of granite, up to 10 cm long, oriented parallel to the lineation are shear-disrupted granitic dykes.

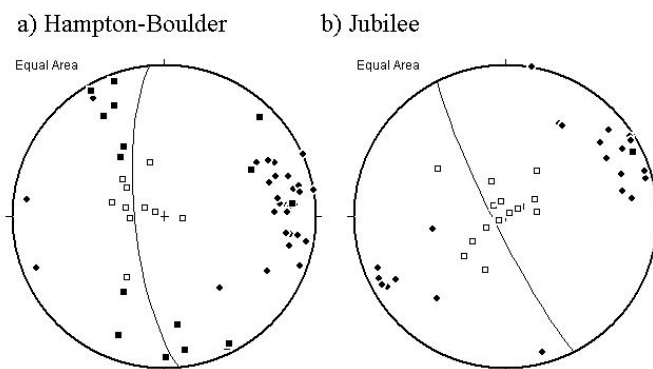


Fig. 2.4.6. Lower hemisphere equal area stereonet projection. a) Mineral and stretching lineation on reverse shear zones (open squares), sinistral strike slip shear zones (black squares) and poles to foliation (black lozenges) from Hampton-Boulder. Great circle indicates the best-fit foliation plane, and strikes N05 W/80 W. b) Same for Jubilee. Notice the absence of strike slip shearing. Average foliation strikes N25 W/75 W.

Notice the absence of strike slip shearing. Average foliation strikes N25 W/75 W.



Fig. 2.4.7. Tightly folded competent granitic body in chlorite schist, associated with a reverse fault indicated by the arrows (note a granite block above the main folded mass of granite). Deformation is indicative of vertical extension (crustal thickening).

On the eastern wall, two sinistral strike-slip shear zones were found (Fig. 2.4.5b). They are parallel to the main NNW-trend of the area and are 2-3 m wide zones of intensely sheared chlorite-talc schist, with gently south plunging mineral and stretching lineation and cut across less sheared rocks with down dip lineation. The oblique sinistral sense of shear is deduced from *S-C* fabric, clearly visible by the asymmetry of weathered fish-shaped blocks, as well as under hand-lenses and in oriented thin sections. Outside the zones of intense shearing, these younger shear zones give rise to anastomosing foliation around less deformed pods, which preserve older down dip lineation. The anastomosing planes glisten due to oriented phyllosilicates (mostly chlorite, but also talc and biotite). Dextral sense of shear was only found along two small shear zones oriented NNE. These planes rotated to become parallel to the NNW-trend sinistral shear planes. Their orientation, physical links with the sinistral shear zones, and their general similarity suggest that they are conjugates to the dominantly sinistral movement.

The southern wall at Jubilee exposes bands of intense shearing, characterized by mylonitic rocks, intercalated with less deformed bands. Mylonites are easily picked out by intensely thinned and disrupted foliation-parallel quartz and carbonate veins, in contrast to more continuous, wider and crosscutting veins on less sheared rocks (Figs. 2.4.8a, b). The general trend of the foliation at Jubilee, like at SOZ, is rotated towards the NW as compared to Hampton Boulder (Fig. 2.4.6). As in Hampton-Boulder, deformation is characterized by a prominent and approximately down dip lineation (Fig. 2.4.6b), and a strong vertical extension (horizontal

shortening) deduced from both west-side up and west-side down sense of shear (depicted by *S-C* fabric, tails around clasts, as well as thrust (Fig. 2.4.8c) and boudins with gently plunging axis.

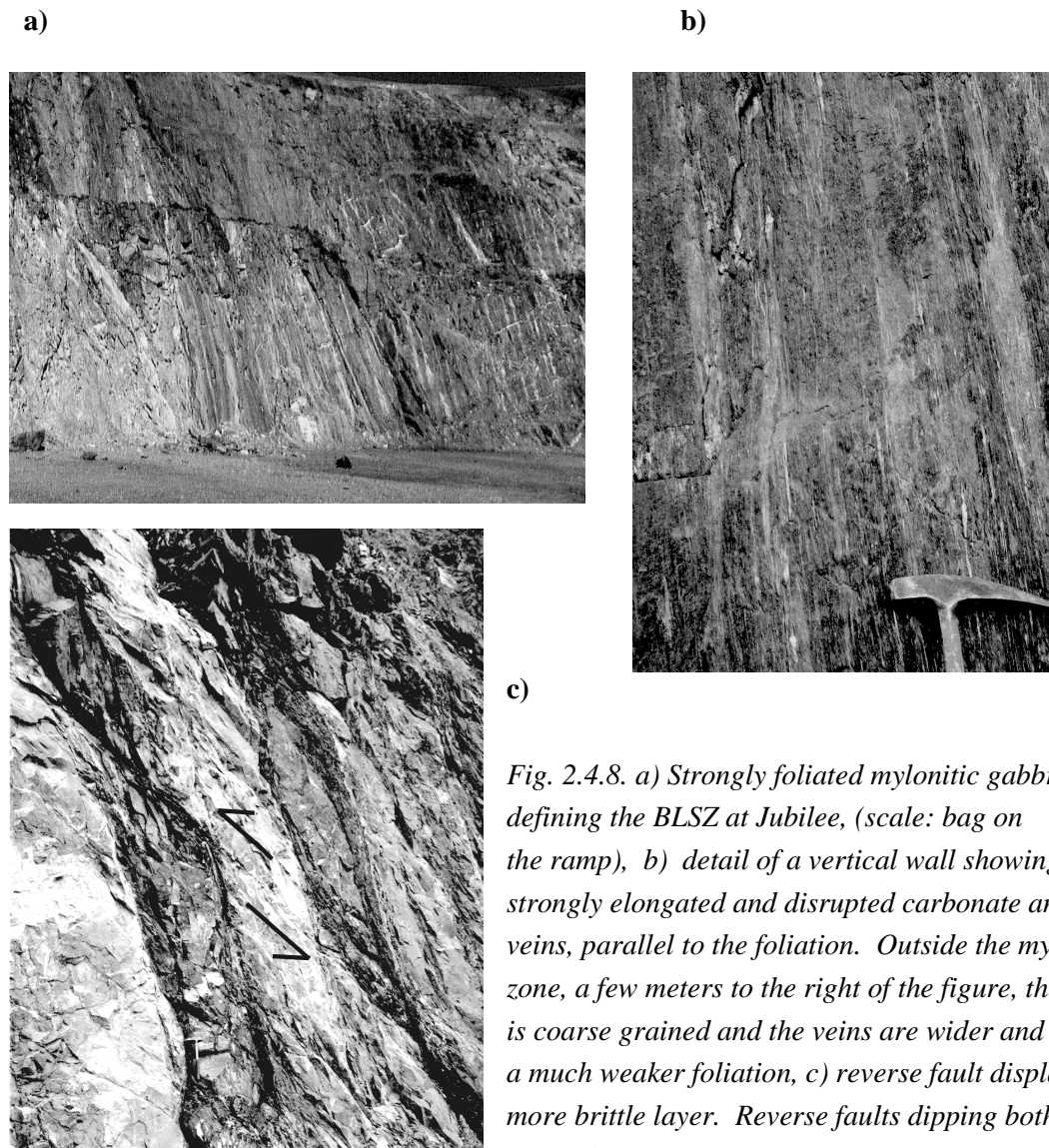


Fig. 2.4.8. a) Strongly foliated mylonitic gabbro defining the BLSZ at Jubilee, (scale: bag on the ramp), b) detail of a vertical wall showing strongly elongated and disrupted carbonate and quartz veins, parallel to the foliation. Outside the mylonitic zone, a few meters to the right of the figure, the gabbro is coarse grained and the veins are wider and cross cut a much weaker foliation, c) reverse fault displacing a more brittle layer. Reverse faults dipping both to the NE and SW are common.

These sheared rocks are exposed for approximately 100 m across strike, and in contrast to Hampton Boulder, there is no evidence for strike-slip reactivation. In summary, our observations here basically confirm Copeland's (1998) conclusions.

Timing of Mineralization. Thin sections were used to determine the relationship between opaque minerals and shear foliation. In the northern wall of Hampton-Boulder, ultramafic rocks displaying a steep lineation contain grains of chromite rimmed by magnetite and grains of pyrite.

Whereas magnetite/chromite commonly deflect the S2 foliation and are elongated along the foliation, indicative of its presence during shearing, smaller euhedral pyrite grains do not deflect the fabric (Fig. 2.4.9a), suggesting it was deposited after the S2 foliation (post- D_2). Figure 2.4.9b shows also that gold is related to these pyrites and is equally late. A thin section of a mineralized porphyry sample from Jubilee, also sheared during D_2 , with a strongly recrystallized fine matrix, has a train of undeformed sulphides, seemingly developed along a later brittle fracture.

Similar relationships could not be determined in thin sections cut from rocks sheared by the D_3 sinistral shear zone at Hampton-Boulder. Thus, we were unable to further detail the timing of mineralization in relation to D_3 . However, Dielemans (2000), as described above, found moderately S-plunging fibre growth on the walls of pyrite suggests a syn- D_3 pyritization.

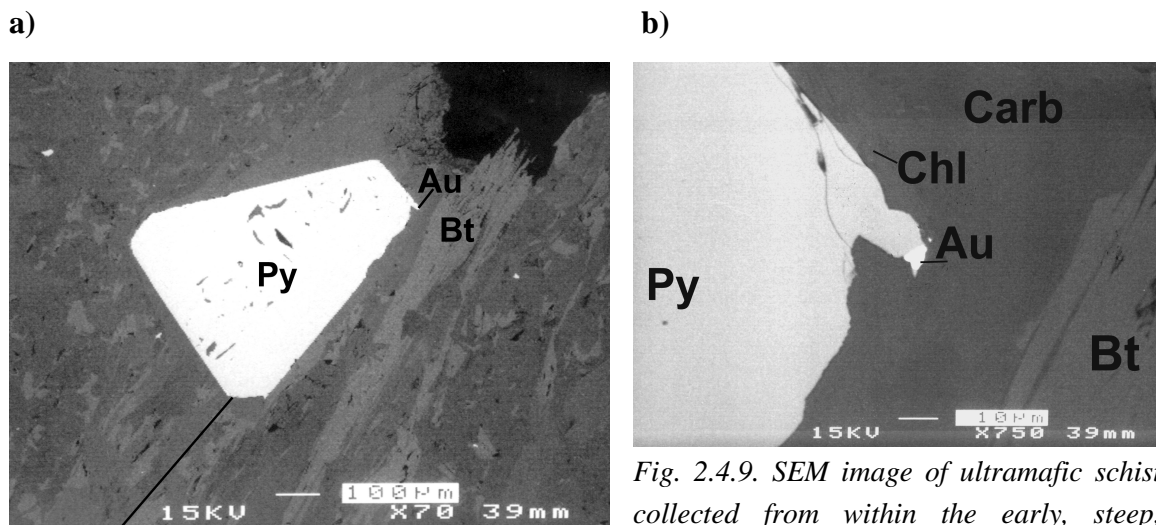


Fig. 2.4.9. SEM image of ultramafic schist collected from within the early, steep, reverse D_2 shear zone, at the western end of the N face at Hampton-Boulder. The thin section was cut perpendicular to foliation (N15W/80W), and parallel to lineation (S/70). a) Coarse euhedral pyrite grain in a zone of talc-chlorite-carbonate-biotite alteration. The foliation (marked by a thin black line and by the orientation of the large biotite on the right-hand-side and other smaller grains) is unaffected by the pyrite grain, suggesting that the pyrite grain grew over a pre-existing fabric. This is typical of all pyrites observed in this rock. By contrast, grains of chromite rimmed by magnetite in the same rock actively interferes with the same foliation. The pyrite grain has a protrusion on it, on the upper-right-hand-side detailed in (b). (b) detail of (a) showing a bleb of gold in contact with the pyrite. Pyrite and gold were therefore deposited after development of S2 and mineralization is post- D_2 .

Interpretation. The BLSZ as exposed in these pits is characterized by an early phase of deformation which gave rise to a zone of intense but variable deformation over 100 m wide, characterized by down dip lineation, horizontal ENE-WSW shortening and vertical extension

(See also Copeland 1998). This was reactivated and overprinted by sinistral strike-slip movement on NNW-trending planes exposed along the eastern wall of the Hampton Boulder pit. The maximum shortening strain axis during this phase would have been rotated clockwise to trend WNW-ESE. The early structures described are likely related to D_2 , while the later sinistral strike slip, to the regional D_3 event.

The difficulty in defining a dominant sense of shear associated with down dip lineation on the mylonitic rocks of the BLSZ in both Hampton-Boulder and Jubilee, suggests either intense flattening and steepening of early formed reverse shear zones, or the simultaneous conjugate pairs gradually flattened to become nearly parallel. Rotation of the main foliation at Hampton-Boulder from northerly at the north to northwesterly at SOZ and Jubilee, is associated with and probably a result of a change in orientation of the main porphyry.

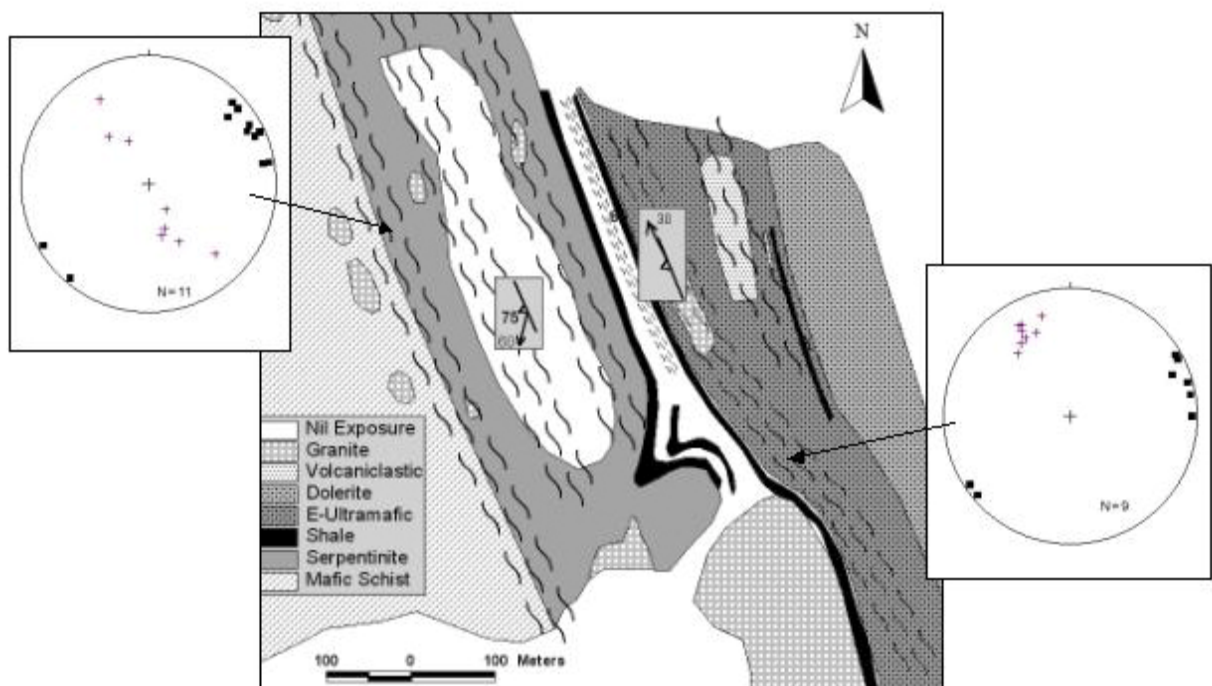
SOZ Reinterpretation. On the basis of our findings, we reinterpret the structures described by Dielemans (2000) at the SOZ. His early penetrative foliation corresponds to the dominant mylonitic foliation in Hampton-Boulder and Jubilee, where it is associated with steep lineation. His anastomosing shear planes correspond to the very similar anastomosing sinistral planes documented by us on the sinistral shear zones of the eastern wall of Hampton-Boulder. If this is correct, the SOZ also records D_2 structures overprinted by D_3 sinistral shearing. The moderately SE-plunging mineral lineation (b) at SOZ and the steep NW-plunging mineral and stretching lineation (c) correspond to the lineations we documented on the sinistral and reverse shear zones, respectively. Thus, rather than representing a single sinistral shearing, as assumed by Dielemans (2000), the different foliations and lineations are a result of D_2 and D_3 .

General Remarks. Main deformation kinematics suggests a swap from a D_2 crustal thickening event, to a D_3 sinistral shearing. The relatively narrow widths of strike slip shear zones suggest a modest amount of sinistral movement, in accordance with regional estimates of no more than 12 km displacement. Kinematic indicators do not confirm early reports of dextral sense of shear along the BLSZ in this District (e.g. Mueller et al. 1988). It is possible however, that such shear zones are exposed elsewhere within the pit, but more likely, they represent relatively minor shear zones (e.g. Copeland 1998). The Pisces Shear Zone, because of its north trend, oblique to the general foliation, may well have accommodated important dextral translations, but was not studied here due to accessibility.

The width, length and intensity of D_2 structures suggest that this was an important deformation phase in the early stages of the BLSZ in this District. Our study of the relationship between pyrite and gold and foliation indicates that mineralization is post- D_2 , in accordance with the finding of fibrous tails around pyrites by Dielemans (2000) suggesting a syn- D_3 timing for the pyrite and possibly gold.

King's Battery. The most complete exposure of the Boulder-Lefroy Shear Zone, away from mineralization, is located on the Western margin of Lake Lefroy, at the historical site of King's Battery (AMG 370333E/6560923N), 6 km SSE of Hampton-Boulder/Jubilee. Fig. 2.4.10 summarizes the geology of the area which is mainly comprised of a NNW-trending supracrustal sequence. Sheared basic rocks crop out on the west side, followed eastwards by ultramafic rocks, and a 3-5 m thick black, chertified slate, known as the Kapai Slate, and then by a zone dominated by 2-3 m thick quartz veins, cropping out as protruding ridges, and porphyries (granitic dykes). These are intruded into ultramafic rocks which weathers to a distinctive pale green colour, and a pyroxenitic layer, in which the pyroxene is now pseudomorphosed by amphibole. The mafic and ultramafic rocks crop out locally in between the protruding ridges of quartz and porphyries. This region is approximately 50 m wide and is followed by a sheared gabbro, a narrow band of shales and quartz-feldspathic rock, followed by a massive gabbro.

Fig. 2.4.10. Geological map of King's Battery indicating the Eastern and Western Shear Zones and their contact in the vicinity of the Kapai Slate. Together these two shear zones comprise the Boulder-Lefroy Shear Zone.



We interpret the sequence east of the Kapaï Slate to represent differentiated mafic sill (ultramafic cumulate at the base followed by pyroxenite and gabbro) intruded by quartz veins and granite dykes close to its contact with the Kapaï Slate. The sequence within the sill indicates east side up. Similar differentiated mafic sills, elsewhere in the region, have been emplaced between the Kapaï Slate and the Paringa Basalt, such as the Williamstown dolerite. The Kapaï Slate sits stratigraphically above the Devon Consols Basalt, indicating that in this instance the ultramafic-Kapaï Slate contact is of a structural nature.

This sequence hosts other small granitic intrusions. One ~20m in length characterized by abundant angular fragments of mafic rocks, of massive appearance and only narrow sheared margins, along which fine pyrite grains are observed. Several small shafts have been sunk on these intrusive rocks and there is considerable evidence for recent exploration efforts focused on the quartz veins. Small porphyritic granites intruded the ultramafic rocks on the western side, and were later sheared and boudinaged. Narrow zones of alteration developed in the ultramafic rocks at the granite contacts, with random growth of amphibole needles and biotite.

Structurally this area is characterized by two shear zones distinguished by different orientation of stretching lineations and sense of shear, and are recorded by different rock types. The western shear zone is characterized by intensely sheared ultramafic rocks (talc+carbonate±chlorite schist) which have narrow, discontinuous pods (5m) of relict spinifex texture preserved within anastomosing shear zones; and a sheared basic unit, which consists of amphibole-feldspar-carbonate schist (upper greenschist to lower amphibolite facies conditions).

The zone of shearing is at least 100m wide, since its western extent is unconstrained due to lack of outcrops. The general attitude of the shear zone is N40°W/70°W for a strike length of ~400m, although considerable internal heterogeneity exists, some of which is described later. Stretching lineation in the talc-carbonate-chlorite schist is defined by elongate carbonate porphyroblasts, and plunges moderately to steeply southeast (typically 145/70), subparallel to a mineral lineation defined by aligned amphibole and plagioclase in the basic schist. Drag folds are observed in the fabric, with axes plunging gently NW (e.g. N35W/22). A well-developed *S-C* fabric, asymmetries around the carbonate porphyroclasts and the asymmetry and orientation of drag-folds, indicate west side down movement, with a minor sinistral component.

The eastern shear is approximately 200 m wide, strikes approximately N20-30W, more northerly than the western shear zone, and has a well-defined stretching lineation plunging gently to the north (Fig. 2.4.11). Lineation is defined by elongated pyrite agglomerates, strained

reduction spots, stretched clasts and striations which can be recognized throughout the eastern shear zone.

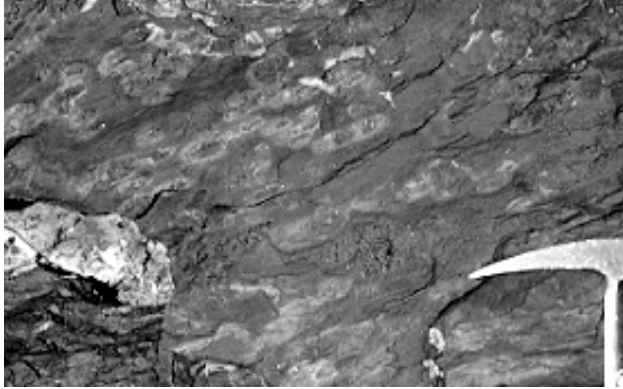


Fig. 2.4.11. Stretched reduction spots in sulphidic Kapai Slate at King's Battery, defining a gently N-plunging lineation parallel to that found over a width of approximately 200 m and defines a sinistral shear zone.

The contact between the two shear zones runs parallel to the contact between the Kapai Slate and the ultramafic rock and is delineated by a sulphidic shale, and a gentle north lineation extends a few meters into the ultramafic unit. The contact itself has not been observed. A well-developed S-C fabric is observed in the coarser grained units, and consistently indicates sinistral shear sense. This has been confirmed in thin-section, where chlorite is seen to wrap coarse tremolite grains with a consistent sinistral stepping. The eastern limit of this sinistral shear zone is defined by an outcrop of dolerite, where shearing is partitioned into narrow (20cm) zones within massive rock, grading eastwards into massive rock with no evidence of shearing.

Towards the southern limit of exposure, the shale beds are folded defining an axial plane trending towards N30°E. Folded laminae within the shale have axial planes that trend towards N35°E. The fold axes of these chevron folds plunge ~ N35°E /70°. There is however some doubts about whether these are tectonic folds or more simply slump folds.

All rocks are overprinted by a weak but pervasive foliation trending towards N10°E, and dips steeply W. Furthermore, a minor (~30cm wide) shear zone, trending N25°E, offsets previously formed shear fabric, which forms a drag fold indicative of dextral movement (no lineation was identified in this fault).

Even though we lack evidence regarding the relative timing of the two shear zones, the similarities to the structures documented at Hampton-Boulder/Jubilee mines suggests that similar events took place here. Thus, we interpret these deformation events in accordance with the better-constrained relative timing determined at the mines. Thus, the down dip movement at the western shear zone is interpreted to have developed as part of the regional D_2 , while sinistral

shearing developed later, during D_3 . The sinistral shear zone here is wider than that exposed at Hampton-Boulder, and its north-plunging lineation contrasts with the varied south and north gentle plunging lineations at the mine. Kings Battery is on the eastern limb of the large-scale Resolution Anticline, which has an axial trace, as interpreted from regional maps, trending N15E. We relate the overprinting, pervasive N10E-trending foliation to the development and tightening of that fold. Folds with such trend have been related to D_3 sinistral shearing, and axial planar foliation generally develops late during a folding event, in accordance with our observation that it overprints all earlier foliations. In summary, the BLSZ as exposed both at Hampton-Boulder/Jubilee mines and Kings Battery have similar structural events, which may be explained in a self-consistent way and in accordance to the regional deformation.

Kalgoorlie District

The Kalgoorlie District lies approximately 40 km NNW along strike from the New Celebration District. A number of workers have described the mineralization and structural evolution of the District (e.g. Phillips 1986; Boulter et al. 1987; Mueller et al. 1988; Swager 1989a; Clout et al. 1990; Ridley and Mengler 2000) with poor agreement on the sequence of events and assignment of deformation phases. Phillips (1986) and Phillips et al. (1996) documented the nature and geometry of the alteration surrounding the Golden Mile deposit. Keats (1987) summarized historical descriptions of the area, which have concentrated on two major deposits: the Fimiston lodes at Golden Mile, a sheared intensely mineralized zone system developed largely within Golden Mile Dolerite, and which produced over 90% of the total production of the Kalgoorlie District; and Mount Charlotte, a system of extensional quartz veins (Ridley and Mengler 2000). Safety reasons have not permitted us to do our own detailed study of this District, thus, we focus on the broad scale deformation and literature descriptions. We first described its general features and then focus on the relative timing of the protracted mineralization of the Golden Mile and Mount Charlotte mines.

The main structures in the area (Fig. 2.4.12) have been interpreted in a number of ways (Table 2). According to Bateman et al. (2001), the earliest recognizable event was thrusting along the Golden Mile Fault, localized within black shales above the Golden Mile dolerite, which they ascribed to a local D_1 (Fig. 2.4.13). The fault is virtually parallel to bedding, caused repetition of the greenstone stratigraphy due to east-over-west movement, and is cross-cut by D_2 shear zones (Mueller et al. 1988, Clout et al. 1990, Bateman et al. et al. 2001). The fault is

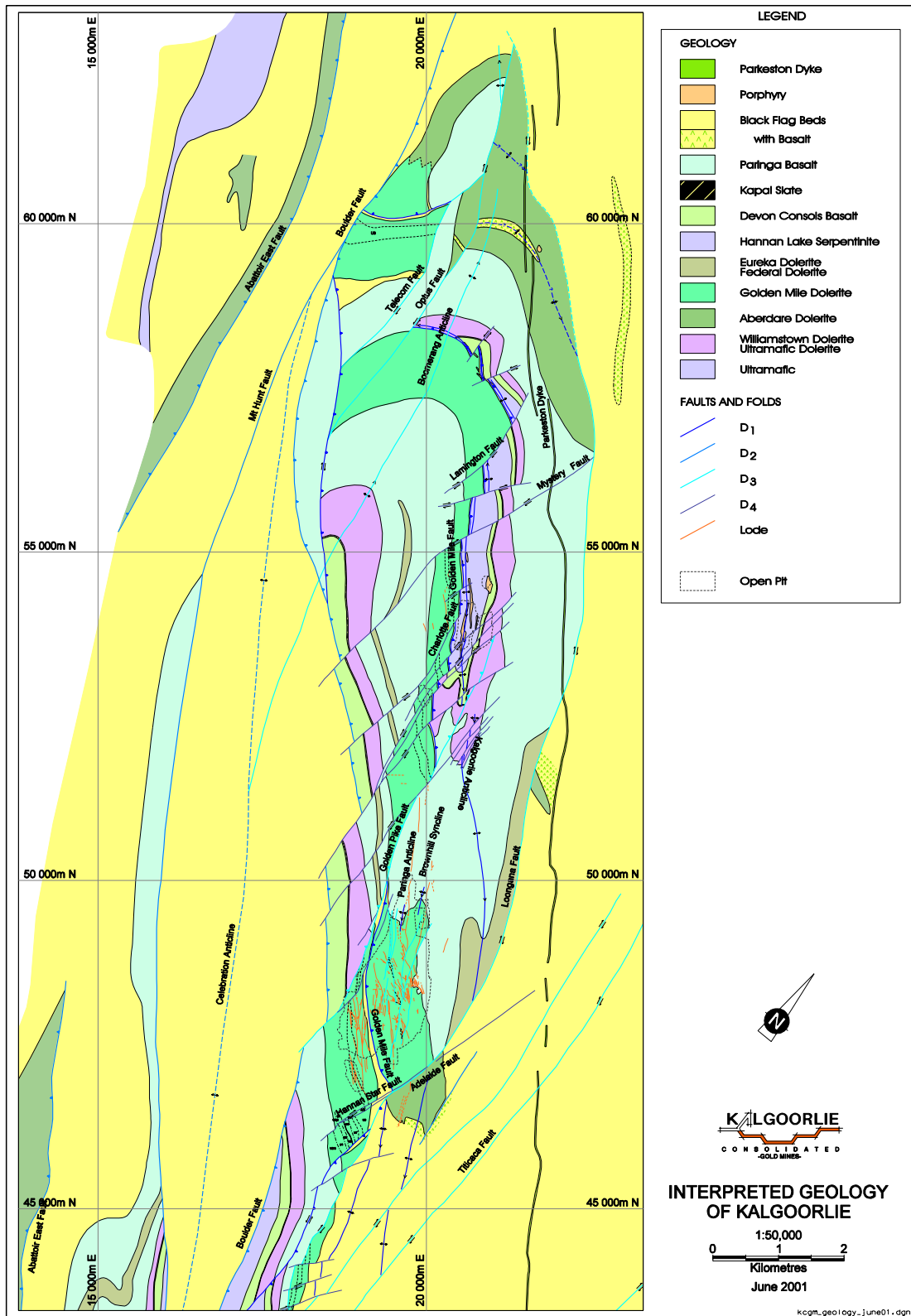


Fig. 2.4.12. Geology of the Kalgoorlie district. Map prepared by Bateman (2001, KCGM).

associated with a hanging wall anticline known as the Kalgoorlie Anticline, with no equivalent synclinal closure at depth (Swager 1989). These early structures are disrupted by D_2 reverse, some eastward thrusting as suggested by seismic sections and small-scale shear zones in Fimiston Western Lodes and elsewhere (e.g. Flanagan Fault, Clout et al. 1990; Mueller et al. 1988). There are also westward thrusting shear zones, such as the Boulder Fault (the northern extension of the BLSZ), which can be matched to a large east-dipping fault revealed by the seismic section (Bateman et al. 2001; Goleby et al. 2000). NNW-trending D_2 folds are associated with these thrusts. The lack of an obvious preferred thrusting direction is similar to our observations at the New Celebration District.

The large scale Boomerang Anticline has folded D_1 structures and has been ascribed to either D_2 or D_3 . Bateman et al. (2001) suggested the Boomerang Anticline is part of D_3 because it has steep ($>60^\circ$) and north-plunging hinge, in contrast to the shallow-plunging, NW-trending hinges of D_2 folds like the Celebration Anticline. In this scenario, the Boomerang Anticline would be an *en echelon* fold. While this may be so, an alternative is that the two folds formed during D_2 and that their different axes resulted from regional variations on the attitudes of lithological contacts caused by previous deformation (e.g. D_1 local). While we interpret this anticline to be part of D_2 , both alternatives remain possible as reflected in Table 2.4.2.

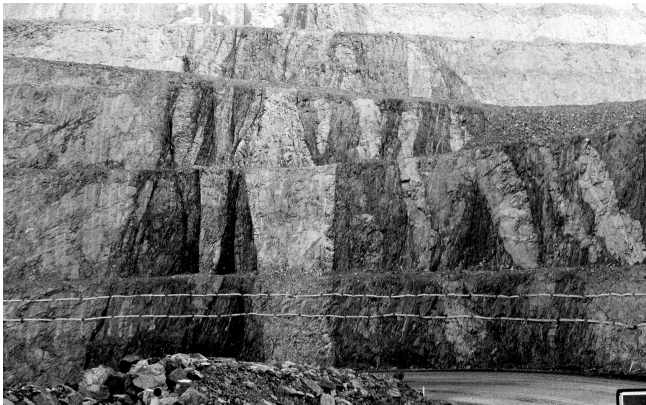


Fig. 2.4.13. The Golden Mile Fault, an early shear zone developed within carbonaceous shale (dark greys) and include numerous felsic lenses that could be either disrupted dykes or slices of volcanoclastic rocks, and which are entirely altered to quartz, ankerite and fuchsite (V-mica). Dolerite crops out on both sides of the shear zone. Scale lowest bench is estimated to be 20 m high.

The final hook-shaped refolded fold comprised by the Golden Mile fault and Kalgoorlie Anticline refolded by the Boomerang Anticline was later segmented by a set of ductile, D_3 dextral, sigmoidal shear zones, trending mainly N-S (e.g. Mueller et al. 1988). Their sigmoidal shape and en-echelon nature suggests they are related to a large-scale NNW-trending sinistral

wrenching, parallel to the regional fabric. These were later reactivated by brittle, dextral D_4 faults a few kilometres long with a few hundred metres of displacement (Ridley and Mengler 2000).

The regional D_1 event is clearly recorded south of Kalgoorlie, between Kambalda and Widgiemooltha, where it is characterized by north-directed thrusting and recumbent folds. Bateman et al.'s (2001) local D_1 can be interpreted either as a regional D_1 structures rotated into the D_2 fabric, or as structures formed early in the D_2 event and became steepened and abandoned as the event progressed, and younger active thrusts and folds developed. There is considerable discussion at present on the nature and thrust directions during D_1 and this will be further discussed below.

Eastward thrusting has also been interpreted from a seismic survey carried out by AGSO (line 99AGSY3 Goleby et al. 2000) which crosses the main structural elements of the region including the Boulder-Lefroy Shear Zone just south of the Golden Mile. The interpretation of the seismic line (Fig. 2.4.14; Goleby et al. 2000), indicates a general change in the trend of seismic reflections broadly coinciding with the position of the BLSZ. To the west of the BLSZ, the main regional shear zones dip west parallel to the main seismic reflections. To the east of the BLSZ, reflections dip east. The regional shear zones sole into a detachment plane at ~6 km depth. The AGCRC-KCGM 1997 seismic survey of the Kalgoorlie area (Bateman et al. 2000) detailed previous results, and defined large-scale thrust duplex dipping west and merging into a detachment surface at depth. This detachment is irregular and limits the width of the overlying greenstone sequence to 5-9 km. A shallow east-dipping structure has also been depicted seismically, which appears to offset the west-dipping thrusts, and may have accommodated east block up movement.

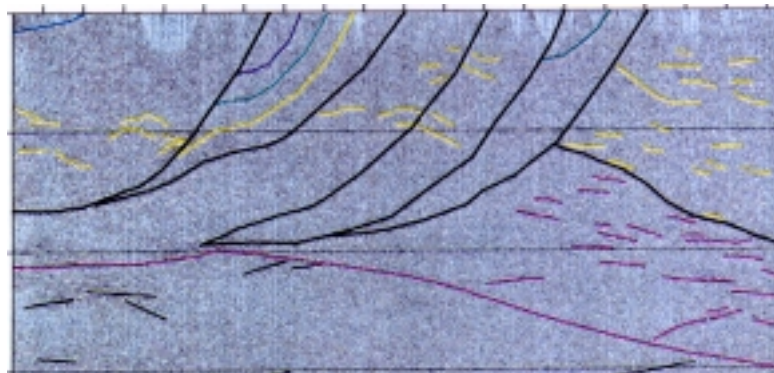


Fig. 2.4.14. Seismic line across the BLSZ, south of Kalgoorlie. From Goleby et al. (2000) Yilgarn Project Line 99AGSY3 (migrated data).

Golden Mile. The Golden Mile, the most endowed gold deposit in the Yilgarn Craton, is characterized by a protracted mineralization (Bateman et al. 2001). Most of the gold is found in “Fimiston-style lodes”, the earliest mineralization, while the slightly later “Oroya-style lodes” include the Oroya Shoot famous for the intensity of its Au-Te mineralization and alteration. The latest mineralization is found in “Mount Charlotte-style” veins which contains relatively smaller amounts of gold as a percentage of the total, but still a considerable 5 Moz of gold.

Fimiston lodes are individually up to 2 km in length and occur over a total length of close to 7 km north-south and 1.3 km in vertical extent (Bateman et al. 2001). Finucane (1941) divided the lodes according to their attitudes (Easterly, Main, Caunter and Cross lodes) and based on their orientations, derived a NE-SW trending maximum compression stress axis. Clout et al. (1990), however, showed a broad spread in lode attitude, with the majority striking NNW and a steep SW dip. Fimiston-style lodes have been variously interpreted as shear zone hosted mineralization (Boulter et al. 1987), or dilational breccias within brittle faults (Clout et al. 1990). But, according to Bateman et al. (2001) the lodes are not shear-hosted mineralization, but are rather breccias and open-cavity fill vein textures, which are in some instances overprinted by foliation.

Boulter et al. (1987) found mineralization to be syn-tectonic with the phase of near-upright regional folding event (D_2), since minerals associated with gold emplacement are strongly modified during ductile shearing. They argued that the main pervasive foliation formed during displacement on the shear zones and that shearing increased rock permeability leading to mineralization. They described also a late D_3 crenulation cleavage of constant orientation overprinting the lodes. In contrast, Clout (1989) and Scott (1997), found that the main foliation (D_2) must have formed after the lodes, but Swager (1989) envisaged the lodes as resulting from D_3 sinistral wrench faulting, and the Mt Charlotte quartz veins from D_4 dextral faulting on North-trending faults (see Table 2.4.2). Groves (1993) considered the Fimiston lodes to be a member of his syn- D_3 crustal continuum, but considerable evidence in the form of structural cross-cutting relationships suggest that this may not be the case.

Structural evidence for a $D_{1\text{local}}$ age for the Fimiston lodes have accumulated over recent years and are listed in Bateman et al. (2001), and the key points are: except for mineralised felsic dykes, they are cut by all other structures, including later foliations, the $D_{1\text{local}}$ Golden Mile Fault and D_2 thrusts, and D_3 - D_4 strike slip shear zones. However, Fimiston mineralization overprints regional metamorphism, which is conventionally ascribed to D_3 , even though Clout et al. (1990) described evidence for syn- D_1 metamorphism. In our view, there is significant

structural evidence to suggest an early phase of mineralization. It is now necessary to determine whether D_1 local corresponds to the D_1 or D_2 regional event.

The Oroya-style lodes, include the ~60t Oroya Shoot, is essentially similar in alteration and fluids to the Fimiston lodes, including V-rich mica, but more intensely mineralised. Structurally the 1500 m long Oroya Shoot is different as it formed in a dilational jog within shear zones, along the contact between the Golden Mile dolerite and the Paringa Basalt. Oroya-related shear zones cut Fimiston lodes and the Golden Mile Fault, suggesting it formed during D_2 . Lungan (1986) suggested that quartz veins that he related to the Oroya Shoot cross cuts Fimiston lodes. Present understanding would relate those quartz veins to a D_4 reactivation of early faults and relate the veins to the syn- D_4 Mount Charlotte mineralization (Bateman 2002, pers. commun.).

Mount Charlotte. In Mount Charlotte, mineralization consists of quartz stockwork, mainly confined to the granophyric unit 8 of the Golden Mile dolerite. Veins are usually 5 to 100 mm wide with two preferred orientations with steep and flat northerly dips (e.g. Ridley and Mengler 2000). North-trending, dextral shear zones known as the Charlotte set (Boulter et al. 1987; e.g. Charlotte, Reward and Golden Pike Faults) overprint earlier D_2 -structures and are important controls on the geometry (Mueller et al. 1988).

Gold at Mount Charlotte is hosted in the wall rocks of quartz veins. Ridley and Mengler (2000) analysed the structures related to the Mt. Charlotte gold deposit and defined a conjugate pair of contemporaneous quartz veins, with no evidence of shear parallel to vein walls. Despite the close presence of shear zones, quartz veins hosting gold developed after movement in these faults had ceased and seem to reflect either a late extensional shearing or bi-directional extension. Ridley and Mengler (2000) concluded that fluid flow in Mt Charlotte was a late event in the structural history, after almost all structures at the deposit and the local terrane were developed. However, the veins crosscut, and are crosscut by D_4 faults which reactivated earlier structures, normally along discrete brittle chlorite-filled fractures, mostly on faults of the Charlotte set (NS-trending set). Bateman et al. (2001) concluded that these D_4 brittle-ductile structures are closely linked to formation of the Mt Charlotte-style deposit, and that mineralization is strictly syn- D_4 .

Kent and McDougall (1995) determined ^{40}Ar - ^{39}Ar ages on hydrothermal muscovite samples associated with gold systems from both Mt. Charlotte and Golden Mile deposits, and found two ages interpreted to represent the time of mineralization: 2602 ± 8 Ma and 2629 ± 9 Ma,

Table 2.4.2. Summary of interpretations of structures from the Kalgoorlie district

	Boulter et al. (1987)	Mueller et al. (1988)	Swager (1989a)	Clout et al. (1990; their Fig. 3)	Bateman (2001)	This work
D₄			<ul style="list-style-type: none"> • NNE dextral faulting • Mt Charlotte Fault • <i>Mt Charlotte deposition</i> 		<ul style="list-style-type: none"> • Brittle, right-lateral faults • <i>Mt Charlotte deposition</i> 	<ul style="list-style-type: none"> • Brittle overprinting • <i>Mt Charlotte deposition</i>
D₃	<ul style="list-style-type: none"> • Open folds (Boomerang) • N-S Charlotte fault set • <i>Mt Charlotte deposition</i> 	<ul style="list-style-type: none"> • dextral shear regime • dextral reactivation of the BLSZ at New Celebration 	Transpression <ul style="list-style-type: none"> • Sinistral wrench faulting and <i>en-echelon</i> folds • NE-SW shortening • <i>Fimiston lodes</i> 	<ul style="list-style-type: none"> • upright cleavage (<i>S₃</i>), small-scale folding • <i>Mt Charlotte deposition</i> (post- <i>S₃</i> cleavage)	<ul style="list-style-type: none"> • upright cleavage (<i>S₃</i>) and small-scale folding • Boomerang Anticline (folds all <i>D₁</i> structures) 	<ul style="list-style-type: none"> • Sinistral shearing overprints BLSZ • N-S trending Charlotte set, Pisces S.Z.
D₂	<ul style="list-style-type: none"> • Kalgoorlie Anticline • Strike slip faults (Golden Mile Fault) • <i>Fimiston lodes</i> 	<ul style="list-style-type: none"> • sinistral BLSZ • Golden Mile Fault as subsidiary of BLSZ • N30W/50W reverse shear zones • doming of Kalg. Ant. and Sync. 	<ul style="list-style-type: none"> • Regional NW-trending folds (e.g. Celebration Anticline) 	<ul style="list-style-type: none"> • N-trending dextral-reverse faults and shear zones • <i>Fimiston lodes</i> (pre-<i>S₃</i> cleavage) 	<ul style="list-style-type: none"> • Large scale reverse faults (W over E) such as the Mt. Hunt, rarely E-over-W like the Boulder Fault 	<ul style="list-style-type: none"> • Thrusts (W-over-E) and folds (Boomerang and Celebration Ant.) • Early D₂ • E-over-W thrusts Golden Mile Fault +Kalgoorlie Anticline • <i>Fimiston lodes</i>
D₁	<ul style="list-style-type: none"> • Recumbent folds 	<ul style="list-style-type: none"> • Kalgoorlie Anticline 	Shortening NE to SW <ul style="list-style-type: none"> • thrust on Golden Mile • Kalgoorlie Anticline • small scale thrusts in interflow slates and Paringa basalt 	<ul style="list-style-type: none"> • Golden Mile and Boulder Faults • Kalgoorlie Anticline+Syncline • Boomerang Anticline 	<ul style="list-style-type: none"> • E-over-W thrusts Golden Mile Fault +Kalgoorlie Anticline • <i>Fimiston lodes</i> 	<ul style="list-style-type: none"> • S-over-N thrusting in Kambalda Tramways, Foster thrusts

respectively. These ages confirmed that mineralization occurred in at least two distinct periods. Recent work, however, has corrected the ages upwards by ~1% (Vielreicher et al. submitted) and cast some doubt on the validity of the older age.

In summary, here, like in New Celebration, an early crustal thickening event gave rise to thrusts and tight to isoclinal folds, associated with a steep and pervasive NNW-trending fabric (D_{1local} and D_2). This structure was subsequently reactivated by a broad zone of regional sinistral shearing, characterized by en-echelon, north-trending, sigmoidal, ductile, local-scale dextral shear zones D_3 . These were later reactivated in a brittle fashion, during D_4 which also gave rise to new faults (Bateman 2002, pers. commun.). Questions remain regarding the absolute and relative timing of different phases of gold mineralization, but structures as well as isotopic dating suggest a lengthy mineralization, with the Fimiston-style lodes possibly pre-dating and the Oroya Shoot seemingly contemporaneous with a crustal thickening event, and the Mt. Charlotte-style mineralization associated with late brittle-ductile deformation.

Kambalda-Saint Ives Goldfield

Previous Work. The Kambalda-Saint Ives goldfield is one of the largest mining centres in the Norseman-Wiluna belt, and has a number of large gold and nickel deposits associated with Archean mafic-ultramafic volcanic and intrusive rocks, and metasedimentary rocks. The goldfield includes several operating and abandoned mines including Victory-Defiance (the largest one), North Orchin (in operation), Revenge (abandoned). Gold deposits are mainly shear zone/quartz vein-hosted, and are localised within low displacement reverse shear zones, up to 1000 m long (Nguyen et al. 1998) and maximum displacement of up to a few hundred metres (e.g. Repulse Fault, Watchorn 1998). The mineralized shear zones are developed adjacent to much larger NNW-trending regional shear zones, to which they are believed to be kinematically related (e.g. Roberts and Elias 1990, Nguyen et al. 1998). The BLSZ is the major regional fault, and is considered to be the first-order structure from which the second-order Playa Shear Zone splays off. The Playa Shear Zone is the largest shear zone in the immediate vicinity of most gold deposits in the area, and extends for about 10 to 15 km south of the Kambalda Dome (Fig. 2.4.15).

Apart from the NNW-trending shear zones, this area is characterized by important and well-defined ENE-WSW striking D_1 thrusts (Archibald 1979) such as the Foster, Tramways, and Republican (Swager and Griffin 1990; Swager et al. 1992). The Tramways thrust has an inferred

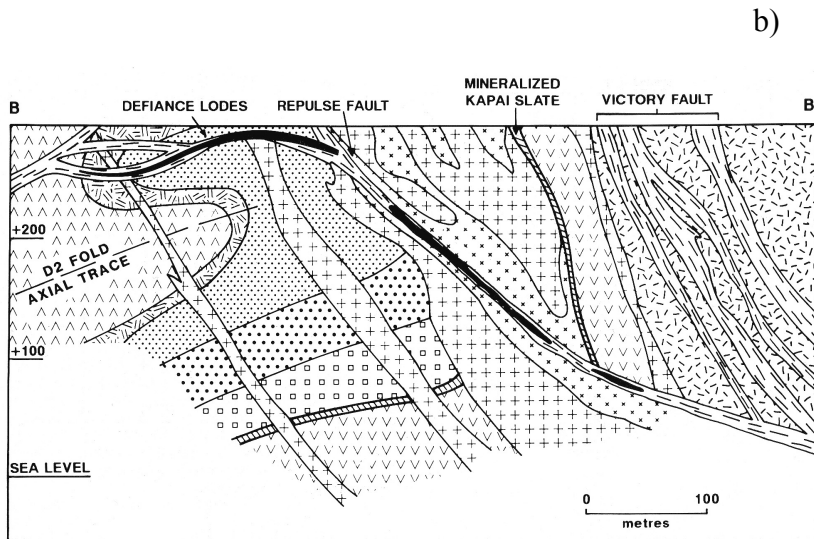
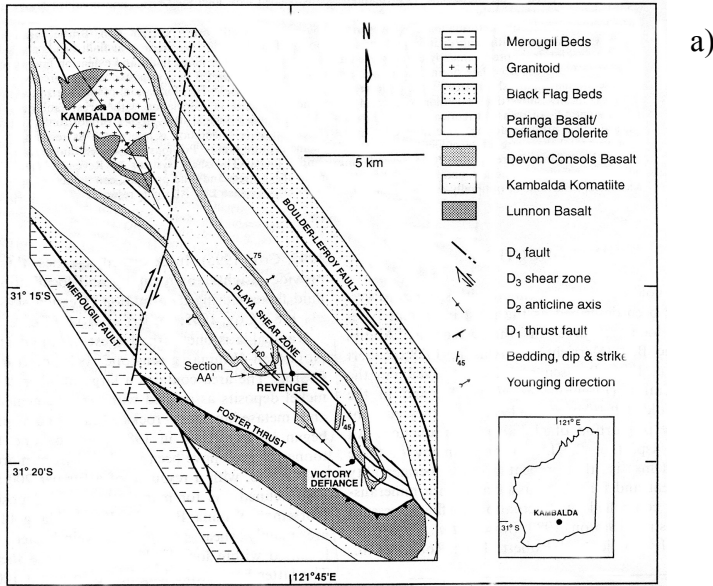


Fig. 2.4.15. a) Solid geology of the Kambalda area (redrawn from Nguyen et al. 1998, based on WMC Resources Ltd maps), b) E-W cross section depicting the shear zones controlling mineralization at Victory-Defiance, Britannia and Sirius. Shear zones are interpreted to be listric and link at depth (redrawn from Roberts and Elias 1990)

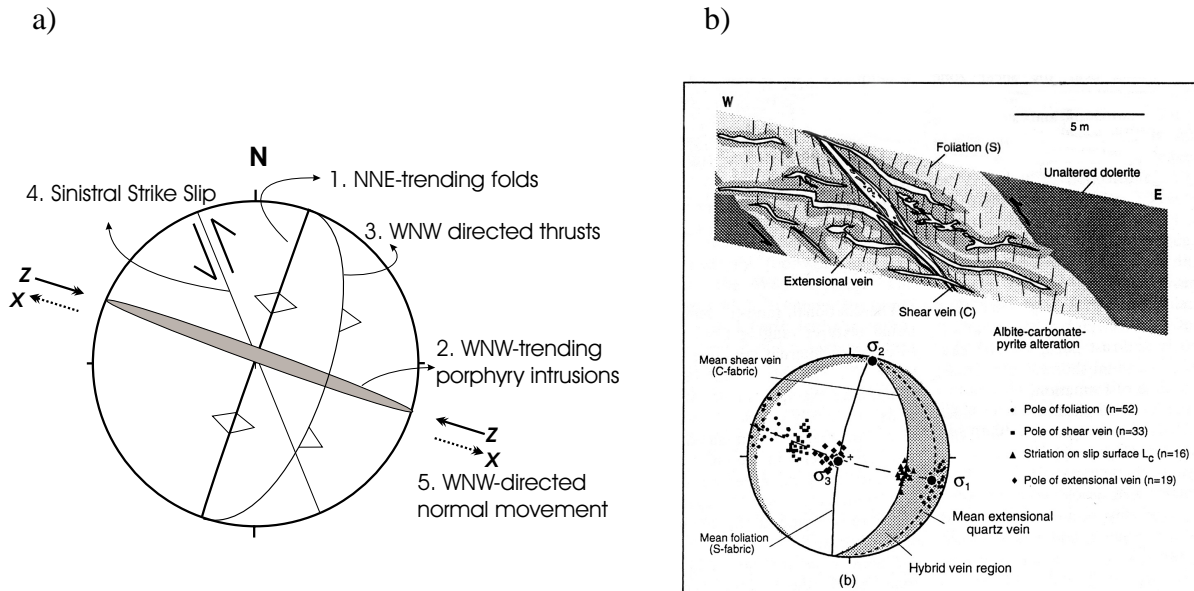
movement of south-over-north (Swager and Griffin 1990) is associated with a recumbent (NNW-vergence), ENE-trending, large-scale fold defined by the Tramways greenstones (Perriam, pers. commun. 2001; and Gresham and Loftus Hill 1981; Griffin 1990). These early structures were later folded by D_2 leading to NNW trending, upright, open folds, possibly associated with NNW-trending shear zones (see Griffin (1990) his table 18). Benett (1995) ascribed to D_2 the framework of reverse faults, depicted in Fig. 2.4.15b and later reactivated by D_3 . The fact that D_2 folds in this area are generally open, in contrast to elsewhere in the terrane, suggests less intense D_2 straining than elsewhere. As discussed below, this has had important consequences in the development of D_3 structures, and preservation of D_1 structures.

D_3 in Kambalda is different than that of the other Districts. Here D_3 gave rise not only to strike slip movement on steep shear zones but also thrusts using gently dipping limbs of the open D_2 folds. Many authors concluded gold mineralization took place during D_3 (e.g. Clark et al. 1986; Roberts and Elias 1990; Benett 1995, Nguyen et al. 1998; Watchorn 1998) and Benett (1995) details its complex structural development as follows:

- 1) early folding with NNE axes, which refolded a NNW fold to give rise to domal structures. D_3 folds tighten to the SSE (see also Clark et al. 1986),
- 2) WNW-striking, steep porphyry dykes cut NNE-trending folds,
- 3) WNW-directed thrusts (such as the Defiance C32 and C33, Revenge N01 and Orchin shear zones) cut these dykes and some of them host gold mineralization which is contemporaneous to shearing (C.J. Nicholson, BSc Thesis),
- 4) pre-existing NNW-striking, D_2 shear zones such as Repulse, Britannia and Sirius Faults (Benett 1995) are reactivated,
- 5) the final stage of D_3 is normal dip-slip movement in a WNW-ESE direction.

Figure 2.4.16 depicts these different structures and the interpreted WNW-ESE orientation of the axis of maximum shortening (z -axis). We note that these different structures, grouped under the same deformation phase, require the strain axes to have swapped places several times as the structures developed. In general agreement with Benett (1995), a detailed study of the structures developed at Revenge (Nguyen et al. 1998) concluded that the structures and kinematic indicators related to gold mineralization, suggest a stress system with a shallow plunging east-southeast σ_1 during mineralization (Fig. 2.4.16 b).

Fig. 2.4.16. a) Schematic stereonet projection of the structures developed during D_3 at Kambalda-SIG according to Bennett (1995) and interpreted orientation of the maximum shortening axis orientation. Structures (1) to (4) are all related to the same WNW-ESE maximum shortening axis (z) as indicated. Final stage normal movement, directed WNW-ESE, (5) in text not shown in the figure), represents a period of extension along the WNW-ESE axis (x strain axis, dashed arrow). b) Equal-area lower hemisphere stereonet projection of structural data from Revenge (from Nguyen et al. 1998).



Nguyen et al. (1998) defined two main types of shear zones: i) NW-trending, sub-vertical first- and second-order regional shear zones like the Boulder-Lefroy and the Playa shear zone, and ii) smaller, more localised E- and W-dipping mineralised shear zones. Likewise Watchorn (1998) divided deposits into two according to the mineralized structures: a) those where gold is hosted by 2-10 m wide thrust zones, trending N- or NW- and dipping moderately either E or W (e.g. Revenge, Defiance, Repulse, Orchin, Junction, Santa Ana, Apollo and Argo); b) those hosted by steep NNW-trending fault zones (e.g. Britannia, Sirius, Ives-Reward and Hunt).

Compston et al. (1985/86) found that gold was emplaced following the peak of metamorphism at 2660 Ma, while Watchorn (1998) concluded that mineralization took place after D_2 upright folding, in rough agreement with Bennett (1995). The structural constrains support a syn- D_3 mineralization. Carbonate alteration surrounding the gold lodes is dated at 2629 Ma (Clarke 1987) and a last episode of mineralization was dated at 2601 Ma (Clarke 1987). Kent and McDougall (1985) report isotopic ages for gold deposits at Kambalda at 2627 ± 14 Ma derived

from Pb-Pb in rutile and ^{40}Ar - ^{39}Ar in actinolite. These ages are similar to those found using Ar-isotopes for Kalgoorlie.

Structural Study. The Kambalda-Saint Ives Goldfield differs from other goldfields along the BLSZ in that many controlling shear zones are moderately dipping. Perriam (pers. commun. 2001) mapped a regionally dominant gentle SE plunge of the mineral lineation, which is also reflected in the major mineralized shear zones. Apart from Nguyen et al. (1998), previous works have not considered in any detail the kinematic information in microstructures. Structural analysis of data collected in North Orchin, Victory-Defiance, Britannia and Sirius open pits will be here compared with data for Revenge (from Nguyen et al. 1998) and with the structural evolution proposed by Benett (1995). Like previous authors, we will first divide the structural information into those related to gently dipping structures and those from steep structures, and later integrate them.

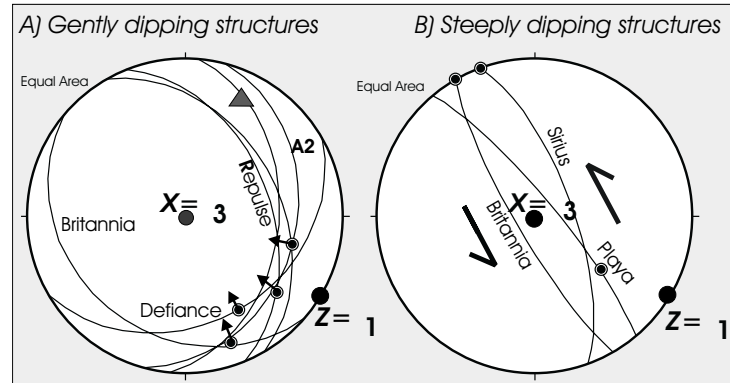
The shallow dipping shear zones exposed in North Orchin, Victory-Defiance and Repulse are plotted in Fig. 2.4.17a. Gold in North Orchin is hosted by the N-S / 45- 50E-striking A2 shear zone. The asymmetry of fibrous tails around pyrite grains (Nicholson, BSc thesis), subhorizontal quartz veins, asymmetric folds and S-C fabric within A2, all indicate the reverse sense of shear. Late 2-cm wide bands with normal sense of shear (S-C fabric) overprint the early reverse structures (also noted by Benett 1995, late D_3 event). Minor isoclinal folds were also observed, with a gently plunging fold axis toward N20E, nearly parallel to a crenulation lineation observed locally (N30E/10) (see Fig. 2.4.17a).

Victory and Defiance orebodies are separated by the Repulse Shear Zone, which is believed to be the sole thrust of a system of splay reverse faults that are linked underground to the Playa Fault, as well as to Britannia and Sirius Shear Zones (Fig. 2.4.15b Profile). The Repulse Shear Zone has a combined sinistral and reverse displacement of 300-600m in a WNW direction, as defined by marker offsets (Benett 1995) and confirmed by S-C fabric. Where exposed in the present pit, the shear zone is approximately 50 cm wide and strikes N22W/ 45E, and has a stretching lineation plunging 130/25. The Defiance ore body lies within a shear zone striking N60E / 32E, with reverse (possibly oblique) movement recorded by displaced markers (Warwick, pers. commun. 2001).

Despite differences in attitude of the shear zones in both North Orchin and Victory-Defiance mines, stretching lineations are roughly parallel, and nearly perpendicular to measured fold/crenulation axis (Fig. 2.4.17a). Together with their sense of shear, the structures suggest a

sub-horizontal WNW-ESE trending maximum shortening strain axis (z) and a vertical maximum extension axis (x). The inferred strain and stress axes are similar to those derived by Nguyen et al. (1998) and Benett (1995).

Fig. 2.4.17. Lower hemisphere equal area stereonet projection of: A) major gently dipping structures from Revenge (from Nguyen et al. 1998), North Orchin (A2 Shear Zone), Victory-Defiance and Britannia deposits, as well as stretching and mineral lineations (dots on great circles). Arrows on dots correspond to the



inferred movement direction (reverse), black triangle corresponds to the orientation of D₃ fold axes and crenulation lineation; B) major steeply dipping shear zones from Playa (from Nguyen et al. 1998), Britannia and Sirius pits. Dots correspond to stretching and mineral lineations, and arrows indicate inferred sinistral shear sense. Interpreted orientation of the strain and stress axes are indicated.

Assuming the inferred strain axes are parallel to stress axes, Fry's method (Fry 1992) for determining maximum shear orientation on any given plane was used. All observed mineral lineations and sense of shear in North Orchin, Victory-Defiance and Revenge may be derived from a nearly uniaxial compression. Interestingly, the kinematics and plunge of mineral lineation in the steep shear zones mapped at Britannia and Sirius (but not the moderate SE-plunging lineation on the Playa shear zone) may be derived from the same stress system.

The shear zones that we investigated at Britannia and Sirius deposits have steep dips and sinistral strike slip shear sense (Fig. 2.4.17b. At Britannia, the main, steep mineralized shear zone, striking N30W / 80E has subhorizontal mineral lineation and kinematic indicators (*S-C* fabric) indicating sinistral sense of shear. This seems to cut across 20-30 cm wide, older gently dipping shear zones (N50W / 20SW), with parallel quartz veins in their cores. Microscale kinematic indicators in the latter were not observed, but drag folds define reverse movement. These older shear zones correspond quite exactly to the W-dipping shear zones described at Revenge (Nguyen et al. 1998), including the presence of quartz veins in their cores. At Sirius, the main shear zone strikes N20W / 70E and has subhorizontal mineral lineation and *S-C* fabric indicating sinistral sense of shear. Evidence for older deformation is preserved in between anastomosing strike slip

Fig. 2.4.18 a) Schematic summary of structures and deformation phases for the three main gold districts along the Boulder-Lefroy Shear Zone. See text for full description.

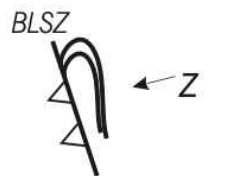
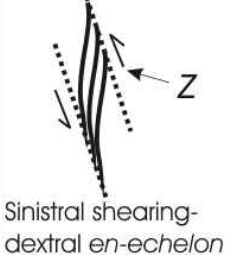
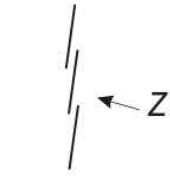
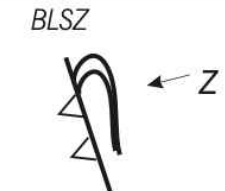
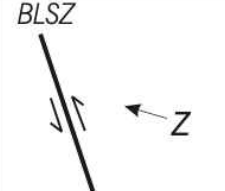
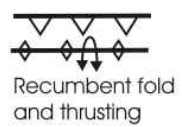
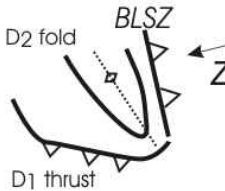
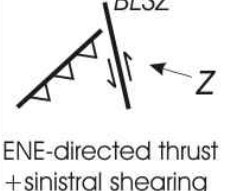

Deform. District	D1 N-thrusting	D1 local-D2 Crustal thickening	D3 NNE-SSW extension	D4 brittle
Kalgoorlie				
New Celebration				
Kambalda Saint-Ives				

Table 2.4.3. Summary of main structures and timing of gold mineralization.

	D1 Crustal thickening N-directed shortening	D1 local	D2 Crustal Thickening BLSZ stage 1	D3 lateral escape BLSZ stage 2	D4 brittle reactivation
Kalgoorlie		<ul style="list-style-type: none"> Golden Mile Fault: E-side-up Kalgoorlie Anticline (recumbent fold) Fimiston lodes 	<ul style="list-style-type: none"> NNW-trending thrusts, W-side-up NNW-trending folds and foliation Oroya lodes 	<ul style="list-style-type: none"> sinistral on NNW planes tightening of D2 folds dextral N-trending en-echelon shear zones 	<ul style="list-style-type: none"> Brittle (semi-brittle) reactivation of early shear zones Mt. Charlotte-style gold
New Celebration			<ul style="list-style-type: none"> NNW-trending, steepened thrusts gently plunging boudin axes 	<ul style="list-style-type: none"> sinistral reactivation dextral N-S Pisces S.Z. Gold deposition, syn-tectonic pyrite 	<ul style="list-style-type: none"> Gold deposition?
Kambalda-Saint Ives Goldfields	N-directed thrusts and recumbent hanging wall folds (e.g. Tramways, Foster, Republican Thrusts)		<ul style="list-style-type: none"> folding of D1 structures NNW-trending foliation, upright gentle folds 	<ul style="list-style-type: none"> WNW-directed thrusts NNE-trending dykes Sinistral, NNW-trending shear zones Gold deposition 	<ul style="list-style-type: none"> Normal and dextral reactivation of D3 shear zones

planes associated with alteration, as steep mineral lineation in unaltered basalt, and is in accordance with E. Baltis (pers. commun. 2001) that the Sirius Shear Zone was initially a reverse fault, linked at depth with the Repulse Thrust.

The sinistral shear zone at Sirius, as well as the A2 thrust place at Orchin have both been reactivated later, when narrow shear zones formed showing dextral movement at Sirius and normal movement at North Orchin. Such movements had previously been recorded by mining personnel (Benett 1995, E. Baltis pers. commun. 2001) and suggest a later relaxation of the maximum shortening axis.

Discussion. The moderately to gently dipping, reverse shear zones controlling gold mineralization in Kambalda-Saint Ives have a common mineral lineation, which results from thrusting from the ESE. This deformation overprints NNW-trending D_2 folds; so that NNE-trending folds refold them, and D_3 porphyry dykes cut both. In its simplest the history of straining in the District may be summarized as initiated with a D_1 north directed thrusting and folding (e.g. Griffin 1990), followed by an open D_2 folding, characterized by ENE-WSW shortening axis and NNW-trending folds, not nearly as significant and penetrative as in the districts to the north. D_3 was an ESE-WNW shortening event, regionally pervasive and associated with porphyry dykes and thrust, as well as steep strike slip shear zones. The regionally dominant lineation in Kambalda-Saint Ives area is roughly parallel to the stretching lineations found in the D_3 mineralized thrusts. This suggests that D_3 has pervasively deformed the area. The more recently found deposits of Argo and Apollo seem to be controlled by NNE-trending shear zones (Benett 1995). Although not investigated here, it is likely that those shear zones are a dextral conjugate set to D_3 .

In summary, the large-scale geometry of the Kambalda Saint-Ives District resulted from D_1 NNW-directed thrusting and associated folding, followed by D_2 folding and thrusting related to NE-SW shortening (Fig. 2.4.18). Thrust planes that define the Victory Complex (including the Playa, Repulse, Britannia and Sirius Shear Zones) could have been initiated as a result of D_2 and later reactivated by D_3 accommodating shortening movement directed from ESE to WNW. D_3 resulted in different structures here than further north. As opposed to the strike-slip shearing of steep, folded lithological contacts, in Kambalda-Saint Ives D_3 reactivated gently dipping limbs of D_2 folds as thrusts. Why was D_3 different? We postulate that differences result from less intense crustal thickening during D_2 , leading to not only preservation of D_1 structures, but also allowing further crustal thickening and thrusting of gently dipping D_2 fold limbs.

Discussion and Conclusions

The strain recorded in different parts of the BLSZ and our interpretation of the structural history are summarized in Fig. 2.4.18 and Table 2.4.3 and will be used as the basis of discussion in this section. The most important result is that although structures may differ, the three main Districts record a common history.

D₄ and dextral reactivation. As mentioned earlier, *D₄* has been poorly defined in the existing literature. Mueller et al. (1988) ascribes to *D₃* a general dextral shear regime, arguing that exposures of the BLSZ (namely the New Celebration District) have dextral fabric anastomosing around and overprinting a sinistral fabric. Outcrops at New Celebration District and good outcrops in the King Battery area allowed documentation of the BLSZ, but these exposures did not reveal the dextral overprinting described by Mueller et al. (1988). We found that not only do *D₃* sinistral shears reactivate previously developed reverse shear zones and tight folds related to *D₂*, but also explains the en-echelon pattern of N-trending dextral shear zones in Kalgoorlie as antithetic bookshelf style shear zones subordinate to the dominant NNW-trending *D₃* sinistral shear set.

We note, however, that some of these N- or NNE-trending shear zones could have had a long history, as they could have been generated during *D₂* ENE-WSW shortening, to accommodate local movement transfer.

Boulder-Lefroy Shear Zone: a two-stage history. Contrary to previous interpretations, this work concludes that the BLSZ is not simply a major sinistral wrench fault but developed as a result of a two-stage history starting with thrusting followed by modest amounts of sinistral movement.

Early in the history, *D₂* crustal thickening gave rise to a number of NNW-SSE trending thrust ramps arranged roughly along strike of the BLSZ. At this stage, the BLSZ was probably not a connected plane but was more likely a number of individual or groups of reverse shear zones, spread along its length. Earlier formed thrusts became steep with the accumulation of strain and incapable of accommodating significant further shortening, they were then abandoned as new ones developed and cross cut and refolded earlier ones. This would explain the refolding of the Kalgoorlie Anticline by the Boomerang Anticline, making *D₁local* part of the regional *D₂*, as well as the cross-cutting relationships of thrust duplexes interpreted on the seismic lines. We postulate that the crust must have reached its maximum sustainable thickness, causing deformation to go into strike slip mode, initiating *D₃*. *D₂* reverse shear zones were reactivated as

sinistral shear zones. A major component in the growth of strike-slip faults is by coalescence of smaller faults. The existence of numerous bends and jogs in the BLSZ argues for such a process whereby sinistral shearing lead to the coalescence of older thrust planes along strike. Modest total sinistral movement along the ~200 km long BLSZ (less than 12 km total apparent movement; e.g. Langsford 1989; Swager 1989) is reflected by the complexity of the trace of the BLSZ, which would tend to get erased with increased displacement (Wesnousky 1988).

D_3 was characterized also by the development of a dextral, N- and NNE-trending set of ductile shear zones (e.g. Pisces Shear Zone at New Celebration, and the early shear zones of the Charlotte set at Kalgoorlie). D_4 was particularly important at Kalgoorlie where it reactivated earlier formed shear zones and gave rise to new N-trending brittle-ductile faults of the Charlotte set.

Timing of Gold Mineralization and Fluid Sources. With the exception of the Golden Mile Fimiston and Oroya lodes, gold deposition along the BLSZ took place during D_3 reactivation of the shear zone or during D_4 (Mt. Charlotte and possibly Hampton-Boulder/Jubilee). The timing of gold mineralization and the origin of fluid sources have been the subject of much discussion (e.g. Groves 1993). Whereas most detailed geochronology work, as well as our own observation, constrain timing of mineralization to late in the history of the Yilgarn Craton (2.64-2.63 Ga), there are a number of deposits and observations which suggest a broader mineralization phase (e.g. Kalgoorlie District).

The discussion of the timing of mineralization is closely linked with our understanding/assumptions about the origin of mineralising fluids. Devolatilization of typical mafic-ultramafic rocks during metamorphism from upper greenschist facies to lower amphibolite facies produces fluids similar in composition to those recorded in typical orogenic lode gold deposits, suggesting that metamorphic devolatilization could be the source of mineralising fluid (Phillips and Powell 1993; Powell et al. 1991). Whereas there may be more than one source of fluids, and there remains intense discussion on the subject, it is plausible that these metamorphic fluids played an important role in the mineralization process.

Simple thermal considerations suggest that the Kalgoorlie terrane would have undergone two distinct metamorphic events since komatiite extrusion at 2.7 Ga. The first event would have been associated with mafic-ultramafic volcanism and extension, whether or not driven by an underlying mantle plume. Because of its extensional nature, the first event would have affected predominantly deeper crustal rocks and is associated with crustal melting and voluminous felsic

volcanism, with a thermal peak within the crust at approximately 2.68-2.66 Ga, the timing of felsic magmatism. The second metamorphic event would result from the 2.65-2.63 Ga D_2 - D_4 crustal shortening phase, and would have affected predominantly the upper part of the crust.

These arguments, together with evidence for several mineralising events in the Kalgoorlie District, suggest the possibility of two terrane-wide phases of gold mineralization each related to devolatilization through heating of basaltic rocks to amphibolite facies temperatures. A detailed numerical study of the thermal evolution of the Kalgoorlie Terrane would further constrain the nature of these two broad metamorphic events between 2.7 and 2.63 Ga, their timing, and the likely volumes of fluids released during each event.

In conclusion, the BLSZ is characterized by an early phase of thrusting and folding related to a crustal thickening event, D_2 . This phase includes the early Golden Mile Fault and Kalgoorlie Anticline at Kalgoorlie, which became abandoned as they became oversteepened and new ones developed. Steep D_2 thrust planes were later reactivated during D_3 as sinistral shear zones, locally accompanied by N- and NNE-trending dextral shear zones, such as the Charlotte set at Kalgoorlie, and large scale N- or NNE-trending folds (Resolution Anticline). D_3 dextral shear zones continued activity through declining temperatures through a brittle-ductile stage and finishing with a brittle stage during D_4 . The change from D_2 to D_3 is probably related to the crust having reached a maximum sustainable thickness, so that further horizontal shortening required lateral escape by means of strike slip shearing. The change from D_3 to D_4 was probably due simply cooling and embrittlement of the upper crust.

During D_3 , the BLSZ probably expanded by linking early thrust planes, and the total displacement was relatively modest (less than 12 km) as expressed not only by marker motion but also by the tortuous trace of the shear zone. D_3 in the southern region of Kambalda-SIG was slightly different than elsewhere in that it had a component of crustal thickening, which was expressed by the reactivation of lithological contacts on gentle D_2 fold limbs. Furthermore, in this region, less intense D_2 , allowed preservation of early formed D_1 , north-directed thrusts. The change from D_2 to D_3 - D_4 may be explained by the crust having reached a maximum stable thickness during D_2 . Most gold deposits seem to have been formed either during D_3 (Hampton-Boulder/Jubilee, Kambalda-SIG) or during later D_4 brittle reactivation (Mount Charlotte-style). However, most *gold* seems to have been deposited during D_1 (Fimiston lodes). The Golden Mile, by far the largest deposit in the Yilgarn Craton, is the only one to have undergone a protracted phase of mineralization, with the first phase and most of the gold probably started during early

D_2 or even earlier. Yilgarn metamorphism remains the most poorly understood of all aspects of its evolution. Thermal history considerations suggest that there *must* have been more than one phase of metamorphism and devolatilization of crustal rocks at the upper greenschist- lower amphibolite facies metamorphism.

2.5. Structural Evolution of the Ida and Zuleika Deformation Corridors

Summary

Gold deposits along the Ida and Zuleika Shear Zones share some similarities, in that, in both areas, mineralization is late in the structural history, and structurally controlled in areas of increased complexity. Economic gold concentrations are preferentially sited at intersections between N-S and NNE-SSW ductile and brittle-ductile structures and the dominant NNW fabric, in particular where there are either low viscosity rocks (shales or ultramafic rocks), or high viscosity or brittle rocks (granites or dolerites). Gold mineralization in both corridors also show a similar chemical signature; for instance ubiquitous potassium, sulphur and silica enrichments, and anomalous arsenic concentrations at shale-hosted deposits.

Although, high-grade, shear-zone hosted deposits have been exploited along both structures, the main factor limiting the development of giant gold deposits would appear to be amphibolite facies metamorphism during or before mineralization. This not only diminishes the competency contrast between lithological units, but also, when accompanied by high strain, produces a pervasive foliation and parallelism of structures and lithologies, thus decreasing heterogeneities which could have focused mineralizing fluids.

Study of deformation of the Ida and Zuleika Structural Corridors suggest that deformation in the Kalgoorlie Terrane resulted from the interaction between a regional ENE-WSW shortening and indentation of competent granitoid blocks into their weaker greenstone matrix. Such interactions at the Terrane and Domain scales is via shear zone and fold rotation, as well as lateral and vertical escape of greenstone sequences on the sides of batholiths. Westward indentation of the large mass of granitoids north of Kalgoorlie into the Southern Cross Terrane explains the intense pure shear flattening with a small dextral component determined along the Ida Shear Zone, as well as the broad flexure of the Zuleika Shear Zone, which has sinistral movement on its northern part and exhumation on its central part around Kundana.

2.5.1. The Ida Shear Zone

Introduction

The Ida Structural Corridor (ISC) is a regional lineament, ~500 km long, on the western side of the Eastern Goldfields Terrane (Fig. 2.5.1) purported to separate the Eastern Goldfields Terrane from the older Southern Cross Terrane (Williams 1974, Gee et al. 1981), either reflecting terrane accretion, or representing the boundary of an early extensional basin into which 2.7-2.66 Ga mafic- ultramafic and felsic rocks were extruded.

The central portion of the Ida Structural Corridor is a narrow zone of high strain developed along the linear Ularring Greenstone Belt (Wyche 2000) that includes the Ida Shear Zone (the term Ida Shear Zone is used in preference to the more common 'Ida Fault', because it better reflects the attributes of the structure). This module has focused on the Ida Shear Zone, and accompanying strain corridor, as part of its regional efforts to understand the evolution of the Kalgoorlie Terrane and gold mineralisation. The structure was selected because of its regional importance as a potential terrane boundary, and also because its poor gold endowment contrasts strongly with that of the Boulder-Lefroy Shear Zone.

On aeromagnetic images, the Ida Structural Corridor can be traced north and south of the Ularring Greenstone Belt. The northward continuation can be traced on the west side of the Agnew-Wiluna belt as the Waroonga Shear Zone (Platt et al. 1978), while the southern continuation correlates with the western margin to the Coolgardie, Widgiemooltha and Chalice Greenstone Belts.

The Ularring Greenstone Belt is further subdivided into local geographic centres (Fig. 2.5.2), namely, from north to south, Mt Alexander, Mt Ida, Riverina and Davyhurst and was selected for study because it incorporates lithologies considered to be representative of the two terranes. The greenstone belt is bounded to the east by the Riverina Gneiss, which is a strongly foliated gneiss that yields a strong linear magnetic fabric that extends along strike for >100km and it is bounded to the north and west by granitoids (Fig. 2.5.2). The Honours Thesis work by Embry (1999) was funded by this project and details the Riverina region with a detailed geological map (available for consultation and copying at UWA, Department of Geology and Geophysics Theses Library, Ms J. Bevan, tel. 08 9380 2681).

Previous Work

The geology of the Ida Structural Corridor, from Davyhurst to Mt Ida, was described by Gibson (1904, 1906), Johnson (1950) and Tomich (1956). Focussing primarily on gold mineralisation, particularly at Timoni (Copperfield), and Riverina gold mines, little attention was paid to poorly exposed crustal breaks, although Tomich (1956) highlighted a contrast between a western ‘jaspelite’ bearing series and an eastern epidiorite series of greenstones within the Ularring belt. Williams (1974) determined that a “linear disruption” defined by the Ida Structural Corridor marked a change in lithology and structural orientations, while noting that the corridor itself was disrupted by granitoid intrusions.

The discovery of the Bottle Creek gold deposit in the Mt Ida area in 1983 led to increased interest in the belt. In his report on Bottle Creek, Legge et al. (1990) placed the Ida Shear Zone at the contact between the eastern margin of the Ularring Belt and the Riverina Gneiss. Wyche and Witt (1992), and Wyche (2000), both suggested that a terrane boundary might correlate with the western extent of ultramafic rocks in the Riverina and Davyhurst areas, which are accompanied by a zone of high strain. No previous detailed structural work on the ISZ has been published, while geochemical analyses of the rocks in the region are limited to a study around the Bottle Creek environs (Binns 1988), and a study in the Riverina area by Embry (1999). The Davyhurst area was mapped and described by Witt and Wyche (1992), and the Riverina area by Embry

(1999) and Wyche (2000). The central (Mt Ida region) and northern (Mt Alexander region) sectors have recently been mapped by AGSO (Ballard, Mt Mason, and Mt Alexander 1:100,000 sheets).

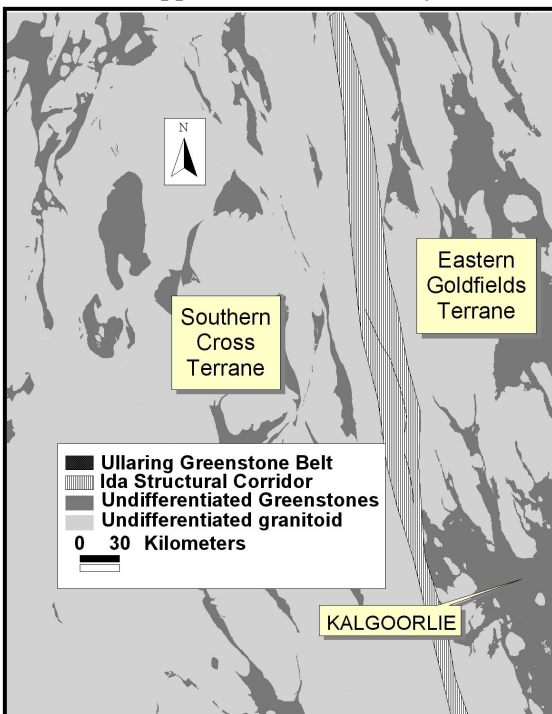


Fig. 2.5.1. The central Yilgarn Craton showing the trace of the Ida Structural Corridor and its relationship to the Eastern Goldfields and Southern Cross Terranes.

Current interpretation of the Ida Shear Zone is largely based on seismic data (Drummond et al. 1993, Swager et al. 1997, Drummond et al. 2000). The structure is interpreted to dip moderately to the east ($\sim 30^\circ$), and to penetrate to 25 km beneath the surface (Drummond et al. 1993). It is one of only a few structures that the seismic data depicts as cutting an apparent detachment fault imaged at the base of the greenstones. A gradual eastward thickening of the crust has been interpreted from the seismic study, and broadly coincides with the position of the Ida Shear Zone (Drummond et al. 1993). This crustal thickening, combined with an easterly decrease in metamorphic grade, led Swager et al. (1997) to interpret the Ida Shear Zone as a late stage normal fault and suggested that greenstones of the Kalgoorlie Terrane once extended west of the Ida Shear Zone, but were subsequently uplifted and eroded.

Stratigraphy

Three distinct stratigraphic sequences are recognised across strike within the Ularring Belt (Fig. 2.5.2). The western sequence consists of interbedded banded iron formation (BIF) and mafic volcanic and possible sedimentary units, which dip moderately to steeply east. The presence of BIF in greenstone belts throughout the Southern Cross Terrane, and their scarcity in the Norseman-Wiluna Belt, have been used to correlate this package with supracrustal rocks to the west (Wyche and Witt 1992).

The central sequence is dominated by thick (<1km), monotonous, east-dipping mafic rocks ranging from fine- to medium-grained (basaltic to doleritic texture), with occasionally preserved pillow structures. Several coarse-grained differentiated mafic intrusive rocks of undetermined dimensions were intruded along the eastern portion of this sequence (van der Borgh, thesis in prep). A series of intermediate to felsic intrusive rocks are also present in this area. In the Mt Ida area (Fig. 2.5.2), the felsic rocks are intensely foliated, tabular bodies, in places discordant to stratigraphy. Individual dykes are several metres thick and persist for several hundred metres along strike. In the Mt Alexander area to the north (Fig. 2.5.2), intrusive rocks tend to be more ovoid and less foliated, and preserve intrusive relationships.

The eastern sequence consists of thinner (5-50m) layers of mafic and ultramafic and interbedded fine-grained sedimentary rocks, tightly folded around NNW- to N-trending, sub-vertical axial planes such as the major Kurrajong Anticline, which incorporates much of the eastern sequence and contains the Copperfield Granite at its core (Figs. 2.5.2 and 2.5.9).

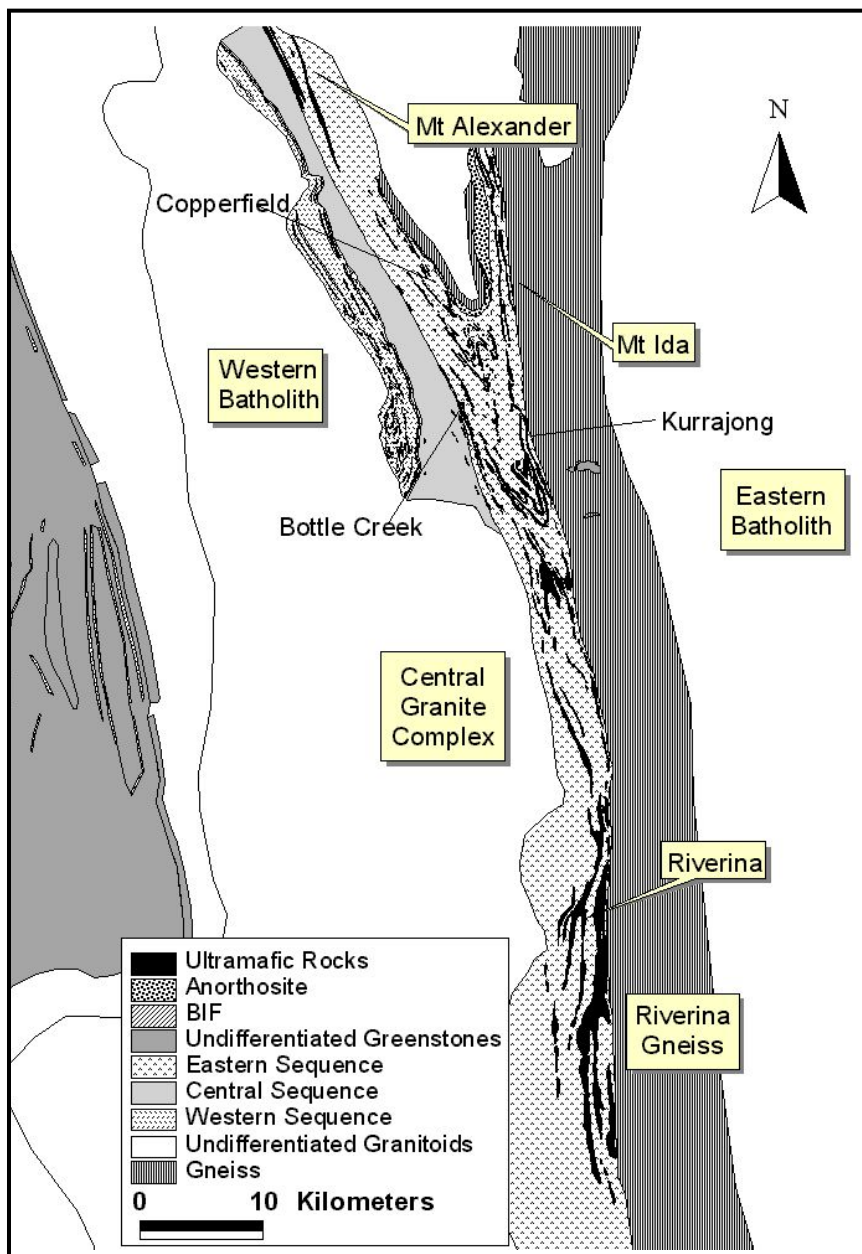


Fig. 2.5.2. Interpretive solid geology map of the Ullaring Greenstone Belt, and the principal regions discussed in the text.

The ultramafic rocks of the eastern sequence at Kurrajong, close to Mt Ida, have been correlated with the Walter Williams Formation (Hill et al. 1995), an extensive (35x150km) ultramafic-mafic package that can be traced along discontinuous outcrop all the way to Ora Banda, east of the Zuleika Shear Zone. The eastern sequence was correlated with similar rocks at Lawlers to the north, and Murrin Murrin to the east of the Keith Kilkenny Fault (Rattenbury 1993). Such interpretations, if correct, imply that the eastern sequence belongs to the supracrustal rocks of the Kalgoorlie Terrane, and that this sequence covers much of the Eastern Goldfields.

In the Mt Ida area, several large porphyritic bodies intrude the ISZ. These, or similar, porphyries can be observed in costeans and intermittent outcrops for >14km northward along the strike of the ISZ. Where observed, the porphyries contain a pervasive foliation, which is consistent with that of the shear zone. The porphyries host mineralisation at Bottle Creek. In the Riverina area, the Clarks Well monzogranite is interpreted to cut the shear zone and to be undeformed (Wyche 2000). A U-Pb zircon SHRIMP age determination yielded 2640 ± 8 Ma and was used to constrain the minimum age of movement along the Ida Shear Zone (SHRIMP U-Pb on zircon; Nelson 1995). However, as discussed in this report on (*Section 2.3*), the error bar on this age covers nearly the entire duration of the Kalgoorlie Orogen (D_2 - D_4). Pegmatite dykes are common in the Mt Alexander and Riverina sectors, but absent in the Mt Ida sector. These crosscut the Ida Shear Zone at high angles, and appear to be undeformed.

In summary, three well-defined sequences can be intermittently traced for the strike length of the greenstone belt (Fig. 2.5.2). The western sequence differs from the others by the presence of BIFs, while the eastern sequence includes extensive ultramafic rocks in the sequence that is related to the Walter Williams Formation at Ora Banda. All sequences are highly attenuated, and, like other regions, they were intruded by mafic sills and porphyries.

Regional Metamorphism

Mafic rocks throughout the Mt Ida and Mt Alexander areas consist of the assemblage amphibole (hornblende or actinolite), plagioclase, ilmenite and titanite. Chlorite forms a minor, retrograde component in some rocks and epidote is rare. Most rocks contain some mineral alignment defining a foliation, although igneous textures are occasionally preserved, such as the inherited ophitic texture (Fig. 2.5.3). Plagioclase compositions of An_{50-90} , and rare epidote and absent garnets in the mafic rocks, together suggest low to mid-amphibolite facies metamorphism.

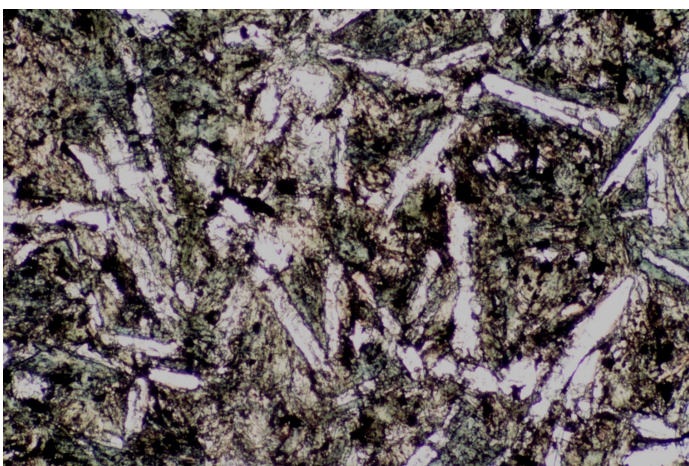


Fig. 2.5.3. A fine grained mafic rock from the Ularring Greenstone Belt, showing an inherited ophitic texture defined by igneous plagioclase laths in a groundmass of metamorphic amphibole, after pyroxene (width of view is 2mm).

Spinifex and cumulate textures are preserved in ultramafic rocks, although the mineralogy is now metamorphic, with massive ultramafic rocks consisting of the assemblage serpentine + magnetite ± tremolite. Sedimentary rocks proximal to the Copperfield Granite are reportedly amphibolite facies (Tomich 1956), and include garnet schists, and staurolite and andalusite schists, which decrease in grade with increased distance from the granitoid (Tomich 1956).

Geochemistry

During the project, a geochemical study was conducted, in collaboration with Dr Derek Wyman (University of Sydney), to define whether basaltic rocks on either side of the Ida Shear Zone are geochemically distinct and therefore belong to different terranes, or different extrusive events (van der Borgh et al., in prep). Fine-grained mafic rocks, considered to be meta-basalts, were sampled throughout the Ularring Greenstone Belt. These were combined with the Riverina data of Embry (1999), and data made available by Stephen Wyche (GSWA), which extended the dataset into greenstone belts within the Southern Cross Terrane. A brief summary of some of our findings follows:

Based on Zr/Y ratios <4.5 , the basalts are all tholeiites according to the criteria used by Barrett et al. (1993) for the Archaean Noranda Mine Sequence, Canada. The tectonic discrimination plot of Pearce and Cann (1973) indicates that the mafic rocks from both terranes are typical of basalts deposited in an ocean floor or island arc environment. Although there is overlap of the data from both sides of the ISZ, the chemistry does indicate that many of the basalts to the east are distinct from those to the west. This is illustrated in a plot of V versus Sc (Fig. 2.5.4), in which many of the eastern samples lie along a trend with their ultramafic counterparts, whereas those to the west lie along a different trend line, probably as a result of pyroxene fractionation (van der Borgh et al., in prep).

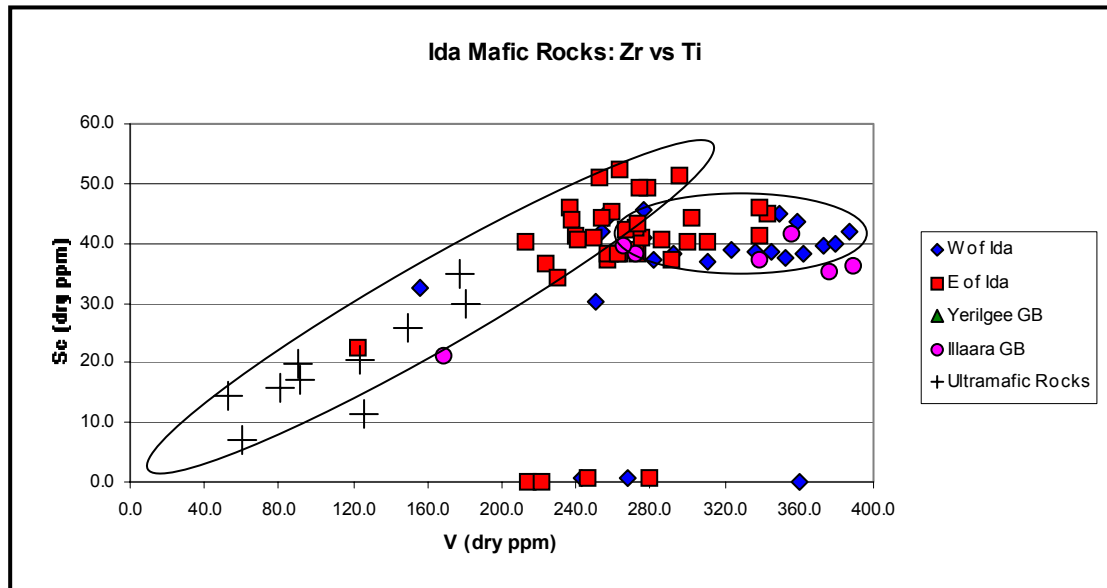


Fig. 2.5.4. Plot of V-Sc for basalts from the Ularring Greenstone Belt, and the Yerilgee and Illaara Greenstone Belts in the Southern Cross Terrane. Most basalts from the eastern sequence (squares) plot along the same trend line as the ultramafic rocks (crosses) in the eastern sequence, whereas basalts to the west of the fault (diamonds), including those from within the Southern Cross Terrane (circles), plot along a different trend.

The geochemistry highlighted a group of ten mafic samples with unusually high REE enrichment, characterized by high Y concentrations between 50 and 1000ppm compared to typical values for basalts of ~25ppm (Hall 1996). SEM analyses revealed the presence of rare-earth phosphates in these samples, including xenotime and monazite. Two attempts to date the phosphates, were unsuccessful, owing to very low *U* and *Th* contents in the phosphate grains. The geochemical aspects of the study will be dealt with in more detail in van der Borgh's PhD Thesis.

Structure and Shearing-Related Metamorphism

The Ida Shear Zone (ISZ). The four regions of the ISZ studied in detail (Fig. 2.5.2) over a strike length of 150 km, exhibit the same structural history and a similar sequence of rocks. Generally the shear zone is 100-200 m wide, and the shear fabric is formed along a sequence of alternating ultramafic and mafic flows and interbedded shales along the western side of the Eastern Sequence. The eastern margin of the shear zone is delineated by a gradual decrease in fabric intensity, commonly towards an ultramafic cumulate, and to the west by the appearance of monotonous pillowed basalt.

The progressive deformation of the ultramafic rocks results first in the flattening of serpentine and magnetite grains, followed by a gradual increase in the modal abundance of tremolite and *Mg*-chlorite at the expense of serpentine. In the most deformed regions, serpentine and magnetite are absent, and the paragenesis is tremolite + actinolite + *Fe*-chlorite. The breakdown of magnetite seems to have liberated *Fe* for chlorite, while *Mg* from *Mg*-chlorite was taken up by actinolite. Thus, shearing has led to the destruction of magnetite and the associated signature in aeromagnetic imagery. The increase of water-poor tremolite at the expense of water-rich serpentine implies deformation was accompanied by devolatilization as reflected in the decrease of LOI from 9.5 wt% in the least deformed rocks, to 4.5 wt% in the core of the shear (ven der Borgh, PhD Thesis in prep).

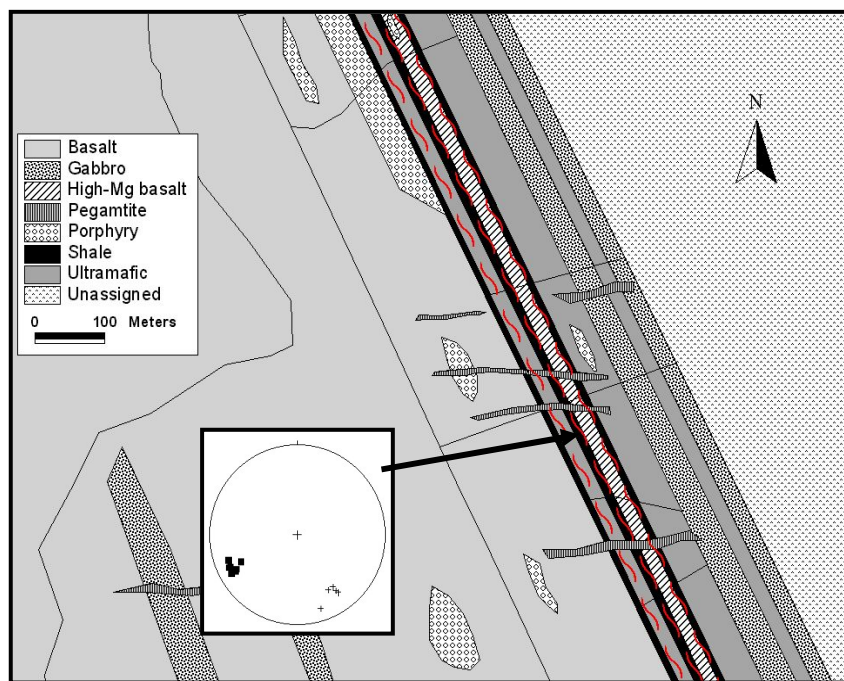


Fig. 2.5.5. Solid geology map of the Ida Shear Zone in the Mt Alexander region, showing the trace of the shear zone along the contact between thinly bedded units of the eastern sequence and massive basalt to the west. The shear zone is marked in the figure by the thick black lines representing shale layers. The lower hemisphere stereographic projection represents structural measurements from within the shear zone (squares are poles to the foliation, crosses are lineations).

The map in Fig. 2.5.5 details the stratigraphic and structural observations from the Ida Shear Zone in the Mt Alexander region, and is representative of observations along the strike length of the structure. The shear zone is typically sited along the contact between thinly bedded mafic-ultramafic rocks and interbedded shales to the east, with massive basalt to the west. The

foliation consistently dips steeply to the east, and contains a gently south plunging mineral lineation (stereonet insert in Fig. 2.5.5). A lack of asymmetries within the shear zone indicates that the deformation is primarily the product of pure strain.

The Riverina Gneiss. The Riverina Gneiss extends along the entire eastern margin of the Ularring Greenstone Belt (Fig. 2.5.2). It is characterized by a banded magnetic fabric that delineates a ~6km-wide belt in aeromagnetic images and was interpreted by Legge et al. (1990) to be a major crustal break. The gneissic banding is very strong for several kilometres in width, suggesting very high strain (Figs. 2.5.6 and 2.5.8).



Fig. 2.5.6. a) Outcrop of Riverina Gneiss at Kurrajong highlighting the gently plunging mineral lineation. b) Polished slab of gneiss from the above locality, showing gneissic banding and lack of consistent asymmetries, indicating deformation was a product of essentially pure shear (scale bar in cm)

The gneissic banding strikes N-S (Fig. 2.5.9 stereonet insert), and contains an intense, sub-horizontal mineral lineation in all outcrops observed (Fig. 2.5.6a). Embry (1999) depicted porphyroblasts showing dextral asymmetry. By contrast we found that the majority of porphyroclasts in the gneiss have either opposing or poorly developed asymmetries, indicating intense flattening or pure shear deformation (e.g. 2.5.6b).

SHRIMP U-Pb dating of fourteen zircon grains separated from the gneiss yielded an age for the zircon cores, interpreted as the crystallization age of the granite precursor, of 2806 ± 5 Ma (Fig. 2.5.7). Interpretation is based on the fact that zircon cores are euhedral, well zoned, and of similar habit, indicating a likely common igneous origin. Also the ages are well centred around

the average age and lack a wider age spread common in a xenocrystic population. Rim overgrowths, which cross-cut core zoning on six crystals, yielded an age of 2667 ± 15 Ma, which is interpreted to represent a resetting age caused by metamorphism or hydrothermal alteration. This interpretation is based on the fact that the concordant analyses have high Th/U ratios, consistent with metamorphic or hydrothermal recrystallisation (N.J. McNaughton, pers comm.), the overgrowths are not concentrically zoned as would be expected from magmatic overgrowths, and no cores yielded the younger age. The implications of these two ages are discussed below.

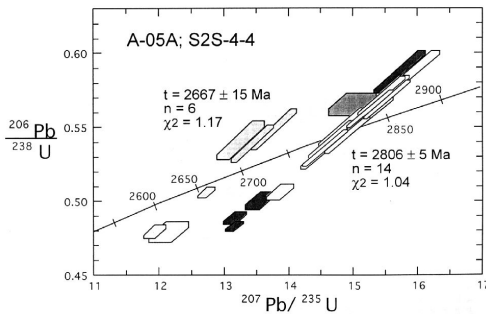


Fig. 2.5.7. Results of SHRIMP U-Pb zircon age determination of the Riverina Gneiss.

The Ballard Shear Zone. In this report, the term Ballard Shear Zone is used to describe a zone of shearing that is developed along the contact between the Riverina Gneiss and the Ullaring Greenstone Belt (Fig. 2.5.9). The contact strikes N10W, and is therefore slightly oblique to the N-S gneissic fabric.

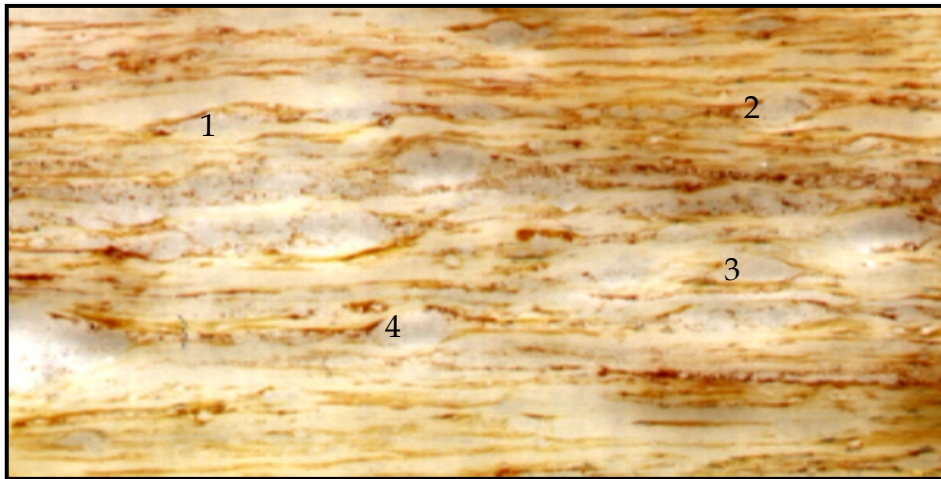


Fig. 2.5.8 Scanned thin-section of the Ballard Shear Zone. Horizontal C-fabric and ENE-WSW S-fabric, in conjunction with asymmetries around quartz porphyroclasts (e.g. 1,2,3 & 4), indicate dextral shear-sense. Width of image is 2 cm.

We studied this shear zone at Kurrajong, where it is ~200m wide and incorporates several rock types, including ultramafic and mafic rocks, porphyries and the margin of the Riverina Gneiss. The shear fabric strikes ~N25W, is sub-vertical, and contains a stretching lineation that

plunges gently both north and south. Shearing of gneiss along the margin of the Riverina Gneiss has resulted in a quartz-mica schist, as a result of extensive recrystallisation of plagioclase and quartz. Asymmetries around porphyroclasts, S-C fabrics, and rotations of porphyroclasts indicate dextral sense of shear (Fig. 2.5.8). The paragenesis and nature of shearing make it distinct from the broader Riverina Gneiss.

The Kurrajong Anticline. The core of the Kurrajong Anticline (Fig. 2.5.9) reflects, in a relatively small area, the regional deformation undergone by the Kalgoorlie Terrane. The lowermost units in the stratigraphy are an amphibolite layer and an anorthosite layer, which are folded around the Copperfield Granite. Around the margin of the granite, a strong gneissic fabric is consistently parallel to the contact and a strong mineral lineation, affecting all minerals, plunges ~30S. The orientation of the lineation is parallel to the axis of the fold, and similar features are observed in the greenstones adjacent to the granite where amphiboles are parallel to the stretching lineation in the granite.

The greenstone corridor to the east of the granite strikes N-S and has dextral kinematic indicators, while the western corridor strikes NW and has sinistral indicators. In many areas however, particularly close to the granite contacts, shearing and flattening has been intense and asymmetries or other kinematic indicators could not be determined.

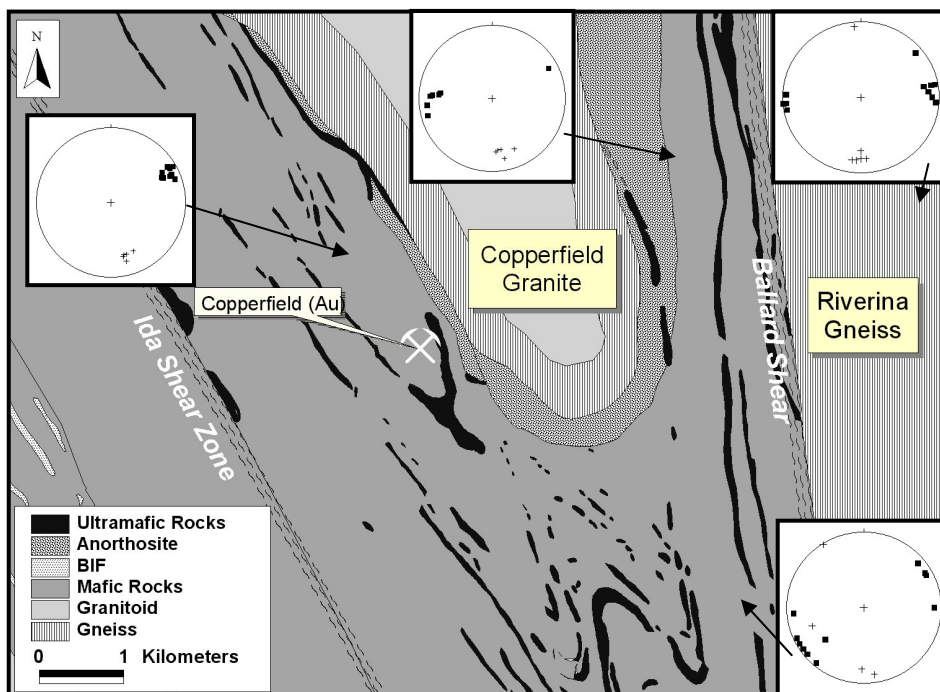


Fig. 2.5.9 Magnetic interpretation of the Kurrajong Anticline in the Mt Ida area. Note the variation in the orientation of foliations in the Riverina Gneiss and adjacent greenstones.

The change in sense of shear as a function of strike on either side of the granite, reflects the regional pattern of deformation observed of the Norseman-Wiluna Belt, where NW-striking shear zones generally register a sinistral movement, Zuleika and Boulder-Lefroy Shear Zones (e.g. *Section 2.4*, and Swager 1997), while NS or NNE-striking shear zones register dextral movement (Waroonga Shear Zone, Platt et al. 1978). This pattern will be discussed in *Section 2.7* where it will be suggested that the two sets represent conjugate shear zones, resulting from D_3 regional deformation event driven by ENE-WSW shortening.

Brittle-Ductile Structures. The Ularring Greenstone Belt contains three sets of brittle-ductile and brittle structures that are observed both on aeromagnetic images and in the field. A set of NNE-SSW brittle-ductile shear zones offset stratigraphy by tens to hundreds of metres. They are recognised in occasional outcrops as a spaced cleavage (Fig. 2.5.10). Macro- and micro-scale asymmetries associated with these shears consistently show dextral shear sense (Fig. 2.5.10). A second set characterized by NE-SW faults are observed, although unlike the previous

set, they have a more localised distribution, for example along the eastern margin of the Copperfield Granite. Offsets are rarely more than tens of metres, and displacements are consistently dextral. These structures have not been observed in outcrop.

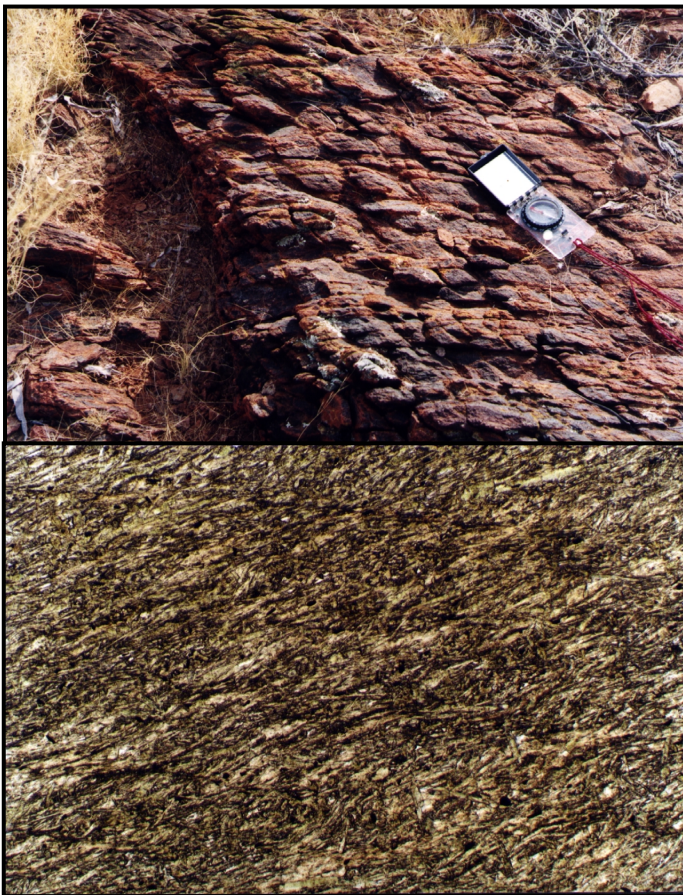


Fig. 2.5.10. a) Early, Ida Shear Zone foliation (horizontal in view) is overprinted by a later spaced NE-SW cleavage, (depicted by orientation of compass). b) Photomicrograph from the above outcrop, showing the same shear fabric (diagonal top right-bottom left) being overprinted by the NE-SW spaced cleavage (horizontal). Note the rotations of the early fabric into the late cleavage showing dextral asymmetry.

The third set consists of ~E-W brittle faults, which also tend to have a localized distribution, such as at the southern end of the Copperfield Granite and along its western margin. This set is usually recognised in the field by buck quartz veins and brecciation of wall rocks. Epidote alteration is observed where the faults are developed in mafic rocks. They consistently show sinistral displacement.

Deviations from Main Trend: Indentation. The Ida Structural Corridor deviates from its dominant regional trends around the Central Granite Complex, CGC (Fig. 2.5.11). The main trend of lithological contacts, the trace of the fold hinge of the Kurradjong Anticline, and the fabric defining the Ballard Shear Zone, are all rotated by ~20°, counter clockwise they approach the CGB. Deflection of the Riverina Gneiss resulted in the development of conjugate fractures dominated by a set of N70W strike-slip faults with sinistral offsets of up to 600m as interpreted from aeromagnetic imagery, and dextral NE faults with undetermined offset (Fig. 2.5.12). We interpret the deflection to be the result of progressive shortening of the greenstones as the CGC, representing a competent indenter to the west, impacted upon them.

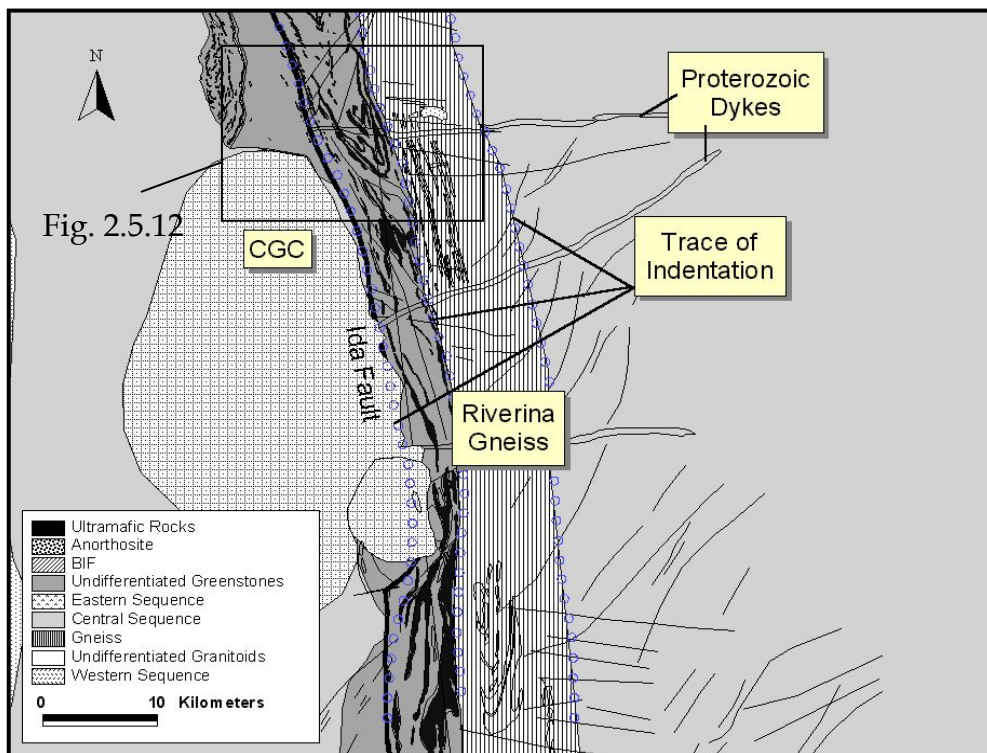


Fig. 2.5.11. Interpretive map of the Central Granite Complex (CGC), located in the area between Mt Ida and Riverina. The image highlights the trace of the 'indentation' observed in the greenstones and gneiss adjacent to the CGC, and the conjugate structures that developed in the gneiss and Eastern Batholith in response to the indentation.

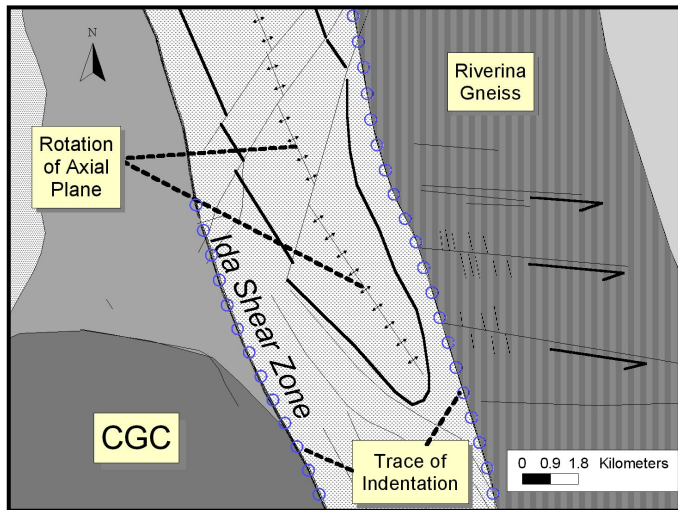


Fig. 2.5.12. Schematic interpretation of the northern part of the CGC, highlighting the 20° counter-clockwise rotation of the Kurrajong Anticline, and associated NNE dextral faults that have accommodated the rotation of blocks. Notice how indentation of the gneiss was accommodated by sinistral ~E-W structures. These structures delineate the northernmost extent of the indentation, which can be observed southwards for ~40 km.

Gold Deposits along the Ida Structural Corridor

Despite being poorly endowed in gold, more than one hundred mines are documented within 10km of the Ida Shear Zone but to date, no deposits have produced >500,000oz. In this section, we focus on three areas where gold production has exceeded 50,000 ounces, namely Copperfield (Fig. 2.5.9) and Bottle Creek in the Mt Ida area, and Iguana, south of Davyhurst.

Copperfield. The camp is located on the western margin, and towards the southern end, of the Copperfield Granite, approximately 2 km east of the Ida Shear Zone (Fig. 2.5.9). To date five parallel lode structures have been mined for a total production of >300,000oz, with the Timoni lode producing >250,000oz. Prior to the mid 1980s, the Timoni mine ranked in the top 12 producing mines in the Eastern Goldfields. All stratigraphic units in the camp, including amphibolite, anorthosite and ultramafic lithologies, host mineralisation.

The Timoni Lode is hosted in amphibolite. Mineralisation occurs in podiform quartz-carbonate veins up to 1m in thickness, enveloped in a biotite-carbonate schist. Mining continued to a depth of 300m, and for a strike length >500m. The majority of gold won was free in the quartz veins, with lesser amounts in pyrite sited along vein margins and alteration selvages. The structural controls on mineralisation are poorly documented and not well understood. The lode is disjointed by several ~E-W trending crosscutting structures, which have been variously interpreted to have been active pre- and post-mineralisation.

Features of the Timoni Lode in common with mineralisation elsewhere include the potassic alteration, a competency contrast owing to its proximity to the granitoid, and the intersection of the lode by cross-structures. Furthermore, schistose ultramafic rocks are adjacent to the lode.

Bottle Creek. The three mines at Bottle Creek are located within the Ida Shear Zone. The pits are currently full of water and inaccessible, however the stratigraphic relationships (ultramafic-mafic-shale lithologies) and easterly dips that characterise the shear zone, as outlined above, are recognisable. The deposit was described by Legge et al. (1990), from which the following is taken. Mineralisation is hosted in a banded amphibolite that defines the upper part of the central sequence, and a porphyry. Shearing along the contact is intense, with the mafic mineralogy being altered to biotite-hornblende-chlorite-epidote-quartz schist, with garnet porphyroblasts, while the margin of the porphyry is quartz-sericite schist. Mineralisation is coincident with an arsenic anomaly (>500ppm), which is similar to many sediment hosted gold deposits in the Yilgarn. Unlike most orogenic lode gold deposits in the Yilgarn Craton, this mineralisation has a Au/Ag ratio <1. In general, gold grades in the primary zone rarely exceeded 3 g/t, while silver grades in the areas of highest gold grade averaged >27 g/t. Gold was very fine grained (<45 μ m diameter), occurring both as free particles, and as inclusions in quartz and sulphides. Gold distribution was very even, and without ‘nugget’ effects. The report does not detail the structural controls on mineralisation.

In some respects, this line of deposits contrasts with typical lode gold deposits, for example the Au/Ag ratio <1, and its location within the plane of a first-order shear zone. Similarities to lode-gold deposits include the ultramafic and porphyry associations. Furthermore, the deposits are situated within a corridor of NNE orientated structures with apparent dextral offset. However, not enough is known of the structure, metamorphism or metasomatism of the deposit to reliably compare these to mineralisation elsewhere in the Kalgoorlie Terrane.

Iguana. The Iguana deposit is located ~30 km south of Davyhurst, and 1.5 km east of the granite-greenstone contact, which marks the Ida Shear Zone in this area. The deposit is of particular interest as it is only ~15 km north of where the 1991 seismic traverse (EGF01) crossed the Ida Shear Zone. There are no published descriptions of the deposit. The pit is located in a sequence of interleaved ultramafic, mafic, and sedimentary rocks. Outcrop in the vicinity of the mine is very poor, and the open pit is intensely weathered, and no detailed mapping is available. The mine stratigraphy is dominated by amphibolite, consisting of *Mg*-hornblende, *Ca*-plagioclase ($An_{>80}$) and titanite. The amphibolite contains numerous grains of HREE-phosphate, including xenotime and other unidentified species as well as small zircon grains. Pyroxene-rich boudins are observed towards the central portion of the pit, and distinguished by their pale green weathering colour. Pegmatite dykes intrude the sequence.

The main shear fabric strikes N40W and dips 80SW. A consistent down-dip mineral lineation is defined by acicular amphiboles. Boudin necks in the pyroxene-rich lenses plunge gently north and south, and provide further evidence for vertical extension. Rare asymmetries around competent porphyroclasts indicate a west-side-up shear sense.

The shear fabric is overprinted by a gently dipping foliation (variable strike N60W to N10W, dipping 20-40NE). The origin of this late foliation is unknown, and clear shear sense indicators could not be found. We note however, that the seismic image depicted a gently E-dipping foliation at depth, south of this locality, which was interpreted to be a result of normal faulting (e.g. Swager 1997). Gold was won from quartz veins, with associated biotite alteration of the amphibole schist. The veins were sited within a narrow zone where the amphibolites have been boudinaged. Arsenopyrite is the main ore mineral, and gold is in these grains (SEM imaging). Gold has also been imaged in one of several potassium feldspar veinlets that brecciates the main shear fabric (Fig. 2.5.13a&b). The veinlets are not sheared or rotated, indicating that

mineralisation took place after the foliation developed

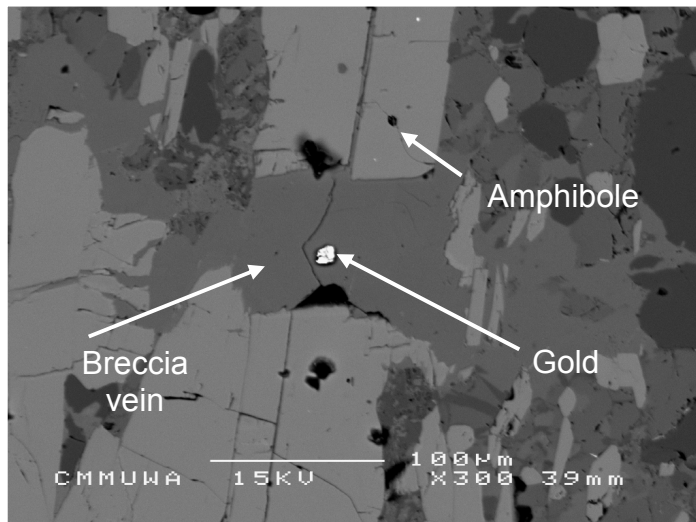
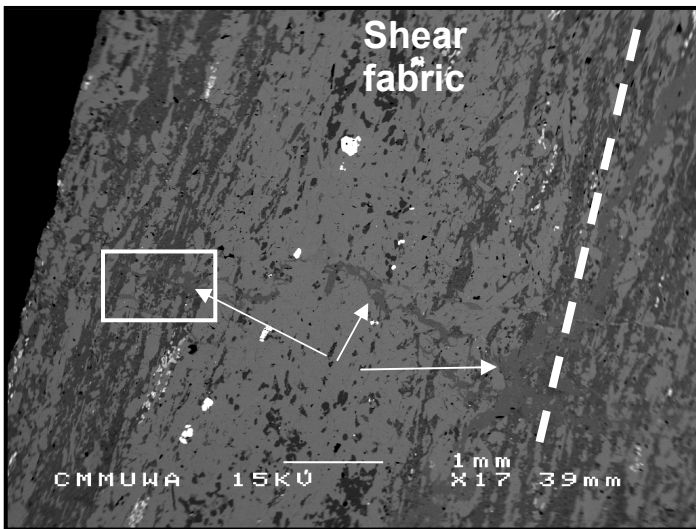


Fig. 2.5.13. Scanning Electron Microscope images of a) the shear fabric at Iguana, highlighting the potassium feldspar breccia veins that cross-cut the main shear fabric, and are themselves undeformed. b) Inset in (a), showing a potassium feldspar breccia-vein hosting a gold inclusion. The undeformed nature of the veinlet, and presence of gold, indicate mineralisation post-dated the main shearing event at Iguana.

In summary, the deposits along the Ida Shear Zone have some characteristics similar to those elsewhere in the Kalgoorlie Terrane, such as: a) the As-anomalies in the two deposits in proximity to sedimentary horizons (i.e. Bottle Creek and Iguana), and the absence of an As-anomaly at Copperfield, where no sediment is present; b) potassic alteration; and c) pyrite and arsenopyrite as the main sulphide mineralogy. Mineralisation at Iguana and Copperfield post-dates the formation of the regional shear fabric. Decreased contrast in the behaviour of rock types under deformation at amphibolite facies conditions, as compared to greenschist facies conditions, might be the single most significant cause for the decreased endowment along this shear zone.

Discussion

The Ida Shear Zone is an intra-greenstone structure within the more extensive Ida Structural Corridor. Strain developed along a stratigraphic break where massive, pillowed tholeiitic basalts to the west, meet a sequence of thinly bedded basalts and ultramafic rocks. The continuity of the ultramafic-mafic stratigraphy along the eastern half of the Ularring Greenstone Belt and possibly into the Ora Banda Domain supports earlier interpretations (Hill et al. 1995, Rattenbury 1993) that it belongs to the Eastern Goldfields Terrane. This interpretation contrasts with suggestions that a major crustal break exists along the margin of the Riverina Gneiss, at the eastern margin of the Ularring Greenstone Belt (Legge et al. 1990).

Contrasting stratigraphy on either side of the ISZ as mapped here suggest that it represents a terrane boundary between the Southern Cross Terrane, which includes banded iron formations in its stratigraphy, with the Norseman-Wiluna Belt, which includes ultramafic rocks in its stratigraphy. Unfortunately, although the geochemistry of basalts highlights different fractionation in rocks on either side of the ISZ, it did not positively discriminate the basaltic sequences on either side. Furthermore, no dateable volcanic rocks have been found to determine any age differences the sequences might have. The fact that the Ida Shear Zone is a fundamental stratigraphic break will be used at the end of this section to build a new model for deformation along the eastern margin of the Eastern Goldfields Terrane.

Lithologies and fabrics in the shear zone consistently strike ~330 and dip ~70E. The south plunging lineation in the Mt Ida and Mt Alexander regions is sub parallel to the axis of the Kurrajong Anticline which controls the orientation of the greenstones in the northern part of the Ularring Greenstone Belt. The structures are interpreted to be a result of intense straining, with a

sub-horizontal or gently south plunging extensional direction associated with folding and flattening of the rock sequence as a result of pure shearing with a minor dextral component.

A late, gently east dipping foliation was documented at Iguana. Owing to its proximity to the position of the seismic traverse, it may represent what was imaged in the seismic reflection survey. However, because this foliation was not observed elsewhere in the Ularring Greenstone Belt, there is a possibility that it represents a relatively local feature. An alternative interpretation for the shallow dipping seismic reflector is that it represents a listric fault that links upwards with the steeply dipping foliation characteristic of the outcropping Ida Shear Zone. Neither interpretation is fully satisfactory as yet, and more structural information and detailed seismic imaging of this important boundary zone is required to further elucidate its nature at depth.

The ages determined from the Riverina Gneiss are broadly consistent with older ages reported from gneisses on the eastern side of the same batholithic mass (west of Leonora, Witt 2001) suggesting that a significant portion of the batholith, including the gneissic margins, represent older continental crust that formed the basement for the 2.7 Ga extrusive and sedimentary sequences.

In some respects, the deformation observed in the Ida Corridor differs slightly from some of the other regions we have documented, and largely reflects the metamorphic conditions that accompanied deformation. Typically, rocks within the deformed corridor are intensely deformed indicating pervasive deformation, and even though competency contrasts between rock types was sufficient to trigger large scale folding (e.g. Kurrajong Anticline; a fold around a granite core), and local boudinage, it was not nearly as strong as in greenschist facies areas, where low-viscosity talc-schist and shales coexists with brittle porphyry dykes and dolerite sills. Brittle fracturing and rock brecciation, though it exists locally, is relatively uncommon in the Ida Corridor.

In general, the major structural features observed in the Ularring Belt are entirely consistent with the pattern of deformation we have observed elsewhere in the Kalgoorlie Terrane. The sinistral and dextral pair of shear zones observed along the western and eastern margins of the Copperfield Granite reflects the influence of the varying orientation of the granite margins in controlling the shear sense in an environment of ENE-WSW shortening. ENE-WSW shortening, and sub-horizontal stretching axis oriented parallel to the regional fabric, is similar to the regional D_3 while upright and tight folds, and reverse movement such as at Iguana, suggest a component of crustal thickening, which probably relates to the regional D_2 . In the Ida Corridor these two phases are not as distinct as they are in the Boulder-Lefroy Shear Zone. It is argued here that

because the ISZ is oriented nearly perpendicular to the maximum shortening axis during D_2 and D_3 most of the shear recorded is pure shear, with little difference between the structures developed during the two phases

The later, brittle-ductile and brittle fault sets that overprint the regional fabric are assigned to the regional D_4 and are similar in their orientation, shear sense, and physical character, to those in other parts of the Terrane (see *Zuleika Shear Zone* below).

We conclude that the deformation pattern in the Ida Structural Corridor is a function of the interaction between a long-lived regional shortening event, and the presence and geometry of pre-existing granitoids, during peak-metamorphic and retrograde conditions. Deformation along the Corridor occurred in an environment of high strain, in which shear sense was a function of the orientation of pre-existing contacts, such as those along granite margins.

2.5.2. The Zuleika Shear Zone

Introduction

The Zuleika Shear Zone was selected for this study because of its intermediate gold endowment and its location between the Boulder-Lefroy and Ida Shear Zones. A high strain corridor can be traced on aeromagnetic images, from a northern limit on the SW margin of the Mt Pleasant Dome, to its southern limit west of Democrat, a distance of ~200km. The Ballard Shear Zone has been interpreted to represent the northward continuation of the Zuleika Shear Zone (Legge 1990, Wyche and Witt 1992).

During the course of this study, we visited the northwest deposits of Chadwin, Ant Hill and Bullant, the central deposits of Centenary, Strezlecki and Barkers at the Kundana camp, and Cave Rocks at the southern end, as well as regional outcrops. This report incorporates existing data with our new data, and provides a new insight into the role of the Zuleika Shear Zone during deformation of the Kalgoorlie Terrane, and associated mineralisation.

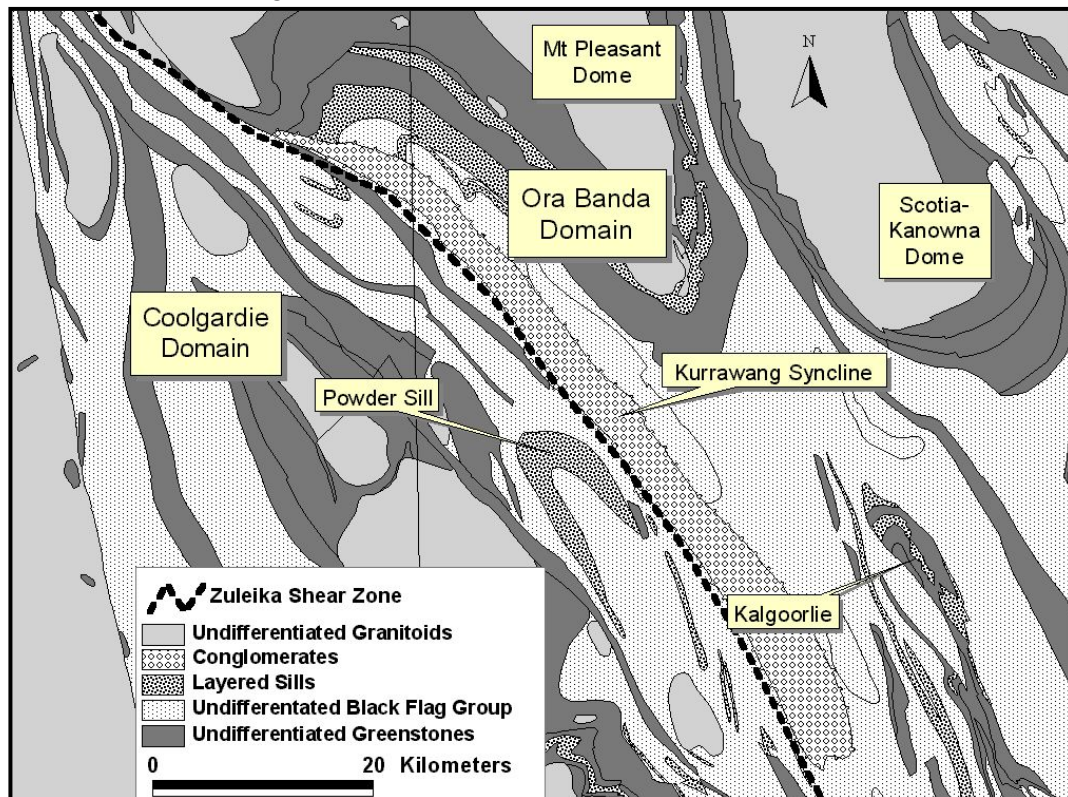


Fig. 2.5.14. Simplified geological map of the northern portion of the Zuleika Shear Zone (modified after Groenwald et al 2000), highlighting the major features discussed in this section of the report. Note the broad curvature of the Zuleika Shear Zone, and corresponding curvature in the Kurrawang Syncline.

Previous Work

Portions of the Zuleika Shear Zone have been documented within the Davyhurst (Swager 1994), Bardoc (Witt 1990), Kalgoorlie (Hunter 1993), and Yilmia (Hunter 1993) 1:100,000 GSWA map sheets. The Zuleika Shear Zone was delineated by these workers as a curved zone, forming the western boundary to the Kurrawang Syncline where it strikes NW and rotates to a more southerly trend to the south (Hunter 1993) cutting west of the Merougil sedimentary rock sequence that forms a synclinal structure similar to that of the Kurrawang Syncline. Swager (1994) defined the Zuleika Shear Zone as a domain boundary fault, separating the Coolgardie Domain from the Ora Banda and Kambalda Domains (2.5.14).

Sparse outcrops of strongly deformed rocks indicate the zone to be as much as 1km wide. On the Bardoc 1:100,000 map, Witt (1990) estimated the width to be between 100m and 1km, and noted that deformation was located between an ultramafic unit to the SW and a sedimentary rock to the NE, although the contact is not exposed. Tripp (2000) studied the ZSZ in the Ant Hill, Bullant, Porphyry and Wattlebird gold deposits on the northwestern section of the shear zone, and concluded that the structure was a zone of interlinked, anastomosing, mylonitic fabric, of sinistral displacement, which preferentially partitioned along lithological contacts and internal heterogeneities such as pillow margins.

Swager (1994) also reported sinistral asymmetries within the zone, a feature also noted by Witt (1993) at Hawkins Find and Zuleika. Witt (1993) documented moderately plunging (~45NW) mineral lineations at these locations, while those at Bullant and Wattlebird are sub-horizontal (Tripp 2000). Stratigraphic mismatch and lack of cross cutting relationships hamper the estimation of the amount of displacement along the shear zone (Swager 1994).

Witt (1993) documented widespread porphyry dykes in the vicinity of the Zuleika Shear Zone and Tripp (2000) described porphyry intrusions preferentially intruded into ultramafic rocks, and interpreted these to be syn- to late-shearing, based on the wrapping and truncation of shear fabrics.

Results from the 1991 and 1999 Yilgarn seismic surveys indicate that the Zuleika Shear Zone itself is not reflective, but displacement of planes cut by it lead to the interpretation that it dips to the east (Goleby et al 2000).

Stratigraphy and Metamorphism

As noted above, the ZSZ is a boundary between the Ora Banda and Coolgardie Domains. The Ora Banda Domain, situated to the NW of the Zuleika Shear Zone, has a well-defined stratigraphy described by Witt (1990), and not repeated here. It is important to note, however, that the Ora Banda Domain includes a significant ultramafic sequence known as the Walter Williams Formation, which has been recognized in several greenstone belts (Hill et al 1995), including the eastern portion of the Ularring Greenstone Belt, as previously mentioned. The two uppermost layers in the ultramafic-mafic sequence, termed the Bent Tree and Victorious Basalts, crop out along, and define, the NE margin of the Zuleika Shear Zone. In the context of the ZSZ and its gold deposits, the two basalt sequences, and rocks at the base of the Black Flag Formation, are particularly important. Particularly important is the role of the Centenary Shale, which is a recognized marker horizon at the interface between the Victorious Basalt, and the Black Flag Formation (Beeson, pers. comm.) within the Ora Banda Domain, and hosts a significant proportion of the mineralisation at Kundana. In the vicinity of the shear zone these rocks are exposed, dipping steeply to the SE, and attenuated.

West of the ZSZ, in the area of Dunnsville (northern section of the shear zone), the stratigraphy has been correlated with that of the Coolgardie Domain (Swager 1994) and consists of a lower basalt and dolerite, overlain by 600m of ultramafic flows and interflow sediments. These mafic-ultramafic rocks are overlain by the Spargoville Formation, which is defined as the felsic volcanoclastic lower section of the Black Flag Group by Krapez et al (2000). To the SW of Kundana, these intermediate to felsic volcanoclastic rocks are intruded by a differentiated dolerite termed the Powder Sill. The stratigraphy of the Coolgardie Domain differs from that of the Ora Banda Domain in that it lacks the Upper Basalt horizons between the ultramafic rocks and the Black Flag Group (Hunter 1993).

An overview of metamorphism in the Kalgoorlie Terrane was presented by Witt (1993). In his metamorphic map (Fig. 2.4.1), much of the Ora Banda Domain is indicated to be low- to mid- greenschist facies, and amphibolite facies rocks occur proximal to the granite domes. West of the ZSZ, metamorphic facies is generally higher than to the east, but the greenschist facies/amphibolite facies isograd cuts the shear zone to the SW of Kundana. The Spargoville Formation is depicted in Witt's (1993) map to be upper greenschist to lower amphibolite facies. Because the isograd cuts the shear zone at a high angle, the ZSZ does not mark a change in metamorphic facies.

Regional Folds

The Kurrawang Syncline forms the NE margin to much of the arcuate central and northern portions of the ZSZ. The axial trace of this fold is parallel to the arcuate shear zone (Fig. 2.5.14). To the SW of the Zuleika Shear Zone, a corridor of intensified deformation is characterized by a broad-scale synclinal structure (the Powder Sill Syncline), and minor folds within the Spargoville Formation (Fig. 2.5.14). These folds are well defined in aeromagnetic imagery.

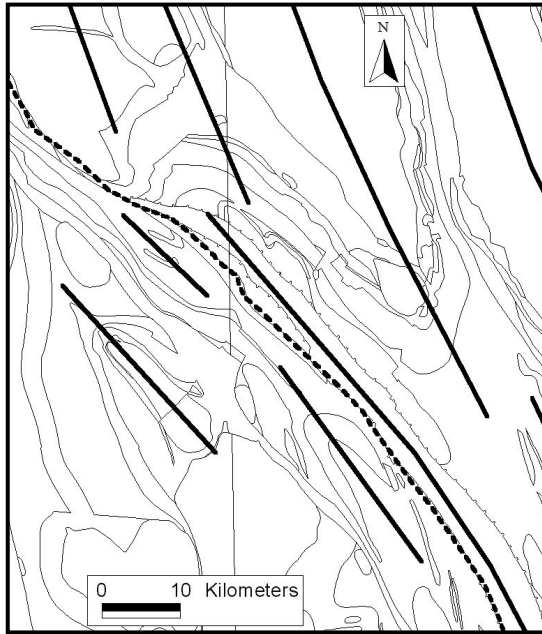


Fig. 2.5.15. Lithological contact map of the area depicted in Fig. 2.5.14, showing the orientation of major folds in the region. Note the obliquity of fold traces adjacent to, and SW of, the Zuleika Shear Zone, relative to those to the NE (see text for explanation). Note also similar orientation of the SW folds to the orientation of the Zuleika Shear Zone.

The open Powder Sill Syncline in the center of the corridor contrasts with increasingly tighter folds towards the ZSZ. At Kundana, rocks that belong to the Powder Sill define a tight anticline with attenuated limbs, as revealed by recent drilling (S. Halley pers. comm.). The NE limb of this anticline forms the SW margin of the ZSZ, where it is in faulted contact with the upper greenstone units of the Ora Banda Domain.

NE of the Kurrawang Syncline, fold structures defining the Mt Pleasant Dome trend ~N25W (Fig. 2.5.15), and formed in response to regional D_2 . The axial traces of these folds are markedly oblique to the N45W-trending folds SW of the ZSZ outlined above (Fig. 2.5.15). The difference in the orientations of these folds is central to understanding deformation in this region and will be dealt with in later discussion.

Late Brittle-Ductile Structures

Numerous N-S to NNE-SSW oriented faults in the region are observable on aeromagnetic images. Several of these can be traced along strike for over 50 km, while many are more than 10

km long. Tripp (2000) defined three principal orientations, a N-S set, a NE-SW set and an E-W set which closely match those in the Ida Structural Corridor. Offsets range from a few metres to a maximum of hundreds of metres, and the sense of displacement is consistently dextral for the N-S and NE-SW sets, and sinistral for the E-W set (Tripp 2000). Furthermore, Tripp (2000) reported the sets of faults to have mutual overprinting relationships, to be brittle-ductile in style, and to crosscut the Zuleika Shear Zone.

Field Observations

Owing to sparse outcrop and degraded sample material, structural analysis of the Zuleika Shear Zone for this project has concentrated on open pit exposures. Ten pits considered to be within the Zuleika Shear Zone were visited over a strike length of ~200 km, from Chadwin in the north to Cave Rocks in the south. Drill core from the recently discovered Raleigh deposit was also observed and sampled for SEM work and microstructural analysis. In this section only the major findings will be described. Full description of the data assembled will be presented in van der Borgh's PhD thesis. For descriptive purposes, individual mines are grouped into geographical camps, namely Chadwin, Bullant, Kundana and Cave Rocks (Fig. 2.5.16).

Chadwin. The Chadwin pit is oriented N45W in its longest dimension, and is located a few hundred meters south of the margin of the Siberia Granite. The pit exposes the contact between interleaved quartzo-feldspathic sedimentary rocks and ultramafic rocks to the SW, and the Victorious Basalt to the NE. A pegmatite dyke lies close to the contact. The western sequence is isoclinally folded and the axial planar cleavage strikes ~N70W and dips 54S, and fold axes plunge ~30/160. The ultramafic layers are boudinaged and boudin necks plunge moderately WNW.

Rocks in this pit are strongly elongated and locally give rise to *l*-tectonites and sheath folds. *S-C* fabric and asymmetries around porphyroclasts indicate NW-directed thrusting, parallel to the lineation. A shear fabric striking N40-45W and dipping 70SW is developed along the axis of the pit, at the contact between the two sequences. The parallelism of the long axis of the pit with this shear zone suggests that it hosted the mineralisation, although this could not be confirmed. The hornblende-plagioclase ($An_{>85}$) mineralogy of the Victorious Basalt implies low- to mid-amphibolite facies metamorphism.

Wattlebird and Bullant. The pit at Wattlebird exposes a 25 m wide, high-*Mg* pillow basalt juxtaposed against ultramafic rocks. A 10-15 m wide shear zone at the contact is

interpreted by Tripp (2000) to represent the Zuleika Shear Zone. Small, attenuated porphyries are observed in the ultramafic schist, while a chlorite-biotite schist in the basalt hosts gold mineralisation. Pillows become increasingly flattened and attenuated towards the zone of shearing, and have long axes parallel to the shear foliation, which in this zone strikes ~N30-40W, and dips >80E, with a gentle north plunging stretching lineation (Fig. 2.5.16). Highest gold grades occur in a ~20m-wide, N-S trending vein array, where the ZSZ is intersected by a N-S trending brittle-ductile fault (Tripp 2000).

At Bullant, the pit is developed wholly within high-Mg pillowed basalt, which is a thickened version of that seen at Wattlebird. The basalt is cut by a series of 0.5-20m-wide ductile shears zones that Tripp (2000) interpreted to be the Zuleika Shear Zone. The average strike-orientation of these shear zones is N28W with a dip of 88/SW (n = 28: Tripp 2000), with gentle to moderate north plunging lineations, all of which was confirmed by our own measurements. In all instances, *S-C* fabric and asymmetries showed sinistral sense of shear (Tripp 2000). High-grade mineralisation at Bullant is also associated with the intersection of the main shear zone and a cross-cutting, NNE orientated, brittle-ductile fault. The foliation in the cross-fault has *S-C* fabric and asymmetries around porphyroclasts indicative of dextral shear sense. The westernmost lode-structure has a dextral jog that is coincident with the intersection of this cross-fault, and also correlates with higher gold tenure. Ore minerals and fine grains of free gold are hosted in quartz-carbonate veins or disseminated in silicates in sheared rocks. Biotite and carbonate are the principal alteration minerals, while ore minerals include galena, sphalerite, pyrrhotite, pyrite and marcasite (Tripp 2000).

Kundana. The Kundana camp incorporates numerous deposits, with mineralisation now recognized along a 14 km strike length, and a total resource >6Moz (S. Halley pers. comm.). Shearing and mineralisation occur along two sub-parallel trends. An eastern line follows the trace of the Centenary Shale, which, owing to the presence of the Ora Banda Domain's Victorious and Bent Tree Basalt to the SW, lies in that Domain. The western line lies within the Coolgardie Domain and is limited to the SW by the Powder Sill.

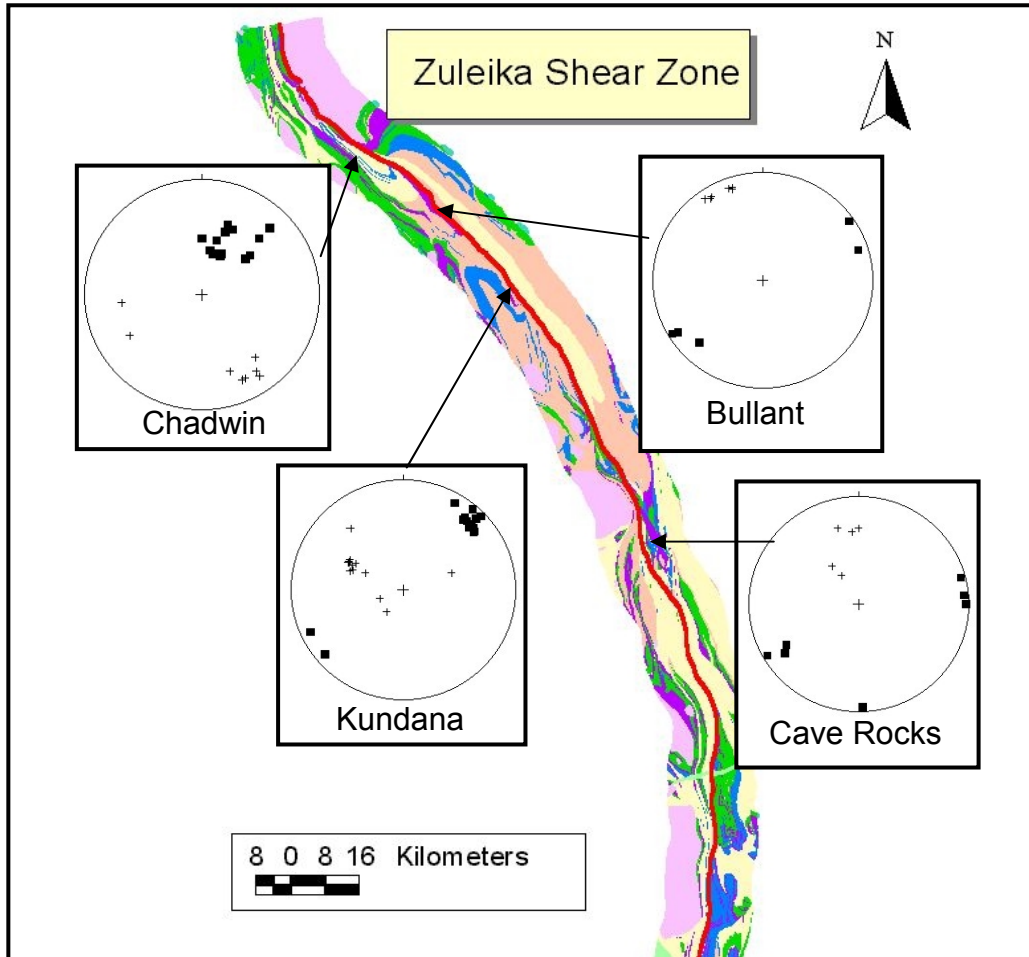


Fig. 2.5. 16. Lower hemisphere equal area projections of structural measurements from the four mine camps visited during this study. Black squares are poles to foliations, crosses are lineations.

The stratigraphy and structures have been segmented and displaced by a series of ~N-S trending brittle-ductile shear zones, and brittle faults with quartz breccias, which show a consistent dextral offset, with up to 600 m displacement. The correlation between N-S faults and gold deposits is typified at Kundana, although the role of the structures in the mineralisation process is obscure. Economic mineralisation is invariably hosted in structures that follow the regional NNW-NW trend, while the N-S to NNE-SSW structures very rarely contain economic gold values. However, grades tend to increase in the vicinity of the N-S and NNE-SSW structures, suggesting a possible relationship between mineralisation and these cross-cutting structures.

Eastern Line (Centenary Shale). The North and South Pits at the Kundana main camp show similar mineralisation styles, and lithological and structural characteristics. Mineralisation occurs in ribboned, crack-seal veins within the *Centenary Shale*. Ore minerals include pyrite,

pyrrhotite, arsenopyrite, and base metals such as galena, sphalerite and scheelite (S. Halley, pers. comm.). An arsenopyrite halo is often observed around the veins.

South Pit exposes a 200m-wide zone of gradational shearing, which incorporates the Centenary Shale at its core, the Victorious Basalt to the SW, and an intermediate volcanoclastic rock to the NE. The shear fabric in the shale and Victorious Basalt is sub-parallel to the contacts, striking N45°W and dipping steeply SW, with well-defined stretching lineation that plunges moderately north (Fig. 2.5.16). In the basalt, the lineation is defined by plagioclase grains, which are significantly flattened and elongated. Plagioclase grains have been wholly replaced by sericite. Chloritoid ‘spots’ are elongate in a similar orientation. A sub-parallel lineation in the shale is defined by stretched clasts, and voids that may represent weathered pyrites.



Fig. 2.5.17. Core from a high-grade intersection on the Centenary Line, showing a 30cm quartz vein within the strongly foliated Centenary Shale. Note the folded veins in the Shale, with axial-planes parallel to the foliation (width of view ~60cm).

Veins within the shear zone are folded and boudinaged (Fig. 2.5.17). The lineation is constant in orientation from the less deformed margin to the core of the shear zone. An *S-C* fabric and asymmetries indicate oblique sinistral shear sense at South Pit but not at North Pit. On the western wall of North Pit, a second structure, the K2B, is exposed along the contact of the Victorious Basalt and underlying Bent Tree Basalt. Here, we measured a steep west-dipping

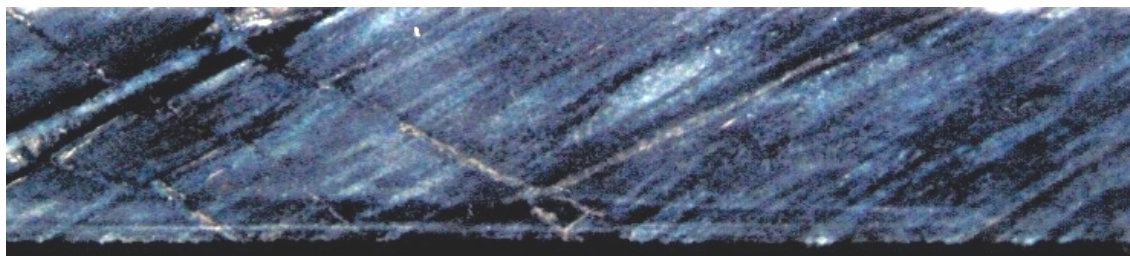


Fig. 2.5.18 Half-core from the Centenary line showing brecciation of the main shear fabric in the Victorious Basalt by mineralized veinlets, indicating that at least part of the mineralisation at Kundana was post the main phase of shearing (length of core is 20 cm).

foliation striking N50W, and a lineation in the Victorious Basalt plunging 70/S along the foliation plane. Asymmetries around the grains showed a consistent west-side-up (reverse) sense of shear. North and South Pits are displaced by a N-S striking fault with dextral offset.

Although the gold mineralisation occurs within the shear zone, there are several lines of evidence to suggest that mineralisation occurred later than the main phase of deformation. Figure 2.5.18 depicts a drill core through sheared Victorious Basalt at South Pit. The shear fabric is brecciated by quartz veinlets that are orientated both parallel, and at high angles, to the shear fabric. The veins host ore sulphides and have biotite selvages and are not sheared.

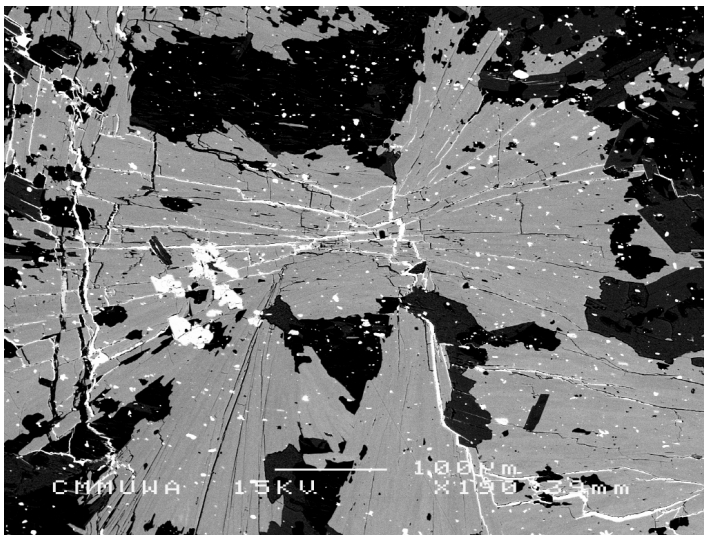


Fig. 2.5.19. SEM image of a chloritoid grain (grey) being brecciated and replaced by sulphides (white). Cross-cutting relationships such as these indicate that at least part of the mineralisation at Kundana post-dated the main phase of shearing.

The veinlets show mutual cross-cutting relationships indicating simultaneous formation, and clearly post-date the main shear fabric. Furthermore, the SEM image in Fig. 2.5.19, depicts a chloritoid grain which is aligned parallel to the shear fabric, brecciated and replaced by sulphides.

Western Line (Barkers-Strezlecki-Raleigh). The Barkers, Strezlecki and Raleigh pits are located approximately 250 m SW of the Eastern Line and define the Western Line. The Strezlecki Main vein is a laminated quartz vein (Fig. 2.5.20b), typically 0.5 m wide, and averages ~55g/t Au locally reaching above 100 g/t. The laminae represent slices of host-rock that became incorporated into the vein during multiple fracturing episodes. Petrographic analysis of the vein indicates laminae commonly take the form of stylolites (Fig. 2.5.21)

The ore at Raleigh and Strezlecki consists of a pair of parallel veins that are developed along the upper and lower surfaces of a 2-14 m wide, moderate SW-dipping felsic sedimentary unit. This unit has been offset along the Lucifer Fault, which strikes N10W, dips sub-vertically,

and has a total dextral displacement of ~600 m (J. Beeson, pers. comm.). The Raleigh and Strezlecki veins pinch out to the north and south respectively, as they approach the Lucifer Fault.

At Strezlecki, the Main vein sits between the upper contact of the felsic sedimentary unit and the Powder Sill. The vein strikes ~N50W and dips ~60SW (Fig. 2.5.20a). An intensely foliated biotite-rich layer is developed along the margins of the vein, and dips steeper than the vein (e.g. N50W/74SW). Laminae within the main vein are oblique to the strike of the vein (e.g. N35W), and have been interpreted to signify sinistral shear sense during vein formation (John Beeson, pers comm.). A stretching lineation on one lamina was measured to plunge 28/320. An increase in the number of laminations within the vein correlates with increased *Au* values (John Beeson, pers comm.).

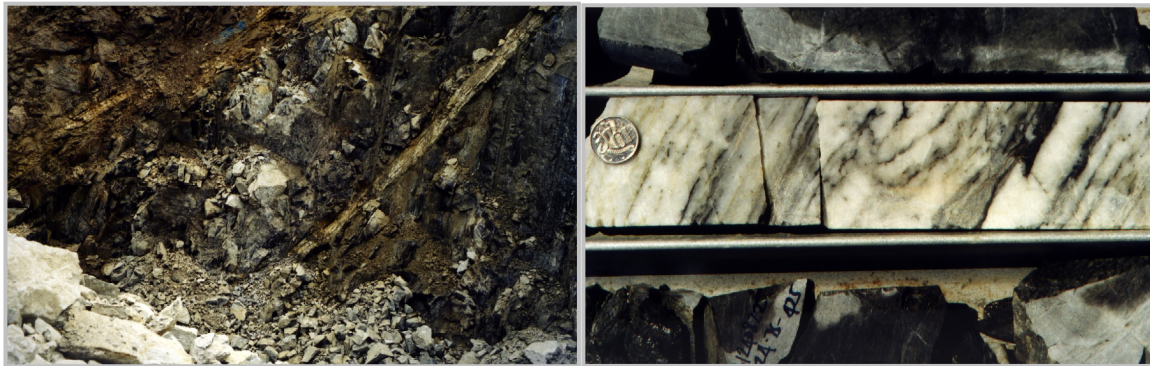


Fig. 2.5.20. a) Looking NW at the moderately SW-dipping Strezlecki Main Vein (top-right to bottom-middle). The Powder Sill forms the hangingwall, while a felsic sedimentary rock forms the footwall. In this exposure the vein is ~30 cm wide, and the vertical height is 5m. b) Half-core showing a portion of the laminated vein at Raleigh, coin for scale.

A second, parallel vein, (the footwall vein) is developed along the lower surface of the felsic unit, where it is in contact with an intermediate volcanoclastic rock. The stratigraphic position of the footwall vein at Strezlecki is equivalent to the position of the main vein at Raleigh. Down dip lineations were observed in several discrete shears along the NE wall of the pit, and in proximity to the footwall vein.

Biotite and chlorite are the principal alteration minerals, with carbonate and epidote forming a minor component. Ore minerals observed include pyrite, galena, chalcopyrite and scheelite. SEM analyses indicate that gold and galena show a close spatial relationship, often forming along, or in close proximity to, stylolitic laminae (Fig. 2.5.21), and occasionally along cracks in pyrite.

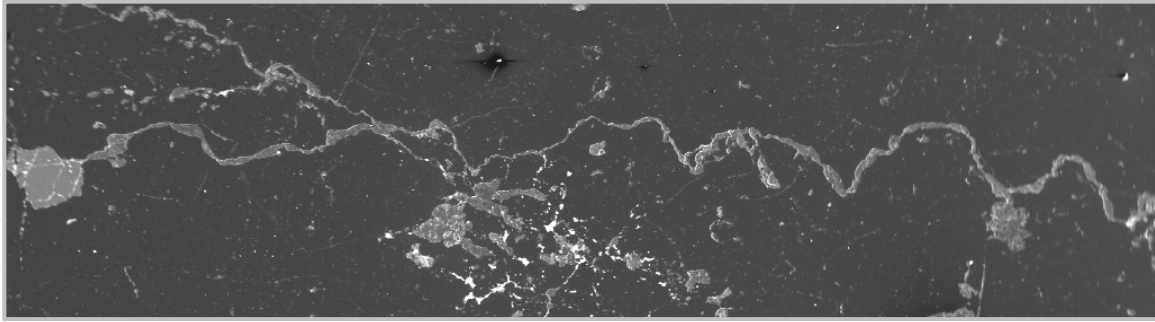


Fig. 2.5.21. SEM image of a sample from a laminated vein at Strezlecki, highlighting the stylolitic form of a lamina. The bright material (bottom-centre) is gold and galena, which generally occur together as aggregates close to, or along, the laminae (width of view is 3.5 mm).

The laminated vein at Barkers has an average trend of N50-60W and dips from 75-85SW. An additional structural component at Barkers is the N-S trending 21-Mile Fault, which intersects the southern end of the pit. The fault is developed along a gabbro-sedimentary rock contact, and has a strong ductile fabric that strikes N8E and dips 70-80E. A very shallow stretching lineation and well-developed *S-C* fabric indicate movement along the fault to have been dextral strike slip. The fault was associated with mineralisation several hundred metres south of the main mineralized trend, and represents a rare occurrence of mineralisation on this trend alone.

Cave Rocks. The Cave Rocks pit is ~65 km south of Kundana and exposes a turbidite (greywacke) package to the east, and ultramafic rocks to the west, separated by a dolerite that hosted the mineralisation. The sedimentary rocks are tightly folded, with vertical axial planes and axial planar cleavage striking N-S. Stretched clasts throughout the sedimentary sequence define a lineation plunging ~30N. The dolerite deformed in a ductile manner, and has a foliation striking N30W and dipping 65E with a stretching lineation plunging down dip. More than one deformation is recorded by the dolerite as reflected by several foliation planes, and no clear tectonic history could be derived as yet. Detailed sampling and microstructural study will be required. Discrete sub-vertical shear zones (~10cm wide) are developed in the ultramafic rock, and trend ~N15W. A stretching lineation plunges 28N along the shear planes, although no asymmetries could be recognized to confirm a shear sense.

Discussion

The Zuleika Shear Zone juxtaposes the Ora Banda Domain against the Coolgardie Domain. The shear zone is developed along a disrupted and attenuated anticlinal corridor that separates two broad, coherent synclines, and was the locus for significant strain partitioning. No marker exists on both sides of the shear zone that would constrain the amount of displacement along it.

The structure is defined by a zone of intense deformation, approximately 1km wide, within which lithological contacts were the dominant loci for shearing. This is typified at Kundana, where at least five steeply west-dipping shear zones are recognized along different lithological contacts. The most central one of these marks the stratigraphic break between the two Domains, juxtaposing the lower surface of the NE-facing Bent Tree basalt, against intermediate volcanoclastic rocks belonging to the Coolgardie Domain.

Steeply plunging lineations and *S-C* fabric asymmetry at Kundana, suggest reverse and oblique-reverse movement. Dominant sinistral strike slip movement was not recorded by us, although it has been interpreted from fold asymmetries within the mine (J. Beeson, pers comm.). However, we documented sinistral strike slip at Bullant/Ant Hill to the NW.

With the exception of Bullant, gold mineralisation along the Zuleika Shear Zone is located at lithological contacts, and reflects the gross pattern of strain partitioning observed along the structure. In the northerly deposits at Bullant, ultramafic rocks and porphyries are present, although it is the mafic lithologies that host the ore. A notable feature of the Kundana camp is the absence of these two rock-types in all known deposits, which is atypical in the Kalgoorlie Terrane. Instead, competency contrast is provided by the presence of low viscosity shales and doleritic rocks.

Biotite is a major alteration mineral in all camps, highlighting the ubiquitous relationship between potassic alteration and gold mineralisation. Carbonate alteration is significant in the regions where ultramafic rocks are present. A relationship between anomalous arsenic values and shale-hosted deposits is highlighted at Kundana, where deposits hosted in the Centenary Shale are associated with an arsenic anomaly, while those along the Western Line lack this anomaly. This is despite the close proximity of the two Lines, their similar temporal relationships, and the presence of similar ore-related sulphides on both Lines. The *As*-shale relationship strengthens the observations along the Ida Shear Zone as outlined earlier in this report.

Gold mineralization at Kundana took place after shearing and foliation development, as exemplified by cross-cutting veinlets and brecciation. Economic mineralisation within one of the

cross-faults (i.e. the 21 Mile Fault at Barkers), implies that some of the cross-faults were active during, or prior to, mineralisation. In contrast, Tripp (2000) suggested that mineralisation commenced during the formation of the shear zone at Bullant, but continued during the formation of cross-faults that cut or displace the main shear fabric.

Stratigraphy and metamorphism. The presence of the Walter Williams Formation (WWF) in both the Ora Banda Domain and along the eastern part of the Ularring Greenstone Belt (Hill et al 1995) implies that the Zuleika and Ida Shear Zones both delineate the western margin of sequences containing the *same* sequence of ultramafic volcanic rocks. In the Mt Ida area, we observe the WWF and rocks beneath it as they are exposed in the Kurrajong Anticline, whereas at Ora Banda the WWF and rocks above it are exposed (i.e. in the Mt Pleasant syncline).

Folds. Folds adjacent to, and SW of, the shear zone, in the Zuleika-Kunanalling Corridor have NW axial traces that are at a small angle to the shear zone (Fig. 2.5.15). These trends are oblique to NNW-trending regional scale axial traces of the Ora Banda Domain and the margins of the main batholiths to the NE (Fig. 2.5.15). This obliquity is here interpreted as resulting from the rotation of regional D2 folds within the Kunanalling-Zuleika Corridor during shearing and deformation. Both orientations of folds are cut by through going brittle-ductile fault sets, which places an upper constraint of the relative timing of the rotational phase of deformation. Rotations are also observed on the southern end of the Mt Pleasant Dome, whereby the trace of the axis of the dome rotates in a counter-clockwise direction as it nears the Zuleika structural Corridor. There are several features in the geology of the Ida, Zuleika and Kunanalling areas that suggests that a process of indentation of competent granitoid blocks into weaker greenstone corridors has played an important role in the structural evolution of the area. These will be detailed below, but most striking is the broad curvature of the Zuleika corridor, the accompanying folding of the southern tips of the large batholiths as they approach the Zuleika Shear Zone; and local deviation of the Ida Corridor trend around the Central Granite.

The Zuleika-Kunanalling Corridor. The Zuleika Shear Zone (ZSZ) at Kundana is predominantly a reverse shear zone, with steeply plunging lineations on steep, W-dipping foliation planes. In many localities, movement was oblique, with a small dextral or sinistral strike-slip component, that varies according to deviations of strike from N45W which corresponds to precise down dip lineations as observed in the Streszlecki pit and is interpreted to be perpendicular to the direction of maximum shortening. By contrast, further north at Bullant

and Ant Hill, movement was predominantly sinistral along gently plunging lineation. In order to understand deformation in this zone, it is necessary to zoom out and investigate the deformation in the Zuleika Deformation Corridor, a zone approximately 20 km wide bounded in the east by the ZSZ and in the west by the Kunanalling Shear Zone.

This corridor contrasts with the less deformed Ora Banda Domain to the NW, and the Coolgardie Block to the SE which has an internal fabric discordant to the regional NW to NNW fabric. The corridor is well defined in aeromagnetic images (Fig. 2.5.22) and includes folds with axial traces trending ~ NW. While folds in the centre of the corridor are broad, they tighten towards both bounding shear zones. Lineaments in the NW end of Fig. 2.5.22 suggests a possible broad sinistral component as determined at Bullant and Ant Hill.

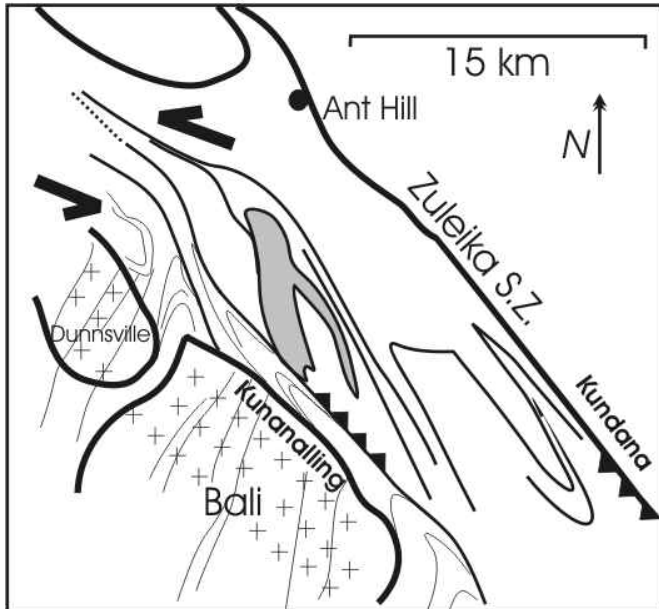


Fig. 2.5.22. The Zuleika-Kunanalling Corridor, limited to the west by the Dunnsville and Bali Granites and to the east by the Ora Banda Domain. Opposite vergence on reverse shear zones at Kundana and Kunanalling accompanied by tight folds suggest the block was exhumed in relation to surrounding areas. The angle between fold traces and the trend of the corridor suggests a possible sinistral component of deformation as was documented at the Ant Hill area.

During this project, open-pits (Kunanalling, London, Blue Bell) along the narrow band of intense folding in the vicinity of the Kunanalling Shear Zone and Bali Granite (Fig. 2.5.22) were studied. This area has been studied by Hunter (1993), who by linking ultramafic rock exposures on either side of the Kunanalling Shear Zone suggested a 12km sinistral movement. This shear sense was not confirmed here. Exposures in the open pits are characterized by NW-striking foliation dipping steeply NE, accompanied with approximately down dip mineral and stretching lineation (Fig. 2.5.23). Sense of shear indicators (*S-C* fabric) suggests SW-thrusting, and in the Kunanalling open pit, ultramafic rocks were thrust over pillow basalts and tight, west-verging folds were also documented (Fig. 2.5.23).

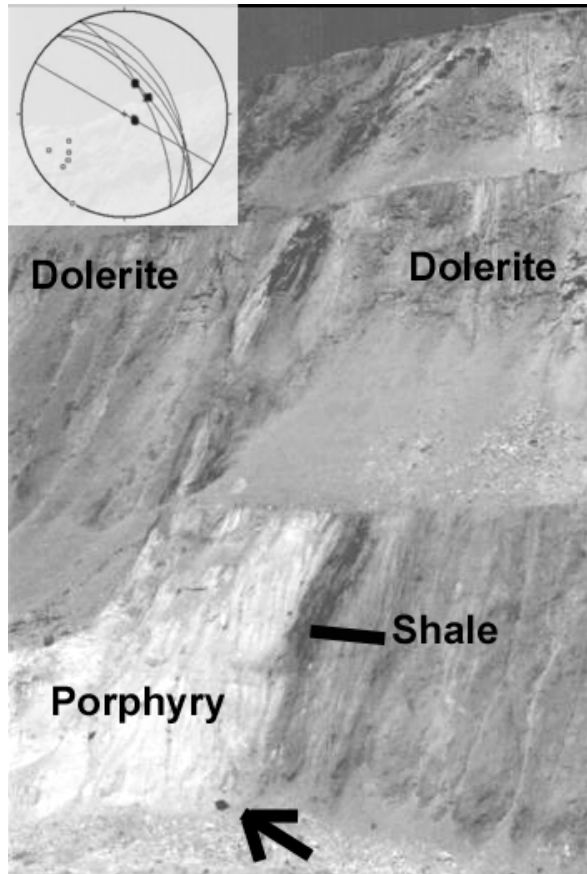


Fig. 2.5.23. A porphyry and a narrow shale layer (darker band) define a tight fold enclosed by dolerite on the SW face of the Kunanalling open pit. Insert: lower hemisphere equal area stereo projection of foliation (N30W/60NE; great circles), their poles (plus signs) and the approximately down dip mineral and stretching lineation (black squares on the great circles). Arrow points to a bag as scale.

These observations suggest that deformation in the Kunanalling Shear Zone was characterized by west-directed thrusting and tight originally recumbent folding, and that these structures probably became steeper as shortening progressed. The sinistral movement previously inferred (Hunter 1993) is based on the incorrect procedure of linking two random parts of complexly folded ultramafic layer.

The symmetric pattern of strain distribution within the corridor between Kundana and Kunanalling, with fold tightening towards the two bounding structures and opposite thrust and fold vergence (Fig. 2.5.24) suggest that folding and thrusting developed broadly contemporaneously and led to the exhumation of the corridor as a *pop-up structure*. Because this deformation event led to a period of crustal thickening, it is most likely related to the regional D_2 event.

As noted above, in contrast to the dominantly reverse movement at Kundana, sinistral shearing along the ZSZ is well-developed at Ant Hill and Bullant, (Tripp 2000; and our own observations) 20 km northwest of Kundana. It could be that either the broad ZSZ lineament has been reactivated as a sinistral shear zone after reverse movement, like the BLSZ, or alternatively,

the sense of shear changes along strike. This will be further discussed below in the section related to the indentation of the Coolgardie Block.

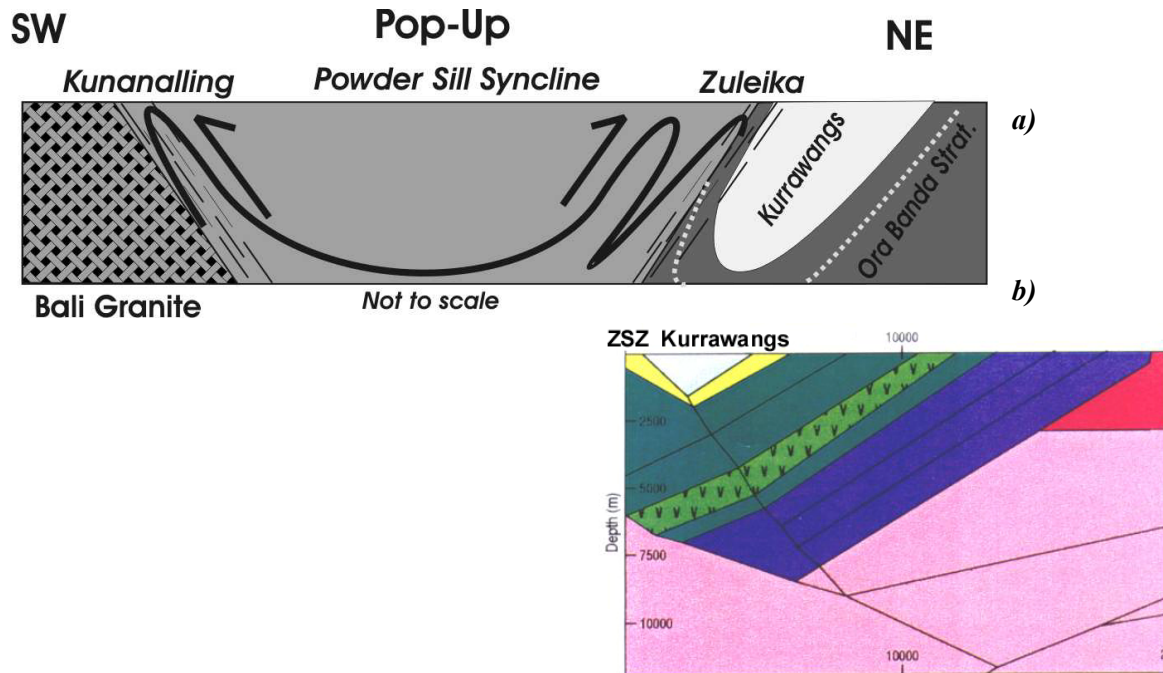


Fig. 2.5.24. a) Schematic profile from Kundana, on the Zuleika Shear Zone, to the Kunanalling pit, on the Kunanalling Shear Zone, 20 km to the west. The profile depicts the tightening of folds towards the shear zones, and their opposite vergence, defining a pop-up structure. Note that the Kurrawangs Sedimentary Sequence has been folded by the same event even though these sedimentary rocks lie in the much less deformed Ora Banda Domain. This profile is only slightly different from that of Hunter (1993), but here shear senses are added to the main shear zones. The profile compares poorly with the seismic interpretation in b) where the stratigraphy is virtually undisturbed by the Zuleika Shear Zone (Goleby et al. 2000).

Escape Tectonics and Deformation of the Kalgoorlie Terrane

Several lines of evidence suggest that large granitoid-dominated masses may have controlled regional deformation, via a process of indentation. Firstly, we described the indentation pattern around the Central Granite Complex on the Ida Shear Zone (Section 2.5.1). Secondly, the Zuleika-Kunanalling Corridor defines a broad flexure and a pop-up structure around the granite dominated Coolgardie Domain. This is associated with a bend of the southern tip of the Siberia Batholith Granitoid, which suggests that the Coolgardie Domain moved eastwards. Thirdly, intensive flattening along the ISZ suggests that the large granite mass to the east may have flattened it against the large granite-dominated Southern Cross Terrane to the west.

A numerical model was designed to test whether some of these features could be explained by indentation of the large granite block north of Kalgoorlie (the Eastern Batholith, Fig. 2.5.2). The code ELLIPSIS developed by Louis Moresi (CSIRO) and run by Chris Wijns (UWA)

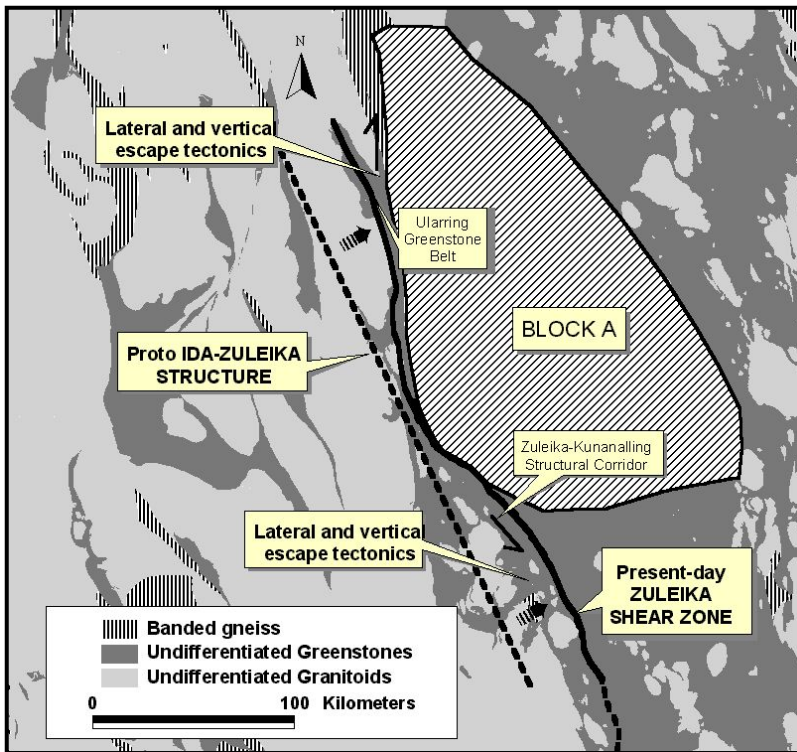
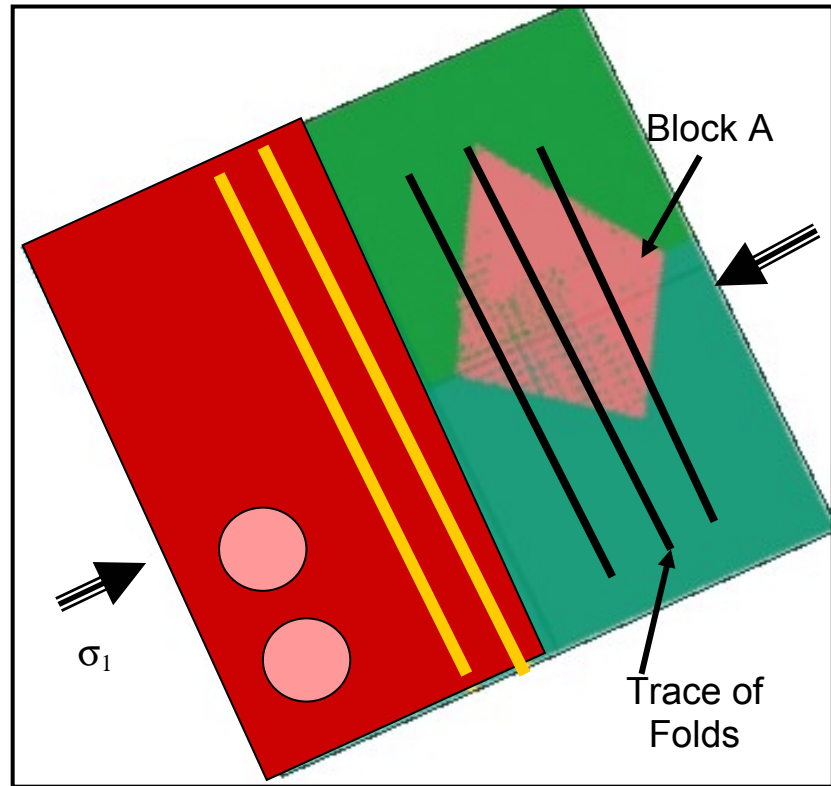


Fig. 2.5.25. Simplified geological map highlighting the principal features on which the ELLIPSIS model is based. Block A broadly defines the Eastern Batholith, which impinged upon the Southern Cross Terrane and surrounding greenstones, resulting in the lateral escape of the greenstone sequences.

was used for this purpose. The model consists of a competent, lozenge-shaped block (Block A, Fig. 2.5.25 and 26), simulating the large, batholithic complex (the Eastern Batholith, Fig. 2.5.2) to the north of Ora Banda and west of the Ularring Greenstone Belt. Block A is surrounded by a less competent matrix, representing the greenstone sequences of the Ida and Zuleika-Kunanalling Corridors. Greenstone sequences are bound to the west by a competent band simulating the

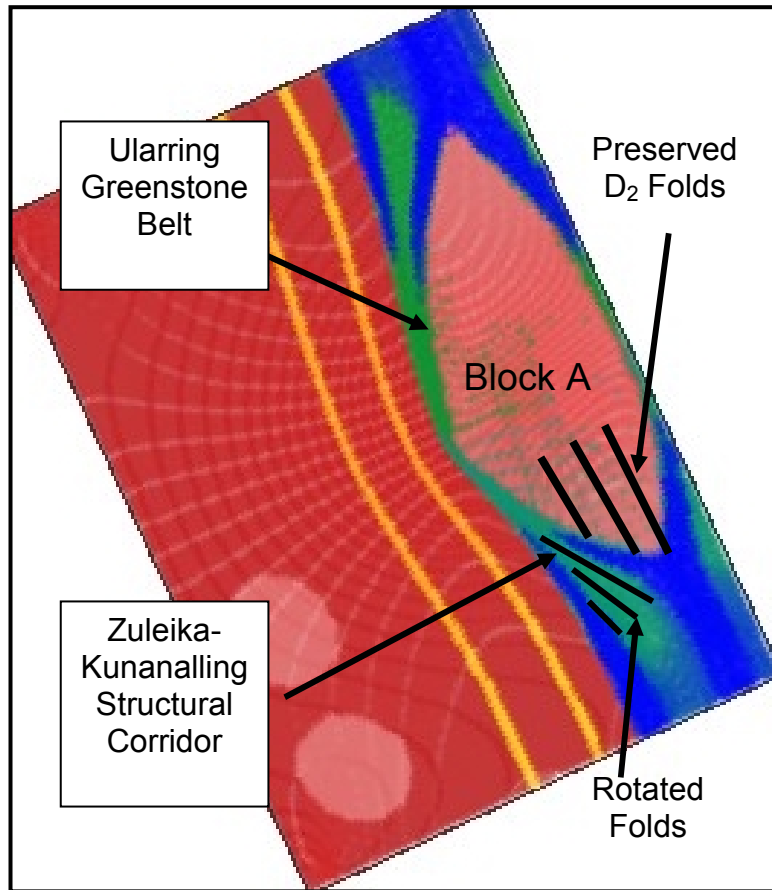
granite-dominated Southern Cross Terrane. Shortening was oriented ENE-WSW (Fig. 2.5.26), as concluded previously in this report.

Fig. 2.5.26. Starting configuration for the ELLIPSIS model to test the hypothesis for escape tectonics in the Kalgoorlie Terrane (see text for details). The model is rotated to match regional orientation.



As the indenting Block A approached the competent Southern Cross Terrane (Fig. 2.5.27) the intervening greenstone sequence was forced to escape laterally, causing the incompetent layer (greenstones) to wrap around Block A, rotating and tightening earlier folds and thrusts. Material immediately in front of the indenter, the region corresponding to the Ida Corridor, accommodated much of the deformation by means of intense flattening. Simultaneously, the Zuleika-Kunanalling Corridor, because of its position on the SW margins of the indenter Block A, was forced to escape towards the southeast by means of rotation and sinistral strike slip. Furthermore, the competent Southern Cross Terrane underwent a broad concave deflection, which caused the Coolgardie Block to move eastwards and led to a general shortening and pop-up of the Zuleika-Kunanalling Corridor. The model also suggests that the region to the NW of the indenter is characterized by a northeastward escape along dextral shear zones, and that is what has been described along the Waroonga Shear Zone (Platt et al. 1978).

Fig. 2.5.27. Result of the numerical model. Areas in green indicate high strain, and correlate well with the Ularring and Zuleika-Kunanalling Corridors (see text for details).



Thus, our simple model suggests that ENE-WSW directed crustal shortening driving the indentation of the competent granite batholith in the middle of the terrane, not unlike the indentation of India into southern Asia, is capable of explaining flattening along the Ida Corridor; the southeast escape and rotation of the Zuleika-Kunanalling Corridor defined by sinistral motion on the northern part of the ZSZ; the eastward motion of the Coolgardie Block and consequent pop-up of the central part of the Zuleika-Kunanalling Corridor; as well as dextral movement on the Waroonga Shear Zone. We suggest also that the Ida and Zuleika might once have been one and the same roughly linear shear zone that was bent into the present shape by the indentation of rigid blocks.

2.6 Controls on Gold Endowment: Shear Zone Comparison

Summary

Field observations suggest that a variety of rock types provides a positive environment for gold deposition, because it provides local zones of dilation as a result of competency contrast, as well as chemical gradients to trigger gold deposition. Field observations, supported by theoretical arguments suggest that competency contrast is strongest at greenschist facies temperatures and decreases at amphibolite facies. This is because at greenschist facies phyllosilicate-rich rocks flow viscously, while coexisting quartz- or feldspar-dominated rocks tend to behave in a brittle fashion. Greenschist facies gold deposits in the Norseman-Wiluna Belt provide numerous examples of this contrast, where granite dykes or dolerite sills are intensely fractured while surrounding talc-schist is strongly sheared.

It is in fact this contrast in behaviour and strength at greenschist facies that ultimately leads to gold deposits because such competency contrasts give rise to local strain incompatibility, and rock rotation during shearing, increasing permeability in dilational zones, particularly close to contacts, and focusing mineralizing fluid flow. At amphibolite facies, by contrast, phyllosilicate schists may be strengthened in comparison to other rocks by the growth of amphiboles and feldspars, or grain size coarsening; while quartz- and feldspar-dominated rocks are weakened and start flowing as ductile materials (e.g. Tullis and Yund 1987). Thus, relatively weak schists may become strong amphibolites, while strong granites and dolerites are weakened by temperature rises. Decreased competency contrast then leads to poorly developed fluid pathways, unfocused fluid flow and impoverished gold deposits.

Three shear zones of regional significance and contrasting gold endowment were previously detailed: the Boulder-Lefroy (BLSZ), the Zuleika (ZSZ) and the Ida Shear Zones (ISZ). This section compares them, focusing particularly on the controls on gold mineralization. The main differences between the shear zones, with direct bearing on gold endowment, are their metamorphic facies, variety of rock types, and shear zone orientation.

The most endowed shear zone (BLSZ) strikes between N20-30W, and cuts through a rich variety of greenschist facies rock types, folded into relatively broad antiforms with good ability to focus fluid flow. The Zuleika Shear Zone, has intermediate gold endowment, and has many intermediate features between the BLSZ and the ISZ. It has a variety of rock types along its length, but these are very tightly folded in the vicinity of the shear zone (reducing fluid focusing ability). Metamorphic temperatures, though varied along strike, are higher than that at the BLSZ, straddling the boundary between greenschist and amphibolite facies. This leads to lower competency contrasts, with negative effects on gold mineralization. The strike of the ZSZ is

curved, varying from a similar strike to the BLSZ in the south, where the larger deposits are (e.g. Cave Rocks and Kundana), to a more westerly strike in the north, with a decrease in the size of deposits (Bullant and Ant Hill). Finally, the least endowed of the three shear zones, the Ida Shear Zone runs parallel to regionally continuous layers, which define a synform within a relatively narrow corridor of strongly attenuated layers of monotonous, amphibolite facies mafic-ultramafic rocks enclosed between more competent granitic batholiths, striking approximately N10-20W. Poor gold endowment results from the combined effects of low competency contrasts, strongly attenuated layers with little variation in attitude due to strong flattening, and amphibolite facies metamorphism.

Introduction

In *Sections 2.3 to 2.5* our study of the Ida, Zuleika and Boulder-Lefroy Shear Zones have been fully described. Fig. 2.6.1 summarizes our findings regarding shear zone kinematics as described in previous sections and compares them with previous interpretations. Detailed comparison will be carried out in Peter van der Borgh's thesis. In this section, the shear zones will be compared (Table 1) focusing on the influences of different shear zone characteristics on gold endowment.

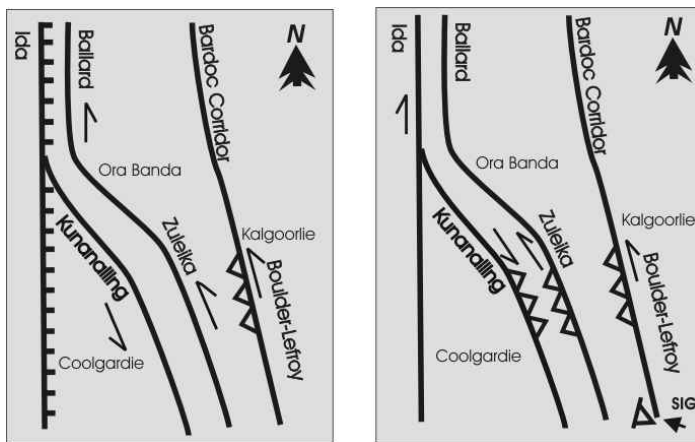


Fig. 2.6.1. a) Kinematics of major shear zones in the Kalgoorlie Terrane as previously reported (Hunter 1993, Swager 1989; Swager et al 1997); b) revised kinematics as detailed in this report and derived from mine-scale structural analyses. The Boulder-Lefroy Shear Zone has a composite history of thrusting and sinistral strike slip. Opposite thrusting directions at Kundana

and Kuranalling suggest a pop-up structure. The Ida Shear Zone has a persistent gently plunging lineation but ambiguous sense of shear due to intense flattening and no evidence for normal faulting.

Spatial distribution of lithologies and variety in contact and structure orientation generally provide a positive environment for gold mineralization. This is because complexity provides increased possibilities of fluid focusing as a result of geometries and variety in rock

permeability and strengths, plus it provides a number of possible local chemical gradients that may saturate gold in the fluids. Our efforts to quantify complexity through fractal dimensions will be described in *Section 3*, here we focus first on the distribution of lithologies around the three shear zones, and subsequently we focus on the role of competency contrast on gold mineralization in creating zones of dilation and focusing fluids.

Competency Contrast

The role of competency contrast in gold mineralization is to increase rock permeability and focus fluid flow. Competency contrast results in strong variations in stress and strain gradients leading to heterogeneous flow close to lithological contacts, fracturing of competent rocks, development of strain shadows, boudin necks or the opening of foliation in incompetent rocks through rotation. In other words, competency contrast disturbs regional stresses giving rise to local zones of dilation and fluid focusing at or close to contacts.

Empirically, it was found that extreme competency contrast between rock types plays a very important role in gold deposition, with a majority of gold deposits in the Norseman-Wiluna Belt having within the mineralized structure either a strongly competent rock (e.g. porphyry dyke, dolerite/gabbro) or an obviously weak, low viscosity schist (e.g. talc schist, shale).

The importance of extreme competency contrast for mineralization should not be underestimated. A simple count of the number of deposits containing sheared ultramafic rocks in contact with more competent rocks in the immediate vicinity of gold mineralization yielded that >60% have ultramafic schist recorded as either the footwall or hangingwall to ore, while <20% record ultramafic as the principal host (n=68). This number increases further when incompetent shales are also counted. Similarly, competent granitic intrusions are so common in gold deposits of the Yilgarn that even a possible genetic relationship to gold has been proposed. In our view their role of either ultramafic rocks or granitic rocks in the mineralization is unrelated to the origin of fluids or gold, but directly related to the origin of high permeability pathways and fluid focusing.

Metamorphic facies has an important effect in decreasing the relative competency contrast of rocks. This is due to the combined effects of the marked weakening of quartz- and plagioclase-dominated rocks (such as granites and dolerites/gabbros) as temperatures rise from 300 °C to 500 °C; and the strengthening of schists by the metamorphism of phyllosilicate minerals into amphibole or plagioclase rocks. The strengthening of ultramafic rocks may be exemplified

by comparing the highly sheared and stretched ultramafic rocks common in greenschist facies deposits, with boudinaged layers of ultramafic rocks in amphibolite facies exposures (Fig. 2.6.2; e.g. at Chadwin, northern ZSZ; Iguana, ISZ).

Thus, we argue further that the reduced endowment of regions dominated by amphibolite facies rocks may be directly related to decreased competency contrasts leading to more homogeneous flow, with decreased opportunity for the creation of high permeability dilational zones during deformation.

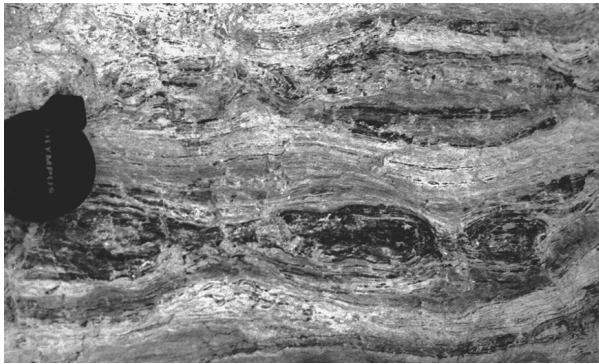
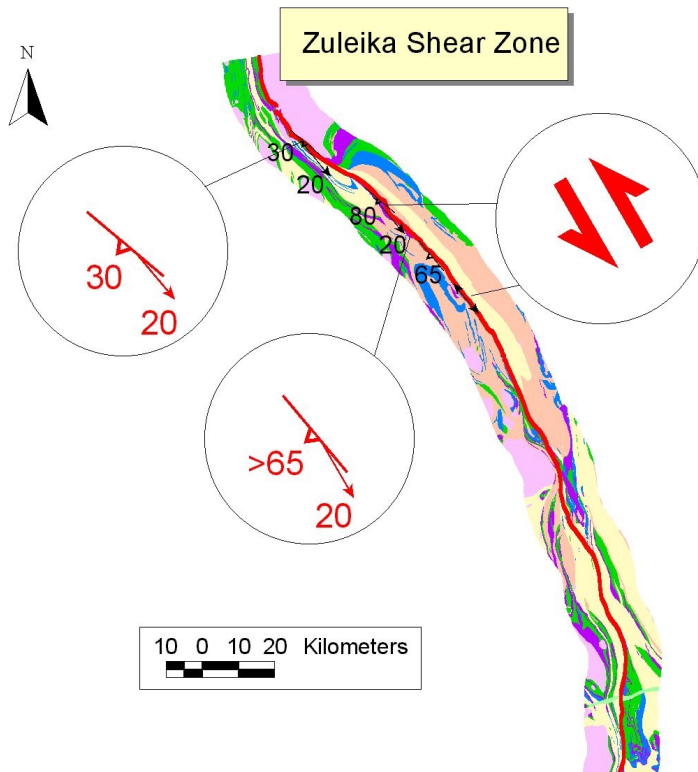
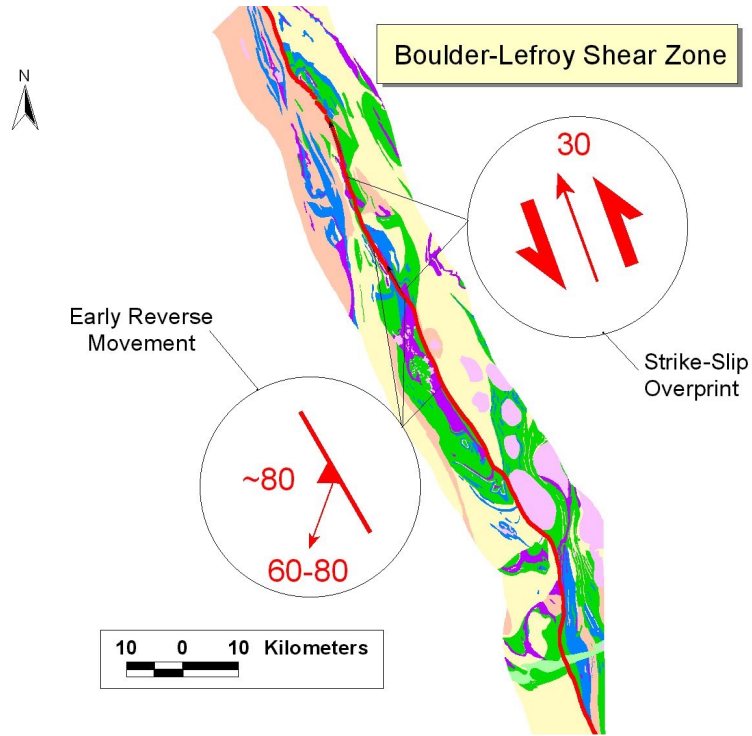


Fig. 2.6.2. Boudinaged narrow layer of ultramafic rock within amphibolite at Iguana on the immediate vicinity of the ISZ.

Lithological Complexity

The ISZ is the least endowed of the three shear zones (Table 2.6.1). It runs parallel to a relatively simple and continuous stratigraphic sequence, composed of monotonous mafic and ultramafic rocks. The stratigraphy is highly attenuated through intensive flattening, so that at the scale of regional maps, complexities are erased (Fig. 2.6.3a). Also through intense flattening, any primary angular discordances have been rotated towards parallelism with the regional trend. In contrast, the Zuleika and Boulder-Lefroy Shear Zones have a wide variety of lithologies in its surroundings, and there are both jogs along strike, plus a number of internal angular discordances, such as caused by cross-cutting intrusions, and folds cut by shear zones.

While all three shear zones have numerous granitic dykes (porphyries) and differentiated mafic sills, the sills are more voluminous and locally fractured and brecciated in the vicinity of the ZSZ and BLSZ, and smaller and sheared along the ISZ. Another significant difference is the lack of carbonate alteration along the ISZ in contrast to extensive alteration along the BLSZ. This difference could be an effect of the higher temperatures of metamorphism and alteration within the Ida Corridor and the decreased stability fields of carbonate minerals in equilibrium with basalts and metamorphic fluids.



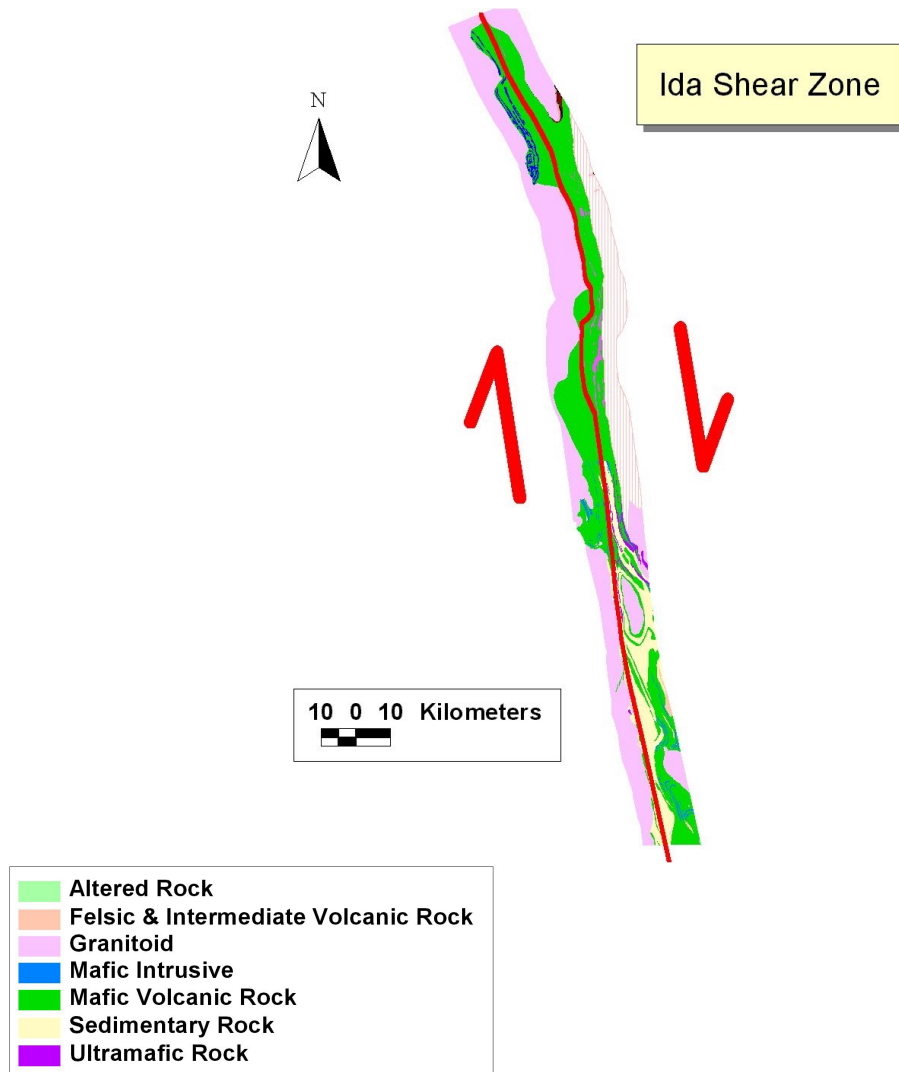


Fig. 2.6.3. Variety of rocks types (colours) in the immediate surroundings of each major shear zone. While a wide variety of rocks crop out in the vicinity of the Zuleika and Boulder-Lefroy Shear Zones; fewer rock types crop out along the Ida Shear Zone. Figures depict also the main trend of the shear zones. Notice that the width of the zone around the BLSZ is twice that around the other shear zones.

In contrast to the ISZ, the better endowed shear zones include significant volumes of volcano-sedimentary rocks (Black Flag Group or Kurrawang Sequence) in their vicinity or within the shear zone. As discussed in *Section 3*, the presence of sedimentary rocks could conceivably be related to gold endowment if they have lower bulk permeability than other rock types. Black Flag Group rocks bound one side of the BLSZ through most of its length, and also crops out immediately north of Kalgoorlie along strike of the BLSZ. If these sedimentary rocks acted as low permeability seals for rising fluids, they would have focused more fluids towards the high permeability neighbouring BLSZ. For the case of Black Flag rocks along strike of the shear zone, lower permeability of the shear zone within these rocks could conceivably have caused deflection of fluids towards other high permeability zones within the shear zone further focusing regional fluids.

Metamorphic facies

Amphibolite facies rocks worldwide tend to be less prospective for gold than greenschist facies rocks (Phillips et al. 1996). This difference is likely to be a compounded result of 1) leaching of gold during prograde metamorphism, 2) less favourable P-T conditions for gold saturation, 3) less voluminous fluids (Powell et al. 1991) and 4) lower rock permeability with increasing depth (Manning and Ingebritsen 1999). To this list, we added above the more homogeneous rock flow at amphibolite facies temperatures as a result of decreased competency and behaviour contrast.

Ultramafic Rocks

Despite the relatively low volumes of komatiites and other ultramafic rocks in the terrane as a percentage of the total, their presence increases in the vicinity of the ZSZ and BLSZ (Fig. 2.6.4). At greenschist facies conditions ultramafic rocks are generally metamorphosed to talc-chlorite schists or serpentinites, both very weak rocks, which tend to focus strain. The abundance of ultramafic rocks along the trace of the shear zones probably results from a combination of strain partitioning to these rocks and them being tectonically emplaced as wedges along the shear zone.

We postulated above that ultramafic rocks, by their low viscosity compared to other rocks at greenschist facies, plays an active role in gold deposition through creating strain gradients and zones of dilation and increased permeability. This very same conclusion can be derived from Fig. 2.6.3 which suggests that ultramafic rocks localize shear zones, which in turn localize regional fluid flow and gold mineralization.

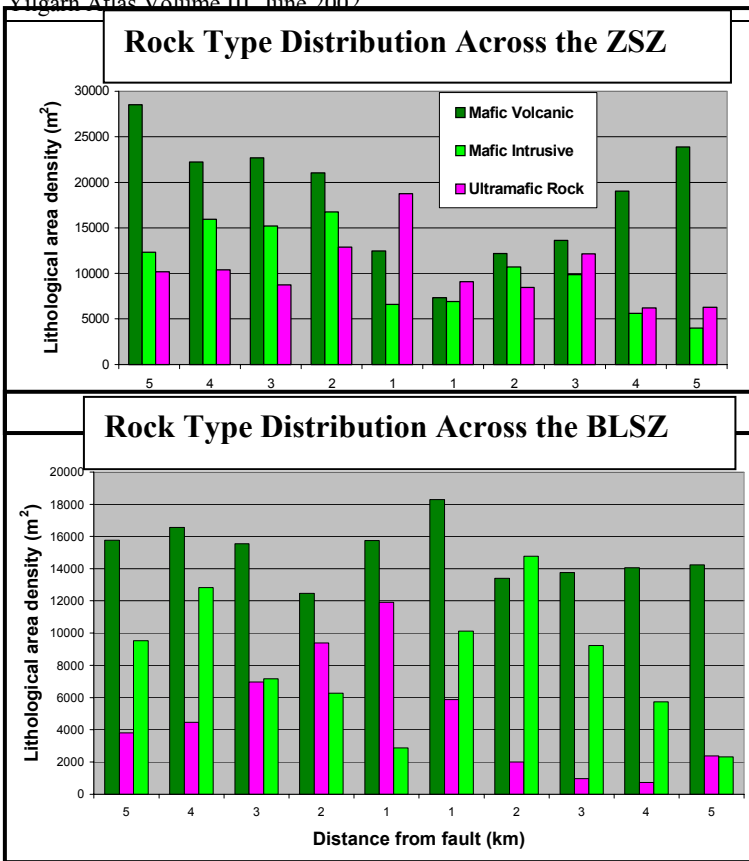


Fig. 2.6.4. Diagrams indicating the increased ultramafic rocks (purple bars) towards the centre of the Zuleika and Boulder-Lefroy Shear Zones at the expense of mafic rock types. Surface area of each rock type is plotted against distance from the shear zone, measured along the length of the shear zone. Felsic rocks have been omitted. Shear zones were either localized by ultramafic rocks, or ultramafic rocks represent tectonically slivers along shear zones.

Role of Folds

Another significant difference between the three shear zones is that the BLSZ cuts across regional, broad antiforms as exemplified by the Boomerang and Celebration Anticlines, while the ISZ runs parallel to the regional foliation and lithological contacts, and the strata in its vicinity defines a tight syncline of strongly attenuated layers. The ZSZ at Kundana defines a zone of intense fold tightening and attenuation of the stratigraphic sequence which defines the Powder Syncline to the west. A similar fold tightening has been observed on the Kunanalling Shear Zone to the west of the Powder Sill Syncline.

If, as it seems likely, antiformal fold closures provide fluid traps for mineralizing fluids and help focus regional mineralization, broad anticlines, cut by a zone of intense shearing such as in Kalgoorlie might play an important role in fluid flow, while tight anticlines like in Kundana will have a much reduced ability to disturb and focus regional hydrothermal fluids. Synforms/synclines, such as along the ISZ, might have no significant ability to focus fluid.

Shear Zone Orientation

A study of the gold content along the BLSZ as a function of its orientation, using geological maps at a scale of 1:1 000 000, found no obvious relationship between the two (Section 3.1). This

could mean either that there is no such a relationship, or most likely that the relationship is hidden at larger scales and to be found in more detailed maps.

The Zuleika Shear Zone provides a good example of the controls of orientation on mineralization. Deposits along the ZSZ are generally smaller than those along the BLSZ, as a result of a number of factors. However, deposits along the ZSZ north of Kundana (Zuleika N), where the shear zone trends predominantly N50°W, are generally small (~1 t Au), whereas from Kundana to the south (Zuleika S), where the shear zone trends N20°-30°W, roughly parallel to the BLSZ, the deposits are larger (see Witt, 1993) (Kundana, >150 t Au total, Cave Rocks, 20 t gold total (Watchorn 1998).

If it is assumed purely empirically that the general orientation of the BLSZ is positive for gold mineralization than the Zuleika N is oriented less favourably, by contrast to the richer Zuleika S, which is parallel to the BLSZ. Furthermore, the Zuleika N seems to lack important bodies of competent rock such as dolerite bodies and porphyry intrusions, which are generally relatively small (e.g. Ant Hill, Witt, 1993, p.6-7), while the Zuleika S, in contrast, has larger dolerite sills (such as at Cave Rocks and close to Kundana). Thus, the Zuleika N is unlikely to yield large deposits, except perhaps at intersections with cross cutting, dilatant N-S and NNE-SSW striking shear zones, while the Zuleika S has a generally more favourable orientation and competent rocks to perturb flow.

The poorly endowed Ida Shear Zone is a good example of a regionally persistent orientation, with relatively little perturbation of rock flow during deformation. The strike of the Ida Shear Zone is nearly perpendicular to the regional axis of maximum shortening which trends ENE-WSW, and being a narrow corridor between more competent batholiths, the belt underwent intensive flattening. Because of the high temperature during deformation and reduced competency contrast, layer attenuation and rotation of angular discordant bodies into parallelism with the regional trend, took place without much flow perturbation and few opportunities for dilation zones to focus regional hydrothermal fluids. Once a narrow, strongly stretched belt developed any subsequent deformation was relatively homogeneous with relatively little perturbation of the regional stresses (Fig. 2.6.5). Nevertheless, mineralization developed in those places where competency contrast existed and gave rise to flow perturbation and zones of dilation. Examples are the surroundings of the Central Granite Batholith indentor (Riverina area; described in *Section 2.5*) and the mineralization in boudin necks at Iguana.

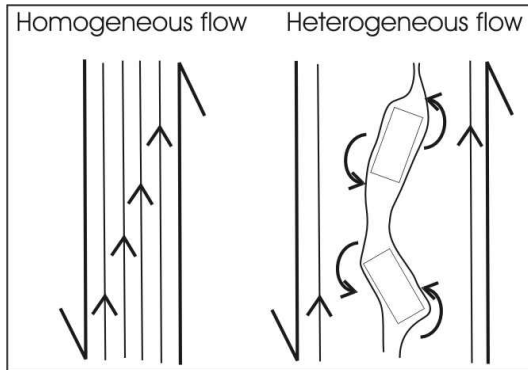


Fig. 2.6.5. Homogeneous flow such as envisaged for the ISZ, and heterogeneous flow, more likely to have taken place along greenschist facies shear zones. Irregular, randomly distributed competent bodies (rectangles) lead to a perturbation of rock flow and rotation of lithological contacts or foliation to dilational (NE-SW) and compressional (NW-SE) orientations, leading to fluid focusing.

Conclusions

Different gold endowment of the three shear zones is related to the combined effects of: *a*) extreme competency contrasts; *b*) degree of straining of the rock package, such as exemplified by the attenuation of the stratigraphy at the Ida Shear Zone (a function of *a*, *c* and *d*); *c*) metamorphic facies, particularly its role in controlling competency contrast; *d*) variety of orientation of lithological contacts and structures giving rise to zones of dilation (function of *b*).

The difference between a rich and a poor shear zone is primarily the result of rock flow disturbance (or stress disturbance) during deformation. In a hypothetical system of perfectly homogeneous, parallel rock flow during deformation, hydrothermal fluid flow will be dispersed through the system and mineralization will not take place. In contrast, in a system where rock flow is perturbed everywhere by the presence of rigid bodies of complex geometry, centers of dilation (divergent flow) and of compression (convergent flow) will develop, leading to fluid focusing and mineralization at dilational spots (Fig. 2.6.5).

Based on these insights we conclude that highly sheared zones, flowing with little perturbation, and including highly attenuated/sheared rocks, with little angular discordance, and including rocks metamorphosed at amphibolite facies, should be assigned low exploration priority. On the other hand, greenschist facies shear zones with varied orientation of lithological contacts and structures, varied lithologies, and close to regional seals, should be assigned highest priorities. The use of fractal dimensions as detailed in *Section 3* should greatly assist the process of quantifying the degree of terrane complexity.

Table 2.6.1. Comparison between major shear zones described in this report. The three shear zones of the Ida Deformation Corridor – the Ida, Ballard and Riverina Gneiss – are listed separately.

Shear Zone	Boulder-Lefroy	Zuleika	Ida	Ballard	Riverina Gneiss
Total Gold Production (from Mine)	>2000 t	269 t	81 t	see Ida	see Ida
Main Features	Reactivated ductile shear zone within greenstone seq. Major Au.	Curved domain boundary (Coolgardie-Ora Banda)	Amphibolite facies, terrane boundary	boundary gneiss/greenstone in Ida Corridor	Strongly sheared gneiss E boundary Ida Corridor
Length	150 km	300 km	250 km	>40 km	> 150 km
Dominant Strike	330°	NW arcuate	340°	350°	360°
Dominant Dip	Vert./Steep E	Vertical	70° E	Vertical	Vertical
Lineation	Steep S/down dip gentle S and N	Steep W at Kundana, gentle S at Ant Hill	Gentle (up to 20-30°) N and S	30° N	Sub-horizontal
Shear Sense	Reverse (E- and W-side up), sinistral	Reverse at Kundana, sinistral at Ant Hill	Flattening (pure shear), locally dextral, horizontal N-S stretching	Dextral	Flattening (pure shear) horizontal N-S stretching
Lithologies (dominant)	Volcaniclastic (Black Flags), greenstone seq. including voluminous differentiated gabbroic sills	Volcaniclastic (Black Flags), komat. -high-Mg basalt, andesite (Kundana)	Gabbro/basalt (W), komat. (E)	Komat. (W), Riverina Gneiss (E)	Gneiss
Other lithologies	Felsic to intermediate intrusions, lamprophyres	Granodiorites boudins and ovoid bodies in sheared komat.	Felsic dykes, pegmatites	Interflow shales	Quartzite (Alan Wittaker, pers. commun.)
Associated Structures	NE-trending dextral faults	NE-trending dextral faults	NE-trending dextral faults	NE-trending dextral faults	NE dextral, E-W sinistral faults
Metam. Facies	Mid to Lower greenschist overprinting higher temperature metam.	Mid to Upper Greenschist	Lower Amphibolite	Upper Greenschist	Lower Amphibolite
Regional Alterat.	Carbonation (including pre-shearing?), potassic and silica alteration	Ultramafic carbonation (pre-shearing?)	Local minor carbonation	Silica	Magnetite, anomalous REE in phosphate
Element Associat.	Major Ni and Au	Major As, moderate Au (Ni absent)	Minor Ni and Au (REE anomalies)	Minor Ni and Au	(REE anomalies)

2.7 Kalgoorlie Orogen

Summary

The late-Archean Kalgoorlie Orogen underwent a continuous deformation cycle known regionally as D_2 - D_4 . While in the central Kalgoorlie Terrane horizontal movement was dominated by a sinistral sense on NW-trending shear zones, at a wider scale, sinistral shearing is counterbalanced by a number of NNE-trending dextral shear zones, and accompanied by NNW- or N-trending flattening zones, such as the Ida Shear Zone. The relatively small total sinistral displacement on sinistral shear zones; the existence of regionally important dextral shear zones and the regional distribution of these shear zones, taken together suggest that deformation resulted from pure shear and not sinistral transpression as previously suggested. The orogeny was characterized by a continuous ENE-WSW directed maximum shortening strain axis and started with a period of the crustal thickening, D_2 , followed by lateral extension on NNW-ESE direction, during D_3 - D_4 after the crust attained its maximum thickness. At the exposed crustal level competent granitoid batholiths played a key role in the deformation. By impinging onto weaker greenstone belts, they controlled the orientation, distribution and sense of shear of regional shear zones.

Introduction

In *Sections 2.2* and *2.3* the several deformation phases of the Kalgoorlie Terrane were introduced and discussed. It was concluded that phases D_2 - D_4 were the result of continuous deformation cycle which characterized a late-Archean, belt-wide Kalgoorlie Orogen which took place between ~2665 and 2630 Ma. This tectono-thermal event was associated with low-Ca granite magmatism, metamorphism and gold mineralization. This section explores our structural findings in the central Kalgoorlie Terrane of *Sections 2.4* and *2.5* and builds on *Section 2.6*.

As discussed previously, the central Kalgoorlie Terrane is dominated by vertical movement on thrusts and folds, accompanied by an important sinistral horizontal component, accommodated by the NW- to NNW-trending shear zones. Because this region has historically attracted most of the research efforts, it has lent its sinistral character to the entire Norseman-Wiluna Belt. We found this is not supported by the regional deformation pattern. The broad geometrical organization of the orogeny and its kinematic significance is only revealed when structures of the central Kalgoorlie Terrane are integrated with those of the northern part of the Norseman-Wiluna Belt.

The bias towards the perception that sinistral shearing dominated the orogeny resulted not only because of the focus on the central Kalgoorlie Terrane but also because of: a) disregard to important N- or NNE-striking dextral shear zones cropping out to the north of Kalgoorlie, such as the Waroonga Shear Zone (Platt 1978) or the south part of the Mount George Shear Zone (south of Leonora); b) erroneous determination of sense of shear; e.g. the Kunanalling Shear Zone was previously described as a sinistral zone when it records a west-verging reverse movement sense (*Section 2.5*); c) bias towards horizontal movement component as a result of focus on aeromagnetic images and geological maps which led to an unintentional disregard for the reverse nature of many regional shear zones.

In this section we argue that regionally important dextral and sinistral shear zones form a conjugate pair that distribute NNW-SSE extension throughout the belt, and that deformation is roughly symmetric, defining a pure shear belt, not a sinistral transpression belt. First, the significance of our findings are discussed in terms of the evolution of the central Kalgoorlie Terrane, followed by a discussion of the patterns of distribution of shear zones in the Norseman-Wiluna Belt as interpreted from aeromagnetic imagery, regional scale maps and literature descriptions.

Shear Zones of the Central Kalgoorlie Terrane: Linking Local to Regional Deformation

The deformation history of the three districts studied along the BLSZ were successfully linked along strike and to the regional deformation phases (*Section 2.4*). The New Celebration the Kalgoorlie Districts revealed that an early D_2 thrusting event was overprinted by a D_3 sinistral strike slip event, in turn overprinted by brittle-ductile D_4 structures. Total sinistral movement of less than 12 km as well as the tortuous nature of the BLSZ suggest that this was not a major regional sinistral wrench shear zone, but that it simply accommodated a sinistral component of the regional shearing.

The deformation history recorded along the NNW-striking Ida Shear Zone is constant throughout its length and defines an early event dominated by pure shear with a minor, possibly earlier dextral component. Deformation is characterized by ENE-WSW shortening, and sub-horizontal stretching axis oriented parallel to the shear fabric (*Section 2.5*) and was interpreted as a result of the combined straining due to D_2 and D_3 . This early shear fabric was cross cut by

brittle-ductile NNE-trending dextral faults and E- to ESE-trending sinistral faults, possibly related to D_4 .

The kinematic history of the NW-striking Zuleika Shear Zone (*Section 2.5*) has not yet been fully uncovered. It varies significantly along strike from a dominantly reverse sense at Kundana, to sinistral strike slip at Ant Hill/Bullant and to reverse-dextral movement at Chadwin to the north at the margin of the Siberia Granite. The latter is of a different nature than most other shear zones, and was interpreted to be a response to complex shearing close to the irregular margin of the granite cropping out in its immediate surroundings. The east-verging reverse movement at Kundana and the sinistral movement at Ant Hill/Bullant are possibly related to the regional D_2 and D_3 phases, respectively. Alternatively they could result from the same deformation event, where their different kinematics result from changes in the shear zone attitude. As discussed in *Section 2.5*, indentation tectonics could explain both the sinistral movement as well as the exhumation of the internally folded Zuleika-Kunanalling Corridor. Like the Ida Shear Zone, distinction between D_2 and D_3 is not entirely clear. The Zuleika-Kunanalling Corridor was also cross cut by the NNE-trending dextral and E- to ESE-trending sinistral brittle-ductile sets. These late fault sets are also clearly visible lineaments in the aeromagnetic images, particularly in the granite batholiths, and will be further discussed below.

In conclusion, based on studies along shear zones of the central Kalgoorlie Terrane, we found that the NNW- to NW- trending shear zones (Boulder-Lefroy, Zuleika and Kunanalling Shear Zones) all have a significant reverse movement, with varying vergence. Sinistral movement is important in two of these (Boulder-Lefroy, Zuleika) but does not define a major sinistral wrenching event. Furthermore, dominant flattening and local dextral *S-C* fabrics along the NNW- to N-trending Ida Shear Zone and surroundings suggests that it lies close to the plane of maximum shortening during deformation.

Indentation Tectonics: the Role of Granitoids

Chen et al. (2001) suggested, based on kinematics around rigid granitoid bodies, that large arcuate structures formed by impingement of the granitoids into greenstone belts as a result of progressive shortening. As discussed in *Section 2.5*, the impingement of granite batholiths may have a wide impact in the development of structures in the Norseman-Wiluna Belt as well. For example, broad deviation of the Ida Structural Corridor from its main trend around the protruding Central Granite Complex was ascribed to granite impingement. More importantly, we have argued that the dextral Waroonga Shear Zone to the north, the sinistral component of the Zuleika

Shear Zone to the south, and the flattening deformation of the Ida Shear Zone in the middle, all resulted from the indentation of the large batholith mass lying between Kalgoorlie and Leonora and Agnew. Indentation tectonics explains not only the shear senses but also rotation and pop-up of the Kunanalling-Zuleika Corridor.

Beyond the large-scale impact of indentation tectonics, the irregular shapes of granite margins may also have local and complex effects on their immediate surroundings. These effects are a result of the margins of competent bodies being stress guides that distort the regional stress distribution. In this way the kinematics in shear zones close to granite contacts such as in Chadwin, is difficult to predict without detailed knowledge of the attitude of the granite contact (commonly poorly exposed in the region). These effects, as best illustrated by mineralization at Granny Smith (Ojala et al. 1993), or at Hampton-Boulder/Jubilee (*Section 2.4*) may play a key role in gold mineralization.

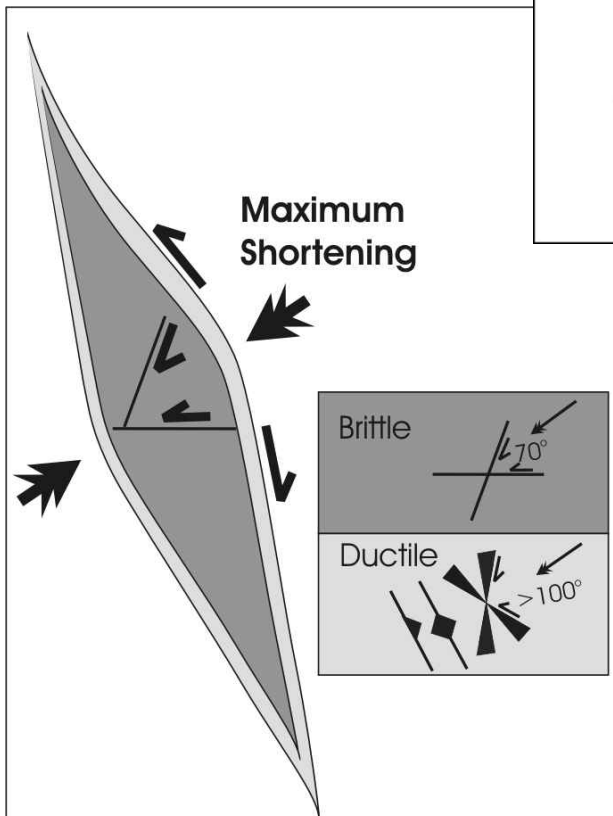
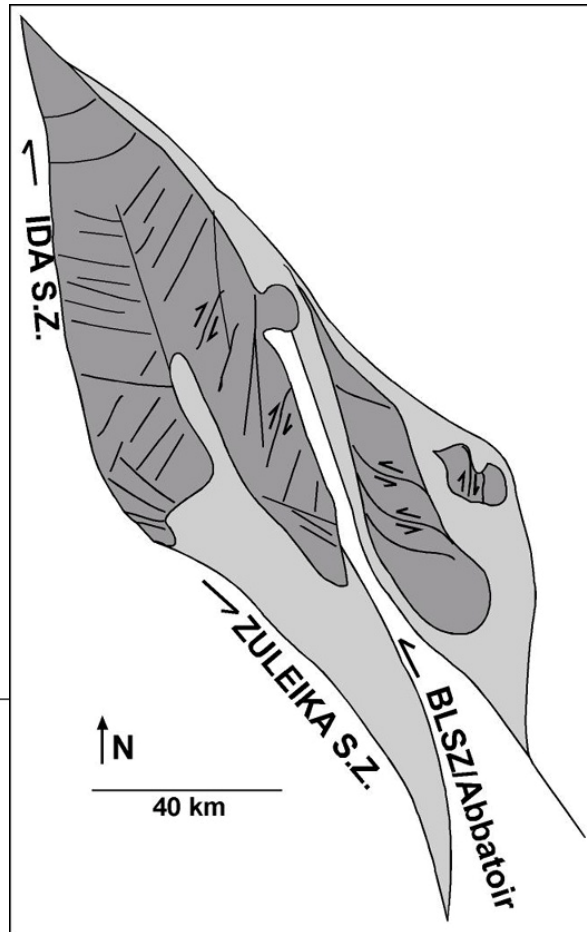
Regional Deformation

Figure 2.7.1 depict the main lineaments in aeromagnetic images in a broad region between the Ida Shear Zone and the Boulder-Lefroy Shear Zone. Lineaments define elongated lozenges and the shear senses on structures will be used to discuss the character of the ductile and brittle deformations in the region.

Ductile deformation is predominantly partitioned to greenstone belts where important folding and regional shear zones developed wrapping around the more competent granite batholiths. Ductile deformation resulted from the combined effects of a deformation cycle driven by ENE-WSW shortening, D_2 – D_4 , and escape related to indentation tectonics. While regional stresses set up the general deformation framework, competent granitoid batholiths tends to redirect them and create their own stress fields.

Regional shortening during D_3 gave rise to a conjugate set of large-scale regional shear zones: sinistral shear zones striking NW to NNW, and dextral shear zones striking NNE to N. This has been clearly documented around the Kurrajong Anticline (Ida Shear Zone, *Section 2.5*) Shear zones striking in between these sets, such as the Ida Shear Zone (NNW to N) tend not to have a dominant sense of shear, as would be expected. These may represent either early, rotated strike-slip shear zones, or shear zones developed close to that orientation as a result of granite batholith impingement. The obtuse angle ($>100^\circ$) between the conjugate strike-slip sets is bisected by the ENE-WSW axis of maximum shortening (Fig. 2.7.1 b) and is probably a result of rotation away from their original orientation, combined with the ductile behaviour of these rocks.

Fig. 2.7.1. a) Schematic map based on aeromagnetic image interpretation. The light grey and white areas represent greenstone belts, and dark grey areas represent granitoid bodies (the Mount Pleasant Dome to the east and the Scotia-Kanowna Dome to the west). Major shear zones and their most significant horizontal movement component are indicated. Important brittle-ductile faults are indicated in the granitic batholiths. These structures show consistently that the NNE-striking set has a dextral horizontal movement component while the ESE-striking ones have a sinistral component.



b) Interpretation of the deformation based on the horizontal component of the motion depicted in a). Ductile shear zones wrap around more competent blocks dominated by granitoid batholiths, while the competent block fractures internally in a brittle or brittle-ductile fashion. Insert shows how the brittle faults can be accounted by the same axis of maximum shortening as the ductile deformation. Difference in orientation is a function of different rheological behaviour of the different domains.

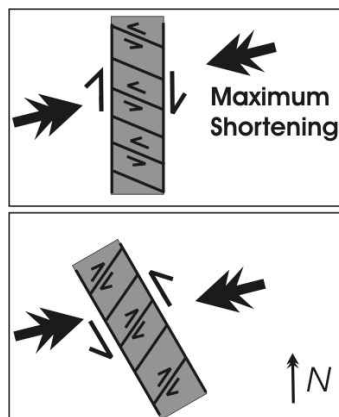
Brittle Deformation. Throughout the Ida and Zuleika-Kunanalling Corridors, and also in the Ora Banda Domain (Vearncombe and Vearncombe 1999) sets of brittle-ductile and brittle faults cross-cut earlier, ductile foliation. Three main sets have been previously reported striking approximately a) NNE-SSW, b) E-W or ESE-WSW and c) NW-SE. We will refer to these

structures as brittle faults for simplicity, and will disregard the NW-SE because no clear horizontal movement could be ascribed to them based on aeromagnetic images.

These fracture sets are very well characterized in aeromagnetic images within the more competent granitoid batholiths (Figure 2.7.1a), where there is a general dominance of the NNE-SSW and the ESE-WNW sets, which in the field, show systematically dextral and sinistral sense of shear, respectively. The same senses are confirmed by aeromagnetic images through the displacement of magnetic anomalies. Their shear sense suggests that they are a conjugate brittle set with an acute angle of $<70^{\circ}$ bisected by the same axis of maximum shortening responsible for the ductile conjugate pair (Fig. 2.7.1b).

The regional distribution of these two sets within the Mount Pleasant and Scotia-Kanowna Domes follow a pattern subtly controlled by changes in the strike of the bounding granitoid margin (Fig. 2.7.2). Even though in some regions both sets may be present, commonly one or the other set dominates. Where the strike of the granitoid contact changes, so does the dominant set. Generally, but not always, the faults are antithetic to the motion on the granitoid margins, so as to produce a bookshelf fault arrangement. In other words, when the contacts are parallel and have a sinistral horizontal component, the dominant fault in the granitoid is the dextral NNE-striking set, while the sinistral set dominates when the granitoid margins undergo dextral motion. In combination, these two fault sets have accommodated a NNW-SSE extension, similar in orientation, but not in intensity, to that in the greenstone sequences.

While in greenstone sequences these brittle structures overprint D_3 strike slip ductile foliation, implying that they are part of D_4 , in the more competent granites, they may have developed contemporaneously with ductile shearing of the greenstones. Thus, the brittle structures in the granitoids are equivalent temporally and in their kinematic role to the ductile strike slip motion on the ductile shear zones in the greenstones. Whereas the latter were overprinted by the same brittle structures upon cooling, the brittle faults remained active in the



granitoid bodies. This is a clear example where terminology must be used carefully.

Fig. 2.7.2. Summary depicting the antithetic relationship between dominant brittle fault set within granitoid batholiths, as depicted in aeromagnetic images, and the dominant movement and orientation of the batholith's main boundary. Based on Fig. 2.7.1a.

Nature of the Kalgoorlie Orogen

While the results from our study in the central part of the Kalgoorlie Terrane are robust, the nature of deformation of the Kalgoorlie Orogen is only revealed when zooming out to the scale of the belt. This is because in the central Kalgoorlie Terrane deformation is predominantly focused on NNW-trending shear zones with a component of sinistral shearing. The full picture must include the equally significant NNE-trending shear zones with a dextral horizontal movement component, such as the Waroonga Shear Zone and the southern part of the Mt. George Shear Zone. When these are included a pattern of the distribution of shear zones emerges. Long NW- to NNW-trending sinistral shear zones tend to join NNW- to N-trending flattening zones such as the Ida Shear Zone, or join NNE-trending dextral shear zones giving rise to a large scale fabric such as depicted schematically in Fig. 2.7.3. The combined effect of these shear zones is to accommodate a NNW-SSE extension and ENE-WSW shortening (Fig. 2.7.1b). The distribution of shear zones was defined early in the deformation event by the distribution and geometry of granitoid batholiths as the low viscosity greenstone sequences escaped away from impinging batholiths. In between these shear zones, competent granite bodies were elongated in the same direction by the brittle-ductile conjugate pair.

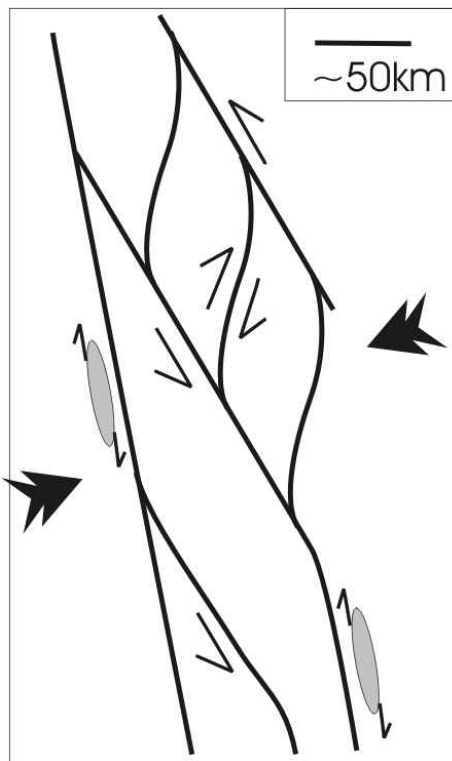


Fig. 2.7.3. Cartoon of the distribution of shear zones within the Norseman-Wiluna Belt. The longest shear zones are either NW- to NNW-trending (e.g. Zuleika and Boulder-Lefroy Shear Zones) with an important sinistral horizontal movement component, or the NNW- to N-trending ones, which record a dominant flattening and minor dextral component (as indicated by a long ellipses with shear arrows). Shorter N- and NNE-trending shear zones have a dextral horizontal movement component, (e.g. the Waroonga Shear Zone; Platt et al. 1978). The pattern suggests that the shear zones resulted from an ENE-WSW shortening event associated with perpendicular horizontal crustal stretching.

Fractal Dimensions and Sulfur Isotopes: Significance of Physical and Chemical Complexity Gradients

Summary

The formation of giant and world-class orogenic gold deposits in the Yilgarn Craton is controlled by both province-scale and process factors. *Province-scale factors* are related to the complexity of geologic features that influence crustal-scale hydrothermal fluid flow. In this study, the geologic complexity of lithologic contacts and structures was quantified using fractal dimensions. Results show that there is a strong correlation between the location of larger (>1 Moz) deposits and steep complexity gradients within greenstone belts. Steep gradients correspond to domain and terrane boundaries, which are possibly crustal-scale zones of weakness with potential for increased levels of heat and fluid flow. The steepest complexity gradients occur across granite-greenstone contacts; however, most of the largest deposits occur on complexity gradients within greenstone belts, along crustal-scale shear zones such as the Boulder-Lefroy Shear Zone and the Laverton Tectonic Zone. Steep complexity gradients within greenstone belts are typically associated with contacts between thick sedimentary units (low complexity units such as the Black Flag Beds) and underlying volcanic and intrusive units. The occurrence of large gold districts at steep complexity gradients suggests a relationship between complexity gradients and hydrothermal fluid flow, where there is a lateral deflection of fluids from areas of low complexity (low permeability) to areas of greater complexity. This deflection leads to increased fluid flow, above regional levels, in the areas with steep gradients. *Process factors* are related to the chemical and isotopic characteristics of hydrothermal ore fluids, and the physical and chemical processes that control fluid flow, gold solubility and gold precipitation. In this study, the focus has been on sulphide sulfur isotopes, as these are sensitive indicators of the physical and chemical conditions of ore formation in orogenic systems. Previous studies suggest that anomalously negative $\delta^{34}\text{S}_{(\text{py})}$ values are related to oxidized magmatic fluids that are responsible for the formation of larger gold deposits. Results of this study indicate that large variations in $\delta^{34}\text{S}_{(\text{py})}$ values (>10‰) in gold-related pyrites are more common in larger (>1Moz) shear-zone hosted deposits, compared to typically smaller ranges (<10‰) in stockwork or rock-hosted deposits. Also, larger sulfur isotope variations commonly occur in dilational structures, compared to narrower ranges in compressional structures. These occurrences suggest that fluid flow associated with dilational and compressional structures may influence $\delta^{34}\text{S}_{(\text{py})}$ values in gold-related pyrites during mineralization. In addition, results of this study show that there is a

larger range of $\delta^{34}\text{S}$ values in sulfides from sedimentary rocks than previously reported. If these rocks were a source of sulfur for the ore fluid, they could be responsible for some of the variability found in gold-related pyrites.

Introduction

The various genetic models proposed for the formation of giant and world-class orogenic gold deposits can be divided into two broad categories: those that emphasize province-scale controls on the structural focussing of hydrothermal ore fluids (Hodgson et al., 1993; Phillips et al., 1996), and those that highlight process controls related to specific ore-depositional mechanisms or unique fluids (Cameron and Hattori, 1987). In this report, the objective is to investigate factors at both scales in order to determine their relative influence on the formation of giant and world-class orogenic gold deposits, with a particular focus on the Eastern Goldfields Province of the Yilgarn Craton. There is considerable debate about the formation of the only giant deposit in the Yilgarn Craton, the Golden Mile at Kalgoorlie, and whether it even belongs to the orogenic deposit style. However, this was not the specific focus of this project, or indeed the UWA Gold Module of AMIRA P511, due to restricted access to the deposit, and on-going research elsewhere. Instead, given the large number of multi-million ounce ("world-class") orogenic deposits in the Yilgarn Craton, and industry interest in finding more of them, the focus of this Section is an investigation of the province-scale and process-related factors associated with them.

Province-scale factors include those related to geologic and structural complexity that may induce fluid focussing and gold deposition. In previous studies, complexity is typically quantified by measuring map features such as relative proportions of rock types, and density and orientation of structures, and comparing proximity, association and abundance relationships between map features and deposit locations (Groves et al., 1990; Knox-Robinson, 1994; Gardoll et al., 2000; Yun, 2000). In general, these are scale-dependent methods. One main objective of this Section is to quantify geologic complexity, as represented on a GIS map of the Yilgarn Craton, in order to discriminate between areas that are more or less favorable for the formation of larger world-class deposits. In this study, the complexity of map-scale geologic features is quantified using fractal dimensions, which is a scale-independent method.

Process factors include those related to ore-depositional mechanisms (i.e., fluid-rock interaction, fluid-mixing and phase separation) and ore fluid sources (i.e., magmatic, mantle, metamorphic, meteoric). The second main objective of this Section is to investigate sulfur

isotopes of gold-related pyrites in order to constrain ore fluid chemical conditions and ore depositional mechanisms. There are three reasons for focussing on sulfur isotopes: (1) gold is transported as a sulfide complex in orogenic gold fluids (Phillips and Groves, 1983; Mikucki, 1998; Loucks and Mavrogenes, 1999), (2) sulfur isotopes are a sensitive indicator of ore fluid oxidation state, which significantly affects the capacity of the fluid to transport and precipitate gold (Golding et al., 1990; Mikucki and Ridley, 1993), and (3) previous studies suggest that anomalously negative sulfur-isotope values in gold-related pyrites from giant and world-class Archean lode-gold deposits may be an indication of unique ore fluids (e.g., oxidized magmatic fluids, (Cameron and Hattori, 1987) and/or specific ore depositional mechanisms (e.g., fluid mixing, Walshe et al., 1999).

In *Section 3.1*, fractal dimensions are used to determine the significance of province-scale geologic complexity, as measured on a GIS map of the Yilgarn Craton, and its relationship to the locations of large orogenic gold deposits. This is used to develop a better understanding of crustal/regional-scale controls on hydrothermal fluid flow. In *Section 3.2*, sulphide sulphur isotopes are used to constrain factors related to ore-depositional processes and ore-fluid sources. The main objective of these two sections is to investigate factors that control the size and location of orogenic gold deposits. This is accomplished, in part, by comparing world-class deposits to smaller deposits in the same mineralized districts. This is not only of academic merit, but also provides the mining industry with improved exploration criteria.

3.1. Fractal Dimensions and Complexity Gradients

Objectives

Orogenic gold deposits are structurally-controlled ore bodies, and genetic models suggest that structural and lithologic complexity are fundamental factors that control their size and location in orogenic belts (Groves et al., 1998; Phillips et al., 1996). An underlying assumption of the continuum model for the formation of orogenic gold deposits is that mineralising fluids are widespread in the crust and require a focussing mechanism for deposit formation (Groves et al., 1995). Structural complexity provides the pathways for focussed fluid flow. Therefore, an investigation of the complexity of geologic features, as represented on GIS maps, should provide a means to distinguish map-scale areas that are more or less favorable for the formation of larger deposits. This can be used to develop a better understanding of factors that control the irregular spatial distribution of larger gold districts in orogenic belts. The objective of this Section is to quantify geologic complexity of regional- to district-scale map features, using GIS techniques, in order to determine the most important factors related to the formation of giant and world-class deposits in the Yilgarn Craton.

Many geologic shapes are self-similar, or have fractal geometries, in which any portion of the system (or geologic map) is a scaled-down version of the whole (Kruhl, 1994; Mandelbrot, 1983; Turcotte, 1997). In this study, self-similarity of geologic patterns, as shown on a GIS map of the Yilgarn, is assumed, and is quantified using fractal dimensions, which are measured using the box-counting method (Mandelbrot, 1983; Hirata, 1989, see below in Methodology;). Previous fractal studies of precious metal deposits have typically examined the distribution of deposit locations (Carlson, 1991; Blenkinsop, 1994; Blenkinsop and Sanderson, 1999). This approach is potentially biased, because it is based on exploration emphasis and success in different areas. In this study, the fractal dimensions of the underlying geology (i.e., lithologic contacts as represented in a GIS map) are measured in order to determine relationships between geologic complexity, which controls regional-scale hydrothermal fluid flow, and the location and size of orogenic gold deposits. Potential biases related to the level of geologic detail in different parts of the map are addressed under *Methodology* below.

Methodology

Scale of observation is a critical issue in any comparison of spatial characteristics. This is especially important in testing the relationship between the spatial distribution of geologic features and the geologic processes that influence gold endowment. This section includes descriptions of the methods used in this study to investigate and quantify the geologic features represented on a GIS map of the Yilgarn Craton (Knox-Robinson et al., 1996).

In this study, geologic complexity in the Yilgarn Craton is quantified within structural and tectonic domains. There is an emphasis on the Eastern Goldfields Province, as it includes the majority of world-class orogenic gold districts, as well as the only giant deposit, the Golden Mile at Kalgoorlie.

Changes in the degree of complexity along and across terrane/domain-bounding structures is investigated in this study as well. The significance of these structures is a controversial issue in Archean research due to uncertainties regarding the nature of Archean tectonic processes (eg, subduction vs plume styles, (Barley et al., 1989; Hamilton, 1998). This study does not directly address these issues. Instead, fractal dimensions are used to quantify the geometry and complexity of domain boundaries, in order to determine any relationships between complexity and hydrothermal fluid flow, which is ultimately responsible for the formation of orogenic gold deposits. The relationship between first-order structures and orogenic gold deposits, which most commonly occur in adjacent, higher-order structures (Eisenlohr et al., 1989), is also a topic of significant recent research related to hydrothermal fluid flow, fluid focussing and structural complexity (Cox et al., 2001; Sibson, 2001), as well as changes in hydrothermal fluid chemistry during migration along structures (Neumayr et al., 2001; Neumayr et al., in prep.). These issues are addressed in this section and the next (3.2) on sulfur isotopes. The most significant structure in the Kalgoorlie Terrane, in terms of gold mineralization, is the Boulder-Lefroy Shear Zone (described in *Section 2.4*). The largest deposits and districts in the terrane occur along, and adjacent, to this structure; it is therefore a focus of this study.

Fractal Dimensions. Self similarity in geology is pervasive. The fact that geologic features tend to be scale-dependent is exemplified by the requirement of scales in any geologic image. This suggests that self-similarity dominates geological systems and that fractal dimensions are an effective means of quantifying such geometries. In this study, the self similarity of patterns of lithologic contacts is measured using the box-counting method for determining fractal dimension [Mandelbrot, 1983 #480; and Hirata, 1989 #461]. In this technique, grids with square boxes of side length, d , are superimposed on a map and the number of boxes containing lines (representing lithologic contacts) N_d is counted (Fig. 3.1.1).

The length of the side of the box, d , is then halved and the process is repeated. N_d is the total number of boxes that contain lines, for a given box size. The fractal dimension D is determined from the slope of a line on a log-log plot of N_d vs d , such that:

$$N_d \propto d^{-D}$$

and D is a value between 1.0 and 2.0 on a two-dimensional map. $D=1$ corresponds to a single line on a two-dimensional surface, and $D=2$ corresponds to the lines covering the entire two-dimensional surface. In this study, the lines represent lithologic contacts. The box-counting computer program used in this study was written by Stephen Gardoll, with assistance from Paul Hodkiewicz and Roberto Weinberg, at the Centre for Global Metallogeny, University of Western Australia, based on the methodology outlined in (Hirata, 1989).

In this study, fractal dimensions of lithologic contacts were calculated on a 10 kilometre grid across the Yilgarn Craton. This grid spacing is appropriate for the level of geologic detail in the 1:500,000 scale map of the Yilgarn Craton, based on the methodologies of (Gillespie et al., 1993; Walsh and Watterson, 1993; Turcotte, 1997;). The grid spacing is related to the map scale; with smaller spaced grids applied to more detailed maps. The fractal dimension includes, in a single value, a measurement of the density and orientation of lines in a given area (Fig. 3.1.2). Fractal dimensions, therefore, provide a better estimate of complexity than simple density measurements which are scale dependent. The advantages of using fractal dimensions to quantify complexity are discussed in more detail below.

For comparison with fractal techniques, GIS techniques were used to produce rose diagrams and evaluate rock type distribution, in a variety of terranes, domains and districts in the Yilgarn Craton. This was done to compare scale-dependent and scale-independent (fractal) methods of measurement.

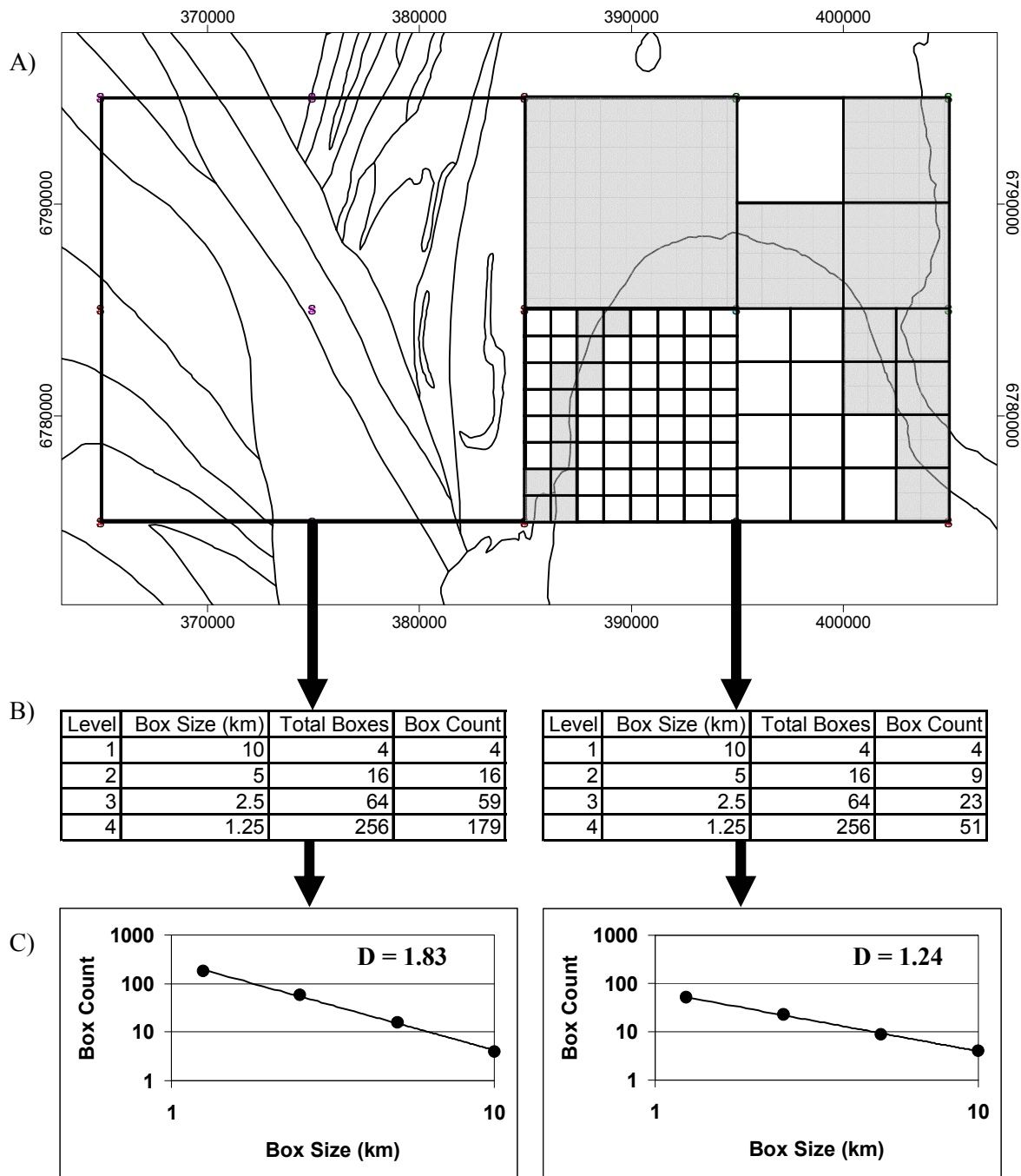


Figure 3.1.1. Example of box-counting method used to determine fractal dimensions of lithologic contacts on a 10 km square grid. (A) Comparison of two 20 km grid squares (centered on 10 km grid points) from the Yilgarn GIS map (Knox-Robinson et al., 1996), with typical greenstone belt contacts at left and an arcuate granite-greenstone contact at right. (B) Results of box counting method. Examples of the different box sizes are shown in the right-hand square. The number in the "Box Count" column equals the number of boxes of a particular size, within which a lithologic contact occurs. These are shown in grey for the granite-greenstone contact in (A). (C) The fractal dimension is obtained from the slope of a line on a log-log plot of box count vs box size. The relatively simple granite-greenstone map pattern (right-hand side) has a fractal dimension of 1.24. The more complex greenstone belt map pattern (left-hand side) has a higher fractal dimension of 1.83.

GIS Geologic Database and Map Homogeneity. In order to quantify and compare complexity of geologic features on maps it is necessary that the maps used have a homogeneous level of detail. If the level of detail varies across the map, the level of complexity will vary independently of geological complexity. Variable levels of map detail may be due to more detailed mapping and exploration effort in well-endowed areas. This is an especially important concern in this study because of its focus on determining relationships between the complexity of geologic features and the location of larger gold deposits.

The GIS geologic database of the Yilgarn Craton used in this study is from AMIRA Project P383 – MERIWA Project M194A and is based on Geological Survey of Western Australia geologic maps at scales of 1:100,000, 1:250,000, and 1:500,000, as well as AGSO regional aeromagnetic data, high-resolution multi-client aeromagnetic data, and gravity data (Knox-Robinson et al., 1996). The GIS database covers approximately 600,000 km² (40 x 1:250,000 GSWA map sheets), with a uniform level of geologic detail across all terranes in the Eastern Goldfields, Southern Cross, and West Yilgarn (Murchison Terrane) Provinces (Knox-Robinson, pers. comm., see below).

The AMIRA P383 project report (Knox-Robinson et al., 1996) includes many references to the uniform level of geologic detail in the Yilgarn GIS geologic database. The consistent and uniform level of geologic detail in the GIS database was required for the types of spatial analyses performed in P383 and subsequent studies (proximity, association, abundance relationships and Bayesian analysis, (Knox-Robinson et al., 1996); shape analysis, (Gardoll et al., 2000), GIS studies, (Yun, 2000). The consistent and uniform level of geologic detail was equally important for the fractal dimension method used in this study.

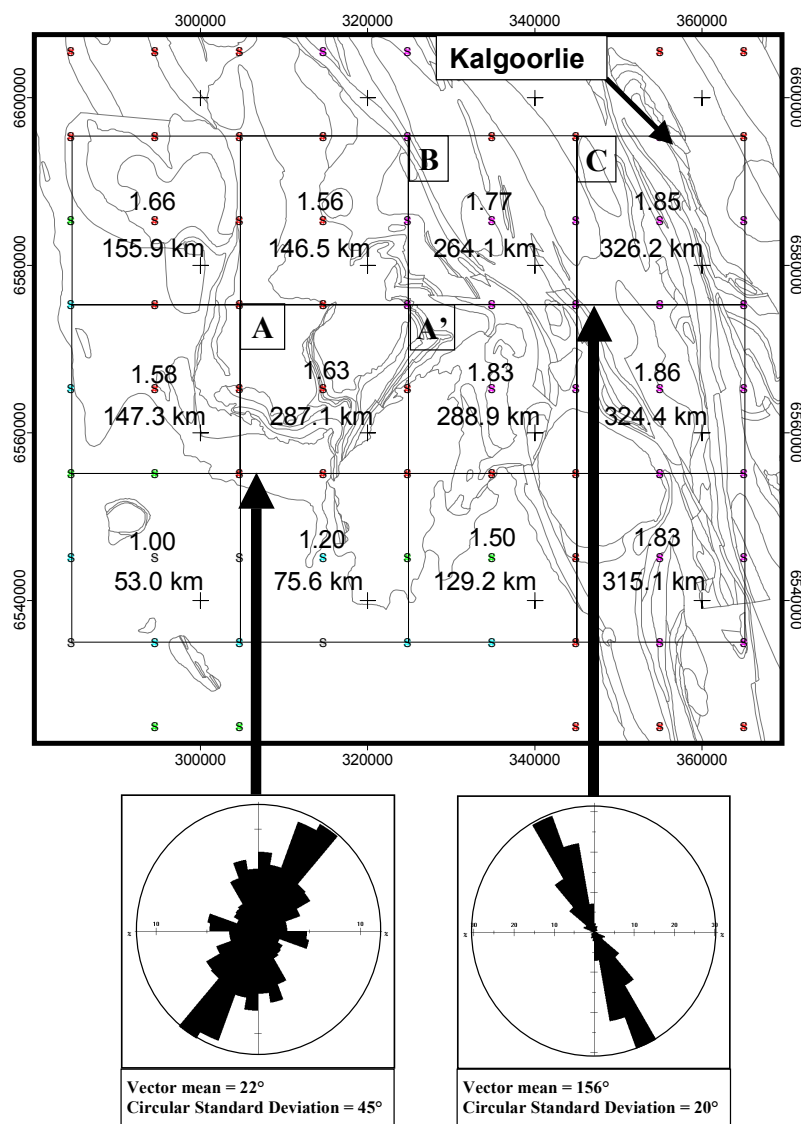


Figure 3.1.2. Map showing the relationship between fractal dimension, density and orientation of lithologic contacts in 10 km grid squares in an area between Kalgoorlie (upper right) and Coolgardie. The number above the grid point at the centre of each square is the fractal dimension. The number below the grid point is the total length in kilometres of lithologic contacts in the grid square. Note that a higher density of contacts does not necessarily correspond to a larger fractal dimension. For example, grid square A, over the granite-greenstone area at Coolgardie, has a density of 287.1 km and a fractal dimension of 1.63. Grid square B, over the greenstone belt west of Binduli, has a lower density of contacts (264.1 km), but has a larger fractal dimension of 1.77. Note also a comparison between A and A', where the density of lines is almost identical in the two grid squares (287.1 km and 288.9 km), yet the fractal dimensions are very different (1.63 and 1.83, respectively). The larger fractal dimensions imply that the distribution of lines in A' covers the square more effectively than that of A. The rose diagrams show the relationship between orientations and fractal dimensions. The orientations are of 100 metre line segments in the grid squares labelled A and C. The lower circular standard deviation of 20° in grid square C indicates lower variation and corresponds to a higher fractal dimension, compared values in grid square A. Geology from AMIRA P383 GIS map (Knox-Robinson et al., 1996).

In addition to relying on statements from the AMIRA report, the GIS map was compared to more detailed maps, normally 1:100,000 scale GSWA maps, in order to visually test the consistent level of geologic interpretation and detail. An example from the Kalgoorlie District is shown in Fig. 3.1.3. The Kalgoorlie District is arguably the most studied area in the Yilgarn, due to its gold endowment, and therefore has the potential to be the most detailed area on the map. Comparison of the two maps in Fig. 3.1.3 (GSWA 1:100,000 Kalgoorlie and Yilmia sheets (Hunter, 1993) and AMIRA GIS map used in this study (Knox-Robinson et al., 1996) shows that there is significantly more detail in the earlier GSWA map. compared to the later AMIRA GIS map, indicating that the geology has been simplified in order to match the level of detail in other areas across the Yilgarn Craton. Due to this uniform level of geologic detail, the map was deemed appropriate for this fractal study.

Gold Deposit Database. The locations and sizes of gold deposits in the Yilgarn were obtained from the Minedex database of the Geological Survey of Western Australia (Townsend et al., 2000). It includes information on production and remaining resources from over 11,000 historic mines and 1,000 recent mines and deposits in the Yilgarn Craton. This is an especially important part of the study, as it allows direct comparisons between geologic complexity and gold endowment. In all cases, estimations of pre-mining resources are given. These estimates include tonnes of gold, corresponding to inferred, indicated, and measured resource categories of the JORC code (JORC, 1999) plus any historic and recent production. The combination of historic production and current resources is the best way to provide order-of-magnitude estimates of the district-scale pre-mining gold endowment for the comparison purposes of this study, despite differences in mining techniques and cut-off grades (i.e., pre-1980 historic production was typically from underground operations that could only support average grades greater than ~30 g/t, while current large-scale open pit operations can profitably mine average grades of less than 5 g/t (Groves et al., 1990).

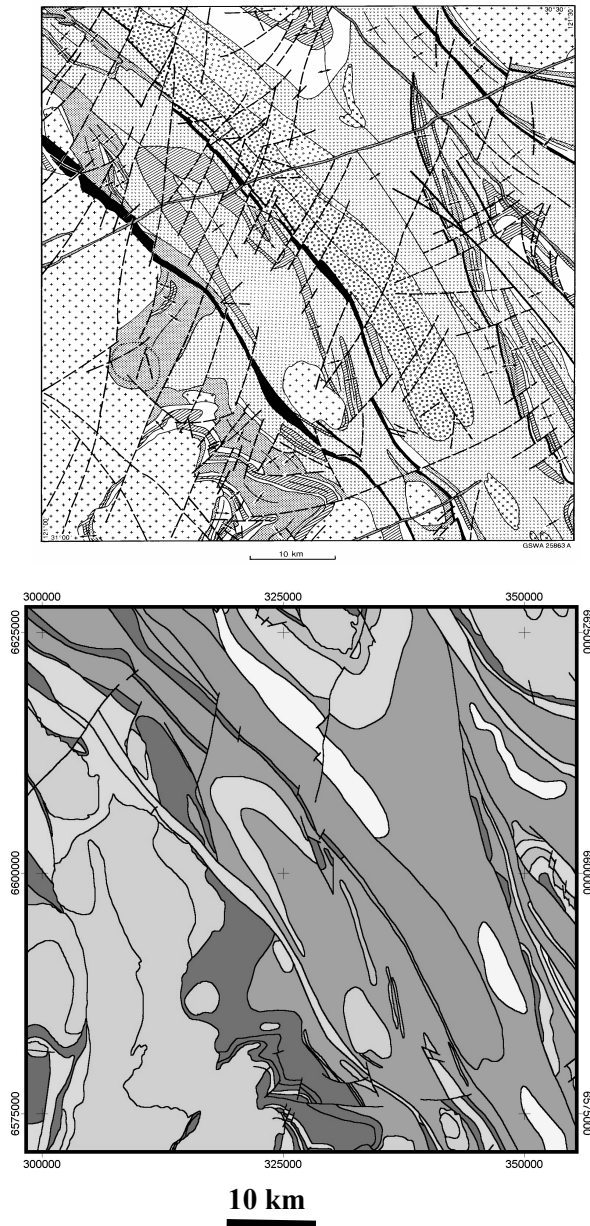


Figure 3.1.3. Comparison of level of geologic detail in maps of the same region in the Kalgoorlie area; (A) from GSWA Kalgoorlie and Yilmia 1:100,000 maps (Hunter, 1993), and (B) from AMIRA P383 GIS map (Knox-Robinson et al., 1996). The Golden Mile is on the centre right margin of both maps. There is significantly more detail in the GSWA map (A), compared to the AMIRA GIS map (B), indicating that the geology has been simplified in this area in order to match the level of detail in other areas across the Yilgarn. This suggests that there is a uniform level of geologic detail across the AMIRA GIS database.

Results - GIS Methods

Attempts to quantify geologic features as displayed on a GIS map require that a scale of observation or measurement be selected first. Whether the scale selected is appropriate, in terms of quantifying some feature that is related to the location or size of gold deposits, is difficult to determine. For example, does the fracture orientation as depicted on a 1:1,000,000 map correspond to the dominant fracture set controlling gold mineralization at 1:100,000?

The orientation of structures is commonly cited as a significant empirical factor related to the location of gold districts at jogs along crustal-scale shear zones (Sibson, 1996). The relationship between gold endowment and orientations was tested by comparing the average orientations of structures and lithologic contacts from rose diagrams and the total pre-mining resource in 12 gold districts along the Boulder-Lefroy Shear Zone (Fig. 3.1.4). Orientations were measured in 100 km² areas centred on the largest gold deposit in each district labelled in Fig. 3.1.4. Plots of average orientation of lithologic contacts and structures, circular standard deviation, and total gold endowment (Fig. 3.1.5) show no systematic relationship, suggesting that if there is a genetic relationship between fabric orientation and gold endowment, it is not being measured at the appropriate scale. This example highlights the difficulty of using scale-dependent methods for quantifying geologic complexity.

In contrast, fractal dimensions include, in a single value, a measurement of the density and orientation of lines in a given area (Fig. 3.1.5) and, therefore, provide a better estimate of complexity than the scale-dependent methods described above. Assuming that a geological map represents a self-similar feature, fractal dimensions can be used as a scale-independent measure of complexity. The advantage of using fractal dimensions is that it does not require initial assumptions regarding preferred structural orientations. It provides an objective method of map analysis that identifies areas of geological complexity.

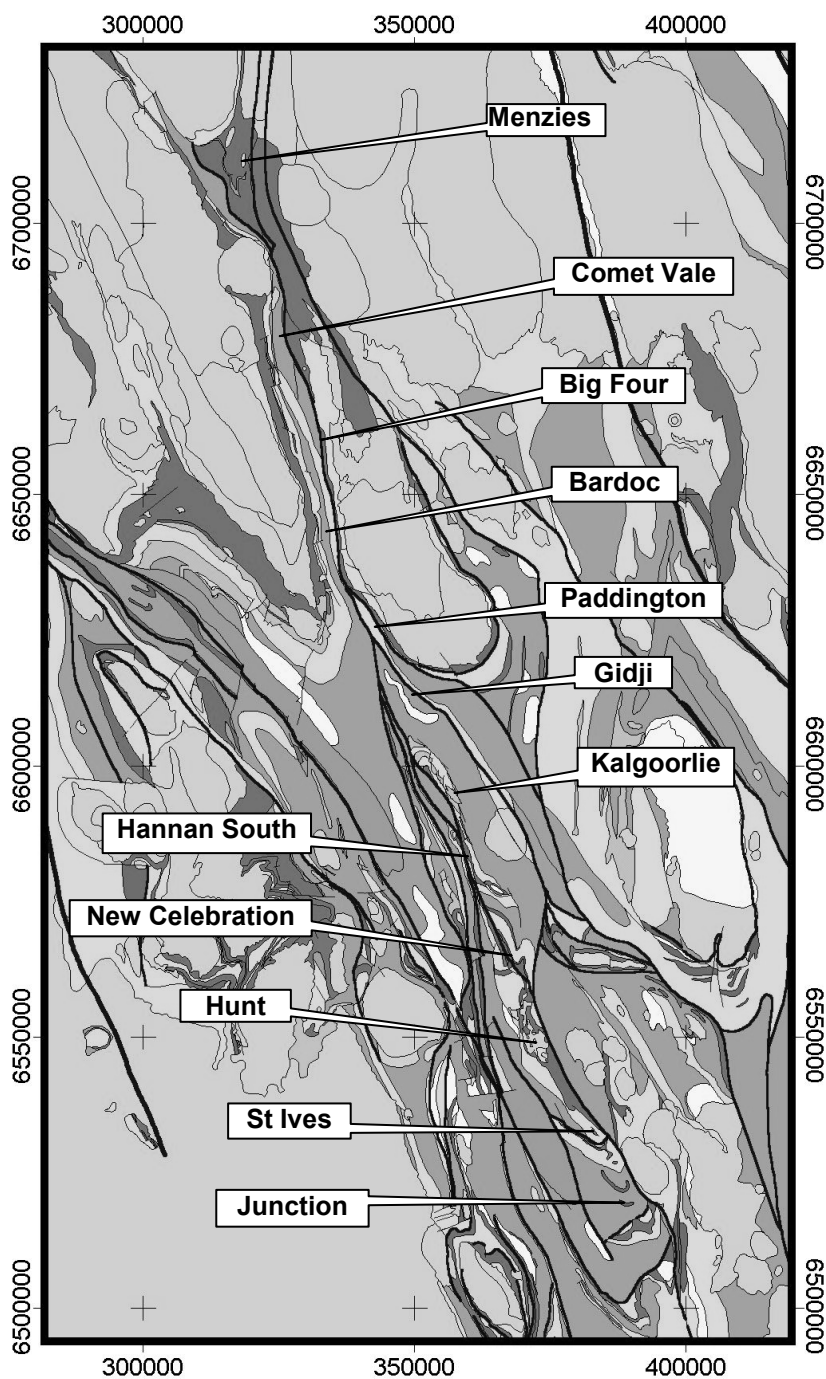


Figure 3.1.4. A) Geologic map of the Kalgoorlie Terrane (Knox-Robinson et al., 1996), showing twelve gold districts along the Boulder-Lefroy Shear Zone. B) (Following two pages) Rose diagrams of structures and lithologic contacts for the twelve gold districts, arranged from north to south. Below each district name, “n” is the number of 100 metre line segments, “cv” is circular variance, and “cstd” is circular standard deviation. In the GIS database, every line representing either a lithologic contact or structure was divided into 100 metre segments. Orientations of each 100 metre segment were measured in 100 km² areas, centred on the largest gold deposit in each district labelled. Comparisons of gold endowment, and average orientation are shown in Figure 3.1.5

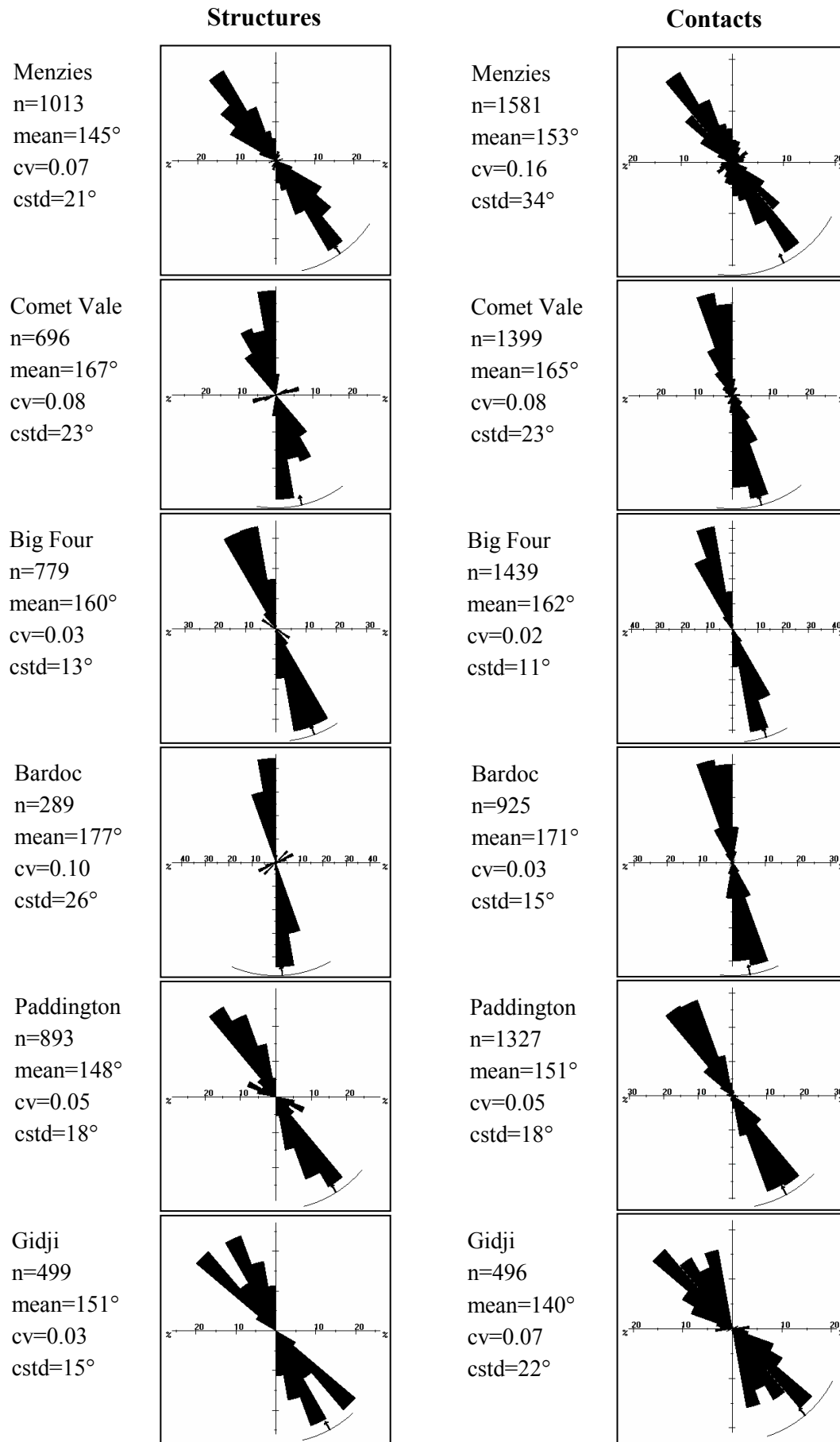


Figure 3.1.4B. Caption on previous page.

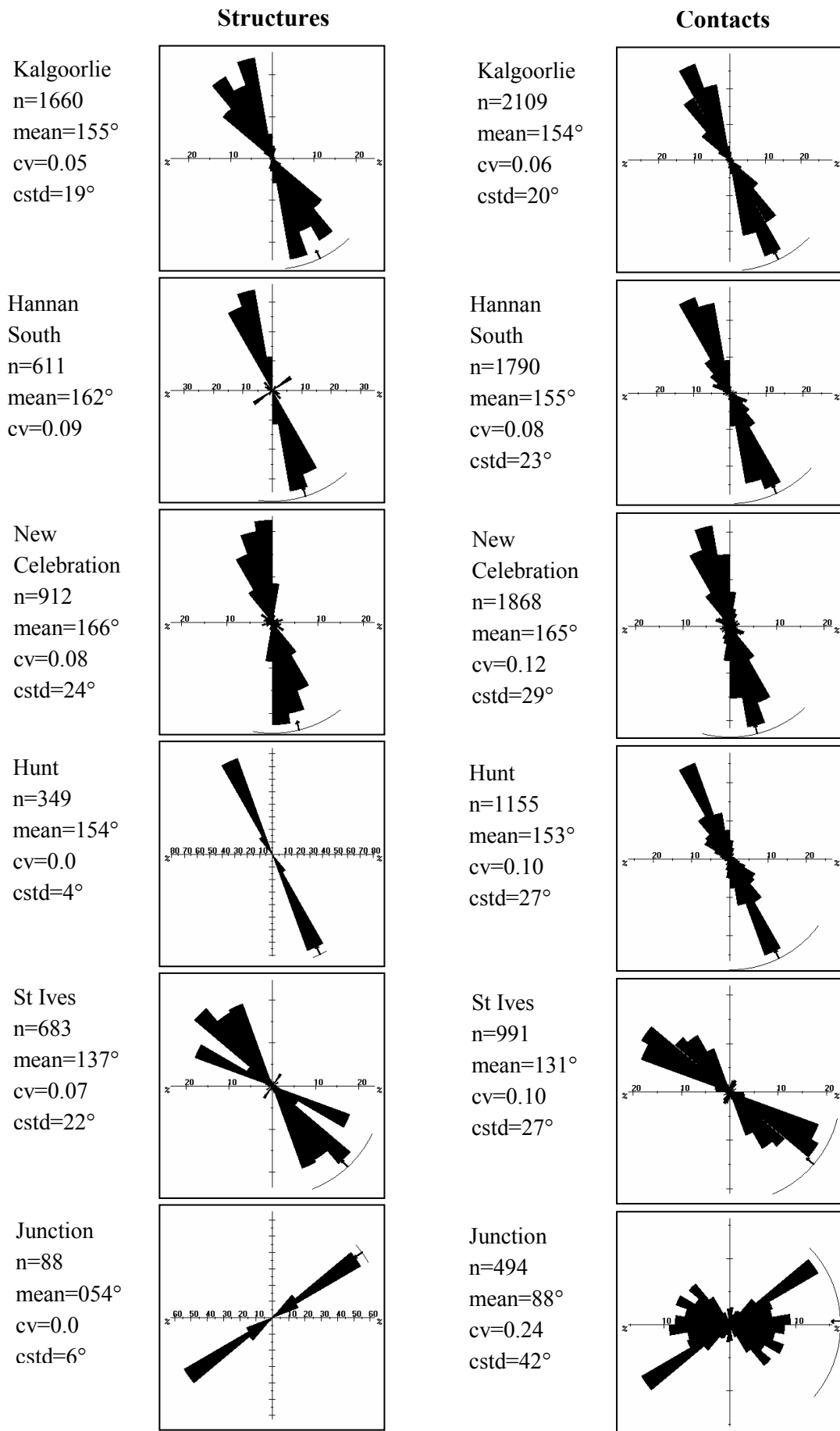
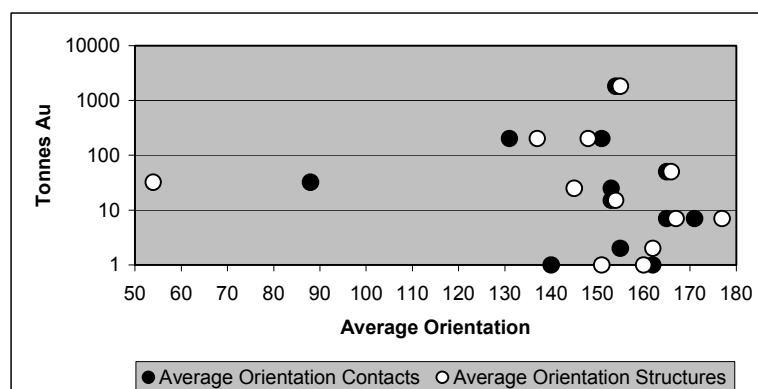


Figure 3.1.4B continued.

A)

Location	Pre-mining Resource (tonnes Au)	Average Orientation Contacts	Circular STD Contacts	Average Orientation Structures	Circular STD Structures
Menzies	25	153	34	145	21
Comet Vale	7	165	23	167	23
Big Four	1	162	11	160	13
Bardoc	7	171	15	177	26
Paddington	200	151	18	148	18
Gidji	1	140	22	151	15
Kalgoorlie	1800	154	20	155	19
Hannan South	2	155	23	162	25
New Celebration	50	165	29	166	24
Hunt	15	153	27	154	4
St Ives	200	131	27	137	22
Junction	32	88	42	54	6

B)



C)

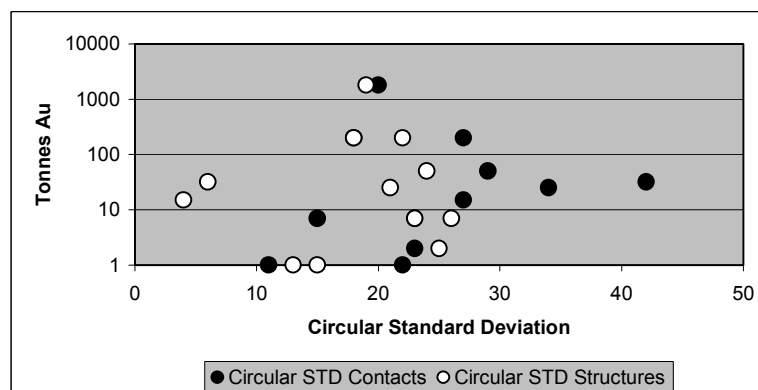


Figure 3.1.5. A) Table with pre-mining gold endowment, average orientation of contacts and structures, and circular standard deviation of contacts and structures, for the twelve districts shown in Fig. 3.1.4. Circular standard deviation corresponds to statistical variation of measurements of 100 m line segments as shown on a rose diagram (see example in Fig. 3.1.2). B) Plot of gold endowment versus average orientation of contacts and structures, showing no direct relationship. C) Plot of gold endowment versus circular standard deviation of contacts and structures, showing no direct relationship. The lack of relationship between average orientation and gold endowment may be a true feature of the system, but the scale dependence of contact and structure orientations means that large maps cannot be used to ascertain this relationship. This highlights the difficulty in determining the appropriate scale of measurement, in order to establish a relationship between map-scale geologic features and gold endowment.

Results - Fractal Dimensions

Fractal dimensions of lithologic contacts were calculated on a 10 km grid across the Yilgarn Craton and used to determine the relationship between geologic complexity and the distribution and size of orogenic gold deposits (Fig. 3.1.6). A contour map of the fractal grid (Fig. 3.1.6C) reveals a pattern of complexity across the craton, coinciding broadly with greenstone belts. The regions of maximum complexity (largest fractal dimensions) occur within greenstone belts, and, initially, we expected the largest gold deposits to occur there, based on suggested empirical relationships between complexity and gold endowment (Phillips et al., 1996; Groves et al., 1997; Groves et al., 2000). Instead, however, we found that the largest gold deposits occur along the steepest complexity gradients (Fig. 3.1.6D and Fig. 3.1.7). The gradients generally correspond to tectonic or structural domain boundaries, and most gold deposits are aligned along these gradients (Fig. 3.1.6D). The steepest complexity gradients occur along granite-greenstone contacts, as would be expected. Within greenstone belts, there are more subtle complexity gradients associated with lithologic contacts. These gradients occur, for example, between sedimentary rock units of low complexity and volcanic and intrusive rock units with more complex lithologic patterns.

The largest, and only giant gold deposit in the Yilgarn Craton, the Golden Mile, occurs at a steep gradient within the Kalgoorlie Terrane greenstone belt (Fig. 3.1.7A). This gradient corresponds to the transitional zone between more complex patterns of geologic contacts, associated with mafic intrusive and basaltic units in the Kalgoorlie area, and less complex patterns associated with a thick, overlying sequence of sedimentary units (Black Flag Beds) to the north. It is significant to note that the peaks for gold endowment occur adjacent to the regions that are depleted in gold, suggesting a relationship between the two (see Discussion below and Figure 2.4.2 in *Section 2.4*). Note also that while gold peaks along the Boulder-Lefroy Shear Zone tend to ≥ 100 tonnes, they are an order of magnitude less along the Bardoc Tectonic Zone, suggesting a fundamental difference in gold endowment.

The profiles of gold and complexity along the Laverton Tectonic Zone, from south to north, show a similar relationship (Fig. 3.1.7B). The largest gold peak (Sunrise Dam ~200 tonnes Au) occurs along the steepest complexity gradient, north of the Celia Lineament. Significantly, this complexity gradient is also associated with a contact between thick sedimentary units and mafic to intermediate volcanic host rocks.

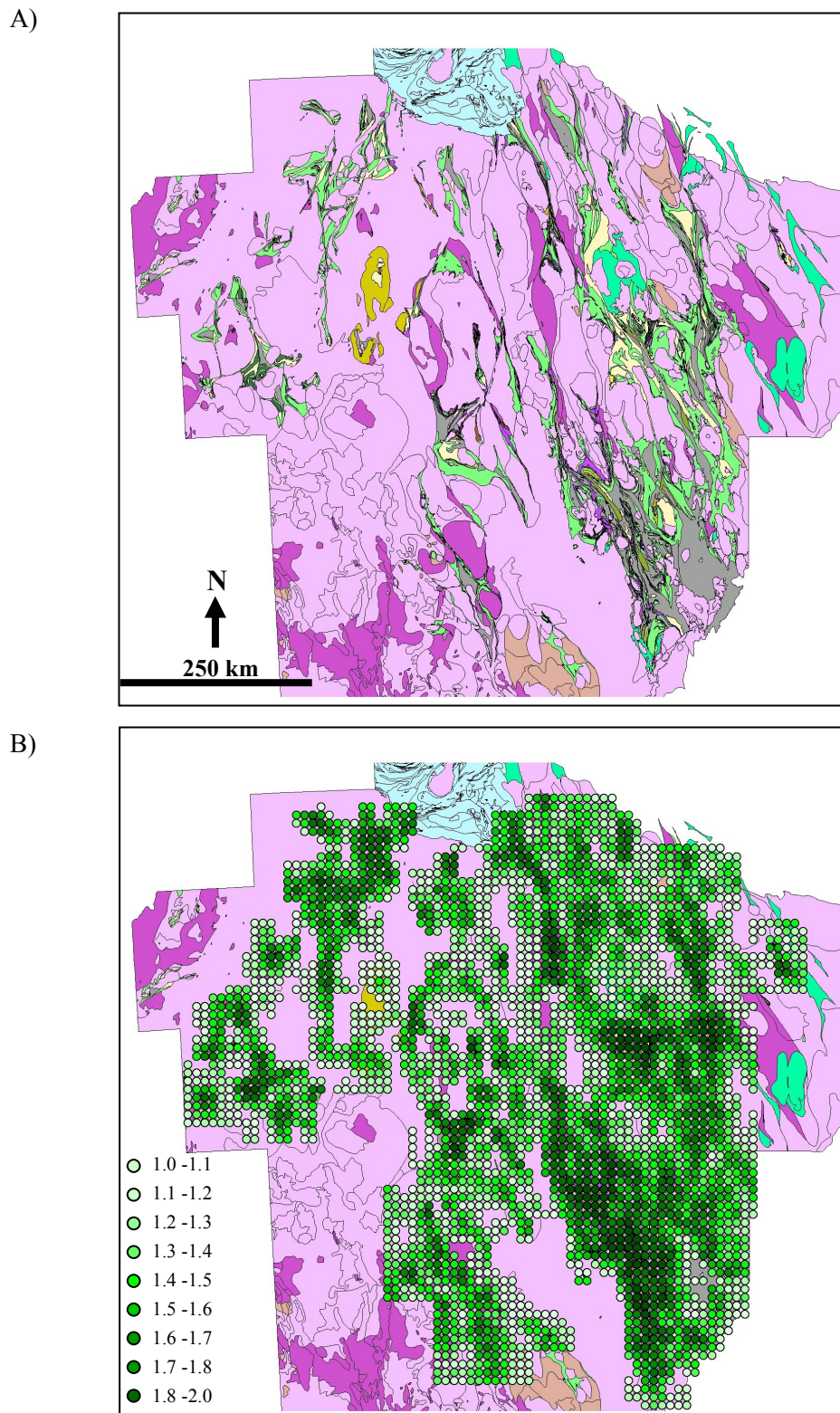


Figure 3.1.6. A) GIS geology map of the Yilgarn Craton (Knox-Robinson et al., 1996). B) Fractal dimensions of lithologic contacts were calculated on a grid with a 10 km node spacing. Grid nodes are shown in green, with darker shades indicating larger fractal dimensions, i.e., greater complexity, coinciding with greenstone belts.

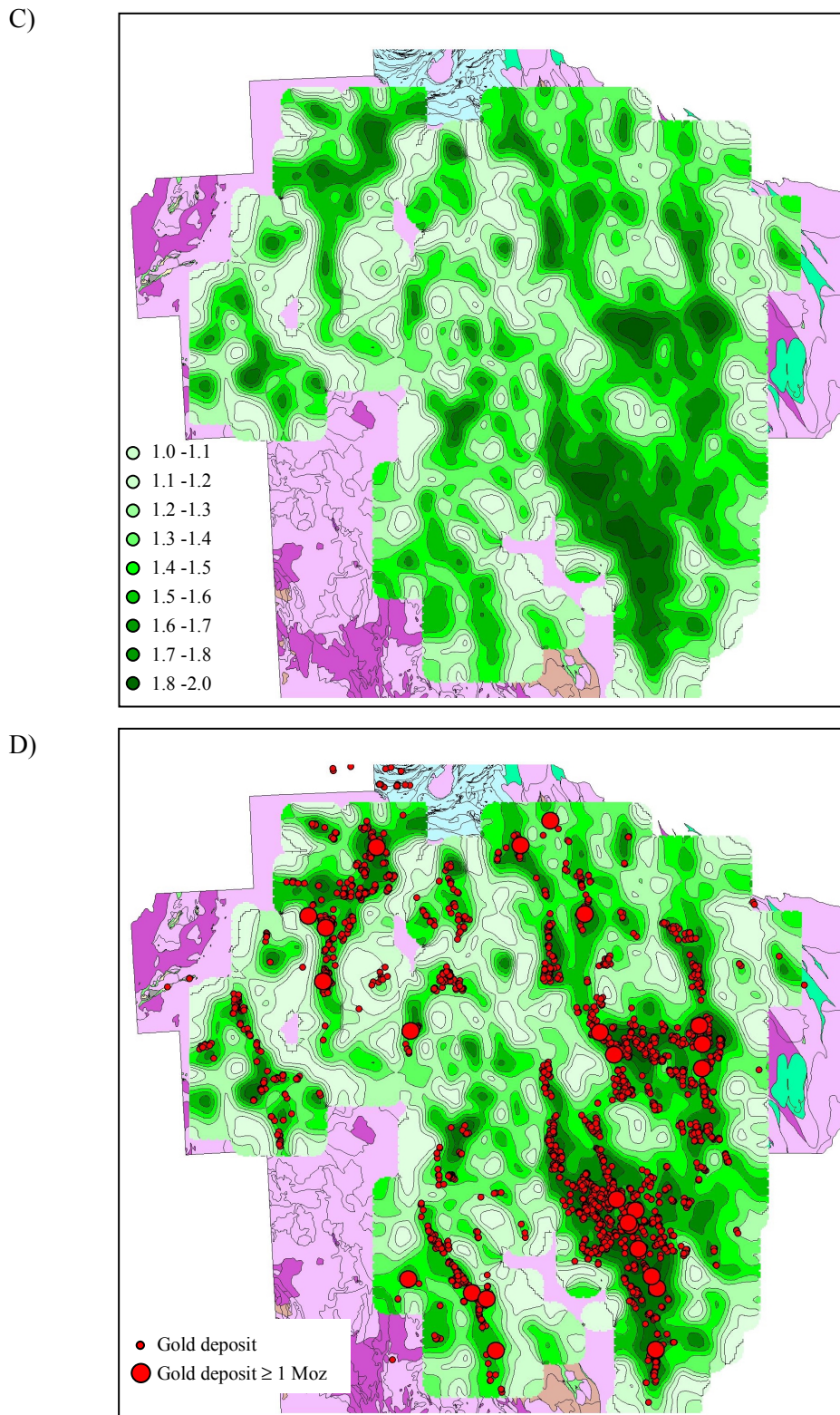


Figure 3.1.6 continued. C) Contour map of fractal dimension grid from (B) with same colour scheme. Darker green colours correspond to areas of greater complexity. D) Locations of over 10,000 historic and recent lode gold deposits, from the GSWA Minedex database (Townsend et al., 2000). Larger circles indicate deposits with ≥ 1 Moz gold; most of these occur adjacent to areas of greatest complexity or in areas with steep complexity gradient.

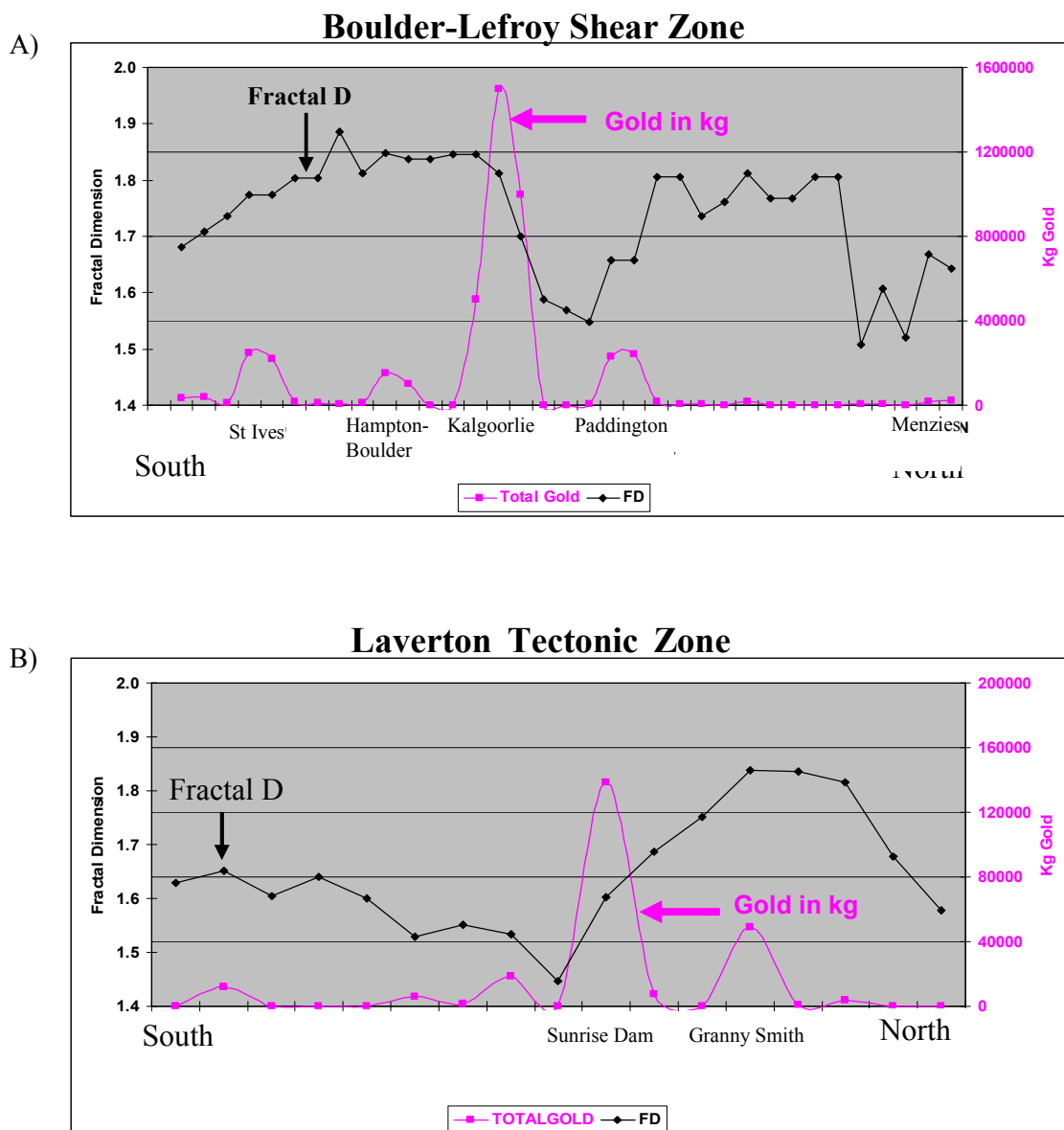


Figure 3.1.7. Profiles showing the relationship between fractal dimension gradients and gold endowment. The gold profiles in these figures are from a compilation of all available data, including historic and recent production, as well as remaining resources (Townsend et al., 2000). This provides the best estimate of a pre-mining gold endowment for the regions in the Yilgarn Craton. A) Profile along the Boulder-Lefroy Shear Zone and Bardoc Tectonic Zone, from south to north (left to right, Junction to Menzies). The Golden Mile (> 1,800 tonnes Au) occurs near the steepest fractal dimension gradient, between the complex geologic features of the Kalgoorlie area and thick sedimentary rock units (Black Flag Beds) to the north at Gidji. Paddington also occurs at a steep gradient north of Kalgoorlie, while to the south, St Ives occurs at a less steep gradient and Hampton-Boulder occurs within the high fractal profile. B) Profile along the Laverton Tectonic Zone, from south to north. Sunrise Dam (>200 tonnes Au) occurs at the steepest fractal gradient. This gradient is associated with the contact between a thick sequence of sedimentary units and more complex mafic volcanic host rocks, north of the Celia Lineament.

This study suggests that large gold deposits generally occur at steep fractal dimension gradients. A steep gradient is defined empirically as a significant change in fractal dimension along at least three consecutive grid nodes on the same gradient. In Fig. 3.1.7, the significant changes in fractal dimension are approximately 0.3 over three grid points at Kalgoorlie and 0.4 over 4 grid points at Laverton. We found that significant gradients to be 0.3 to 0.5 fractal dimensions over 3 to 5 consecutive grid points. Because the distance between grid points depends on map scale, the same definition of significant or steep gradient should apply to any map. Testing this on a series of more detailed maps is suggested as a topic for further study.

This has significant implications for exploration. Fractal dimensions provides a method of map analysis that can efficiently focus exploration efforts into smaller (ie, district-scale) areas of regional-scale maps. The use of fractal dimensions on more detailed maps may allow delineation of deposit-scale areas for exploration targeting.

Discussion and Conclusions

This study demonstrates that the use of scale-dependent methods for quantifying map features is not only cumbersome, requiring maps at several different scales, but also sometimes irrelevant because of incorrect choice of scale (Fig. 3.1.5). Fractal dimensions, by contrast, is a method of quantifying complexity that is independent of scale because it is based on the self-similarity of geologic patterns. As shown above in ***Methodology***, fractal dimension combines components of density and orientation in a single value, which can be used to represent the geologic complexity of a given area. Because the orientation and density of potential fluid pathways affect hydrothermal fluid flow, a map of fractal dimension distributions can be used to highlight areas of increased potential for focussed fluid flow, and therefore increased potential for gold deposit formation.

Complexity of geological structures, including lithological contacts, not only indicates areas of increased likelihood for focussed fluid flow, but also the variety of rocks provides chemical gradients that can favor gold-depositional mechanisms, such as fluid-rock interaction (Cox, 1999), as well as phase separation and “back-mixing” of evolved ore fluids (Sibson, 2001). This is significant because there is commonly evidence for multiple ore-depositional processes in larger orogenic deposits (Hodgson et al., 1993).

The movement of hydrothermal fluids through pathways in the crust is driven primarily by pressure gradients. The large volumes of focussed fluid flow necessary for the formation of large orogenic gold deposits requires the accumulation and intermittent, high-flux discharge of strongly over-pressured fluids in the mid-crust (Sibson, 2001). Hydrothermal fluids can become over-pressured if there is a cap or seal on the hydrothermal system, such as thick, low-permeability sedimentary units. At Kalgoorlie and Laverton, the

thick sedimentary (i.e., low complexity) rock units that occur adjacent to the largest gold deposits, may have acted as seals that caused the hydrothermal system to become locally overpressured. This suggests that map-scale patterns of lithologic contacts can provide an indication of crustal-scale controls on hydrothermal fluid flow.

Fluid flow in hydrothermal systems can be either focussed or dispersed, depending on the degree of connectivity and permeability in the network of fluid pathways (Cox et al., 2001). The most significant factor in the formation of large orogenic gold deposits is focussed flow of large volumes of hydrothermal fluid in well-connected, or linked, networks of fluid pathways. This requires focussing of fluids from a large volume of well-connected rocks at depth, towards a narrow, focussed and high permeability zone at around the level of deposit formation. Connectivity is an indirect measure of permeability, and the degree of connectivity is related to the density and orientation of fluid pathways, which are quantified by fractal dimensions. Thus, fractal dimensions are a measure of the potential for increased connectivity and permeability. Lithologic complexity, as measured by larger fractal dimensions, implies that a certain area has the potential to produce interconnected pathways, or zones of high connectivity.

Large networks with very high connectivities generate more dispersed fluid flow, which will not allow high enough fluid fluxes to generate economic gold deposits (Cox, 1999). Thus, changes in connectivity are required to focus fluids. If fractal dimensions can be used as a measure of potential connectivity/permeability, fractal dimension gradients can be thought of as connectivity or permeability gradients. Changes in connectivity, which are related to changes in permeability and porosity, cause pressure gradients that influence fluid flow. This is possibly the reason why the largest gold districts occur at steep gradients, adjacent to areas with the largest fractal dimensions. At steep gradients, fluids that were unable to rise through regions of poor connectivity/permeability would become focussed. These would create the potential for the high fluid fluxes required to form large gold deposits.

In this scenario, the main assumption about crustal-scale hydrothermal fluid flow is that it is homogenous everywhere at depth. This is a fundamental assumption of the continuum model (Groves et al., 1995), and a reasonable one considering the large volumes of fluid generated by metamorphic devolatilisation of greenstones at depth (Powell et al., 1991; Phillips and Powell, 1993; Oliver, 1996). The method outlined in this study establishes possible links between map-scale geologic complexity and crustal-scale controls on hydrothermal fluid flow that influence the formation of larger orogenic gold deposits. This is significant in that it explains the occurrence of larger gold districts through flow of a

homogenous, deeply-sourced ore fluid, controlled by pressure gradients, without necessarily requiring input from shallow, intrusion-related magmatic fluids.

3.2. Sulfur Isotopes

Objectives

Sulfides in orogenic gold deposits typically have sulfur isotope ($\delta^{34}\text{S}$) values that are in a narrow range between 0 to +9‰, indicating precipitation from a dominantly reduced ore-fluid and a sulfur source that was isotopically uniform (McCuaig and Kerrich, 1998). However, some giant orogenic gold deposits (e.g., Golden Mile, Kirkland Lake, Timmins) have much larger ranges of $\delta^{34}\text{S}$ values in gold-related pyrites, indicating that oxidized fluids may have played a role in ore formation (Ohmoto and Rye, 1979). These anomalous $\delta^{34}\text{S}_{(\text{py})}$ values typically occur with alteration mineral assemblages that include hematite±anhydrite±V-micas, also indicating deposition under oxidizing conditions. Various studies propose that such oxidized fluids were responsible for the anomalously large gold endowment in several giant deposits (Cameron and Hattori, 1987; Walshe et al., 1999; Hall et al., 2001). Whether the ore fluids were originally oxidized (i.e., magmatic volatiles) or whether they became oxidized through ore-depositional processes (i.e., fluid-rock reaction, phase separation and/or fluid mixing) is a highly controversial issue in genetic models of orogenic gold-deposit formation (Phillips et al., 1986; Cameron and Hattori, 1987; Hattori, 1987; Cameron, 1988; Kerrich, 1989; Phillips et al., 1996;). This Section focuses on deposits in the Eastern Goldfields Province of the Yilgarn Craton, to determine whether anomalously negative $\delta^{34}\text{S}_{(\text{py})}$ values, or significantly large ranges of $\delta^{34}\text{S}_{(\text{py})}$ values, are an indication of fluid sources and/or gold depositional processes that are directly related to the formation of larger (i.e., world-class or multi-million ounce) orogenic gold deposits.

In order to determine these relationships, we document $\delta^{34}\text{S}_{(\text{py})}$ values in a variety of orogenic gold deposits and sedimentary rocks from the Eastern Goldfields Province, with new analytical results from this study and results compiled from previous studies. We also document relationships between variations in sulfide sulfur-isotope composition and district-to deposit-scale factors, such as host rock composition, hydrothermal alteration assemblages, and structural setting.

New analytical results of $\delta^{34}\text{S}_{(\text{py})}$ suggest that Archean orogenic gold deposits in the Eastern Goldfields Province fall into two distinct groups (Fig. 3.2.1). One group of deposits has a restricted range of positive $\delta^{34}\text{S}_{(\text{py})}$ values between 0 and +9‰, with a mean value of approximately 3.0‰, and rare occurrences of anomalously positive and negative $\delta^{34}\text{S}_{(\text{py})}$ values between –6 and +12‰ (Fig. 3.2.1A). The second group of deposits has a broader range of negative $\delta^{34}\text{S}_{(\text{py})}$ values between –8 and 0‰, with a mean value of –2.4‰ (Fig. 3.2.1B). Importantly, both groups include world-class (>100 tonnes of gold) and smaller deposits. In

contrast, unmineralized sulfides in sedimentary rocks throughout the Eastern Goldfields Province have a broad range of positive $\delta^{34}\text{S}_{(\text{py})}$ values between 0 and +12‰, with a mean value of approximately +5.6‰ (Fig. 3.2.1C). In this Section, various geologic characteristics of the three groups in Fig. 3.2.1 are documented, with specific examples, in order to determine geologic constraints on sulfur isotopic composition and variation.

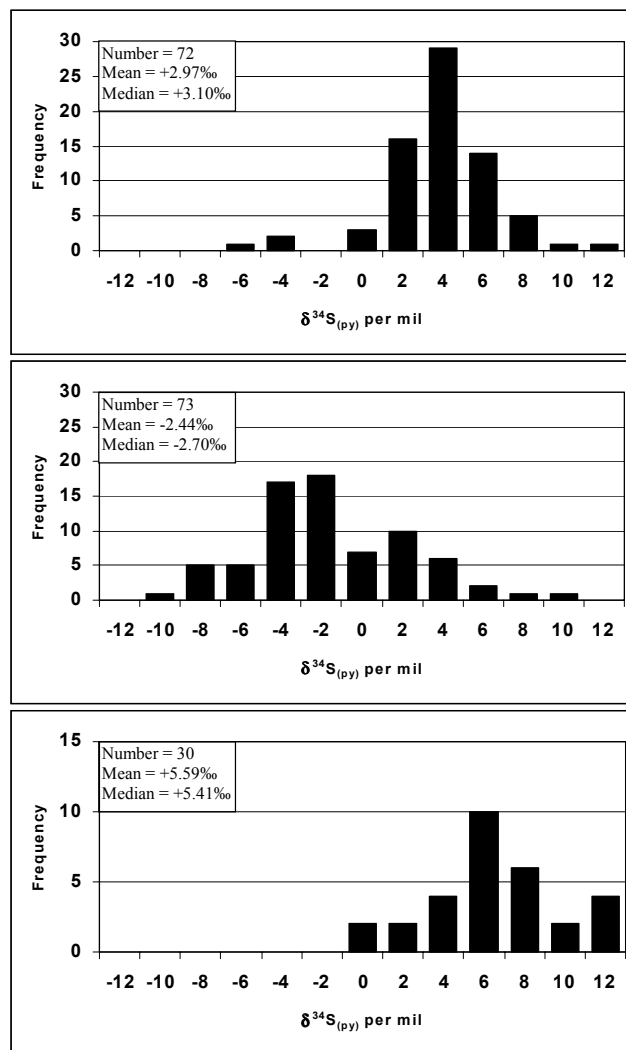


Figure 3.2.1. Histograms of sulfide sulfur-isotope values from the Yilgarn Craton. Analytical results are from this and previous studies, as listed in Table ref. (A) Typical distribution in normal deposits with average $\delta^{34}\text{S}_{(\text{py})}$ values approximately +3‰ and rare occurrences of anomalously positive and negative values, ranging from -8 to +12‰. (B) Typical distribution in anomalous deposits, with average $\delta^{34}\text{S}_{(\text{py})}$ values of -2.4‰ and abundant negative values. (C) Typical distribution in unmineralized sedimentary sulfides with average $\delta^{34}\text{S}$ values of approximately +5.5‰ and mostly positive values ranging from 0 to +12‰.

Methodology

A total of 185 sulfur isotope analyses were performed for this study. Results are summarised in Tables 3.2.1 (gold-related pyrites) and Table 3.2.3 (sedimentary sulfides).

Sample Selection. A total of 92 samples were selected for sulfide sulfur-isotope analysis from a wide variety of orogenic gold deposits and regional locations in the Eastern Goldfields Province. These include 79 samples from orogenic gold deposits and 13 unmineralized samples from interflow sedimentary units in mafic and ultramafic rocks. Deposit samples were selected to investigate variations in sulfur isotope composition related to deposit-scale factors, such as host rock composition, hydrothermal alteration assemblages, and structural setting. Samples of unmineralized sedimentary sulfides were selected to determine the $\delta^{34}\text{S}$ composition of potential source regions in various lithologic units. The majority of the samples were selected from archived PhD and BSc Honours collections at the Edward de Courcy Clarke Geological Museum at UWA. The remaining samples were collected during field visits to various mines and drill core storage yards in the Eastern Goldfields Province.

Sulfur Isotope Analysis of Pyrites. Analytical techniques used in this study include laser ablation of *in-situ* sulfides (Huston et al., 1995) and conventional digestion techniques for pyrite separates (Robinson and Kusakabe, 1975) and whole rock pulps (Canfield et al., 1986). All results are reported as $\delta^{34}\text{S}$ values in parts per thousand (per mil = ‰), relative to the Canyon Diabolo Triolite (CDT). Results include 161 laser ablation analyses, 20 conventional analyses of pyrite separates, and 4 conventional analyses of whole rock pulps. All analytical work was completed at the Central Science Laboratory and the Centre for Ore Deposit and Exploration Studies, Department of Earth Sciences at the University of Tasmania.

Recent advances in laser ablation technology allow individual pyrite crystals, or different parts of pyrite crystals (e.g., cores and rims), to be analysed with a laser spot size of less than 100 microns (Crowe et al., 1990; Huston et al., 1995). Analytical precision is typically less than 0.05‰. Conventional analytical techniques, used in most previous sulfur isotope studies (Lambert and Donnelly, 1990), commonly results in homogenisation of grain-scale variations in isotopic composition. Analytical precision is typically greater than 0.1‰.

District	Deposit Name	Deposit Tonnes Au	Number of Samples	Number of Analyses	Minimum $\delta^{34}\text{S}_{(\text{sulfide})}$ value	Maximum $\delta^{34}\text{S}_{(\text{sulfide})}$ value	Analytical Results of	Analytical method
Mt Magnet	Water Tank Hill	1.3	24	24	-0.90	4.10	Lambert et al., 1982, WMC unpubl. data	CONV
	Morning Star	7.3	14	14	0.70	3.50	Lambert et al., 1982, WMC unpubl. data	CONV
Wiluna	Wiluna	86.0	?	?	-2.50	1.00	Hagemann, 1992	CONV
Leinster	Great Eastern	14.7	1	2	1.51	2.52	this study	LA
	Great Eastern		12	12	-0.60	2.10	Mikucki, 1997	CONV
Leonora	Forrest Mine	1.0	1	2	0.58	2.57	this study	LA
	Harbour Lights	10.0	2	3	-1.13	5.09	this study	LA
	Leonora Gold Blocks	1.0	1	1	7.12	7.12	this study	LA
	Sons of Gwalia	132.0	3	5	0.67	3.21	this study	LA
	Trump Mine	1.0	1	2	2.69	2.85	this study	LA
	Tarmoda	~100		34	-2.60	3.80	Duuring, 2001, unpubl. data	CONV
Laverton	Granny Smith	49.5	7	11	0.30	4.50	Ojala, 1995	CONV
	Lancefield	46.0	18	18	-6.40	3.20	Hronsky, 1993, WMC unpubl. data	CONV
	Sunrise Dam	~200	2	4	-6.84	2.46	this study	LA
	Sunrise Dam		17	17	-8.00	4.00	S. Brown unpubl. data	CONV
	Wallaby	~170	7	11	-6.80	6.16	this study, P. Kitto unpubl. data	LA
BTZ	Aphrodite	14.0	6	9	-0.29	4.10	this study	LA
	Paddington	200.0	2	6	2.67	10.62	this study	LA
Kumapli	Porphyry	10.6	14	20	-10.19	9.95	this study	LA
	Porphyry		3	3	5.13	10.76	this study	CONV/S extr.
Ora Banda	Golden Kilometre	16.6	5	5	0.60	3.70	Gebre-Mariam, 1994	CONV
	Golden Kilometre		2	5	3.14	6.95	this study	LA
	Golden Swan	1.0	1	2	3.42	5.35	this study	LA
	Lady Bountiful	11.4	4	9	2.27	9.45	this study	LA
	Lady Bountiful		5	5	-1.14	3.36	this study	CONV
	Mt Pleasant	16.6	1	3	-4.33	3.26	this study	LA
	Ora Banda	17.8	1	2	1.74	2.97	this study	LA
	Racetrack	12.6	3	3	2.70	3.50	Gebre-Mariam, 1994	CONV
	Racetrack		2	3	1.63	7.26	this study	LA
	Royal Standard	1.0	1	1	3.58	3.58	this study	LA
Binduli	Sand King	1.9	1	2	5.69	6.02	this study	LA
	Sand King	1.8		9	0.90	5.00	WMC unpubl. data	CONV
	Binduli	~50	4	5	-5.38	7.56	this study	LA
Kanowna Belle	Kanowna Belle	132.0	17	17	-3.50	3.60	Ren and Heithersay, 1997	CONV
	Kanowna Belle			75	-5.50	10.90	Ren and Heithersay, 1997; Ross, unpubl. data	LA
Kalgoorlie	Golden Mile	1800.0		90	-8.70	9.20	Hagemann et al., 1999	LA
	Golden Mile		212	212	-9.80	12.70	Clout, 1989	CONV
	Mt Charlotte	160.0	27	27	-3.80	8.90	Harbi, 1997	CONV
BLFZ	New Celebration	~50	5	8	-8.64	5.54	this study	LA
Kambalda	Hunt	10.0	3	7	1.02	4.92	this study	LA
	Hunt			3	4.40	8.00	Lambert et al., 1982	CONV
	Junction	57.0	6	6	2.20	5.10	Polito, unpubl. data	CONV
	Victory-Defiance	~200	8	13	-5.70	-1.49	this study	LA
	Victory-Defiance		20	45	-6.26	5.10	this study, Palin and Xu, 2000	CONV
	Poseidon South	10.0	1	2	7.28	7.88	this study	LA
	Chalice	18.3		14	1.80	3.50	Bucci et al., 2001	CONV
Norseman	North Royal	59.0	4	9	0.25	10.38	this study	LA
	Princess Royal		4	4	1.60	2.90	Golding et al., 1990	CONV

Table 3.2.1. List of gold deposits, indicating sources of sulfur isotope data used in this study. Locations are shown in Figure 3.2.2. Includes approximate size of deposit, in tonnes of gold, number of samples, number of analyses, and analytical method (CONV is conventional analysis and LA is laser ablation analysis).

Results

Results of 133 laser ablation analyses and 24 conventional analyses from 79 deposit samples, performed for this study, are presented in this section. Deposit locations and ranges of values are shown in Fig. 3.2.2.

Deposits with Normal $\delta^{34}\text{S}_{(\text{py})}$ Values This section includes brief descriptions of six orogenic gold deposits in the Eastern Goldfields Province that display normal ranges of $\delta^{34}\text{S}_{(\text{py})}$ values in gold-related pyrites, as shown in the histogram in Fig. 3.2.1A. The deposits are Hunt, Sunrise Dam, Lady Bountiful, Mt Pleasant, North Royal at Norseman, and Great Eastern/Lawlers. Photographs of rock samples from these deposits, with $\delta^{34}\text{S}_{(\text{py})}$ values, are shown in Fig. 3.2.3. The $\delta^{34}\text{S}_{(\text{py})}$ values shown in Fig. 3.2.3 highlight the **rare** occurrences of anomalous values in samples from deposits with otherwise normal sulfide sulfur-isotopic compositions. Deposits with **abundant** occurrences of anomalous $\delta^{34}\text{S}_{(\text{py})}$ values are described in the next section.

Hunt Mine, Kambalda. The Hunt mine is located in the Kambalda district of the Kalgoorlie Terrane, and contained a pre-mining resource of approximately 10 tonnes of gold (Witt, 1992a). Gold mineralization is hosted in 10 to 20 m thick, steeply-dipping, brittle-ductile shear zones within the Lunnon Basalt (the lowest in the local stratigraphy), and occurs in pyritic alteration halos around quartz veins and as free gold associated with tellurides and nickel sulfides in veins and vein margins (Neall and Phillips, 1987). Previous studies show a narrow range of $\delta^{34}\text{S}_{(\text{sulfide})}$ values (using conventional analytical techniques), with gold-related pyrite values ranging from +4.4 to +8.0‰ (Phillips and Groves, 1984) and nickel sulfide and sedimentary sulfide values ranging from +0.9 to +4.6‰ (Donnelly et al., 1978; Seccombe et al., 1981). Results from this study support this narrow range, with $\delta^{34}\text{S}_{(\text{py})}$ values ranging from +3.41 to +4.92‰ (n=5) in vein-related wall rock alteration (Fig. 3.2.3A) and auriferous quartz veins (Fig. 3.2.3B) in the sheared biotite-chlorite-carbonate schist host rock. Additional results from this study include $\delta^{34}\text{S}_{(\text{py})}$ values of +1.02 and +1.07‰ in an unaltered minor intrusion (“megacrystic malchite”, sample 108484 of (Perring, 1989)) approximately 800 m southeast of the Hunt mine.

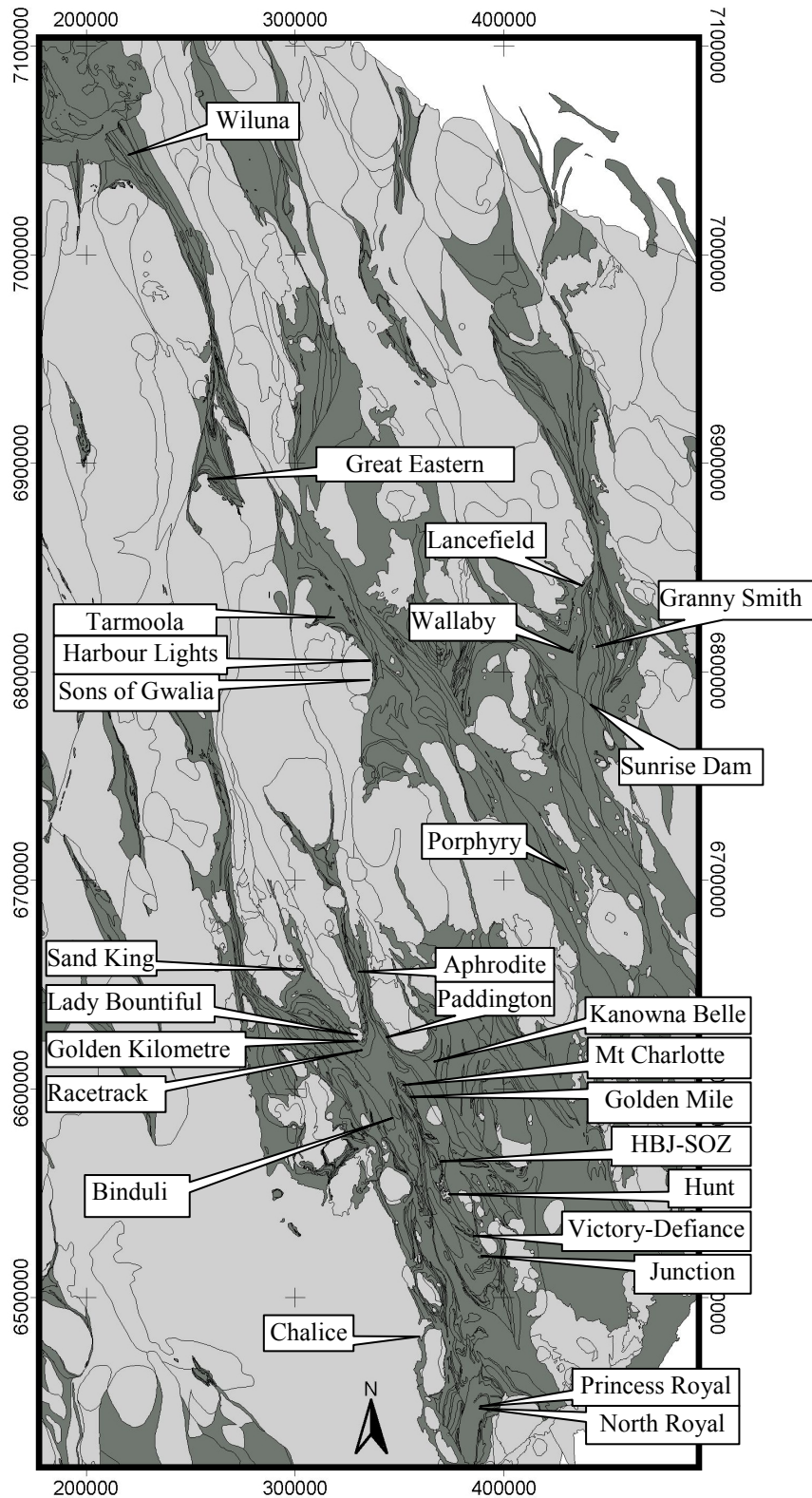


Figure 3.2.2. (A) Map of the Eastern Goldfields Province (modified from Knox-Robinson *et al.*, 1996), showing locations of deposits with sulfur isotope data from this study and previous studies. Results are shown in Table 3.2.1 and (B) on next page. Greenstones are dark grey and granitoids are light grey. Map grid is in AMG coordinates, in metres.

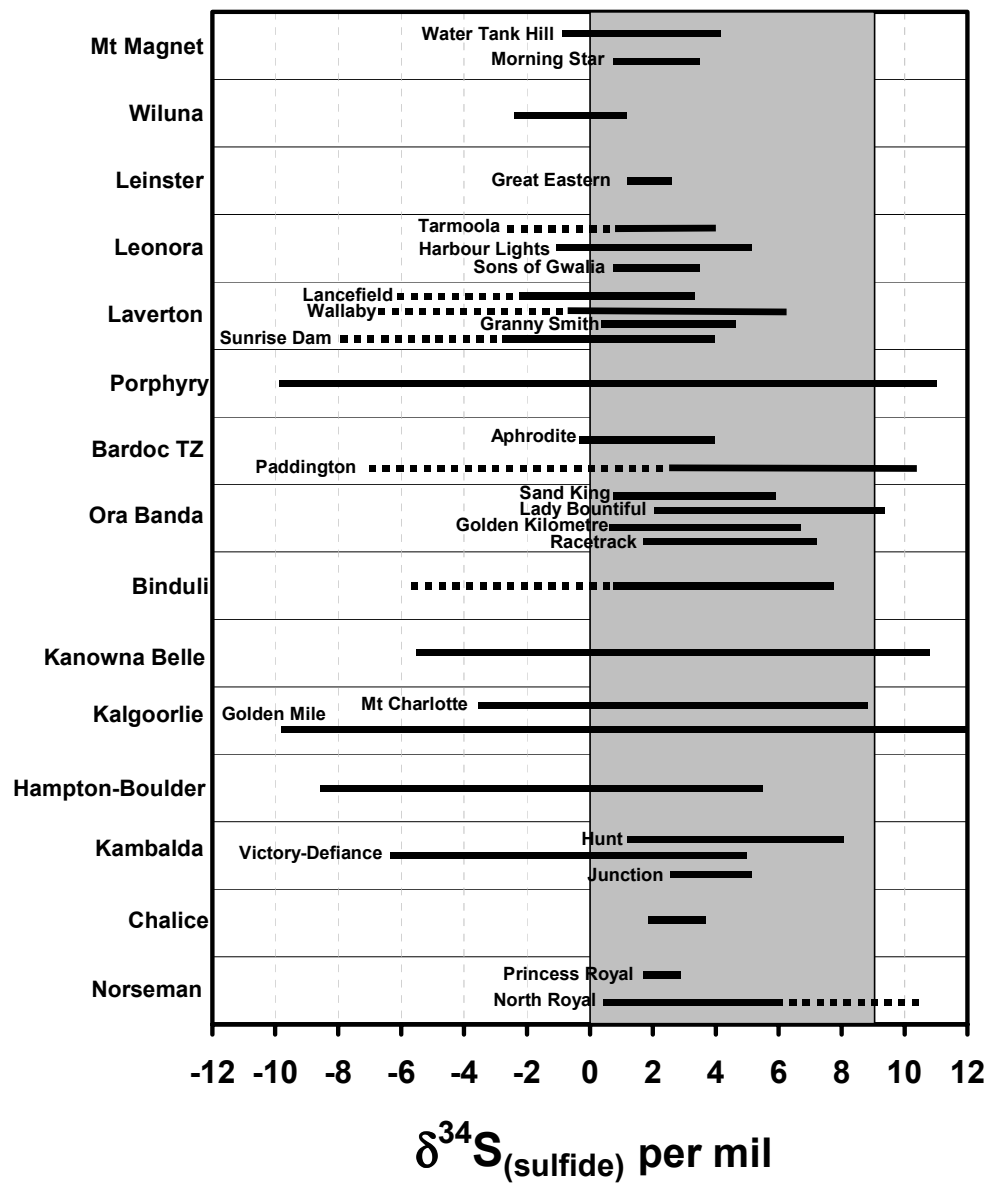


Figure 3.2.2. (B) Ranges of sulfide sulfur-isotope values by district, arranged from north to south and corresponding to locations in (A) on previous page. Note that the values from Water Tank Hill and Morning Star (in the Mt Magnet district in the Murchison Province) are shown only for comparison purposes. Dashed lines correspond to $\delta^{34}S_{(P)}$ values based on limited data (i.e., one sample or analysis). The grey area corresponds to the typical range of values (0 to +9‰) for Archean orogenic gold deposits (McCuaig and Kerrich, 1998).

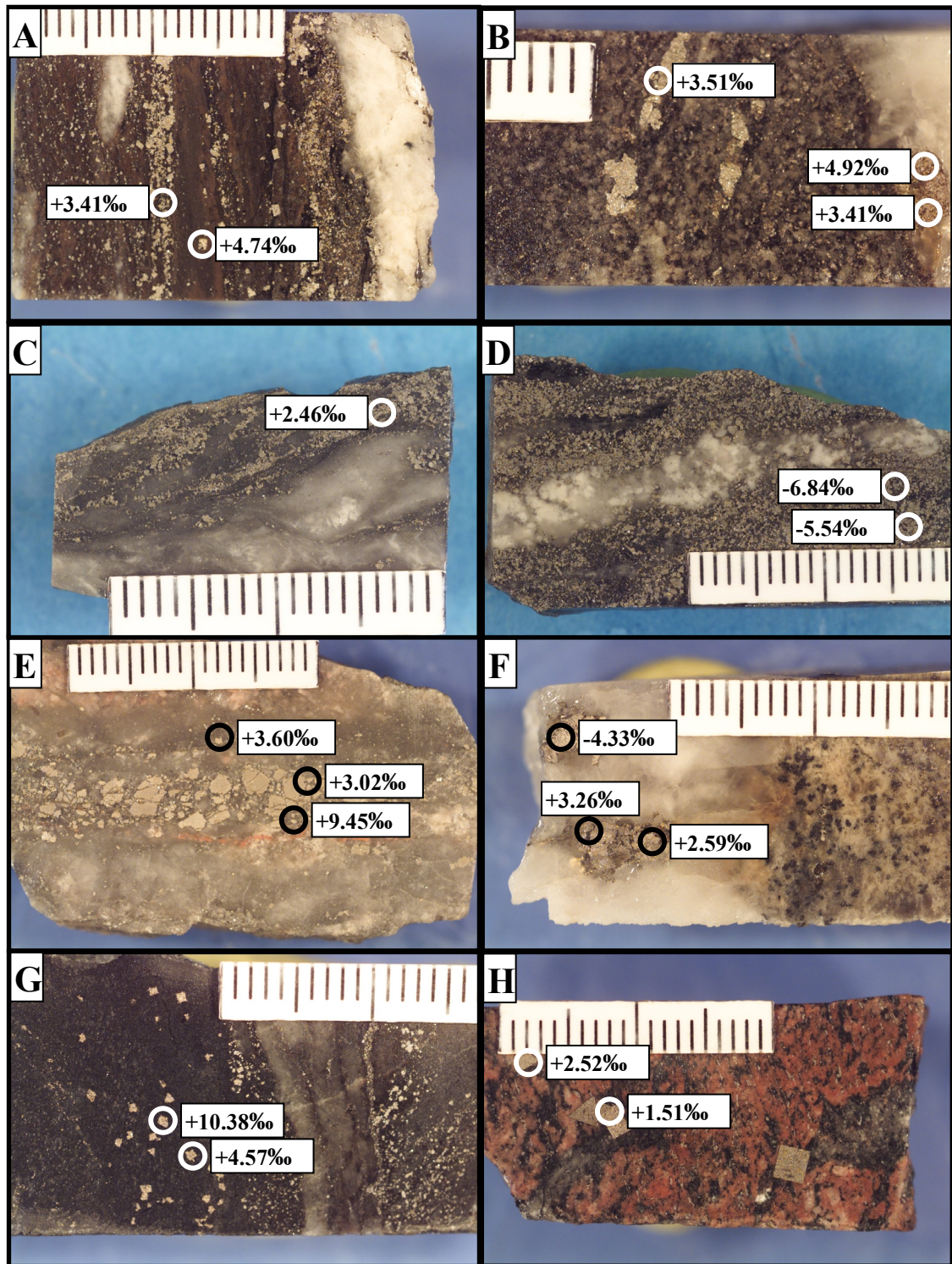


Figure 3.2.3. Photographs of samples from deposits in the Eastern Goldfields Province, with results of $\delta^{34}S_{(py)}$ analyses from this study. (A) Hunt Mine, Kambalda (sample 109673 of Mueller, 1990) weakly mineralized pyrite-biotite-chlorite-ankerite schist from the 12 Level, 1221 east drive, A Fault, with $\delta^{34}S_{(py)}$ values of +3.4‰ and +4.7‰. (B) Hunt Mine, Kambalda (sample 109681 of Mueller, 1990) highly mineralized pyrite-biotite-ankerite schist adjacent to scheelite-bearing quartz vein from 10 Level, 1020 east drive, A-Fault, with $\delta^{34}S_{(py)}$ values of +3.5‰, +4.9‰ and +3.4‰. (C) Sunrise Dam (sample CD191 of Brown, 2002) with a $\delta^{34}S_{(py)}$ value of +2.46‰. (D) Sunrise Dam (sample CD373 of Brown, 2002) with $\delta^{34}S_{(py)}$ values of

–6.84 and –5.54‰. This is a difference of 9.3‰ in two samples less than 30 metres apart, from the same mineralized horizon. (E) Lady Bountiful (sample 107862 of Cassidy, 1992) from the Liberty Granodiorite, near the contact with the Mt Ellis Sill (lower gabbro) and the Cashmans metasedimentary unit. The pyrite in the central portion of the vein has a $\delta^{34}\text{S}_{(\text{py})}$ value of +3.6‰, while a pyrite only 3 mm away on the vein margin has a $\delta^{34}\text{S}_{(\text{py})}$ value of +9.4‰, a shift of 5.8‰. Note that the heavier value is adjacent to a thin seam of hematite on the vein margin. (F) Mt Pleasant, Ora Banda (sample 107958 of Mueller, 1990) at the contact between a quartz-vein and sericite-ankerite altered metagabbro. Two euhedral pyrites in the vein have $\delta^{34}\text{S}_{(\text{py})}$ values of +2.6 and +3.3‰. An adjacent subhedral pyrite, less than 5 mm away, has a $\delta^{34}\text{S}_{(\text{py})}$ value of –4.3‰, a shift of 6.9‰. (G) North Royal, Norseman (sample 109622 of Mueller, 1990), in the transition zone between inner chlorite-biotite and outer chlorite-bearing alteration assemblages. Subhedral pyrites less than 3 mm apart show a large range of $\delta^{34}\text{S}_{(\text{py})}$ values, from +4.6‰ to +10.4‰, a shift of 5.8‰. (H) Great Eastern, Agnew, (sample 106711 of J. Mikucki, 1997). This late-stage chlorite-hematite alteration is associated with gold-telluride-mineralisation from a relatively oxidized, low XCO_2 , low-salinity ore fluid (J. Mikucki, 1997). Two pyrites analyzed in the sample have $\delta^{34}\text{S}_{(\text{py})}$ values of +2.52 and +1.51‰, values not typical in sulfides precipitated from oxidized fluids.

Sunrise Dam, Laverton. The Sunrise Dam deposit is located at the southern end of the Laverton Tectonic Zone, and contained a pre-mining resource of over 200 tonnes of gold (ref). Gold mineralization is hosted mainly in lodes and shear zones in a sequence of volcanoclastic units, magnetite-bearing shales, and rhyodacite porphyry dikes, and occurs with pyrite±arsenopyrite in alteration zones characterized by disseminated sericite±ankerite/dolomite (Brown, 2000). Based on conventional sulfur isotope analyses, the average $\delta^{34}\text{S}_{(\text{py})}$ value in ore is approximately +2.0‰ (n=17, S. Brown unpublished PhD data), and there is no appreciable difference in the two main mineralized structures, the Sunrise Shear Zone and the Western Lodes, despite significant differences in styles of mineralization and average gold grades (Brown, 2000). However, there is evidence for rare occurrences of anomalously negative $\delta^{34}\text{S}_{(\text{py})}$ values. The two mineralized samples analyzed in this study (Fig. 3.2.3C and D) are from the same magnetite-bearing shale unit in the Sunrise Shear Zone and show a large difference in $\delta^{34}\text{S}_{(\text{py})}$ values. A euhedral pyrite in Fig. 3.2.3C has a $\delta^{34}\text{S}_{(\text{py})}$ value of +2.46‰, whereas subhedral and inclusion-rich pyrites in Fig. 3.2.3D have $\delta^{34}\text{S}_{(\text{py})}$ values of –6.84 and –5.54‰, a difference of 9‰.

Lady Bountiful, Ora Banda. Lady Bountiful is located in the Ora Banda Domain, approximately 36 km NW of Kalgoorlie, and contained a pre-mining resource of approximately 11.4 tonnes of gold (Cassidy, 1992). Gold mineralization is hosted primarily in brittle quartz-vein arrays in the Liberty Granodiorite and zones 5 to 8 of the Mount Pleasant layered mafic sill, and occurs both as free gold and in pyrite±tellurides (Cassidy and Bennett,

1993). Wall rock alteration assemblages include quartz-albite-muscovite-calcite±chlorite±pyrite±rutile (Cassidy et al., 1998). Nine laser ablation and five conventional $\delta^{34}\text{S}_{(\text{py})}$ analyses were performed for this study, with 13 analyses ranging from -1.14 to $+4.79\%$, in both quartz veins and proximal alteration halos, and one anomalous value of $+9.45\%$ in a hematite-altered auriferous quartz vein (Fig. 3.2.3E). This anomalous sample in Fig. 3.2.3E is from the Liberty Granodiorite, near the contact with the Mt Pleasant Sill. The pyrite in the central portion of the vein has a $\delta^{34}\text{S}$ value of $+3.6\%$, whereas a pyrite 3 mm away near the vein margin has a $\delta^{34}\text{S}$ value of $+9.4\%$, a shift of 5.8% . The more positive value is adjacent to a thin seam of hematite on the vein margin. Analyses from this study, of pyrite+telluride from stage II gold mineralization (not shown), include $\delta^{34}\text{S}_{(\text{py})}$ values of $+2.45$ and $+4.79\%$.

Mount Pleasant, Ora Banda District. The Mount Pleasant deposit is approximately 35 km NW of Kalgoorlie and contained a pre-mining resource of approximately 16.6 tonnes of gold (Witt, 1992b). Gold mineralization occurs in narrow ($<10\text{m}$) brittle-ductile shear zones hosted in a low-grade tholeiitic metagabbro sill (Mueller, 1990; Witt, 1992b). The alteration assemblage in the ore zone includes sericite, biotite, ankerite and chlorite, and the ore mineral assemblage includes pyrite-pyrrhotite-arsenopyrite-sphalerite-galena with minor rutile and scheelite (Mueller, 1990; Witt, 1992b). Results from the present study include $\delta^{34}\text{S}_{(\text{py})}$ analyses from the contact between a scheelite-bearing quartz-vein and sericite-ankerite altered metagabbro (Fig. 3.2.3F). Two euhedral pyrites in the vein have $\delta^{34}\text{S}$ values of $+2.6$ and $+3.3\%$. An adjacent subhedral pyrite, less than 5 mm away in the same quartz vein, has a $\delta^{34}\text{S}$ value of -4.3% , a difference of 6.9% .

North Royal, Norseman. The North Royal mine is located in the Norseman Terrane, approximately 10 km north of the town of Norseman. The Royal reef lodes account for approximately 60 tonnes of the pre-mining resource of over 140 tonnes of gold in the Norseman district (ref). Gold mineralization is hosted in laminated quartz veins in brittle-ductile shear zones, mainly within the gabbroic Royal Dyke, and occurs with pyrite±pyrrhotite and Ag-Pb-Au tellurides (McCuaig et al., 1993). Wall rock alteration assemblages include chlorite-biotite-carbonate-pyrite-gold±scheelite (McCuaig et al., 1993). Nine laser ablation $\delta^{34}\text{S}_{(\text{py})}$ analyses were performed for this study, from both quartz veins and proximal wall-rock alteration halos, with eight values ranging from $+0.25$ to $+5.81\%$, and one anomalous value of $+10.38\%$ (Fig. 3.2.3G). The sample in Fig. 3.2.3G is from the transition zone between inner chlorite-biotite and outer chlorite-bearing alteration assemblages, and shows a large range of $\delta^{34}\text{S}_{(\text{py})}$ values, from $+4.57\%$ to $+10.38\%$, in adjacent pyrites.

Great Eastern, Agnew District. The Great Eastern deposit, also known as Lawlers, is located in the Leinster district, and contained a pre-mining resource of approximately 14.7 tonnes of gold (Cassidy, 1992). Gold mineralization is hosted in diorite and tonalite, and occurs as two distinct structural styles: 1) early shear zones with pyritic biotite-calcite alteration; and 2) late-stage chlorite-hematite altered, gold-telluride-bearing, brittle vein arrays and breccias [Cassidy, 1992 #497; J. Mikucki, 1997 #498]. Results of a previous stable isotope study show $\delta^{34}\text{S}_{(\text{py})}$ values ranging from -0.6 to +2.1‰ (using conventional techniques), with no apparent difference in values between the two mineralization styles (n=12; Mikucki, 1997 #498). Results from this study include laser ablation analyses of two pyrites from a sample of the late-stage chlorite-hematite, gold-telluride mineralization, with $\delta^{34}\text{S}_{(\text{py})}$ values of +2.52 and +1.51‰ (Fig. 3.2.3H).

Deposits with Abundant Anomalous $\delta^{34}\text{S}_{(\text{py})}$ Values In contrast to the deposits described above, there are a number of deposits in the Eastern Goldfields Province with abundant occurrences of anomalously negative and positive $\delta^{34}\text{S}_{(\text{py})}$ values (Fig. 3.2.1B and Fig. 3.2.2B). Documentation of these occurrences has increased with the more widespread application of laser ablation techniques that allow more detailed in-situ analysis of sulfides in orogenic gold deposits (e.g. Kalgoorlie, (Hagemann et al., 1999); and Kanowna Belle, (Ren et al., 1994)). Deposits with abundant anomalous $\delta^{34}\text{S}_{(\text{py})}$ values discussed in this section include Victory-Defiance and Hampton-Boulder Southern Ore Zone (described in Section 2.4), both located along the Boulder-Lefroy Fault in the Kalgoorlie Terrane, and the Porphyry deposit, in the Yilgangi/Keith-Kilkenny Fault Zone in the Kurnalpi/Mulgabbie Terrane.

Victory-Defiance, Kambalda Victory-Defiance is located 15 km southeast of the town of Kambalda in the Kalgoorlie Terrane. In terms of total contained gold, it is the second largest deposit, after Kalgoorlie, that occurs along the Boulder-Lefroy Shear Zone, with pre-mining resources of over 200 tonnes of gold (Watchorn, 1998). Gold mineralization is hosted in brittle-ductile shear zones, quartz breccia zones and brittle quartz-vein arrays, in the Defiance Dolerite, Paringa Basalt, and the Kapai Slate; minor host rocks include the Flames Porphyry and the Tripod Hill Komatiite (Clark et al., 1986). Detailed geologic and geochemical studies of Victory-Defiance include those of (Clark et al., 1986; Clark et al., 1989; Roberts and Elias, 1990; Ho et al., 1994; Watchorn, 1998). Geochronological studies constrain the timing of mineralization to 2627 ± 14 Ma (Clark, 1987; Kent, 1994). Geochemical studies indicate that the hydrothermal ore fluid was dominantly $\text{H}_2\text{O}-\text{CO}_2 \pm \text{CH}_4$ with low to moderate salinity of 8-9 wt% NaCl equivalent, and pressure conditions of ore formation ranged from 170 to 200 MPa (Clark et al., 1989). Studies of mineral equilibria, mineral pair geothermometry and fluid inclusions indicate temperatures of approximately 370° to 390°C for proximal hydrothermal alteration (Clark et al., 1989). The temperature of quartz vein formation ranged from 270° to $>500^\circ\text{C}$, based on oxygen isotope geothermometry (Xu et al., 1997).

The distribution of $\delta^{34}\text{S}_{(\text{py})}$ values at Victory-Defiance is revealed by combining new results from this study with those of previous studies (Palin and Xu, 2000; Xu, 1999). Results are shown in Table 3.2.2. Samples analyzed for this study are mainly from the 32 Ore Zone (a gently dipping shear zone) at Victory ($n=23$, from samples and pyrite separates of Ho et al., 1994), whereas samples analysed by Xu (1999; $n=21$) are from areas to the south and east of the Victory deposit. By combining the results from these two studies into a more comprehensive data set, the spatial distribution of variations in sulfur isotopic composition are more apparent. Ho et al., (1994) selected the 32 Ore Zone for a study of the lead-isotopic

composition of pyrites because it is well studied and precisely dated (Clark et al., 1986; Clark et al., 1989) and it includes a wide range of mineralization styles and host rocks. This also makes it an ideal location to determine the causes of variations in $\delta^{34}\text{S}_{(\text{py})}$ values associated with gold mineralization.

Sample Number	Host Rock	Estimated Au (g/t)	$\delta^{34}\text{S}_{(\text{py})}$ per mil	Host Structure
CD2427, 469.7m	Devon Consols Basalt	0.10	1.60	Distal
104367EQC	Devon Consols Basalt	6.00	-2.70	32 Shear Zone
104355AC	Devon Consols Basalt	12.00	-5.61	Repulse Fault
104355BD	Devon Consols Basalt	12.00	-6.26	Repulse Fault
VU4-4, 62.75m	Defiance Dolerite	0.10	5.10	32 Shear Zone
VU4-4, 73.3m	Defiance Dolerite	0.10	3.50	32 Shear Zone
CD2423, 389.5m	Defiance Dolerite	5.00	-3.00	32 Shear Zone
VO13	Defiance Dolerite	5.00	-1.60	32 Shear Zone
VO16	Defiance Dolerite	5.00	-1.80	33 Shear Zone
VO34	Defiance Dolerite	5.00	-2.70	33 Shear Zone
VU4-10, 71.5m	Defiance Dolerite	5.00	1.10	32 Shear Zone
VU4-4, 38.2m	Defiance Dolerite	9.00	-3.10	31 Shear Zone
104370ACi	Defiance Dolerite	15.00	-5.79	Repulse Fault
104369BE	Defiance Dolerite	26.00	-5.01	Repulse Fault
CD2693, 403.3m	Kapai Slate	0.10	1.60	Distal
104352CF	Kapai Slate	0.40	-1.16	Victory Fault
VO27	Kapai Slate	5.00	-1.00	Britannia Shear Zone
VO49	Kapai Slate	5.00	0.20	Britannia Shear Zone
VO50	Kapai Slate	5.00	2.70	Britannia Shear Zone
104352AB	Kapai Slate	18.00	-1.49	Victory Fault
104352DB	Kapai Slate	33.00	-2.53	Victory Fault
CD2193, 274.6m	Paringa Basalt	0.50	-2.00	32 Shear Zone
104364CAi	Paringa Basalt	0.70	-3.62	32 Shear Zone
VU4-13, 120.75m	Paringa Basalt	1.00	3.30	32 Shear Zone
VO40	Paringa Basalt	5.00	2.00	Sirius Shear Zone
CD2193, 87.3m	Paringa Basalt	10.00	-3.50	31 Shear Zone
CD2231, 171.7m	Paringa Basalt	30.00	-2.60	32 Shear Zone
VO01	Paringa Basalt	50.00	-4.40	32 Shear Zone
104366BE	Paringa Basalt	114.00	-3.03	Repulse Fault
104362AA	Paringa Basalt	117.00	-4.44	Repulse Fault
104360BA	Flames Porphyry	0.07	-3.88	Repulse Fault
104358ACi	Flames Porphyry	0.30	-3.74	Repulse Fault
104361AA	Flames Porphyry	0.50	-3.94	Repulse Fault
104357AA	Flames Porphyry	1.00	-4.71	Repulse Fault
VO15	Flames Porphyry	5.00	-2.30	Repulse Fault
104350BB	Flames Porphyry	20.00	-2.15	Victory Fault
104350BE	Flames Porphyry	20.00	-2.12	Victory Fault
104350AE	Flames Porphyry	80.00	-2.01	Victory Fault
104373AD	Tripod Hill Komatiite	0.50	-4.37	Repulse Fault
104372AD	Tripod Hill Komatiite	0.70	-5.26	Repulse Fault
104371BE	Tripod Hill Komatiite	2.00	-5.08	Repulse Fault
CD4997, 237.45m	Tripod Hill Komatiite	60.00	0.20	Repulse Fault
104354AC	Xenolithic fine-grained spessartite	6.00	-5.17	Repulse Fault
104354BD	Xenolithic fine-grained spessartite	3.00	-5.81	Repulse Fault

Table 3.2.2 Pyrite sulfur isotope values from Victory-Defiance. Samples analyzed in this study are highlighted in grey ($n=23$), from samples of Ho et al. 1994. Other results are from Xu (1999, $n=21$). Sample numbers correspond to those used in respective studies. Host structures are shown in Fig. 3.2.4B. Gold grades are from Ho et al. (1994) and Xu (1999).

The cross section in Fig. 3.2.4B shows the spatial distribution of gold-related $\delta^{34}\text{S}_{(\text{py})}$ values at Victory-Defiance. The $\delta^{34}\text{S}_{(\text{py})}$ values range from -6.84 to $+5.10\%$ (n=44), with distinct ranges in certain host rocks and structures. The most consistently negative $\delta^{34}\text{S}_{(\text{py})}$ values are along the Repulse Fault, including -5.55 to -3.06% in the Flames Porphyry (n=4), -6.26 to -5.61% in the Devon Consols Basalt (n=2), and -5.26 to $+0.20\%$ in the Tripod Hill Komatiite (n=4). More steeply-dipping structures in the hanging wall of the Repulse Fault have distinctly heavier $\delta^{34}\text{S}_{(\text{py})}$ values, including $+2.00\%$ in Paringa Basalt in the Sirius Shear (n=1); -1.00 to $+2.7\%$ in Kapai Slate in the Britannia Shear Zone (n=3); and in the Victory Fault -2.15 to -1.71% in Flames Porphyry (n=3) and -2.53 to -1.16% in Kapai Slate (n=3). The largest range of $\delta^{34}\text{S}_{(\text{py})}$ values is in the 31, 32, and 33 Ore Zones, which are gently-dipping structures in the footwall of the Repulse Fault, and include -4.44 to $+3.33\%$ in the Paringa Basalt (n=8), and -5.79 to $+5.10\%$ in the Defiance Dolerite (n=10).

In addition to the apparent structural control on the range of $\delta^{34}\text{S}_{(\text{py})}$ values, there are also distinct ranges of values in certain rock types. The more mafic units (Defiance Dolerite, Devon Consols Basalt, and Paringa Basalt) have larger ranges, from approximately -6.26 to $+5.10\%$, whereas there are more restricted ranges in the Flames Porphyry (-4.71 to -1.71% , n=8) and the Kapai Slate (-2.53 to $+2.7\%$, n=7), particularly in the steeper structures, as discussed above.

The relationship between gold grade and $\delta^{34}\text{S}_{(\text{py})}$ value is shown in Fig. 3.2.5A. In general, there is weak negative correlation for the mafic units (Defiance Dolerite, Devon Consols Basalt, and Paringa Basalt) and the Kapai Slate, across a range of $\delta^{34}\text{S}$ values from -5.81 to $+5.5\%$ and gold grades ranging from >100 to 0.10 ppm. There is also a distinct group of Flames Porphyry and Tripod Hill Komatiite samples that lies below this trend. These are from samples with less than 10 wt% pyrite. Similarly, in plots of wt % pyrite vs $\delta^{34}\text{S}_{(\text{py})}$ value and gold grade (Fig. 3.2.5B and C), the samples with the lowest wt % pyrite have the most negative $\delta^{34}\text{S}_{(\text{py})}$ values and the lowest gold grades. These relationships suggests that the chemical composition of host rocks may influence the $\delta^{34}\text{S}_{(\text{py})}$ value of gold-related pyrites during gold mineralization.

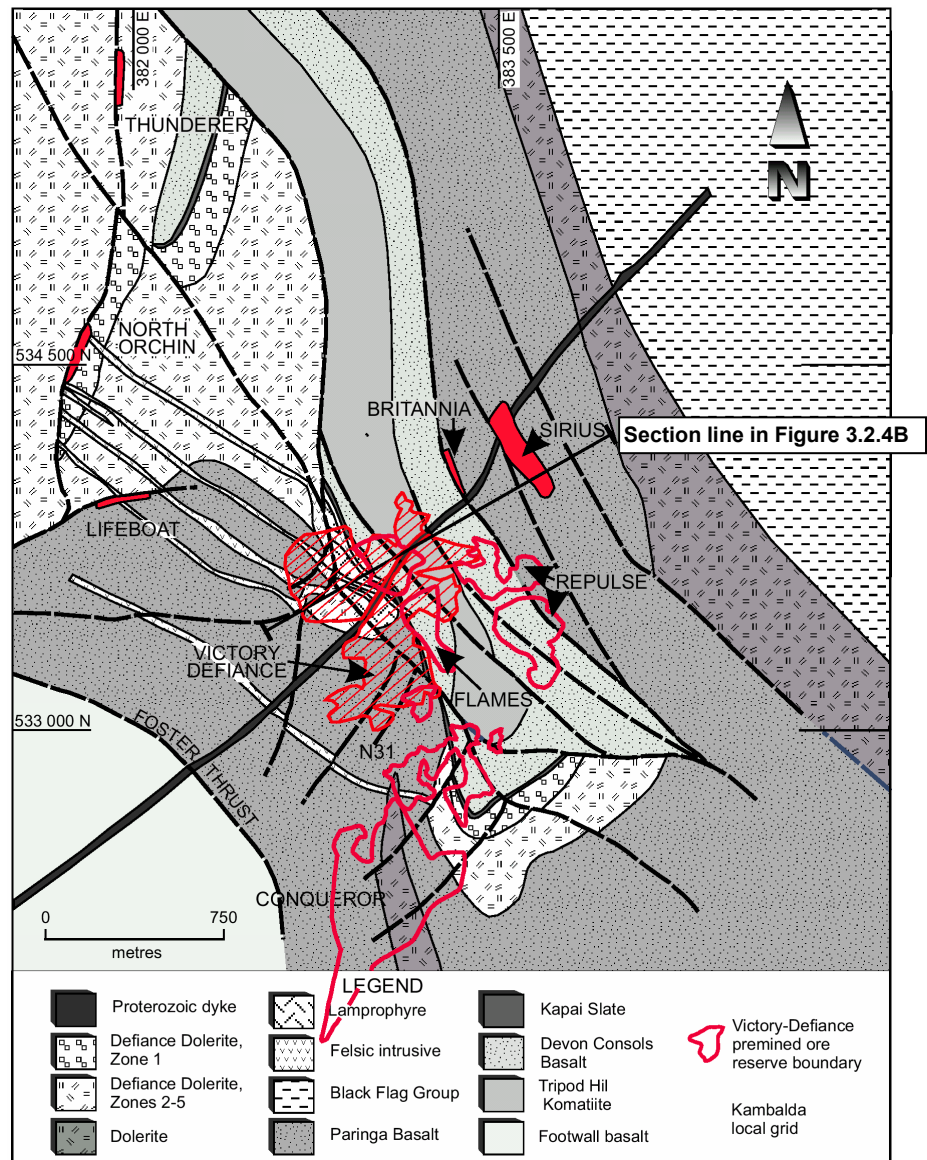


Figure 3.2.4. (A) Plan map of the Victory-Defiance area (Watchorn, 1998). $\delta^{34}S_{(py)}$ values listed in Table 3.2.2 have been projected on to the cross section line, as shown in (B) on the next page.

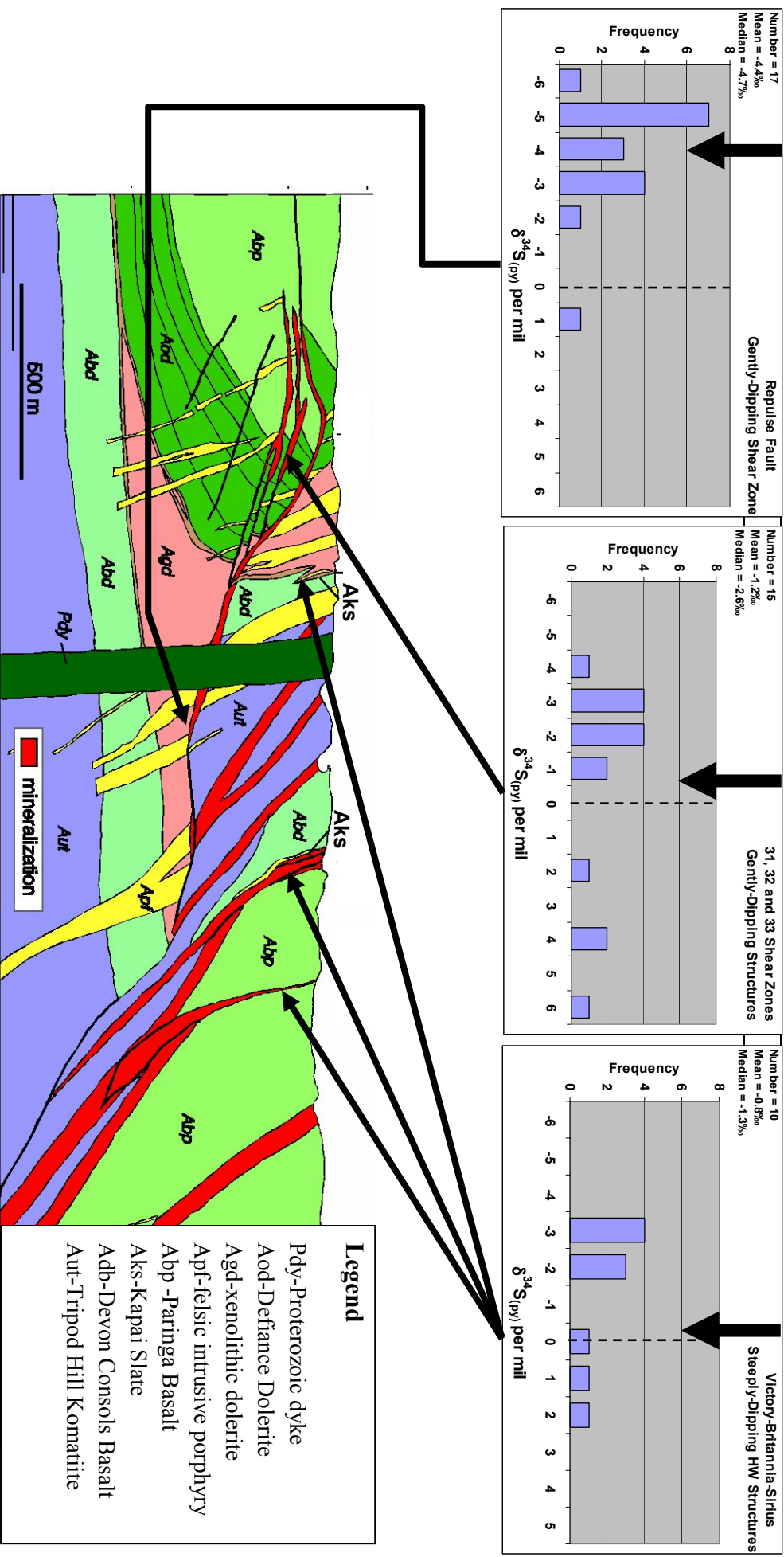


Figure 3.2.4. (B) Cross section of the Victory-Defiance area (see section line on previous page) view to the northwest (from (Vanderhor and Groves, 1998)). Histograms show spatial distribution of $\delta^{34}\text{S}(\text{per})$ values listed in Table 3.2.2, with distinct values or ranges of values in certain host rocks and structures (see discussion in text). Large arrows on histograms indicate mean $\delta^{34}\text{S}(\text{per})$ value; vertical dashed lines at 0‰ shown for reference.

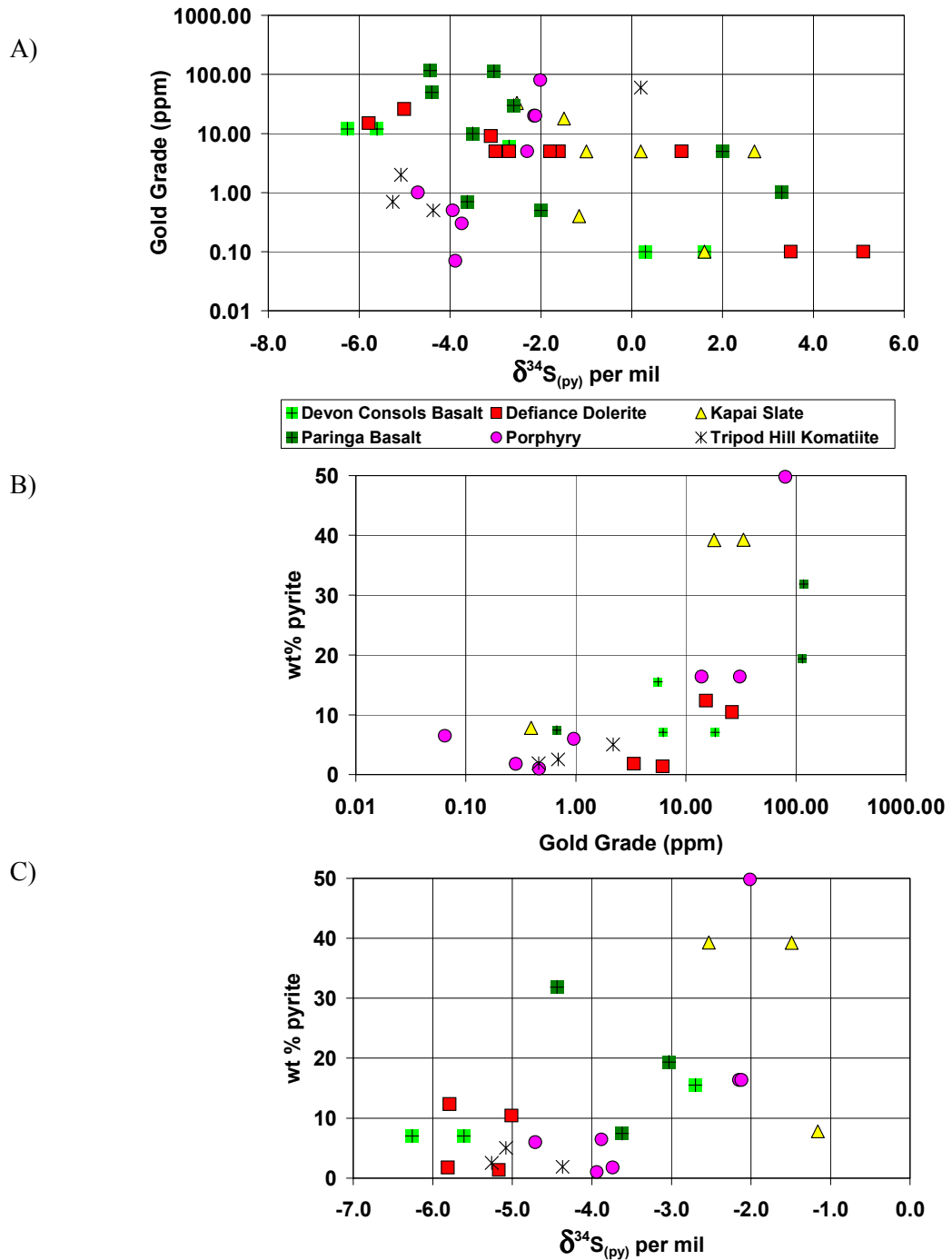


Figure 3.2.5. Plots of gold grade, $\delta^{34}S$ value and wt% pyrite from Victory-Defiance pyrites. Data from this study, Ho et al. (1994), and Xu (1999) as shown in Table 3.2.2. (A) Gold grade vs $\delta^{34}S$ value. There is weak negative correlation for the mafic units (Defiance Dolerite, Devon Consols Basalt, and Paringa Basalt) and the Kapai Slate, across a range of $\delta^{34}S_{(py)}$ values from -5.81 to $+5.5\%$ and gold grades ranging from >100 to 0.10 ppm. There is also a distinct group of Flames Porphyry and Tripod Hill Komatiite samples that lies below this trend. These are from samples with less than 10 wt% pyrite. (B) Wt% pyrite vs gold grade and (C) Wt% pyrite vs $\delta^{34}S_{(py)}$ value. In both plots, the samples with the lowest wt % pyrite have the most negative $\delta^{34}S_{(py)}$ values and the lowest gold grades.

Hampton-Boulder Jubilee - Southern Ore Zone. The Hampton-Boulder Jubilee deposits are located on the Boulder-Lefroy Shear Zone, approximately 30 km north of Victory-Defiance. The pre-mining resource included approximately 100 tonnes of gold, hosted in brittle-ductile shear zones and brittle quartz-vein arrays, in mafic schists and porphyry intrusions in the hanging wall of a steeply dipping mafic/ultramafic contact (Williams, 1994). Based on the results of this reconnaissance study (seven analyses from five samples), there is a large range of $\delta^{34}\text{S}_{(\text{py})}$ values in gold-related pyrites in a variety of host rocks (Fig. 3.2.6), similar to the ranges at Victory-Defiance. Previous geologic studies by (Langsford, 1989; Norris, 1990; Williams, 1994) are summarized briefly below. Hydrothermal assemblages associated with gold mineralization vary with host rock, and reflect increasing intensities of $\text{K}\pm\text{Na}$ metasomatism, carbonation and sulfidation towards the ore zones. In the tholeiitic mafic schist, proximal alteration zones are characterized by alkali feldspar-albite-ankerite-pyrite, intermediate alteration zones by sericite-ankerite-albite-biotite \pm magnetite, and distal alteration zones by chlorite-calcite-biotite-oligoclase-magnetite assemblages. In the felsic porphyry, proximal alteration zones are characterized by albite-pyrite, intermediate zones by sericite-hydrothermal biotite, and distal zones by albite-quartz-biotite assemblages. Gold mineralization overprints regional-scale carbonate alteration and is contemporaneous with magnetite alteration of chlorite schists. The last stage of hydrothermal alteration is represented by post-gold, quartz-carbonate-chlorite-hematite veins (Fig. 3.2.6B). Fluid inclusion studies (Williams, 1994) indicate that the hydrothermal ore fluid was H_2O - CO_2 -rich and low to moderate salinity (5 to 10.6 wt% NaCl equivalent), with temperature of mineralization estimated to be $330^\circ \pm 20^\circ\text{C}$.

Results of this reconnaissance sulfur isotope study show that $\delta^{34}\text{S}_{(\text{py})}$ values range from -8.64 to $+5.54\text{‰}$. There is a large range of $\delta^{34}\text{S}_{(\text{py})}$ values in the tholeiitic mafic schist, with values of -5.49 and -4.84‰ in proximal alteration, and a value of $+5.54\text{‰}$ in distal alteration. A more restricted range of negative $\delta^{34}\text{S}_{(\text{py})}$ values was found in the felsic porphyry unit, with values of -8.64 and -6.04‰ in proximal alteration and a value of -1.41‰ in distal alteration (19.5 m from the ore zone). A sample of ultramafic schist from the footwall of the deposit has a $\delta^{34}\text{S}_{(\text{py})}$ value of $+3.92\text{‰}$. This large range of $\delta^{34}\text{S}_{(\text{py})}$ values, especially in felsic porphyry and mafic host rocks, is similar to that described above at Victory-Defiance.

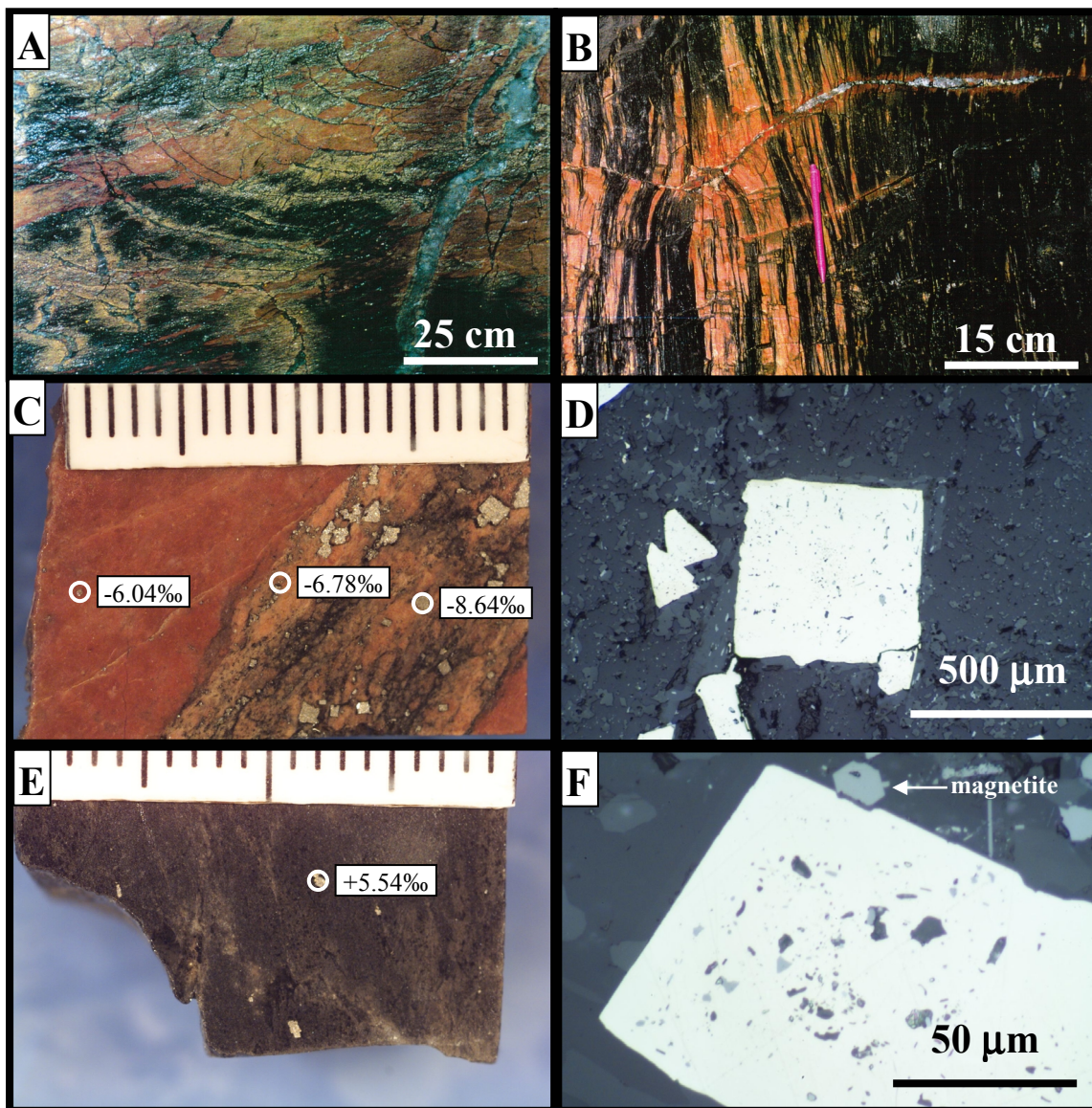


Figure 3.2.6. Host rocks, hydrothermal alteration, and $\delta^4S_{(py)}$ values in the Hampton-Boulder Jubilee Southern Ore Zone. (A) Photograph of quartz-carbonate±pyrite veins, with yellow feldspar-ankerite-pyrite selvages, cross-cutting black tholeiitic mafic schist and orange, hematite-altered felsic porphyry (from Williams, 1994). (B) Photograph of sub-vertical lenses of hematite-altered felsic porphyry (orange unit) in black tholeiitic mafic schist, and cross-cutting, sub-horizontal, quartz-carbonate-chlorite veins with hematite-altered selvages (from Williams, 1994). (C) Photograph of mineralized felsic porphyry (sample #121784, 3.65 g/t Au) and $\delta^4S_{(py)}$ values, and (D) photo-micrograph of euhedral pyrite from same sample. (E) Photograph of unmineralized tholeiitic mafic schist (sample #121776) and $\delta^4S_{(py)}$ value, and (F) photo-micrograph of euhedral pyrite and magnetite from same sample.

Porphyry Deposit. The Porphyry deposit, in the Yarri mining district of the Mulgabbie Terrane, is a small deposit with a total pre-mining resource of 10.6 tonnes of gold (Cassidy, 1992). However, it is significant in that, except for the Golden Mile, it has the largest range of $\delta^{34}\text{S}_{(\text{py})}$ values in the Yilgarn, from -10.19 to $+9.95\%$. Recent geologic studies, summarized briefly below, include those of (Allen, 1986; Allen, 1987; Weatherstone, 1990; Cassidy, 1992; Hill et al., 1992; Cassidy et al., 1998).

Gold mineralization at Porphyry is hosted in a NNW-striking shear zone that dips 20° - 25° ENE, along the margin of a small, porphyritic quartz-monzonite intrusion. The NNW strike orientation of the shear zone is sub-parallel to both the regional tectonic fabric in the Mulgabbie Terrane (Swager, 1995) and the Keith-Kilkenny/Yilgarn Fault zone, which is 12 kilometers to the west of the deposit. The majority of the gold is hosted in the quartz monzonite, with minor ore hosted in overlying quartz andesite. Increasing gold grades correlate with increases in wt% pyrite, degree of shearing and fabric development, and intensity of hematite alteration (Allen, 1987). Hydrothermal alteration zones associated with gold mineralization indicate large volume increases with additions of SiO_2 , K_2O , Na_2O , CO_2 , S and Mo, and depletion of MgO. Modal mineralogy shows increases in quartz, carbonate, muscovite, and pyrite, and decreases in biotite and epidote proximal to the ore zone. The shear fabric is defined by sericite, which has replaced biotite. Based on trace element studies of (Allen, 1986) and (Cassidy, 1992), there is no enrichment of As and Te with gold. A reconnaissance fluid inclusion study by (Allen, 1986) suggests a CO_2 - H_2O rich, low salinity fluid. Geochronological studies of emplacement of the quartz monzonite provide ages of 2676 ± 21 Ma, based on whole rock Pb/Pb (Cassidy, 1992) and 2667 ± 4 Ma, based on a single zircon U-Pb SHRIMP analysis (Hill et al., 1992).

A plan map of Porphyry is shown in Fig. 3.2.7. As mentioned above, the Porphyry deposit has the largest range of $\delta^{34}\text{S}_{(\text{py})}$ values, from -10.19 to $+9.95\%$ ($n=17$), compared to other orogenic gold deposits in the Yilgarn, except for the Golden Mile. The largest shifts in $\delta^{34}\text{S}_{(\text{py})}$ values occur within and adjacent to the ore zones, with the most negative values in the highest grade ore-zones and the most positive values in weakly altered zones adjacent to the lodes (Fig. 3.2.8). The relationship between $\delta^{34}\text{S}_{(\text{py})}$ values, gold mineralization, shear-zone fabric development, hematite alteration and pyrite shape is shown in Fig. 3.2.8. High gold grades (> 5 g/t) are associated with the most negative $\delta^{34}\text{S}_{(\text{py})}$ values (-10.19 and -9.44%), strongest shear fabric development, strongest hematite alteration, and least euhedral pyrites (Fig. 3.2.8A and B). With increasing distance from the lodes and decreasing gold grades, hematite alteration and shear fabric development decrease and $\delta^{34}\text{S}_{(\text{py})}$ values increase, approaching 0% (Fig. 3.2.8C and D). Weakly mineralized samples adjacent to the lode have

the heaviest $\delta^{34}\text{S}_{(\text{py})}$ values (+9.95‰) in small euhedral pyrites (Fig. 3.2.8E and F). These samples suggest significant sulfur isotope fractionation associated with lode formation. Two samples of small (sub 10 μm) disseminated pyrite in distal, unaltered quartz monzonite on the western margin of the intrusion have similar values of +5.13 and +5.53‰, providing an estimate of distal $\delta^{34}\text{S}_{(\text{py})}$ values, although the relative timing of formation of this distal pyrite is unknown.

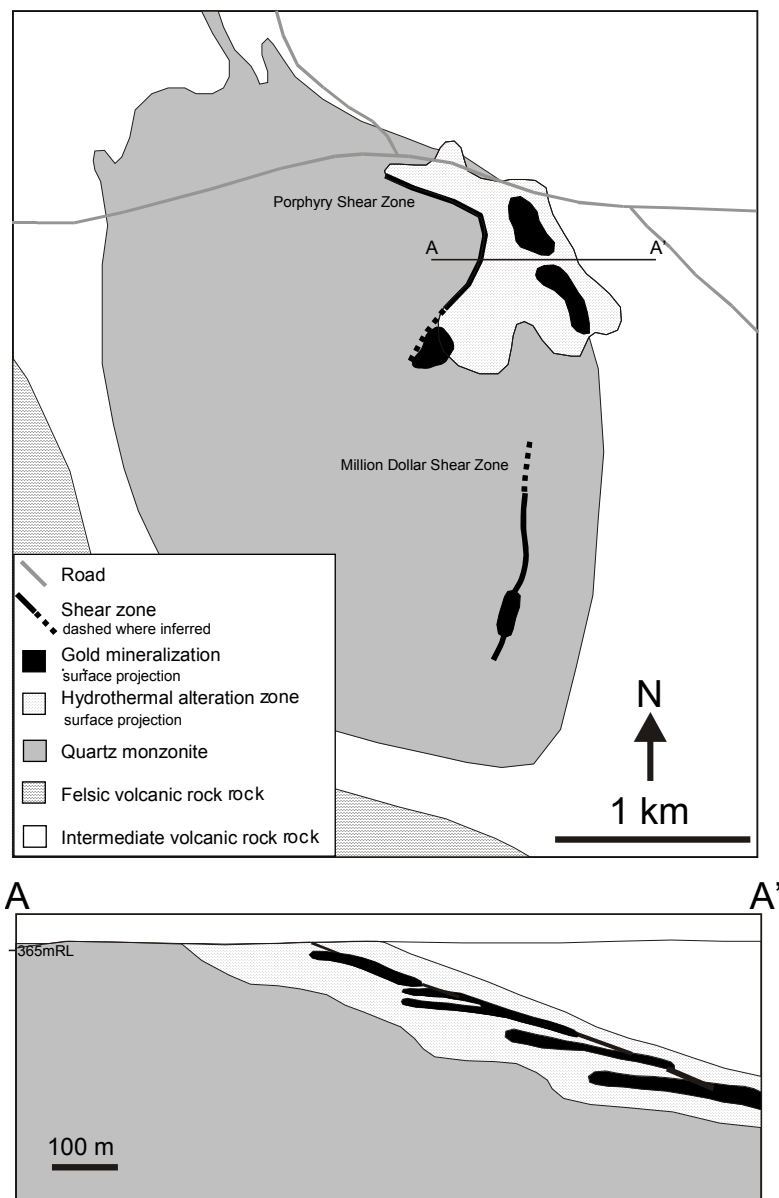


Figure 3.2.7. Plan and cross section of the Porphyry mine, modified from (Allen, 1987). Two distal samples of unaltered quartz monzonite on the western margin of the intrusion have similar values of +5.13 and +5.53‰, providing an estimate of distal $\delta^{34}\text{S}_{(\text{py})}$ values. The largest shifts in $\delta^{34}\text{S}_{(\text{py})}$ values occur within and adjacent to the ore zones, with the most negative values (-10 to -6‰) in the highest-grade ore zones and the most positive values (+7 to +10‰) in weakly altered zones adjacent to the lodes.

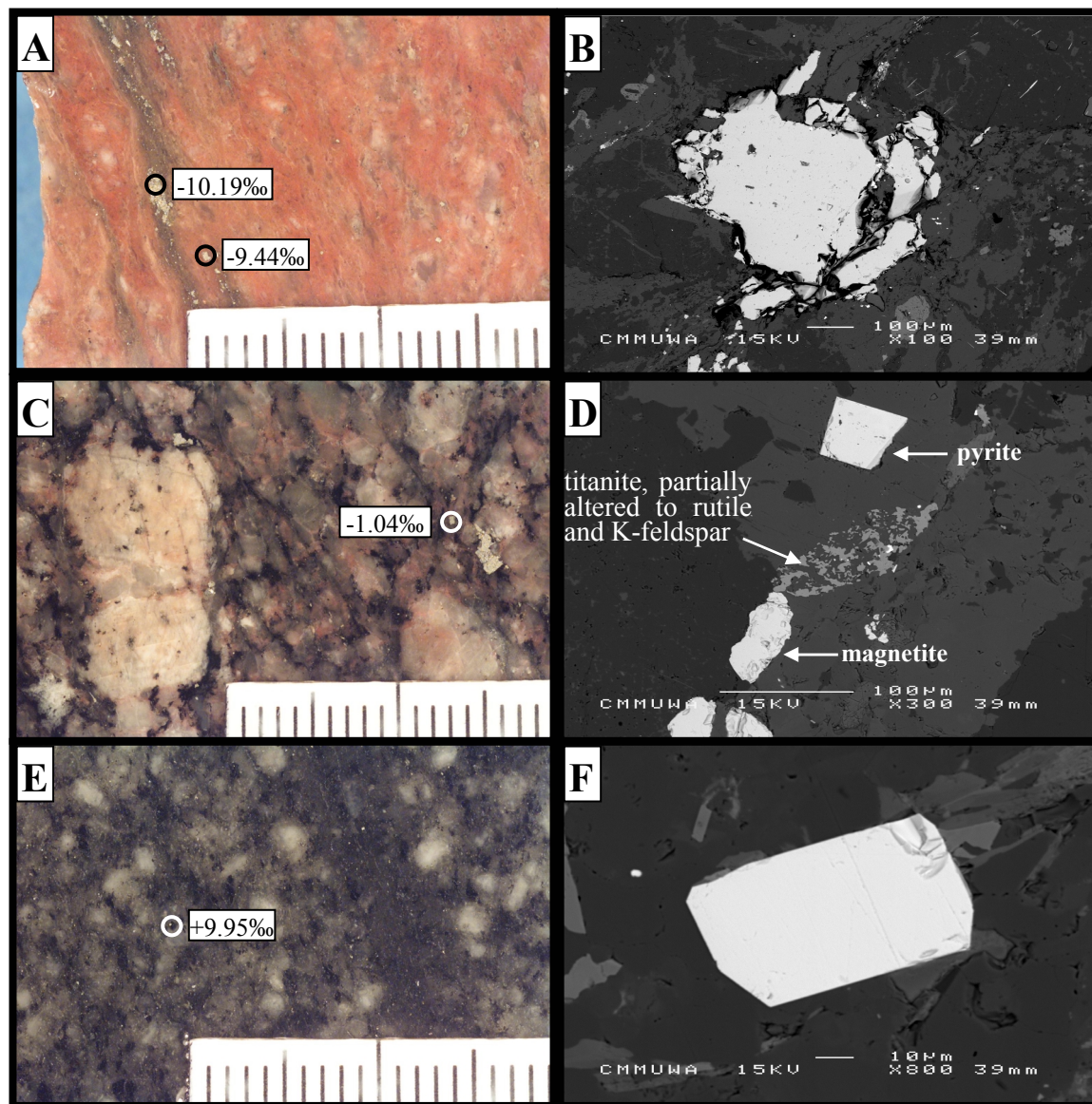


Figure 3.2.8. Photographs and SEM images of quartz-monzonite host rock from Porphyry, showing relationship between $\delta^{34}S_{(pyrite)}$ values, gold mineralization, shear zone fabric development, hematite alteration and pyrite shape. (A) Well-mineralized sample (#101956, > 5 g/t Au) with strong hematite alteration and well-developed shear fabric defined by pyrite and muscovite, and (B) SEM image, from same sample, of anhedral pyrite. (C) Weakly-mineralized sample (#101958, < 0.5 g/t Au) with weak hematite alteration and minor fabric development, and (D) SEM image, from same sample, of euhedral pyrite, magnetite and titanite partially altered to rutile and K-feldspar. The above samples are from the same drill hole, three meters apart. (E) Unmineralized sample (#101951, < 0.01 g/t Au) of quartz monzonite with very weak fabric development, from approximately ten metres below mineralized shear zone; (F) SEM image, from same sample, of small, euhedral pyrite. This sample is from a drill hole, approximately 320 meters south of samples described above.

Sedimentary Sulfides Previous studies show that $\delta^{34}\text{S}$ values of unmineralized Archean sedimentary sulfides generally fall within a restricted range between +1 and +5‰ (Donnelly et al., 1978; Seccombe et al., 1981; Lambert et al., 1984). This range of values constrains the $\delta^{34}\text{S}$ value of sulfur in gold ore fluids, if these sedimentary sulfides are considered to be a potential sulfur source (Kakegawa and Ohmoto, 1999). Sulfur isotope analyses were performed in this study in order to test the narrow range of $\delta^{34}\text{S}$ values in Archean sedimentary sulfides. The results of 28 laser ablation analyses from 13 samples of unmineralized interflow sedimentary units in the Eastern Goldfields Province are presented in this section. Combined with results from previous sulfur isotope studies, these data are used to document the range of $\delta^{34}\text{S}_{(\text{sulfide})}$ values in potential sulfur reservoirs for gold-ore fluids. Analytical results of this study, and results compiled from previous studies, are listed in Table 3.2.3. Sample locations and ranges of $\delta^{34}\text{S}_{(\text{sulfide})}$ values are shown in Fig. 3.2.9.

There is a large range of $\delta^{34}\text{S}_{(\text{sulfide})}$ values in samples of unmineralized sedimentary sulfides from the Eastern Goldfields Province, from -7.60 to $+12.68\text{‰}$ (Fig. 3.2.9B). Although the majority of the $\delta^{34}\text{S}_{(\text{sulfide})}$ values fall in the restricted range between +1 and +5‰, there are distinctly negative and positive values associated both with specific locations in the Eastern Goldfields Province and within particular sedimentary rock types. The locations in Fig. 3.2.9B are arranged from north to south and correspond to labels on the map in Fig. 3.2.9A. The most negative $\delta^{34}\text{S}$ values are from locations in the northern portion of the map.

Samples of interflow sedimentary units from Kalgoorlie and the Kambalda district, and corresponding $\delta^{34}\text{S}$ values, are shown in Fig. 3.2.10. The heaviest $\delta^{34}\text{S}$ values analyzed in this study are from Kalgoorlie (Fig. 3.2.10A, $+10.30\text{‰}$) and from the Tramways Fault at Kambalda (Fig. 3.2.10D, $+12.68\text{‰}$).

District	Location	Host	Number of Samples	Number of Analyses	Minimum $\delta^{34}\text{S}_{(\text{sulfide})}$ value	Maximum $\delta^{34}\text{S}_{(\text{sulfide})}$ value	Analytical Results of	Analytical method
Mt Magnet	Mt Magnet	black shale	1	1	3.40		Donnelly et al., 1977	CONV
Mt Keith	Mt Keith	black shale	3	4	0.70	1.50	Donnelly et al., 1977	CONV
	Mt Keith Ni	nickel	1	2	-4.60	-0.50	Donnelly et al., 1977	CONV
	Perserverance	nickel	3	3	-2.50	-2.00	Donnelly et al., 1977	CONV
Laverton	Eulaminna	black shale	1	2	-1.80	-1.70	Donnelly et al., 1977	CONV
	Mt Windarra	nickel	2	2	-2.00	-1.40	Donnelly et al., 1977	CONV
Kurnalpi	Carr Boyd	nickel	1	1	1.50		Donnelly et al., 1977	CONV
	Mt Jewell	black shale	3	3	-5.40	0.90	Donnelly et al., 1977	CONV
	Black Swan	nickel	1	1	1.60		Donnelly et al., 1977	CONV
BTZ	Bardoc	black shale	1	2	-0.40	1.24	this study	LA
	Scotia	nickel	1	1	3.60		Donnelly et al., 1977	CONV
	Scotia	black shale	1	2	4.38	5.78	this study	LA
	Scotia East	black shale	1	1	1.86		this study	LA
Kanowna	Kanowna	black shale	4	4	-7.60	0.10	Donnelly et al., 1977	CONV
Kalgoorlie	Kalgoorlie	black shale	1	2	6.88	10.30	this study	LA
	Kalgoorlie	black shale	7	9	-0.10	5.20	Donnelly et al., 1977	CONV
Central EGP	Lake Yindarigooda	black shale	1	3	4.52	10.91	this study	LA
	Carnilya Hill	black shale	1	3	2.42	5.60	this study	LA
	Mt Martin	nickel (vein)	1	1	0.90		Donnelly et al., 1977	CONV
Nepean	Mt Martin	black shale	1	2	-1.25	3.86	this study	LA
	Nepean	black shale	1	2	6.35	6.42	this study	LA
	Nepean	black shale	1	1	3.60		Donnelly et al., 1977	CONV
	Nepean	nickel	3	4	1.00	3.50	Donnelly et al., 1977	CONV
	Kambalda	Kambalda Dome	black shale	1	2	4.15	5.62	this study
Kambalda	Kambalda Dome	black shale	18	18	1.00	4.60	Donnelly et al., 1977	CONV
	Kambalda Ni	nickel		68	-0.50	3.80	Seccombe et al., 1981	CONV
	Republican Hill	black shale	1	1	3.29		this study	LA
	St Ives	black shale	1	4	3.91	5.08	this study	LA
	Tramways	black shale	1	2	8.39	12.68	this study	LA
Norseman	Mt Thirsty	siltstone	1	1	0.40		Donnelly et al., 1977	CONV
	Norseman	black shale	1	2	7.31	7.84	this study	LA
	Norseman	black shale	3	3	-2.20	2.40	Donnelly et al., 1977	CONV

Table 3.2.3. List of locations of regional samples of sedimentary sulfides and nickel sulfide deposits, indicating sources of sulfur isotope data shown in Figure 3.2.9B. Includes rock type, number of samples, number of analyses, and analytical method (CONV is conventional analysis and LA is laser ablation analysis).

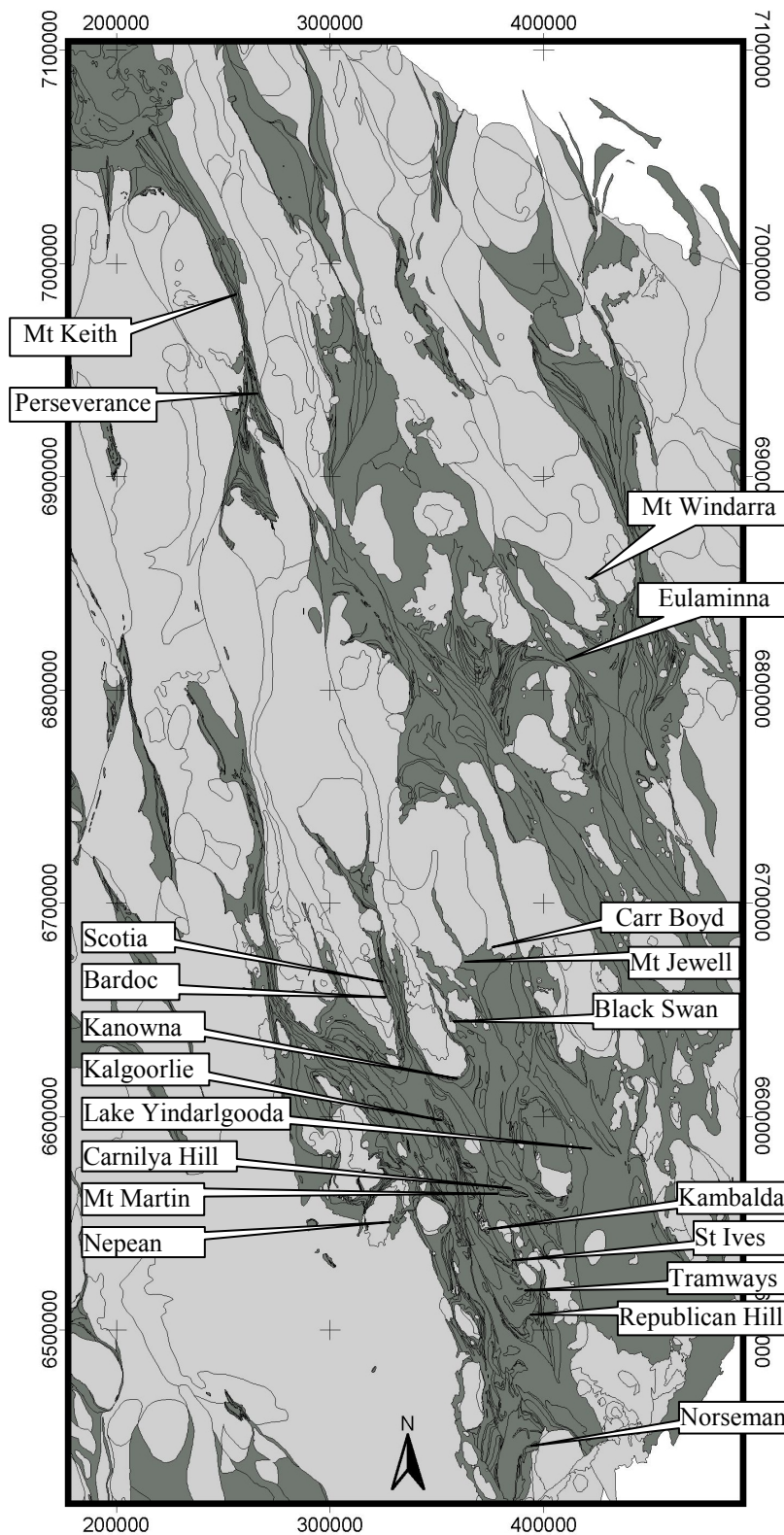


Figure 3.2.9. (A) Map of the Eastern Goldfields Province, showing locations of regional samples of sedimentary sulfides and nickel sulfide deposits with sulfur isotope data from this study and previous studies. Greenstones are dark grey and granitoids are light grey. Map grid is in AMG coordinates, in metres.

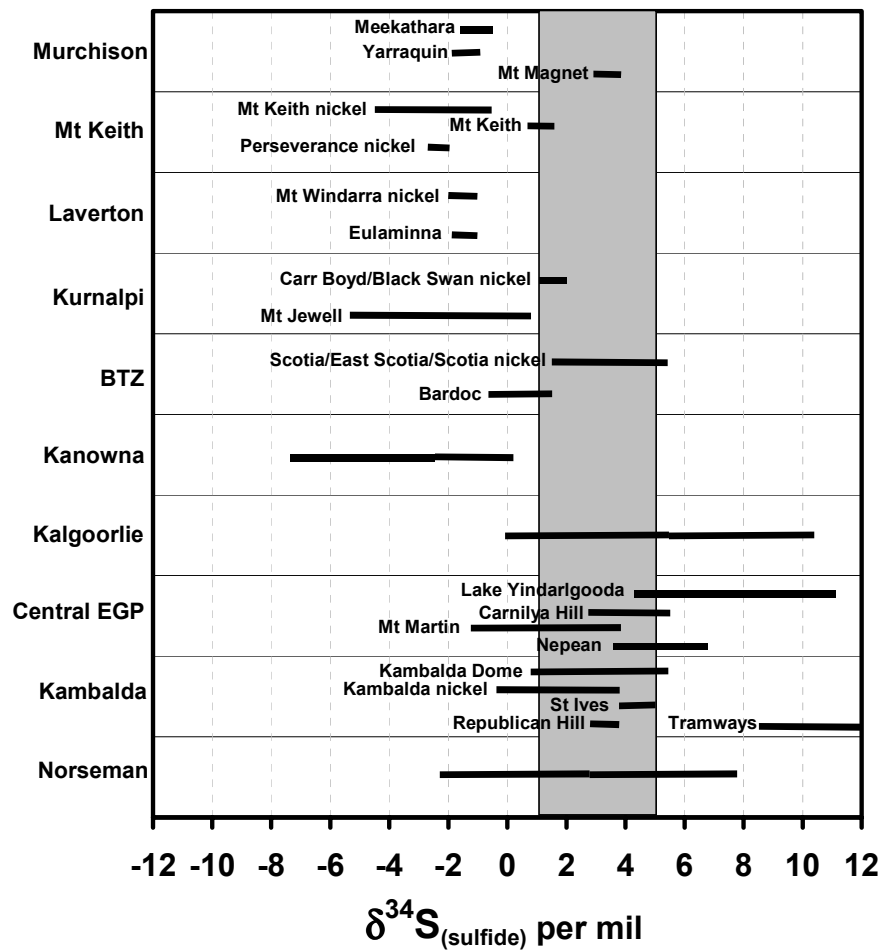


Figure 3.2.9. (B) Ranges of sulfide sulfur-isotope values, arranged from north to south and corresponding to locations in (A). Values from the Murchison Province are shown only for comparison. The grey area corresponds to the typical range of $\delta^{34}\text{S}$ values (+1 to +5‰) for Archean sedimentary sulfides (Donnelly et al., 1977, Seccombe et al., 1981, Lambert et al., 1984). Details of analytical results are shown in Table 3.2.3.

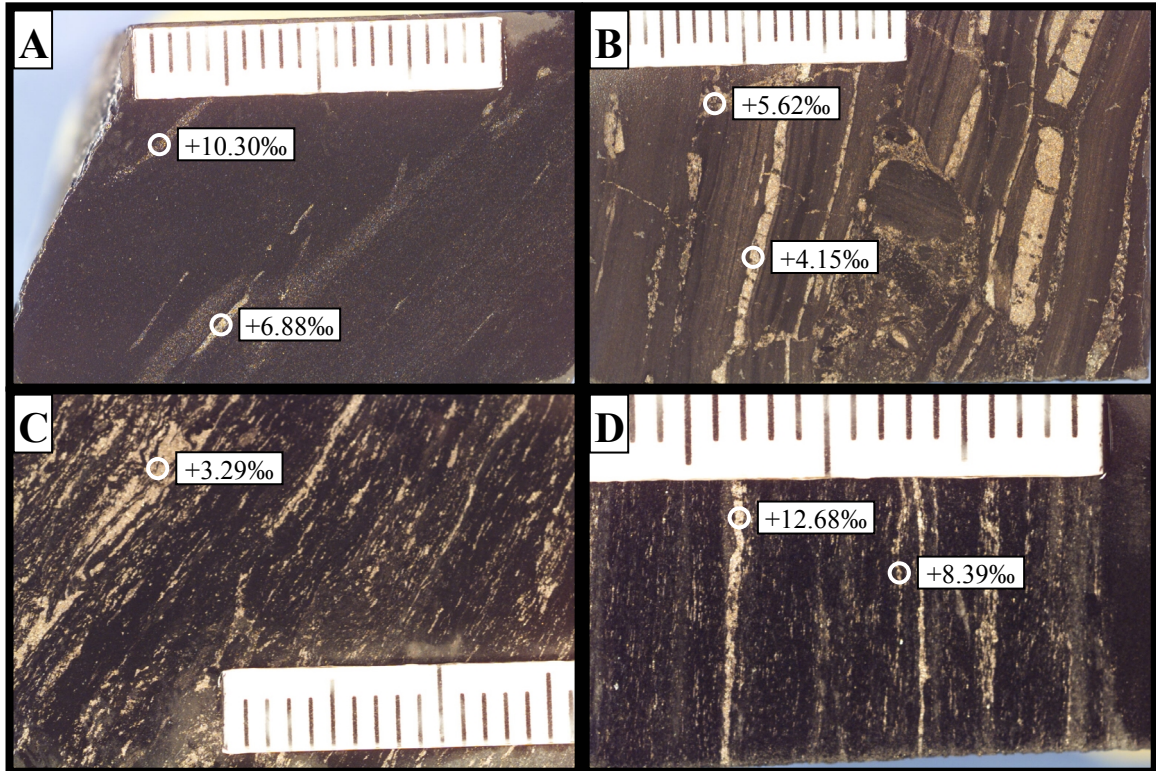


Figure 3.2.10. Photographs of interflow sedimentary units from within mafic and ultramafic rocks, showing results of $\delta^{34}\text{S}(\text{sulfide})$ analyses from this study. All samples from (Chapman, 1980) (A) Kalgoorlie - carbonaceous unit from mafic/ultramafic contact (sample 87826). (B) Kambalda Dome - carbonaceous unit from within hanging wall basalt (sample 87802). (C) Republican Hill - chlorite-rich unit from within basalt sequence (sample 79913b). (D) Tramways - chlorite-rich unit from within ultramafic sequence (sample 87796).

Discussion and Conclusions

Based on the results presented in this *Section*, the occurrence of anomalously positive and negative $\delta^{34}\text{S}_{(\text{py})}$ values in Archean orogenic gold deposits is more common than previous studies suggest. This is due, in part, to the laser ablation analytical technique used in this study, which allows *in-situ* measurement of variations between and within sulfide grains. Previous studies generally used conventional digestion techniques that require larger samples, resulting in more homogenised analytical results. The recognition of larger variations in $\delta^{34}\text{S}_{(\text{py})}$ values is important because sulfur isotopes are a sensitive indicator of ore fluid oxidation state, which significantly affects the capacity of the fluid to transport and precipitate gold. This has implications for constraining ore depositional processes and ore fluid sources.

The occurrence of hematite alteration and anomalously negative $\delta^{34}\text{S}$ values in gold-related pyrite is commonly used as possible evidence for oxidized hydrothermal ore fluids (Cameron and Hattori, 1987). However, results of this study indicate that there is not always a consistent relationship between them. For example, we describe hematite-altered samples that include anomalously negative $\delta^{34}\text{S}$ values in gold-related pyrites (-8.6‰ at Hampton-Boulder SOZ (Fig. 3.2.6C) and -10.2‰ at Porphyry (Fig. 3.2.8A)), anomalously positive values (+9.5‰ at Lady Bountiful (Fig. 3.2.3E)) and normal values (+2‰ at Great Eastern Fig. 3.2.3H)). The sample from Great Eastern is especially interesting in that gold-telluride mineralization is associated with late-stage chlorite-hematite alteration, with $\delta^{34}\text{S}_{(\text{py})}$ values between +1.5 and +2.5‰. These relationships suggest that hematite and pyrite did not always form in equilibrium conditions, and that constraining the timing relationships between oxidation and mineralisation is critical. They also suggest that a variety of ore-depositional mechanisms may be operating. For example, phase separation of reduced gases, such as H_2 , CH_4 , and H_2S , from the ore fluid may account for anomalously positive $\delta^{34}\text{S}$ values in hematite-rich ore (Drummond and Ohmoto, 1985).

The occurrence of tellurium minerals and anomalously negative $\delta^{34}\text{S}_{(\text{py})}$ values in pyrite is also used as evidence for possible oxidised ore fluids. Tellurium minerals occur in a number of the deposits described in this *Section*, including Hunt, Lady Bountiful, North Royal and Great Eastern. As discussed above, the sample from Great Eastern has gold-telluride mineralization associated with chlorite-hematite alteration, and $\delta^{34}\text{S}_{(\text{py})}$ between +1.5 and +2.5‰. These values are not typical of those precipitated from an oxidized fluid, which would be expected given the occurrence of telluride minerals and hematite. These results indicate that the relationship between anomalous $\delta^{34}\text{S}_{(\text{py})}$ values and telluride minerals is complex and not fully understood as yet. Cooke (2001) proposes that tellurium-bearing gas

condensation into auriferous fluids is the most viable mechanism for the deposition of high-grade gold telluride ore. Given the occurrence of tellurium in a number of orogenic gold deposits in the Eastern Goldfields Province, further research into its significance is warranted.

The distribution of $\delta^{34}\text{S}_{(\text{py})}$ values at Victory-Defiance (Fig. 3.2.4B) suggests a relationship with structural style of mineralization, which is controlled mainly by zones of dilation and compression along structures of different orientations (Roberts and Elias, 1990). The most negative $\delta^{34}\text{S}_{(\text{py})}$ values, and the largest range in values, occur in gently-dipping, dilational structures, in the Repulse Fault (a reverse shear zone) and the 31, 32 and 33 Shear Zones in the footwall of the Repulse Fault (Fig. 3.2.11). In contrast, more positive $\delta^{34}\text{S}$ values, and a narrower range of values, occur in steeply-dipping, compressional structures in the hangingwall of the Repulse Fault (Victory Fault, Britannia Shear and Sirius Shear). This suggests that fluid flow associated with dilational and compressional structures may influence $\delta^{34}\text{S}$ values in gold-related pyrites during mineralization. Similar relationships between stable isotopes (carbonate carbon and oxygen), gold mineralization and orientations of structures have been documented at the Revenge gold mine (Nguyen, 1997), suggesting that fluid flow in different structures can influence the isotopic signature of ore fluids (Cox, 1999; Nguyen et al., 1998).

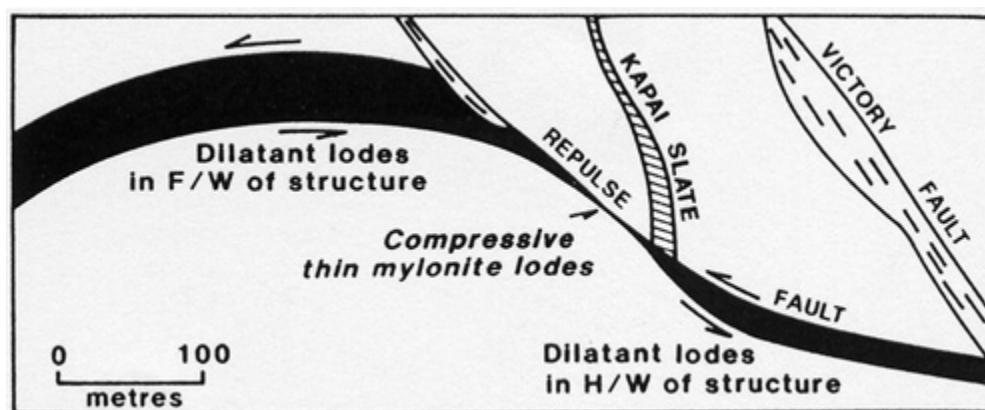


Figure 3.2.11. Schematic cross section of Victory-Defiance area (Roberts and Elias, 1990) showing areas of dilation and compression developed in variably oriented structures. The area in this section corresponds to the left-hand side of the section in Fig. 3.2.4B, including the Victory Fault and the 31, 32 and 33 Shear Zones in the footwall of the Repulse Fault. Negative $\delta^{34}\text{S}_{(\text{py})}$ values occur in dilational structures associated with the Repulse Fault; more positive $\delta^{34}\text{S}_{(\text{py})}$ values typically occur in steeply-dipping structures in the hangingwall.

A plot of gold endowment vs total variation in $\delta^{34}\text{S}_{(\text{py})}$ values (Fig. 3.2.12A) shows that larger gold deposits (>1 Moz) commonly have larger ranges of $\delta^{34}\text{S}_{(\text{py})}$ values (>10‰). Most of the deposits in this group are dominantly shear-zone hosted. This also suggests a relationship between structural style of mineralization, sulfide sulfur isotopes and gold mineralization. In addition, deposits with anomalously positive or negative values tend to have large ranges, overall (Fig. 3.2.2B and Fig. 3.2.12B and C), suggesting that the positive and negative anomalous values may be related to similar processes. The relationships in Fig. 3.2.12B and C show that a large range of values can be expected, given the presence of either anomalously positive or negative values. The plots and equations in Fig. 3.2.12B and C could be used to test this relationship in further studies of sulfur isotope variability in orogenic gold deposits. This is also useful for exploration, considering the relationship between sulfur isotope variability and gold endowment (Fig. 3.2.12A).

The large range of $\delta^{34}\text{S}$ values (>10‰) in sulfides from interflow sedimentary rocks, documented in this study (Table 3.2.3 and Fig. 3.2.9B), contrasts with the narrow ranges reported in previous studies. If these rocks were a source of sulfur for the ore fluid, they could be responsible for some of the variability found in gold-related pyrites discussed above. The large range in $\delta^{34}\text{S}$ values also suggests that constraints on the isotopic composition of Archean sulfur sources are not well understood. The redox condition of the Archean atmosphere, and implications for ore-forming processes, are controversial issues (Phillips et al., 2001) that are beyond the scope of this study. However, large variations in $\delta^{34}\text{S}$ values in hydrothermal pyrite could be related to the microbial reduction of seawater sulfate, and suggest an alternative to a magmatic source for oxidized ore fluids (Thode et al., 1991; Kakegawa and Ohmoto, 1999).

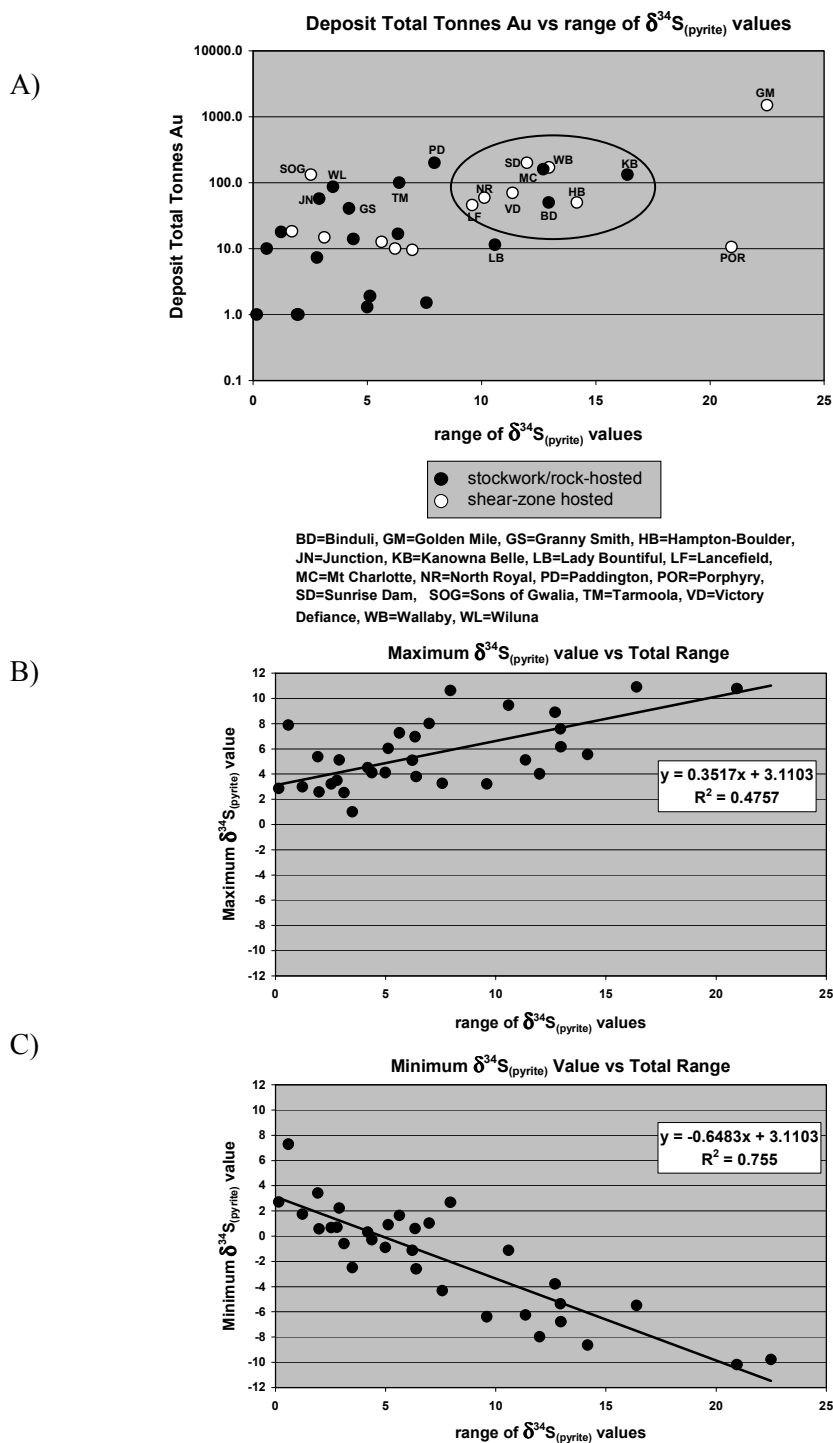


Figure 3.2.12. (A) Plot showing relationship between gold endowment and total range of $\delta^{34}\text{S}_{(\text{py})}$ values by dominant structural style of mineralization. Most of the larger gold deposits (>1Moz) have larger ranges of $\delta^{34}\text{S}_{(\text{py})}$ values (>10%). Six out of nine in this group (circled) are dominantly shear-zone hosted. (B) Plot of maximum $\delta^{34}\text{S}_{(\text{py})}$ value and total range. (C) Plot of minimum $\delta^{34}\text{S}_{(\text{py})}$ value and total range. See discussion in text.

GIS and Gold Endowment

4.1 Introduction

During the GODs Project, there were several presentations relating to GIS analysis of gold endowment, or prospectivity, in the Yilgarn Block, with emphasis on the Kalgoorlie Terrane. There was also a presentation of a preliminary database prepared by David Groves, Paul Hodkiewicz and Peter Neumayr. These are all included on the CD (distributed by AMIRA to all participants, file *Groves_emp.pdf* in archive *1-2_Aug_2001*), and are not repeated here. The principles and all published research on the topic are reviewed in Groves et al. (2000).

It is, however, useful to summarise the critical parameters, which in conjunction, control the location of the world-class to giant gold deposits in the Eastern Goldfields Province. In concert with the aims of AMIRA P511, they are summarised in terms of a minerals system approach of sources, fluid pathways, depositional sites, caps and outflow zones. It is hoped that this provides an exploration-friendly context in which to summarise the critical parameters.

The majority of the research is not proprietary to AMIRA P511, the significant exception being the concepts on chemical gradients developed by John Walshe in collaboration with Ed Mikucki and David Huston, which are not discussed in Groves et al. (2000).

4.2 Major Factors Controlling World-Class Gold Deposits

The critical factors controlling the siting of world-class orogenic gold deposits in the Eastern Goldfields Province are summarised in Table 4.1. These are largely derived from research into controls on orogenic gold deposits, which have been tested using a variety of GIS-based methodologies over the past decade or so. An attempt is made to place the critical factors into a minerals system, with the factors arranged in a broad hierarchical order related to their scale within each of the genetic categories. The empirical parameters defined by GIS-based analysis are explained in terms of their potential genetic significance and some examples of districts or deposits where these parameters apply are also given.

Table 4.1 Parameters considered critical for location of world-class orogenic gold deposits in the Eastern Goldfields Province of the Yilgarn Block. Parameters are ordered in terms of their significance to 1. Source, 2. Fluid Pathways, 3. Depositional Site, 4. Caps to System, and 5. Outflow Zones: subdivisions are given where appropriate. Empirically desired parameters are explained in terms of genetic significance. Examples are given where appropriate: names in brackets are well-documented deposits worldwide.

ORE SYSTEMS	OBSERVED PARAMETERS (Empirical)	GENETIC SIGNIFICANCE (Theoretical)	EXAMPLES
1. SOURCE* A. Deep Fluid (metamorphic?)	Gold deposits at all metamorphic grades but greenschist facies favoured.	Fluid is ubiquitous leading to widespread deposits and prospects. Greenschist facies broadly equals brittle-ductile transition: hence enhanced structurally permeability.	Most world-class deposit worldwide.
B. Magmatic (Proximal)	Widespread association with felsic porphyries and lamprophyres. In some deposits, more obvious association with specific porphyry or syenite dyke swarms or plutons.	Undoubted structural control by intrusions that control heterogeneous stresses. May be genetic relationship with magmas providing a critical fluid component. Timing needs resolution.	Wallaby (?) Jundee (?) Mt Pleasant District (?) (Parts of Abitibi Belt).
2. FLUID *** PATHWAYS			
A. Classical Structural Controls	Within 5-10 km of crustal-scale deformation zones, particularly those with abundant ultramafic rocks: first-order "worms" from geophysical datasets.	Probably crustal-scale fluid conduits from deep crust/mantle. Align greenstones broadly perpendicular to far-field stress. Also suggested that they act as aquacludes.	Many world-class deposits worldwide.
	Flexures (jogs) from normal NNW or NNE trends in these crustal-scale deformation zones.	Zones of simple rather than pure shear, producing oblique-slip rather than flattening and generating low minimum stress zones.	Kalgoorlie, Kambalda-St Ives, New Celebration Districts (Timmins).
	Clusters of regional-scale, largely NNE to ENE trending, faults across these flexure zones.	Second or third order, discontinuous fluid channels; isolate competent blocks; if non-parallel, rotate and dilate early structures.	Hill 50, Mt Charlotte, Paddington, Kundana.
	Curvilinear thrust and/or strike-slip duplexes that tend to be concentrated in these flexures and may accommodate them: traditionally considered folded D1 structures.	Produce additional complexity, particularly opportunity to increase numbers of contacts between rheologically different rock units; dilatant zones in reactivated thrust tips.	Kalgoorlie and Kambalda Districts (Timmins, Ashanti, Carlin).
	Complex stratigraphy with abundant contacts between units with contrasting geochemistry and theology.	Small-scale discontinuous fluid conduits; internal blocks with structurally induced permeability.	Most world-class deposits in Norseman-Wiluna Belt.
B. Heterogeneous Stress Controls Around Rigid Bodies	Pressure shadows of granitoid batholiths.	Overall zones of low minimum stress.	Kanowna Belle, Mt Pleasant.
<i>continued</i>	Zones in which greenstones "escape" between closely spaced batholith pairs and where transitions in metamorphic grades may occur.	Complex zones of strike-slip to thrust duplexes which accommodate volume change in greenstones; changes from ductile to brittle-ductile deformation.	Southern Cross Belt, Thunderbox (?), (Red-Campbell Lake).

ORE SYSTEMS ... continuation of B. Heterogeneous Stress Controls etc.	OBSERVED PARAMETERS (Empirical)	GENETIC SIGNIFICANCE (Theoretical)	EXAMPLES
	Similar zones where one granitoid body is in proximity to another rigid body in the greenstone belt.	Similar to above. Complex volume changes related to variable proximity between the rigid bodies.	Bronzewing, Coolgardie District (?)
	Small (<5km diameter) granitoid, porphyry or gabbro “larrikins” within the greenstone sequence, particularly in incompetent rock units or foliated rocks.	Large variations in stress orientations and magnitude of minimum stresses: dilation around irregularities in the contact or around dykes and sills.	Granny Smith, Jundee, Sons of Gwalla (?), New Celebration.
3. DEPOSITIONAL SITE ***			
	Within structural architectures as described above for fluid pathways: essentially ends or tips of fluid conduits.	May be tips or “blind ends” of more regional-scale fluid conduits; fluid pressure drives deformation.	Most world-class deposits.
	Localised structural complexities, particularly interference structures produced during progressive or superimposed deformation.	Local complexities causing variable orientation of structures to far-field stresses and consequent selective reactivation.	Most world-class deposits.
	Anticlinal or uplifted zones, particularly domal culminations.	Traps for upward fluid advection; compare with oil traps.	Kalgoorlie – New Celebration – St Ives trend (Telfer, Cosmo-Howley, Callies).
	Specific rock sequences with strong contrasts in units, and/or magnetite alteration zones around intrusions. Rocks with high Fe/ (Fe+Mg+Ca) or anomalous Fe ³⁺ /Fe ²⁺ . Rocks with anomalous magnetic signatures.	Competency contrasts for selective failure and production of structural permeability; strong chemical gradients; destruction of pre-existing magnetite.	Deposit in Kalgoorlie Terrane, Wallaby (Ashanti Belt)
	Evidence of overprinting ore-deposit or alteration styles.	Incremental addition of gold; early style produces additional contrasts in rock strength and/or geochemistry.	Kalgoorlie (Hemlo, Timmins, Bulyanhulu?)
	Evidence of anomalously oxidised (e.g. hematite/magnetite, anhydrite, V-mica, Te minerals, negative δ ³⁴ S) or anomalously reduced (e.g. pyrrhotite-arsenopyrite-loellingite, graphite) ore environments.	Steep chemical gradients to cause highly efficient gold precipitation; may relate to mixing of deep fluid with magmatic vapour (?), backmixing of “spent” fluid, or evolution of fluids along different structural pathways.	Golden Mile, other Yilgarn world-class deposits (oxidised), (Ashanti, Sheba-Fairview, Geita, Kolar-reduced).
	Fluid inclusion evidence in quartz veins for phase separation; more extreme separation, the better.	Phase separation can change oxidation state of fluid (liberation of CH ₄), pH (liberation of H ⁺), and/or reduce aH ₂ S.	Most world-class deposits, particularly Precambrian examples.

ORE SYSTEMS	OBSERVED PARAMETERS (Empirical)	GENETIC SIGNIFICANCE (Theoretical)	EXAMPLES
4. CAPS TO SYSTEM **	Regional-scale contacts where thick sedimentary sequences overlie greenstone-belt lithologies; particularly anticlinal zones.	Sedimentary sequence acts as an aquaclude on a regional to local scale.	Deposits in Kalgoorlie Terrane (Ashanti, Stawell).
	More local-scale contact zones where ultramafic rocks or porphyry-lamprophyre dykes provide large competency contrasts.	Local aquaccludes where ultramafic to felsic bodies are in appropriate orientation.	New Celebration (?) Jundee (?)
	Thrust duplexes or tips where segments of the stratigraphy may be more gently dipping than adjacent segments; or where thrusts may be flat-lying.	Local aquaccludes where rocks with more gentle dips overlie steeper dipping units, or where thrusts are more flat-lying than the rock sequence.	Victory-Defiance (?) Cleo-Sunrise (?) (Carlin).
5. OUTFLOW ZONES* (MAY BE INFLOW ZONES?)	Regional-scale alteration zones (chlorite-calcite or magnetite-bearing) that post-date peak-metamorphic assemblages in greenschist facies zones.	Possible large outflow zones around major deposits.	Kalgoorlie (Timmins, Red Lake).
	Geochemical dispersion of critical elements such as As, Sb, Te and W across or along strike.	Large outflow zones around major deposits.	Deposits studied by Pasi Eilu and co-workers: see Eilu and Groves (2001).

Final Remarks

5.1. Structural Evolution: the late Archean Kalgoorlie Orogen

The structural research carried out during this project has convinced us of the appropriateness of the division of major deformation phases in the Kalgoorlie Terrane into D_1 - D_4 . While considerably more work is still required to fully understand their regional significance and timing, considerable advances have been made here. We proposed a new time chart in *Section 2.3* which revises previously proposed timing and duration of these deformation phases.

D_1 is a north-directed thrusting phase accompanied by recumbent folds, which took place before the deposition of the <2655Ma Kurrawangs sedimentary sequence. D_1 is a shortening event separate from D_2 - D_4 and is most clearly expressed in the stratigraphic repetition in an E-W belt from Kambalda to the Widgiemooltha Dome, but also around the steepened sides of granite domes to the north such as Kanowna and Dunnsville.

Most importantly, however, is the conclusion that D_2 - D_4 represents a single continuous tectonic event defining the late-Archean Kalgoorlie Orogen, which was accompanied by low-Ca granite intrusion, regional metamorphism and gold mineralization. This orogen took place between ~ 2655 and 2630 Ma and involved the different terranes that compose the Norseman-Wiluna Belt, as evidenced by their similar deformation histories (e.g. Passchier 1994), and by the distribution of large scale NW- and NNE-trending shear zones forming large (100-km-scale) lozenges.

It was proposed that the orogen was a result of pure shear, such as typically results from head-on continental collision or gently dipping subduction below a continent. The orogen was initiated by a phase of crustal thickening (D_2 thrusting and folding), followed by a phase of lateral extension which evolved from ductile (D_3 strike slip shear zones) to (semi-) brittle (D_4 strike slip faults), once the crust became too thick for any further thickening. Arguments against a sinistral transpression deformation for the Kalgoorlie Terrane are: a) whilst sinistral movement is important in the central part of the Kalgoorlie Terrane, it did not account for large translation as expected in transpressional terranes; b) important regional N- and NNE-trending dextral shear zones (e.g. Waroonga Shear Zone) impose a symmetry to the Norseman-Wiluna Belt which is unexpected of transpressional domains, and more likely in pure shear environments; c) important NNW- to N-trending corridors such as the Ida Shear Zone were intensely flattened with unimportant sinistral shearing.

There is considerable discussion among practitioners working in the Yilgarn, about the nature of each deformation phase, and whether they developed synchronously or diachronously across the terrane. Our findings in *Section 2.4* are illustrative of the complexities of an evolving orogen and exemplify different expressions of D_2 and D_3 in different districts along the BLSZ. The swap from D_2 thrusting and folding, to D_3 strike slip shearing was not marked everywhere by the same structures, as exemplified by the contrast in deformation between the Kalgoorlie and Kambalda-SIG Districts. While in Kalgoorlie D_3 was characterized by sinistral deformation, in Kambalda D_3 was expressed by thrusting roughly contemporaneous with sinistral motion on steep shear zones. As discussed in *Section 2.4* this difference was probably a result of less intense D_2 shortening in Kambalda.

Although it is possible that the change from D_2 to D_3 occurred diachronously across the region, it is more likely that changes in one area triggered immediate changes elsewhere in the orogen, implying contemporaneity. Once again comparison between the evolution of the Kalgoorlie and Kambalda-SIG districts seems to exemplify this connectedness. When the region around Kalgoorlie reached its maximum crustal thickness and D_3 was initiated, the Kambalda district was probably forced to respond to the changes occurring to the north, initiating its own D_3 , with slightly different characteristics.

Similarly important for understanding the link between local structural evolution and regional evolution of the belt is the role of large granitoid bodies in controlling deformation. Deformation in greenstone belts in the vicinity of these large competent bodies is a compounded result of external tectonics and the attitude of the margins granitoid (e.g. Chadwin, *Section 2.5*). Low viscosity greenstones surrounding granitoids flowed away from impinging granites. Granitoid impingement explains the deviation of the main structural fabric of the Ida Corridor around the Central Granite, and also explains the arcuate shape of the Zuleika-Kunanalling Corridor and its pop-up around the Coolgardie Domain, granitoid-dominated area.

Considerable advances have been made during this project with regards to understanding the structural development of the Kalgoorlie Terrane but more work is required to firmly establish the timing of deformation in different districts. Future efforts should be directed towards detailing the structural evolution of other terranes in the Norseman-Wiluna Belt, and towards better understanding D_1 and the preceding extensional phase. These early phases are particularly important for understanding possible terrane amalgamation, and for exploration of nickel deposits in refolded ultramafic sequences.

5.2. Gold Mineralization

In all localities where the structural timing of gold mineralization has been constrained, it appears that the mineralization has taken place late, either during D_3 or D_4 . The only exception being the Golden Mile which has had a prolonged history of mineralization, starting with the Fimiston lodes, which can be firmly placed early in the structural development of the belt, possibly during D_2 or even before; followed by the D_2 Oroya lodes and by the D_4 Mount Charlotte veins. Could this be the underlying reason for it being the only giant in the Craton?

One of the main controls on gold mineralization is the existence of extreme competency contrast, such as between low viscosity talc schists or shales and competent granites or coarse-grained dolerites/gabbros. Maximum competence contrast is found at greenschist facies conditions, decreasing as temperatures decrease or increase. At amphibolite facies rocks will tend to flow more homogeneously with decreased ability to focus fluid flow into localized zones of dilation.

Geological complexity is generally associated with gold mineralization. This is most likely a result of complex areas having statistically higher ability to focus fluid flow and provide an appropriate host for the mineralization. Fractal dimensions were used in order to quantify geological complexity. Our initial expectation, based on empirical knowledge, was that regions of maximum complexity would host large gold deposits. Surprisingly, this expectation was not fulfilled. Results showed that large gold deposits are located at regions of steep lateral change in complexity (change in fractal dimensions). These regions correspond to domain boundaries, such as obvious boundaries between granite and greenstone dominated regions, or more subtle, but more important, intra-greenstone boundaries. The Golden Mile is located at one of these intra-greenstone zones of change in complexity where to the north, along strike of the BLSZ, there is a marked decrease in fractal dimensions related to the region dominated by Black Flag sedimentary rocks.

Gold endowment distribution along the BLSZ shows a regular pattern, with regularly spaced peaks of high gold endowment (every ~35 km), followed systematically by regions of low gold endowment. The two areas with the lowest gold endowment are immediately adjacent to the Golden Mile, the richest district. This pattern indicates that mineralising fluids were focused at the scale of the crust (35 km) and that the intervening gold-poor zones, were depleted of either gold or fluids. Furthermore, the region coincides with a steep variation in fractal dimensions, a measure of structural and lithological complexity. This finding suggests that complexity does

control crustal fluid flow, and that regions of transition in complexity levels as measured by fractal dimensions focus regional fluids more effectively.

5.3. Sulphur isotopes

Sulphide sulphur isotopes are sensitive indicators of the physical and chemical conditions of ore formation in orogenic systems. In this study, they were used to constrain factors related to ore-depositional processes and ore-fluid sources. Previous studies suggest that anomalously negative $\delta^{34}\text{S}_{(\text{py})}$ values are related to oxidized magmatic fluids that are responsible for the formation of larger gold deposits. Results of this study indicate that large variations in $\delta^{34}\text{S}_{(\text{py})}$ values (>10‰) in gold-related pyrites are more common in larger (>1Moz) shear-zone hosted deposits, compared to typically smaller ranges (<10‰) in smaller stockwork or rock-hosted deposits. Also, larger sulphur isotope variations commonly occur in dilational structures, compared to narrower ranges in compressional structures. These occurrences suggest that fluid flow associated with dilational and compressional structures may influence $\delta^{34}\text{S}_{(\text{py})}$ values in gold-related pyrites during mineralization. In addition, results show that there is a larger range of $\delta^{34}\text{S}$ values in sulphides from sedimentary rocks than previously reported. If these rocks were a source of sulfur for the ore fluid, they could be responsible for some of the variability found in gold-related pyrites.

This report concludes that the next major step in building up our understanding of the evolution of the Norseman-Wiluna Belt and constrain gold mineralization is to understand the thermal evolution of the region. Knowledge of the timing and nature of magmatic and deformation events is now sufficiently mature to provide well-constrained inputs for thermal and dynamic constraints to any thermal numerical modelling. However, knowledge of the metamorphic evolution of the Norseman-Wiluna Belt is lagging behind all other major areas. Future work should focus on these two areas: metamorphic evolution and thermal modelling

Acknowledgements. We would like to thank Louis Moresi for discussions and introducing RW to his computer code Ellipsis which was used to run many numerical models to support some of the work carried out in this project. Derek Wyman is thanked for his contribution during the initial stages of the project, and ensuing discussions. Nick Archibald, Ed Baltis, Mark Barley, Roger Bateman, John Beeson, Stu Brown, Ian Copeland, Brett Davis, Steve Devlin, Jack Hallberg, Scott Halley, Nick Hayward, John Hronsky, Greg Job, Clive Jones, Kevin Joyce, Paul Kitto, Bryan Krapez, Charter Matheson, Neal McNaughton, Ed Mikucki, Peter Neumayr, Bob Perriam, Gerard Tripp and Steve Wyche for discussions, helpful comments, and field support during this project. Steve Wyche is also thanked for the use of geochemical data. The Staff at the Centre for Microscopy and Microanalysis, UWA, are thanked for their expertise, Janet Thickett for all her logistical support, and students at the Centre for Global Metallogeny for their tolerance of the 'illusiv' GOD Squad. The parameters in *Section 4* are derived through the co-operative research of Warick Brown, Stephen Gardoll, Carl Knox-Robinson, and Grace Yun of the Centre for Global Metallogeny, together with Rich Goldfarb, Peter Holyland and Juhani Ojala.

Reference List

- Allen, C.A., 1986. Mineralisation controls and alteration of the Archaean quart-monzonite-hosted Porphyry gold deposit. Honours Thesis, University of Western Australia, Perth, 73 pp.
- Allen, C.A., 1987. The nature and origin of the Porphyry gold deposit, Western Australia. In: S.E. Ho and D.I. Groves (Eds.), Recent advances in understanding Precambrian gold deposits. University of Western Australia, Geology Department and Extension Service, Perth, pp. 137-145.
- Allibone, A.H., Norris, R.J. 1992. Segregation of leucogranite microplutons during syn-anatectic deformation: an example from the Taylor Valley, Antarctica. *J. Metam. Geol.* 10: 589-600.
- Archibald, N.J. 1979. Tectonic-metamorphic evolution of an Archaean Terrain. Ph.D. Thesis, University of Western Australia, Perth.
- Archibald, N.J., Bettenay, L.F. 1977. Indirect evidence for tectonic reactivation of a pre-greenstone sialic basement in Western Australia. *Earth Planet. Sci. Lett.* 33, 370-378.
- Archibald, N.J., Bettenay, L.F., Bickle, M.J., Groves, D.I. 1981. Evolution of the Archaean crust in the Eastern Goldfields Province of the Yilgarn Block, Western Australia. *Geol. Soc. Aust. Spec. Publ.* 7: 491-504.
- Archibald, N.J., Bettenay, L.F., Binns, R.A., Groves, D.I., Gunthorpe, R.J. 1978. The evolution of Archaean greenstone terrains, Eastern Goldfields Province, Western Australia. *Precambrian Res.* 6: 103-131.
- Barley, M.E., Eisenlohr, B.N., Groves, D.I., Perring, C.S., Vearncombe, J.R. 1989. Late Archean convergent margin tectonics and gold mineralization: a new look at the Norseman-Wiluna Belt, Western Australia. *Geology* 17: 826-829.
- Barrett, T. J., Cattalani, S., and MacLean, W. H., 1993. Volcanic lithogeochemistry and alteration at the Delbridge massive sulfide deposit, Noranda, Quebec. In: E.L. Hoffman, and D.W. Moore, (Eds.), Deep exploration using lithogeochemistry. *Journal of Geochemical Exploration* 48, pp. 135-173.
- Bateman, R., Owen, A.J., Goleby, B.R. and Drummond, B. 2000. The 1997 AGCRC-KCGM seismic survey - internal structure of the Kalgoorlie greenstone belt in the Kambalda domain, W.A., based on seismic reflection profiling, *Crustal Structure and Fluid Flow in the Eastern Goldfields, Western Australia*, pp. 48-51.
- Bateman, R., Costa, S., Swe, T., Lambert, D., in press. Archaean mafic magmatism in the Kalgoorlie area of the Yilgarn Craton, Western Australia: a geochemical and Nd isotopic study of the petrogenetic and tectonic evolution of a greenstone belt. *Precambrian Res.*
- Bateman, R.J., Hagemann, S.G., McCuaig, T.C., Swager, C.P. 2001. Protracted gold mineralization throughout Archaean orogenesis in the Kalgoorlie camp, Yilgarn Craton, Western Australia: structural, mineralogical, and geochemical evolution. In S.G. Hagemann, P. Neumayr, W.K. Witt, (Eds.), *World-class gold camps and deposits in the eastern Yilgarn Craton, Western Australia, with special emphasis on the Eastern Goldfields Province*. Western Australia Geological Survey Record 2001/17: 63-98.
- Bickle, M.J., Archibald, N.J. 1984. Chloritoid and staurolite stability: implications for metamorphism in the Archaean Yilgarn Block, Western Australia. *J. Metam. Geol.* 2: 179-203.
- Blenkinsop, T., 1994. The fractal dimension of gold deposits: two examples from the Zimbabwe Archaean Craton. In: J.H. Kruhl (Ed.), *Fractals and Dynamic Systems in Geoscience*. Springer-Verlag, Berlin, pp. 247-258.

- Blenkinsop, T.G. and Sanderson, D.J., 1999. Are gold deposits in the crust fractals? A study of gold mines in the Zimbabwe Craton. In: K.J.W. McCaffrey, L. Lonergan and J. Wilkinson (Eds.), *Fractures, Fluid Flow and Mineralization*. Geological Society of London Special Publications. London, pp. 141-151.
- Binns, R.A., 1988. Preliminary report on petrological and geochemical studies at Bottle Creek, Western Australia. CSIRO, Restricted Investigation Report 1767R, Open File, Sydney.
- Boulter, C.A., Fotios, M.G., Phillips, G.N. 1987. The Golden Mile, Kalgoorlie: a giant gold deposit localized in ductile shear zones by structurally induced infiltration of an auriferous metamorphic fluid. *Econ. Geol.*, 82(7): 1661-1678.
- Brown, S.M., 2000. The world-class Sunrise Dam gold mine, Western Australia: geologic setting and lode characteristics, In *Exploration Significance of Linking New Regional and Deposit Studies in the Eastern Yilgarn*, 12 December 2000, Centre for Global Metallogeny UWA, Seminar proceedings.
- Cameron, E.M. and Hattori, K., 1987. Archean gold mineralization and oxidized hydrothermal fluids. *Economic Geology*, 82(5): 1177-1191.
- Cameron, E.M., 1988. Archean gold: relation to granulite formation and redox zoning in the crust. *Geology*, 16(2): 109-112.
- Campbell, I.H., Hill, R.I. 1988. A two-stage model for the formation of the granite-greenstone terrains of the Kalgoorlie-Norseman area, Western Australia. *Earth Planet. Sci. Lett.* 90 11-25.
- Canfield, D.E., Raiswell, R., Westrich, J.T., Reaves, C.M. and Berner, R.A., 1986. The use of chromium reduction in the analysis of reduced inorganic sulfur in sediments and shales. *Chemical Geology*, 54(1-2): 149-155.
- Carlson, C.A., 1991. Spatial distribution of ore deposits. *Geology (Boulder)*, 19(2): 111-114.
- Cassidy, K.F., 1992. Archean granitoid-hosted gold deposits in greenschist to amphibolite facies terrains: a high P-T to low P-T depositional continuum equivalent to greenstone-hosted deposits. PhD Thesis, University of Western Australia, Perth, 296 pp.
- Cassidy, K.F. and Bennett, J.M., 1993. Gold mineralisation at the Lady Bountiful mine, Western Australia. *Mineralium Deposita*, 28: 388-408.
- Cassidy, K.F., Groves, D.I. and McNaughton, N.J., 1998. Late-Archean granitoid-hosted lode-gold deposits, Yilgarn Craton, Western Australia: Deposit characteristics, crustal architecture and implications for ore genesis. *Ore Geology Reviews*, 13: 65-102.
- Champion, D.C., Sheraton, J.W. 1997. Geochemistry and Nd isotope systematics of Archean granites of the Eastern Goldfields, Yilgarn Craton, Australia: Implications for crustal growth processes. *Precambrian Res.* 83: 109-132.
- Chapman, D.G., 1980. Gold distribution and content of sulfide-rich interflow metasediments in the Eastern Goldfields, Western Australia. BSc Hons Thesis, UWA, 102 pp.
- Clark, M.E., Archibald, N.J. and Hodgson, C.J., 1986. The structural and metamorphic setting of the Victory gold mine, Kambalda, Western Australia. In: A.J. Macdonald (Ed.), *Gold '86: an international symposium on the geology of gold deposits; proceedings volume*. Gold '86, Toronto, ON, Canada, pp. 243-254.
- Clark, M.E. 1987. The geology of the Victory gold mine, Kambalda, Western Australia. Ph.D. Thesis, Queen's University, Kingston, Ontario.
- Clark, M.E., Carmichael, D.M., Hodgson, C.J. and Fu, M., 1989. Wall-rock alteration, Victory gold mine, Kambalda, Western Australia: processes and P-T-X (sub CO₂) conditions of metasomatism. In: R.R. Keays, W.R.H. Ramsay and D.I. Groves (Eds.), *The geology of gold deposits: the perspective in 1988*. Economic Geology Publishing Company, Denver, pp. 445-459.
- Clemens, J.D., Holloway, J.R., White, A.J.R. 1986. Origin of an A-type granite: experimental constraints. *Am. Mineral.* 71: 317-324.
- Clout, J.M.F., Cleghorn, J.H., Eaton, P.C. 1990. Geology of the Kalgoorlie gold field. In: Hughes, F.E. (Ed.), *Geology of the Mineral Deposits of Australia and Papua New Guinea*. The Australasian Institute of Mining and Metallurgy, Parkville, Australia, pp. 411-431.
- Compston, W., Williams, I.S., Campbell, I.H., Gresham, J.J. 1985/86. Zircon xenocrysts from the Kambalda volcanics: age constraints and direct evidence for older continental crust below the Kambalda-Norseman greenstones. *Earth Planet. Sci. Lett.*, 76: 299-311.
- Cooke, D.R., 2001. The trouble with tellurium. Report and presentation to AMIRA P511, August 2001: 7.1-7.2.

- Copeland, I.K. and al., e. 1998. Jubilee gold deposit, Kambalda. In: D.A. Berkman and D.H. Mackenzie (Eds.), *Geology of Australian and Papua New Guinean Mineral Deposits*. The Australian Institute of Mining and Metallurgy, Melbourne, pp. 219-224.
- Cox, S.F., 1999. Deformational controls on the dynamics of fluid flow in mesothermal gold systems. In: K.J.W. McCaffrey, L. Lonergan and J. Wilkinson (Eds.), *Fractures, Fluid Flow and Mineralization*. Geological Society of London Special Publications, London, pp. 123-140.
- Cox, S.F., Knackstedt, M.A. and Braun, J., 2001. Principles of structural control on permeability and fluid flow in hydrothermal systems. In: J.P. Richards and R.M. Tosdal (Eds.), *Structural Controls on Ore Genesis*. Society of Economic Geologists, Boulder, pp. 1-24.
- Crowe, D.E., Valley, J.W. and Baker, K.L., 1990. Micro-analysis of sulfur-isotope ratios and zonation by laser microprobe. *Geochimica et Cosmochimica Acta*, 54(7): 2075-2092.
- Davis, B.K. 1993. Mechanism of emplacement of the Cannibal Creek Granite with special reference to timing and deformation history of the aureole. *Tectonophysics* 224, 337-362.
- Davis, B.K. 2002 in press. Complexity of structural-mineralization history in the Eastern Goldfields Province, Yilgarn Craton: evidence and implications from study of mineralized systems. *Econ. Geol.*, 48.
- Davis, B.K., Forde, A. 1994. Regional slaty cleavage formation and fold axis rotation by re-use and reactivation of pre-existing foliations; the Fiery Creek slate belt, North Queensland. *Tectonophysics* 230: 161-179.
- Davis, B.K., Pollard, P.J., Lally, J.H., McNaughton, N.J., Blake, K., Williams, P.J. 2001. Deformation history of the Naraku Batholith, Mt Isa Inlier, Australia: implications for pluton ages geometries from structural study of the Dipvale granodiorite and Levian granite. *Australian J. Earth Sci.* 48,
- Dielemans, P. 2000. Structural controls on gold mineralisation in the Southern Ore Zone, of the Hampton Boulder Deposit, New Celebration Gold Mine, Western Australia. Ph.D. Thesis, University of Western Australia, Perth 166 pp.
- Donnelly, T.H. et al., 1978. A reconnaissance study of stable isotope ratios in Archaean rocks from the Yilgarn Block, Western Australia. *Journal of the Geological Society of Australia*, 24(Part 7-8): 409-420.
- Drummond, S.E. and Ohmoto, H., 1985. Chemical evolution and mineral deposition in boiling hydrothermal systems. *Economic Geology*, 80: 126-147.
- Drummond, B.J., Goleby, B.R., Swager, C.P., Williams, P.R. 1993. Constraints on Archaean crustal composition and structure provided by deep seismic sounding in the Yilgarn Block. *Ore Geol. Rev.* 8: 17-24.
- Drummond, B.J., Goleby, B.R. and Swager, C.P., 2000. Crustal signature of Late Archaean tectonic episodes in the Yilgarn Craton, Western Australia: evidence from deep seismic sounding. *Tectonophysics* 329: 193-221.
- Eilu, P., Groves, D.I., 2001. Primary alteration and geochemical dispersion haloes of Archean orogenic gold deposits in the Yilgarn Craton: the pre-weathering scenario. *Geochemistry, Environment, Analysis* 1: 183-200.
- Eisenlohr, B.N., Groves, D.I. and Partington, G.A., 1989. Crustal-scale shear zones and their significance to Archaean gold mineralization in Western Australia. *Mineralium Deposita*, 24(1): 1-8.
- Embry, R., 1999. The structural architecture of the Ida Fault Zone in the Riverina area, Yilgarn Craton, Western Australia. Honours Thesis, University of Western Australia, Perth, 38 pp.
- Fry, N. 1992. Direction of shear. *J. Struct. Geol.* 14(2): 253-255.
- Gardoll, S.J., Groves, D.I., Knox-Robinson, C.M., Yun, G.Y. and Elliot, N., 2000. Developing the tools for geological shape analysis, with regional- to local-scale examples from the Kalgoorlie Terrane of Western Australia. *Australian Journal of Earth Sciences*, 47: 943-953.
- Gee, R.D., Baxter, J.L., Wilde, S.A. and Williams, I.R., 1981. Crustal development in the Archaean Yilgarn Block, Western Australia. In: J.E. Glover and D.I. Groves (Eds), *Archaean geology; Second international symposium*. Special Publication, Geological Society of Australia, pp. 43-56.
- Gee, R.D. 1979. Structure and tectonic style of the Western Australia Shield. *Tectonophysics* 58: 327-369.
- Gibson, C.G., 1904. The geological features and mineral resources of Mulline, Ularring, Mulwarrie and Davyhurst, Geological Survey of W.A., Bulletin No 12, pp. 3-31.
- Gibson, C.G., 1906. The geology and mineral resources of the Lawlers, Sir Samuel and Darlot (East Murchison Goldfield) Mt Ida (North Coolgardie Goldfield) and a portion of the Mt. Margaret Goldfield, Geological Survey of W.A. Bulletin No. 28, pp. 3-66.

- Gillespie, P.A., Howard, C.B., Walsh, J.J. and Watterson, J., 1993. Measurement and characterisation of spatial distributions of fractures. *Tectonophysics*, 226: 113-141.
- Golding, S.D., Groves, D.I., McNaughton, N.J., Mikucki, E.J. and Sang, J.H., 1990. Source of ore fluid and ore components: Sulphur isotope studies. In: S.E. Ho, D.I. Groves and J.M. Bennett (Eds), *Gold deposits of the Archaean Yilgarn Block, Western Australia; nature, genesis and exploration guides*. Publication - Geology Department and Extension Service, University of Western Australia. University of Western Australia, Geology Department and Extension Service. Perth, West, Aust., Australia, pp. 259-262.
- Goleby, B.R., Korsch, R.J., Fomin, T., Owen, A.J., Bell, B. 2000. The AGCRC's 1999 Yilgarn Deep Seismic Survey, Crustal Structure and Fluid Flow in the Eastern Goldfields, Western Australia, pp. 52-64.
- Goleby, B.R., Rattenbury, M.S., Swager, C.P., Drummond, B.J., Williams, P.R., Sheraton, J.W., Heinrich, C.A. 1993. Archaean crustal structure from seismic reflection profiling, Eastern Goldfields, Western Australia. *Austr. Geol. Surv. Org. Rec.* 15: 1-54.
- Griffin, T.J. 1990. Geology of the granite-greenstone terrane of the Lake Lefroy and Cowan 1:100 000 sheets, Western Australia. Geological Survey of Western Australia, Report 32: 44.
- Groenewald, P.B., McCabe, M., Roberts, I., Painter, M.G.M., 2000. Eastern Goldfields, Menzies to Norseman 1:100,000-scale Digital Data package. Geological Survey of Western Australia, Perth.
- Groves, D.I., Batt, W.D. 1984. Spatial and temporal variations in Archaean metallogenic associations in terms of evolution of granitoid-greenstone terrains with particular emphasis on the Western Australian Shield. In: Kröner, A., Hanson, G.N., and Goodwin, A.M. (Eds.), *Archaean Geochemistry: The Origin and Evolution of the Archaean Continental Crust*. Springer-Verlag, Berlin, pp. 73-98.
- Groves, D.I., Knox-Robinson, C.M., Ho, S.E. and Rock, N.M.S., 1990. An overview of Archaean lode-gold deposits. In: S.E. Ho, D.I. Groves and J.M. Bennett (Editors), *Gold deposits of the Archaean Yilgarn block, Western Australia: nature, genesis and exploration guides*. Geology Department and University Extension, UWA, Perth, pp. 2-18.
- Groves, D.I. 1993. The crustal continuum model for late-Archaean lode-gold deposits of the Yilgarn Block, Western Australia. *Mineral. Deposita* 28: 366-374.
- Groves, D.I. et al. 1995. Lode gold deposits of the Yilgarn block: products of late Archaean crustal-scale overpressured hydrothermal systems. *Geological Society of London Special Publications*, London, 95: 155-172.
- Groves, D.I., Ojala, V.J. and Holyland, P.W., 1997. Use of geometric parameters of greenstone belts in conceptual exploration for orogenic lode-gold deposits. In: K.F. Cassidy, A.J. Whitaker and S.F. Lui (Eds.), *An International Conference on Crustal Evolution, Metallogeny and Exploration of the Yilgarn Craton - an update*. Australian Geological Survey Record 1997/41, pp. 103-108.
- Groves, D.I., Goldfarb, R.J., Gebre-Mariam, M., Hagemann, S.G. and Robert, F., 1998. Orogenic gold deposits: a proposed classification in the context of their crustal distribution and relationship to other gold deposit types. *Ore Geology Reviews*, 13: 7-27.
- Groves, D.I., Goldfarb, R.J., Knox-Robinson, C.M., Ojala, J., Gardoll, S., Yun, G.Y., Holyland, P. 2000. Late-kinematic timing of orogenic gold deposits and significance for computer based exploration techniques with emphasis on the Yilgarn Block, Western Australia. *Ore Geol. Rev.* 17: 1-38.
- Guineberteau, B., Bouchez, J.-L., Vigneresse, J.L. 1987. The Mortagne granite pluton (France) emplaced by pull-apart along a shear zone: structural and gravimetric arguments and regional implications. *Bull. Geol. Soc. Am* 99: 763-770.
- Hagemann, S.G., Bateman, R., Crowe, D. and Vielreicher, R.M., 1999. In situ sulfur isotope composition of pyrites from the Fimiston- and Oryoa-style gold lodes in the Golden Mile Camp, Kalgoorlie; implications for sulfur source(s) and depositional processes. In: Anonymous (Ed.), *Geological Society of America, 1999 annual meeting. Abstracts with Programs - Geological Society of America*. Geological Society of America (GSA), Boulder, CO, United States, pp. 32.
- Hall, A., 1996. *Igneous Petrology*. Longman Group Ltd, Harlow, 551 pp.
- Hall, G.A., Wall, V.J. and Massey, S., 2001. Archaean pluton-related (thematic aureole) gold: the Kalgoorlie exploration model, 2001 - A Hydrothermal Odyssey. James Cook University EGRU, Townsville, pp. 66-67.
- Hallberg, J.A. 1986. Archaean basin development and crustal extension in the northeastern Yilgarn Block, Western Australia. *Precambrian Res.* 31: 133-156.

- Hamilton, W.B., 1998. Archean magmatism and deformation were not products of plate tectonics. *Precambrian Research*, 91: 143-179.
- Hammond, R.L., Nisbet, B.W. 1992. Towards a structural and tectonic framework for the central Norseman-Wiluna greenstone belt, Western Australia. In: Glover, J.E., and Ho, S.E. (Eds.), *The Archaean: Terrains, Processes and Metallogeny: Geology Department (Key Centre) & University Extension, University of Western Australia, Perth*, pp. 39-50.
- Hattori, K., 1987. Magnetic felsic intrusions associated with Canadian Archean gold deposits. *Geology*, 15(12): 1107-1111.
- Hill, R.I., Chappell, B.W. and Campbell, I.H., 1992. Late Archean granites of the southeastern Yilgarn Block, Western Australia. *Transactions of the Royal Society of Edinburgh*, 83: 211-226.
- Hill, R.E.T., Barnes, S.J., Gole, M.J. and Dowling, S.E., 1995. The volcanology of komatiites as deduced from field relationships in the Norseman-Wiluna greenstone belt, Western Australia. In: I. Campbell and C.M. Leshner (Eds), *Picrites, komatiites and their ore deposits*. *Lithos*, pp. 159-188.
- Hirata, T., 1989. Fractal dimension of fault systems in Japan: fractal structure in rock fracture geometry at various scales. *Pure and Applied Geophysics*, 131(1-2): 157-170.
- Ho, S.E., McNaughton, N.J. and Groves, D.I., 1994. Criteria for determining initial lead isotopic compositions of pyrite in Archaean lode-gold deposits; a case study at Victory, Kambalda, Western Australia. *Chemical Geology*, 111(1-4): 57-84.
- Hodgson, C.J., Love, D.A. and Hamilton, J.V., 1993. Giant mesothermal gold deposits: descriptive characteristics, genetic model and exploration area selection criteria. In: B.H. Whiting, C.J. Hodgson and R. Mason (Eds), *Giant ore deposits*. *Society of Economic Geologists*, pp. 157-211.
- Howard, L.E., Sass, J.H. 1964. Terrestrial heat flow in Australia. *J. Geophys. Res.* 69 1617-1626.
- Hunter, W.M., 1993, *Geology of the granite-greenstone terrain of the Kalgoorlie and Yilmia 1:100,000 sheets: Western Australia Geological Survey, Report 35*, 80pp.
- Huston, D.L., Power, M., Gemmell, J.B. and Large, R.R., 1995. Design, calibration and geological application of the first operational Australian laser ablation sulphur isotope microprobe. *Australian Journal of Earth Sciences*, 42(6): 549-555.
- Hutton, D.H.W. 1982. A tectonic model for the emplacement of the Main Donegal granite, NW Ireland. *J. Geol. Soc. London* 139: 615-631.
- Jardim de Sá, E.F., Trindade, R.I.F., Hollanda, M.H.B.M., Araújo, J.M.M., Galindo, A.C., Amaro, V.E., Souza, Z.S., Vignerese, J.-L., Lardeaux, J.-M. 1999. Brasiliano syntectonic alkaline granites emplaced in a strike slip/extensional setting (eastern Seridó, NE Brazil). *An. Acad. Bras. Ci.* 71: 17-27.
- Johnson, W., 1950. Report on the Timoni workings of the Mt. Ida Gold Mines Ltd., Copperfield. Menzies District, North Coolgardie Goldfield, Geological Survey of Western Australia, Annual Report, pp. 53-57.
- JORC, 1999. *Australasian Code for Reporting of Mineral Resources and Ore Reserves (The JORC Code)*, The Joint Ore Reserves Committee of the Australasian Institute of Mining and Metallurgy, Australian Institute of Geoscientists and Minerals Council of Australia.
- Kakegawa, T. and Ohmoto, H., 1999. Sulfur isotope evidence for the origin of 3.4 to 3.1 Ga pyrite at the Princeton gold mine, Barberton greenstone belt, South Africa. *Precambrian Research*, 96(3-4): 209-224.
- Keats, W. 1987. Regional geology of the Kalgoorlie-Boulder gold-mining District. Geological Survey of Western Australia, Report 21: 44p.
- Kent, A.J.R., Cassidy, K.F., Fanning, C.M. 1996. Archean gold mineralization synchronous with the final stages of cratonization, Yilgran Craton, Western Australia. *Geology* 24: 879-882.
- Kent, A.J.R., 1994. Geochronological constraints on the timing of Archean gold mineralisation in the Yilgarn Craton, Western Australia, Australia National University, Canberra, 268 pp.
- Kent, A.J.R., McDougall, I. 1995. ⁴⁰Ar-³⁹Ar and U-Pb age constraints on the timing of gold mineralization in the Kalgoorlie gold field, Western Australia. *Econ. Geol.* 90: 845-859.
- Kerrick, R., 1989. Archean gold: relation to granulite formation or felsic intrusions? *Geology*, 17: 1011-1015.
- Knight, J.T., Groves, D.I., Ridley, J.R. 1993. The Coolgardie Goldfield, Western Australia: District-scale controls on and Archaean gold camp in an amphibolite facies terrane. *Mineral. Deposita* 28: 436-456.
- Knight, J.T., Ridley, J.R., Groves, D.I. 2000. The Archean amphibolite facies Coolgardie Goldfield, Yilgarn Craton, Western Australia: nature, controls, and fold field-scale patterns of hydrothermal wall-rock alteration. *Econ. Geol.* 95: 49-84.

- Knox-Robinson, C.M., 1994. Archaean lode-gold mineralisation potential of portions of the Yilgarn Block, Western Australia: development and implementation of methodology for the creation of regional-scale prospectivity maps using conventional geological map data and a Geographic Information System (GIS). PhD Thesis, University of Western Australia, Perth, 169 pp.
- Knox-Robinson, C.M., Groves, D.I., Robinson, D.C. and Wheatley, M.R., 1996. Improved resource evaluation using geoscientific information systems (GIS): a pilot study, Final report for AMIRA Project P383/MERIWA Project M194A.
- Krapez, B., Brown, S.J.A., Hand, J., Barley, M.E., Cas, R.A.F. 2000. Age constraints on recycled crustal and supracrustal sources of Archaean metasedimentary sequences, Eastern Goldfields Province, Western Australia: evidence from SHRIMP zircon dating. *Tectonophysics* 322: 89-133.
- Kruhl, J.H. (Editor), 1994. *Fractals and Dynamic Systems in Geoscience*. Springer-Verlag, Berlin, 421 pp.
- Langsford, N. 1989. The stratigraphy of locations 48 and 50. In: I.M. Glacken (Ed.). *The 1989 Kalgoorlie Gold Workshop*, pp. B2-B8.
- Lambert, I.B., Phillips, G.N. and Groves, D.I., 1984. Sulphur isotope compositions and genesis of Archaean gold mineralization, Australia and Zimbabwe. In: R.P. Foster (Editor), *Gold '82; the geology, geochemistry and genesis of gold deposits*. A.A. Balkema, Rotterdam, Netherlands, pp. 373-387.
- Lambert, I.B. and Donnelly, T.H., 1990. The palaeoenvironmental significance of trends in sulphur isotope compositions in the Precambrian: a critical review. In: H.K. Herbert and S.E. Ho (Eds.), *Proceedings of the conference on stable isotopes and fluid processes in mineralization*. University of Western Australia, Geology Department and Extension Service, Perth, pp. 260-268.
- Langsford, N., 1989. The stratigraphy of locations 48 and 50. In: I.M. Glacken (Editor), *1989 Kalgoorlie Gold Workshop - the geology and mining operations of the Kambalda region*. Australasian Institute of Mining and Metallurgy, Kalgoorlie, pp. B1-B8.
- Leaman, D.E., 1994. Some aspects of the magnetic signature of the Bottle Creek gold deposit, Western Australia. In: M.C. Dentith et al. (Eds.), *Geophysical signatures of Western Australian mineral deposits*, University of Western Australia, Geology Department and Extension Service. Perth, pp. 277-282.
- Legge, P.J., Mill, J.H.A., Ringrose, C.R. and McDonald, I.R., 1990. Bottle Creek gold deposit. In: F.E. Hughes (Ed.), *Geology of the mineral deposits of Australia and Papua New Guinea*. Monograph Series - Australasian Institute of Mining and Metallurgy, pp. 357-361.
- Loucks, R.R. and Mavrogenes, J.A., 1999. Gold solubility in supercritical hydrothermal brines measured in synthetic fluid inclusions. *Science*, 284(5423): 2159-2163.
- Mandelbrot, B.B., 1983. *The fractal geometry of nature*. Freeman, New York, 468 pp.
- Manning, C.E. and Ingebritsen, S.E. 1999. Permeability of the continental crust: implications of geothermal data and metamorphic systems. *Rev. Geophys.*, 37(1): 127-150.
- Martyn, J.E. 1987. Evidence for structural repetition in the greenstones of the Kalgoorlie District, Western Australia. *Precambrian Res.* 37: 1-18.
- McCuaig, T.C. and Kerrich, R., 1998. P-T-t deformation-fluid characteristics of lode gold deposits: evidence from alteration systematics. *Ore Geology Reviews*, 12: 381-453.
- McCuaig, T.C., Kerrich, R., Groves, D.I. and Archer, N., 1993. The nature and dimensions of regional and local gold-related hydrothermal alteration in tholeiitic metabasalts in the Norseman goldfields: the missing link in a crustal continuum of gold deposits? *Mineralium Deposita*, 28: 420-435.
- McLaren, S., Sandiford, M., Hand, M. 1999. High radiogenic heat-producing granites and metamorphism—an example from the western Mount Isa inlier, Australia. *Geology* 27: 679-682.
- McNaughton, N.J., Cassidy, K.F., Groves, D.I., Perring, C.S. 1990. Timing of mineralization. In: Ho, S.E., Groves, D.I., and Bennett, J.M. (Eds.), *Gold Deposits of the Yilgarn Block, Western Australia: Nature, Genesis and Exploration Guides*. Department of Geology and University Extension, University of Western Australia Publication, Perth, pp. 221-225.
- Mikucki, E.J. and Ridley, J.R., 1993. The hydrothermal fluid of Archaean lode-gold deposits at different metamorphic grades: compositional constraints from ore and wallrock alteration assemblages. *Mineralium Deposita*, 28: 469-481.
- Mikucki, J.A., 1997. Contrasting fluid sources and mineralization styles in the Great Eastern Archaean lode-gold deposits, Lawlers, Western Australia. PhD Thesis, University of Western Australia, Perth.
- Mikucki, E.J., 1998. Hydrothermal transport and depositional processes in Archean lode-gold systems: A review. *Ore Geology Reviews*, 13: 307-321.

- Moresi, L., Muhlhaus, H.-B., Dufour, F. 2000. *Particle- in-Cell Solutions for Creeping Viscous Flows with Internal Interfaces*. In: H-B Muhlhaus, H.-B, Dyskin, A. and Pasternak, E. (Eds). Proceedings of the 5th International Workshop on Bifurcation and Localization in Geomechanics (IWBL'99), Perth, W. A., Australia: Australia, Balkema, Rotterdam. To appear: Dec 2000
- Mueller, A.G., Harris, L.B., Lungan, A. 1988. Structural control of greenstone-hosted gold mineralization by transcurrent shearing: a new interpretation of the Kalgoorlie Mining District, Western Australia. *Ore Geol. Rev.* 3: 359-387.
- Mueller, A.G., 1990. The nature and genesis of high- and medium-temperature Archaean gold deposits in the Yilgarn block, Western Australia, including a specific study of scheelite-bearing gold skarn deposits. PhD Thesis, University of Western Australia, Perth.
- Mueller, A.G., McNaughton, N.J. 2000. U-Pb ages constraining batholith emplacement, contact metamorphism, and the formation of gold and W-Mo skarns in the Southern Cross area, Yilgarn Craton, Western Australia. *Econ. Geol.* 95: 1231-1257.
- Myers, J.S., and Hocking, R.M., 1998. Geological map of Western Australia, 1:2,500,000 (13th edition): Western Australia Geological Survey.
- Neall, F.B. and Phillips, G.N., 1987. Fluid-wall rock interaction in an Archean hydrothermal gold deposit; a thermodynamic model for the Hunt Mine, Kambalda. *Economic Geology*, 82(7): 1679-1694.
- Nelson, D.R. 1997. Evolution of the Archaean granite-greenstone terranes of the Eastern Goldfields, Western Australia: SHRIMP U-Pb zircon constraints. *Precambrian Geol.* 83: 57-81.
- Neumayr, P., Hagemann, S.G. and Groves, D.I., 2001. Stable isotope and fluid inclusion signatures of hydrothermal fluid in transcrustal fault zones: significance of orogenic Archaean lode-gold mineralization, 2001 - A Hydrothermal Odyssey, Townsville, James Cook University, pp. 150-151.
- Neumayr, P. et al., in prep. The hydrothermal connection of the transcrustal Cadillac Tectonic Zone and mineralized second- and third-order shear zones in the Val-d'Or Camp, Canada: evidence from fluid inclusions, stable isotopes, gas and ion-analyses.
- Neves, S.P., Vauchez, A., Archanjo, C.J. 1996. Shear zone-controlled magma emplacement or magma-assisted nucleation of shear zones? Insights from northeast Brazil. *Tectonophysics* 262: 349-364.
- Nguyen, T.P., 1997. Structural controls on gold mineralisation of the Revenge deposit and its setting in the Lake Lefroy area, Kambalda, Western Australia. PhD thesis, The University of Western Australia.
- Nguyen, P.T., Cox, S.F., Harris, L.B., Powell, C.M. 1998. Fault-valve behaviour in optimally oriented shear zones: an example at the Revenge gold mine, Kambalda, Western Australia. *J. Struct. Geol.* 20(12): 1625-1640.
- Norris, N.D. 1990. New Celebration gold deposits. In: F.E. Hughes (Editor), *Geology of the Mineral Deposits of Australia and Papua New Guinea*. The Australasian Institute of Mining and Metallurgy, Melbourne, pp. 449-454.
- Ohmoto, H. and Rye, R.O., 1979. Isotopes of sulfur and carbon. In: H.L. Barnes (Editor), *Geochemistry of hydrothermal ore deposits*. John Wiley and Sons, New York, pp. 509-567.
- Ojala, V.J., Ridley, J.R., Groves, D.I., Hall, G.C., 1993. The Granny Smith gold deposit: the role of heterogeneous stress distribution at an irregular granitoid contact in a greenschist facies terrane. *Mineral. Deposita* 28: 409-419.
- Oliver, N.H.S., 1996. Review and classification of structural controls on fluid flow during regional metamorphism. *J. Metam. Geol.*, 14(4): 477-492.
- Palin, J.M. and Xu, Y., 2000. Gilt by association? Origins of pyritic gold ores in the Victory mesothermal gold deposit, Western Australia. *Economic Geol.*, 95: 1627-1634.
- Passchier, C.W. 1994. Structural geology across a proposed Archaean terrane boundary in the eastern Yilgarn craton, Western Australia. *Precambrian Res.* 68, 43-64.
- Paterson, S.R., Tobisch, O.T. 1988. Using pluton ages to date regional deformation: problems with commonly used criteria. *Geology* 16: 1108-1111.
- Pearce, J. A., and Cann, J. R., 1973, Tectonic setting of basic volcanic rocks determined using trace element analyses: *Earth Planet. Sci. Lett.* 19, pp. 290-300.
- Perring, C.S., 1989. The significance of "porphyry" intrusions to Archaean gold mineralization in the Norseman-Wiluna belt of Western Australia. PhD Thesis, University of Western Australia, Perth.
- Phillips, G.N. and Groves, D.I., 1983. The nature of Archaean gold-bearing fluids as deduced from gold deposits of Western Australia. *J. Geol. Soc. Australia*, 30(1-2): 25-39.
- Phillips, G.N. and Groves, D.I., 1984. Fluid access and fluid-wall rock interaction in the genesis of the Archaean gold-quartz vein deposit at Hunt Mine, Kambalda, Western Australia. In: R.P. Foster (Ed.),

- Gold '82; the geology, geochemistry and genesis of gold deposits. A.A. Balkema, Rotterdam, Netherlands, pp. 389-416.
- Phillips, G.N. 1986. Geology and alteration in the Golden Mile. *Kalgoorlie. Econ. Geol.*, 81: 779-808.
- Phillips, G.N., Groves, D.I., Neall, F.B., Donnelly, T.H. and Lambert, I.B., 1986. Anomalous sulfur isotope compositions in the Golden Mile, Kalgoorlie. *Economic Geology*, 81: 2008-2015.
- Phillips, G.N., Powell, R. 1993. Link between gold provinces. *Econ. Geol.*, 88: 1084-1098.
- Phillips, N., Groves, D.I., Kerrich, R. 1996. Factors in the formation of the giant Kalgoorlie gold deposit. *Ore Geol. Rev.* 10: 295-317.
- Phillips, G.N., Law, J.D.M. and Myers, R.E., 2001. Is the redox state of the Archean atmosphere constrained? *Society of Economic Geologists Newsletter*, 47, October 2001: 1, 9-18.
- Pitcher, W.S., Berger, A.R. 1972, *The geology of Donegal: a study of granite emplacement and unroofing: Regional Geology Series: New York, John Wiley & Sons*, 435 p.
- Platt, J.P., Allchurch, P.D., Rutland, R.W.R. 1978. Archean tectonics in the Agnew supracrustal belt, Western Australia. *Precambrian Res.* 7: 3-30.
- Powell, R., Will, T.M., Phillips, G.N. 1991. Metamorphism in Archean greenstone belts: calculated fluid compositions and implications for gold mineralization. *J. Metam. Geol.*: 9: 141-150.
- Qiu, Y. 1997. Long-lived granitoid magmatism in the Southern Cross Province, Yilgarn Craton, Western Australia, and its relationships with Archean lode-gold mineralization, Ph.D. thesis: University of Western Australia 297 p.
- Rattenbury, M.S., 1993. Tectonostratigraphic terranes in the northern Eastern Goldfields. In: P.R. Williams and J.A. Haldane (Eds.), *Crustal evolution, metallogeny and exploration in the Eastern Goldfields*. AGSO, Kalgoorlie, pp. 73-75.
- Ren, S.K., Heithersay, P.S. and Ballinger, T.A., 1994. The Kanowna Belle gold deposit and implications to Archean gold metallogeny of the Yilgarn Craton, Western Australia. In: *Proceedings of the Ninth Quadrennial IAGOD Symposium, Beijing, China, August 12-18, 1994*, R.D. Hagni. (Ed.) Stuttgart: E. Schweizerbart'sche Verlagsbuchhandlung (Nagel u. Obermiller), Beijing and Perth.
- Ridley, J. 1993. Implications of metamorphic patterns to tectonic models of the Eastern Goldfields. In: Williams, P.R. and Haldane, J.A. (Compilers), *Kalgoorlie 93 - An international conference on crustal evolution, metallogeny and exploration of the Eastern Goldfields*. AGSO, pp. 95-100.
- Ridley, J., Mengler, F. 2000. Lithological and structural controls on the form and setting of vein stockwork orebodies at the Mount Charlotte Gold Deposit, Kalgoorlie. *Econ. Geol.* 95: 85-98.
- Roberts, D.E., Elias, M. 1990b. Gold deposits of the Kambalda-St Ives region. In: F.E. Hughes (Editor), *Geology of the Mineral Deposits of Australia and Papua New Guinea*. The Australasian Institute of Mining and Metallurgy, Melbourne, Australia, pp. 479-491.
- Robin, P.-Y. 1979. Theory of metamorphic segregation and related processes. *Geoch. Cosmoch. Acta* 43: 1587-1600.
- Robinson, B.W. and Kusakabe, M., 1975. Quantitative preparation of sulfur dioxide for ³⁴S/³²S analyses from sulfides by combustion with cuprous oxide. *Analytical Chemistry*, 47: 1179-1181.
- Sandiford, M., Hand, M. 1998. Australian Proterozoic high-temperature, low-pressure metamorphism in the conductive limit. In: Treloar, P.J., and O'Brien, P.J. (Ed.), *What Drives Metamorphism and Metamorphic Reactions*. *Geol. Soc. London Sp. Publ.*, 138: 109-120.
- Scott, R.J. 1997. Fault control on fluid flow and mineralization at Mount Charlotte and the Golden Mile. In: K.F. Cassidy, A.J. Whitaker and S.F. Liu (Editors), *Crustal evolution, metallogeny and exploration of the Yilgarn Craton — an update*, Kalgoorlie 97: pp. 145-150.
- Secombe, P.K., Groves, D.I., Marston, R.J. and Barrett, F.M., 1981. Sulfide paragenesis and sulfur mobility in Fe-Ni-Cu sulfide ores at Lunnon and Juan Main shoots, Kambalda: textural and sulfur isotopic evidence. *Economic Geol.*, 76: 1675-1685.
- Sibson, R.H., 1996. Structural permeability of fluid-driven fault-fracture meshes. *J. Struct. Geol.*, 18(8): 1031-1042.
- Sibson, R.H., 2001. Seismogenic framework for hydrothermal transport and ore deposition. In: J.P. Richards and R.M. Tosdal (Eds.), *Structural Controls on Ore Genesis*. *Society of Economic Geologists, Boulder*, pp. 25-50.
- Skwarnecki, M.S. 1987. Controls on Archean gold mineralization in the Leonora District, Western Australia. In: S.E. Ho and D.I. Groves (Editors), *Recent Advance in Understanding Precambrian Gold Deposits*. The University of Western Australia, Perth, pp. 109-135.

- Smithies, R.H., Champion, D.C. 1999. Late Archaean felsic alkaline igneous rocks in the Eastern Goldfields, Yilgarn Craton, Western Australia: a result of lower crustal delamination? *J. Geol. Soc. London* 156: 561-576.
- Sulsky, D., Zhou, S.-J., Schreyer, H. L. 1995. Application of a particle-in-cell method to solid mechanics, *Comput. Phys. Commun.* 87: 236-252.
- Swager, C. 1989a. Structure of the Kalgoorlie greenstones — regional deformation history and implications for the structural setting of the Golden Mile gold deposits. *GSWA Prof. Papers, Report 25*: 59-84.
- Swager, C.P. 1989b. Dunnsville 1:100 000 Sheet. *Geol. Surv. West. Australia*: 11-42.
- Swager, C., Griffin, T.J. 1990. An early thrust duplex in the Kalgoorlie-Kambalda greenstone belt, Eastern Goldfields Province, Western Australia. *Precambrian Res.* 48: 63-73.
- Swager, C.P., Witt, W.K., Griffin, T.J., Ahmat, A.L., Hunter, W.M., McGoldrick, P.J., Wyche, S. 1992. Late Archaean granite-greenstones of the Kalgoorlie Terrane, Yilgarn Craton, Western Australia. In: Glover, J.E., and Ho, S.E. (Eds.), *The Archaean: Terrains, Processes and Metallogeny: Geology Department (Key Centre) & University Extension, University of Western Australia, Perth*, pp. 107-122.
- Swager, C.P., 1994. *Geology of the Dunnsville 1:100,000 sheet, Western Australia: Western Australia Geological Survey, Perth*, 16pp.
- Swager, C.P., 1995. *Geology of the greenstone terranes in the Kurnalpi-Edjudina region, southeastern Yilgarn Craton, Geological Society of Western Australia, Report 47*, pp. 31.
- Swager, C.P. 1997. Tectono-stratigraphy of late Archaean greenstone terranes in the southern Eastern Goldfields, Western Australia. *Precambrian Res.* 83: 11-42.
- Swager, C.P., Goleby, B.R., Drummond, B.J., Rattenbury, M.S., Williams, P.R. 1997. Crustal structure of granite-greenstone terranes in the Eastern Goldfields, Yilgarn Craton, as revealed by seismic reflection profiling. *Precambrian Res.* 83: 43-56.
- Swager, C.P. Griffin, T.J., Witt, W.K., Wyche, S., Ahmat, A.L., Hunter, W.M., and McGoldrick, P.J., 1995. *Geology of the Archaean Kalgoorlie Terrane. Report 48, Geological Survey of Western Australia, Perth, Western Australia*, 26 pp.
- Thode, H.G., Ding, T. and Crocket, J.H., 1991. Sulphur-isotope and elemental geochemistry studies of the Hemlo gold mineralization, Ontario; sources of sulphur and implications for the mineralization process. *Canadian Journal of Earth Sciences = Journal Canadien des Sciences de la Terre*, 28(1): 13-25.
- Tomich, S.A., 1956. Summary Report on the geology of a portion of the Mt. Ida district, North Coolgardie Goldfield. *Geological Survey of Western Australia, Annual Report*, pp. 18-20.
- Townsend, D.B., Mai, G. and Morgan, W.R., 2000. Mines and mineral deposits of Western Australia: digital extract from MINEDEX - an explanatory note, *Geological Survey of Western Australia, Record 2000/13*, pp. 28.
- Tripp, G.I., 2000. *Structural Geology and Gold Mineralisation of the Ora Banda and Zuleika Districts, Eastern Goldfields, Western Australia. M.Sc. Thesis, Curtin University of Technology, Western Australia*, 378pp.
- Tullis, J. and Yund, R.A. 1987. Transition from cataclastic flow to dislocation creep of feldspar: mechanisms and microstructures. *Geology* 15: 606-609.
- Turcotte, D.L., 1997. *Fractals and Chaos in Geology and Geophysics*, 2nd edition. Cambridge University Press, Cambridge, 398 pp.
- Ulmer, P. and Trommsdorff, V., 1995. Serpentine stability to mantle depths and subduction-related magmatism. *Science* 268: 858-861.
- Vanderhor, F. and Groves, D.I., 1998. Systematic Documentation of Archean Lode Gold Deposits in the Yilgarn Craton, MERIWA Report # 193.
- Vearncombe, J.R., Barley, M.E., Eisenlohr, B.N., Groves, D.I., Houstoun, S.M., Skwarnecki, M.S., Grigson, M.W., Partington, G.A. 1989. Structural controls on mesothermal gold mineralization: examples from the Archean terranes of southern Africa and Western Australia. *Econ. Geol. Monogr.* 6 124-134.
- Vearncombe, J.R., Vearncombe, S. 1999. The spatial distribution of mineralization: applications of Fry analysis. *Econ. Geol.* 94: 475-486.
- Vielreicher, N.M., Snee, L.W., Marshall, S.A., McNaughton, N.J., Groves, D.I., Baggott, M.S., Vielreicher, R.M., submitted. Precise age constraints on gold mineralization in the eastern Yilgarn Craton, Western Australia. *Econ. Geol.*
- Vielreicher, N.M., and McNaughton, N.J., 2002. SHRIMP U-Pb geochronology of magmatism and thermal events in the Archaean Marymia Inlier, Central Sestern Australia. *Int. J. Earth. Sci.*, 96: 406-432.

- Walsh, J.J. and Watterson, J., 1993. Fractal analysis of fracture patterns using the standard box-counting technique: valid and invalid methodologies. *Journal of Structural Geology*, 15(12): 1509-1512.
- Walshe, J.L., Hobbs, B.E., Hall, G.C. and Ord, A., 1999. Towards an understanding of giant gold systems, SME Annual Meeting. Society of Mining Engineers, Metallurgists and Explorationists (USA), Denver, pp. 1-6.
- Watchorn, R.B. 1998. Kambalda-St Ives gold deposits, Kambalda. In: D.A. Berkman and D.H. Mackenzie (Editors), *Geology of Australian and Papua New Guinean Mineral Deposits*. The Australian Institute of Mining and Metallurgy, Melbourne, pp. 243-254.
- Weatherstone, N., 1990. Porphyry gold deposit. In: F.E. Hughes (Editor), *Geology of the Mineral Deposits of Australia and Papua New Guinea*. Australasian Institute of Mining and Metallurgy, Melbourne, pp. 525-530.
- Weinberg, R.F. 1996. The ascent mechanism of felsic magmas: news and views. *Trans. R. Soc. Edinburgh: Earth Sciences* 87: 95-103.
- Weinberg, R.F., Podladchikov, Y.Y. 1995. The rise of solid-state diapirs. *J. Struct. Geol.* 17: 1183-1195.
- Wesnowsky, S.G. 1988. Seismological and structural evolution of strike-slip faults. *Nature*, 335: 340-343.
- Williams, H. 1994. The lithological setting and controls on gold mineralization in the Southern Ore Zone, of the Hampton Boulder Deposit, New Celebration Gold Mine, Western Australia. Honours Thesis, University of Western Australia, Perth, 58 pp.
- Williams, I.R., 1974. Structural subdivision of the Eastern Goldfields Province, Yilgarn Block, Geological Survey of Western Australia, Annual Report, pp. 53-59.
- Williams, P.R., Currie, K.L. 1993. Character and regional implication of the sheared Archaean granite-greenstone contact near Leonora, Western Australia. *Precambrian Res.* 62, 343-365.
- Williams, P.R., Nisbet, B.W. and Etheridge, M.A. 1989. Shear zone, gold mineralization and structural history in the Leonora District, Eastern Goldfields Province, Western Australia. *Aust. J. Earth Sci.*, 36: 383-403.
- Williams, P.R., Whitaker, A.J. 1993. Gneiss domes and extensional deformation in the highly mineralized Archaean Eastern Goldfields Province, Western Australia. *Ore Geol. Rev.* 8: 141-162.
- Wintsch, R.P., Christoffersen, R., Kronenberg, A.K. 1995. Fluid-rock reaction weakening of fault zones. *J. Geophys. Res.* 100: 13021-13032.
- Witt, W.K. 1990. The geology of Bardoc 1:100,000 sheet, Western Australia: Western Australia Geological Survey, Perth, Record 1990/14, 111pp.
- Witt, W.K. 1991. Regional metamorphic controls on alteration associated with gold mineralization in the Eastern Goldfields Province, Western Australia: implications for the timing and origin of Archean lode-gold deposits. *Geology* 19: 982-985.
- Witt, W.K., 1992a. Gold deposits of the Kalgoorlie-Kambalda-St Ives areas, Western Australia: Part 3 of a systematic study of the gold mines of the Menzies-Kambalda region, Geological Survey of Western Australia, Record 1992/15, pp. 107.
- Witt, W.K., 1992b. Gold deposits of the Mt Pleasant-Ora Banda areas, Western Australia: Part 2 of a systematic study of the gold mines of the Menzies-Kambalda region, Geological Survey of Western Australia, Record 1992/14, pp. 103.
- Witt, W.K. 1993. Gold deposits of the Kalgoorlie-- Kambalda areas, Western Australia -- Part 3 of a systematic of the gold mines of the Menzies-Kambalda region. Geological Survey of Western Australia, Record 1992/15: 108.
- Witt, W.K. 1994. Geology of the Melita 1:100 000 Sheet, Explanatory Notes. Geological Survey of Western Australia 63 pp.
- Witt, W.K. 2001. Tower Hill gold deposit, Western Australia: an atypical, multiply deformed Archaean gold-quartz vein deposit. *Australian J. Earth Sci.* 48: 81-99.
- Witt, W.K., Swager, C.P. 1989. Structural setting and geochemistry of Archaean I-type granites in the Bardoc-Coolgardie area of the Norseman-Wiluna Belt, Western Australia. *Precambrian Res.* 44: 323-351.
- Wyche, S., 2000. Geology of the Riverina 1:100,000 sheet, Western Australia. Western Australia Geological Survey, Perth.
- Wyche, S. and Witt, W.K., 1992. Geology of the Davyhurst 1:100,000 Sheet, Western Australia. Western Australia Geological Survey, Perth. Record 1991/3, 48 pp.
- Xu, Y., Palin, J.M. and Campbell, I.H., 1997. Large variations in temperature of hydrothermal vein precipitation in the Victory gold deposit, Kambalda, WA. In: Anonymous (Ed.), *New developments in*

- research for ore deposit exploration; Third national conference of the Specialist Group in Economic Geology. Abstracts - Geological Society of Australia. Geological Society of Australia, Sydney, N.S.W., Australia, pp. 76.
- Xu, Y., 1999. The stable isotope and trace element geochemistry of the Victory gold deposit, Western Australia. PhD Thesis, Australian National University, Canberra, 163 pp.
- Yeats, C.J. et al. 1999. Evidence for diachronous Archean lode gold mineralization in the Yilgarn Craton, Western Australia: a SHRIMP U-Pb study of intrusive rocks. *Econ. Geol.*, 94: 1259-1276.
- Yun, G.Y., 2000. GIS-based methodology for prospectivity analysis of orogenic lode-gold deposits, PhD Thesis, University of Western Australia, Perth.

PART II

**A Generic Assessment of Orogenic Gold
Provinces**

**Factors Controlling the Formation of World-
Class and Giant Deposits**

**Hydrothermal Systems,
Giant Ore Deposits
&
A New Paradigm for
Predictive Mineral Exploration**

AMIRA Project P511

Author: David Groves
with contributions from Derek Wyman and Richard Goldfarb

JUNE, 2002

PREAMBLE

The previously released Generic Assessment document (February, 2000) has now been revised and expanded to include a list of critical criteria over a decreasing scale, from terrane to goldfield. The summary of generic observations and interpretations is based on the view that orogenic lode gold deposits constitute a distinct and recognisable ore deposit class. They correspond to deposits that have been variously termed “gold only”, “greenstone belt-hosted”, “slate-hosted”, “mesothermal”, “Mother Lode-style”, etc (Groves et al., 1998).

The orogenic gold deposit class is characterised by epigenetic, structurally-controlled deposits with $Au/Ag > 1$ and a lack of associated economic base-metal mineralisation. Unlike most other gold deposit types, the orogenic deposits are predominantly formed at crustal depths in excess of 5 km. They are characterised by potassic and carbonate alteration assemblages, $\delta^{18}O_{\text{quartz}}$ values between 10 and 14 per mil, and low-salinity aqueous fluid inclusions with 3-30 % CO_2 . Conversely, Archaean or younger deposits characterised by high Ag or base-metal contents, or $\delta^{18}O_{\text{quartz}}$ that departs significantly from 10 to 14 per mil, or high-salinity and/or CO_2 - poor ore fluids, are **not** considered to be part of this deposit class.

Given that the orogenic gold deposits are a coherent deposit class, individual deposits or districts are considered to have formed by the same fundamental processes. Accordingly, evidence is applied from the approximately 75 known orogenic gold provinces (Goldfarb et al., 2001) towards a generic or generalised resolution of the five questions addressed by AMIRA Project P511. An implicit assumption of the approach is that a single-source fluid type is dominant in all examples of the deposit class, rather than distinct source fluids being related to different shallow crustal environments (e.g., the source fluids for slate belt gold are directly analogous to the source fluids for greenstone belt gold). This assumption is based on comparisons of fluid inclusion data from a variety of orogenic gold provinces (numerous papers in *Ore Geology Reviews* volume 13, 1998 and references therein). It is, however, realised that chemical gradients are important in producing high gold grades and that local mixing may occur. Whether this mixing is related to different degrees of modification of a single fluid, or whether it reflects mixing of an externally-derived fluid with the major fluid is controversial.

Using these assumptions, differences between orogenic gold districts are evaluated in order to constrain factors that contribute to the formation and preservation of world- and giant-class examples of the deposit type, rather than the more common smaller examples. Initially, each of the five questions posed in P511 is addressed, with a Summary of Constraints followed by an Interpretation and a list of Outstanding Problems and related positive and negative Exploration Criteria. This is followed by a list of potentially critical criteria that could be used for area selection for giant to world-class gold deposits from the terrane to goldfield scale.

Table of Contents

- 1. What is the Size And Structural-Lithological Architecture of World-Class Giant Orogenic Gold Systems?**
 - 1.1 Constraints
 - 1.1.1 Size*
 - 1.1.2 Architecture*
 - 1.2 Interpretation
 - 1.3 Outstanding Problems
 - 1.4 Exploration Criteria
 - 1.4.1. Positive Criteria*
 - 1.4.2. Negative Criteria*

- 2. What is Geodynamic History of World-Class/Giant Orogenic Gold Systems?**
 - 2.1 Constraints
 - 2.2 Interpretation
 - 2.3 Outstanding Problems
 - 2.4 Exploration Criteria
 - 2.4.1. Positive Criteria*
 - 2.4.2. Negative Criteria*

- 3. What is the Nature of Fluid Reserviors?**
 - 3.1 Constraints
 - 3.1.1 Fluid*
 - 3.1.2 Reservoirs*
 - 3.2 Interpretation
 - 3.3 Outstanding Problems
 - 3.4 Exploration Criteria
 - 3.4.1. Positive Criteria*

- 4. What is the Method of Fluid Advection/Convection?**
 - 4.1 Constraints
 - 4.2 Interpretation
 - 4.3 Outstanding Problems
 - 4.4 Exploration Criteria
 - 4.4.1. Positive Criteria*
 - 4.4.2. Negative Criteria*

- 5. Mechanisms of Metal Transport and Deposition**
 - 5.1 Constraints
 - 5.2 Interpretation
 - 5.3 Exploration Criteria

- 6. Executive Summary of Positive Geological Exploration Criteria for Giant to World-Class Deposits: Listed in Order of Decreasing Scale: (Regolith Geochemistry And Geophysical Targetting Excluded)**
 - 6.1 Terrane or Province Selection Scale
 - 6.2 Goldfield or Camp Selection Scale
 - 6.3 Indicative Target-Scale Geological Guides (Not Exclusive to Large Deposits)

1. What is the Size and Structural-Lithological Architecture of World-Class/Giant Orogenic Gold Systems?

1.1 Constraints

1.1.1 Size

- Orogenic gold deposits of similar age (generally ± 20 m.y.) are present in collisional or orogenic belts (or preserved segments of them) or segments of terranes which extend for strike lengths on the order of several 100 km to 1000 km (e.g., Norseman–Wiluna; Abitibi –Wawa; Alaska). Maximum Orogenic Belt widths are on the order of 100 km to 500 km for early Precambrian deposits, but tend to be narrower for younger examples (the Lachlan Fold belt excepted).
- Within these Orogenic Belts, World-Class ($> 100t$ Au) or Giant ($>> 100t$ Au) deposits occur in more restricted sub-regions (“Provinces”) with maximum lengths of 200 to 300 km and 100 km widths (e.g., Kalgoorlie Terrane). World-Class Goldfields or Districts within the Provinces are typically on the order of 10 to 20 km by 10 to 15 km in area (Golden Mile; Timmins; Ashanti; Bendigo) and probably represent original vertical-depth extents of up to 5 km.

1.1.2 Architecture

- At the largest scale, deposits occur in Orogenic Belts that tend to be elongate features comprising accreted back arc–arc and ocean island or wacke–flysch forearc accretionary prisms. In the latter, basal mafic volcanic sequences appear to be critical. The sequences have preserved thicknesses of 10 km to 20 km. The nature of the underlying lithosphere appears to be important. The highest quality ore deposits are sited in terranes where there is evidence for oceanic lithosphere (e.g. Abitibi, Ashanti) or thinned continental lithosphere (e.g. Norseman-Wiluna). Terranes with evidence of unconformably overlying greenstone belts (e.g. Southern Cross, Zimbabwe) are less endowed and terranes with anomalously long histories of greenstone-belt development (e.g. Pilbara) are least endowed.
- Anomalously large amounts of granitoids are common, particularly in Archaean-Palaeoproterozoic Orogenic Belts.
- Within the Orogenic Belts, deposits exhibit a spatial association with major crustal-scale fault systems, most commonly steep oblique-slip systems but including, for example, postulated thrust tips in the Bendigo–Ballarat district. Segments of the crustal-scale fault systems that deviate from the mean trend are particularly well-endowed.
- Important orogenic gold provinces are characterised by large proportions of low-strain domains (typically comprising 95% of the province) and volumetrically minor high-strain zones, commonly sited at regional-scale contacts between rocks of different competency, and containing anomalous concentrations of ultramafic rocks in Archean terranes.
- World-Class deposits tend to occur in regions of complex lithostratigraphy: greenstone belt associations commonly contain mafic/ultramafic volcanic units, doleritic intrusions and upper sedimentary sequences, whereas slate belts typically include thrust slivers of mafic volcanic rocks and(or) dolerites, felsic dykes and sills, and lamprophyres. Greenschist-facies terranes are favoured because there is brittle-ductile deformation with contrasting behaviour of adjacent rocks with different competency.
- World Class Districts commonly exhibit structural complexities such as stratigraphic and (/or) tectonic interleaving of rock types and complex geometries, such as:
 - i) isolated greenstone belt blocks in sedimentary rocks (Kalgoorlie – Timmins),
 - ii) irregular geometries around thick, competent, granitoids or quartzites (Ashanti), or

- iii) thrust-decollement structures (Bendigo–Ballarat?).

1.2 Interpretation

- The size of orogenic gold provinces suggests a process that is an integral part of the orogenic event. The elongate nature of orogenic gold districts, and the association with large (regional) faults zones, appear conducive to fluid focussing from deep crustal levels. The occurrence of significant orogenic gold deposits in extensive ductile or ductile-brittle shear zones in amphibolite-facies belts also attests to this interpretation.
- The association of mantle-derived lamprophyres and lower crustal-sourced porphyries indicates that the 1st order structures, in some form, have extensions to the lower crust. The long-lived nature of the structures, as documented by recurring post-gold lamprophyres and kimberlites (up to ~ 2.5 G.y.), attests to the magnitude of these structures and supports their role as conduits for deeply-sourced fluids. The gravity “worms” produced by Nick Archibald and Fractal Graphics also support this interpretation.

1.3 Outstanding Problems

- The dominance of volcanic-intrusive units in early Precambrian Provinces versus the prominence of slate/wacke accretionary prisms in Phanerozoic Provinces requires clarification. The transition is almost certainly related to changes in orogenic style since the Late Archaean (differing slab dip, oceanic crust thickness, etc.). Resolution of this “problem” will better clarify which aspects of the orogenic process are crucial for gold mineralisation, given that the deposits occur in both types of orogens.
- The apparent increase in granitoid-hosted orogenic gold deposits with time (e.g. Jiadong Peninsular, China), also requires explanation. This appears to correlate with the increasing emergence of “gold-only” intrusion-related gold deposits in the Phanerozoic (e.g. Tombstone Belt, Yukon-Alaska).

1.4 Exploration Criteria

1.4.1 Positive Criteria

1. Orogenic belts with supracrustal back arc, arc or fore-arc rocks, particularly those formed on oceanic lithosphere or anomalously thinned continental lithosphere.
2. Anomalous volumes of granitoids at the province-scale.
3. Numerous crustal-scale structures with segments of anomalous geometry. In some districts, these may be cryptic thrusts rather than upright structures.
4. Evidence that structures are mantle-tapping, as expressed by lamprophyres, deep crustal porphyries or syenites.
5. Low strain belts with \pm 5% high strain zones, particularly where these are sited along regional contacts of competency contrasts.
6. Complex structural geometries with isolated curvilinear faults and competent blocks: evidence of reworked duplex structures or flower structures.
7. Belts which contain areally significant greenschist-facies domains where brittle-ductile deformation is dominant.

1.4.2. Negative Criteria

1. Orogenic belts containing only reworked older crust with no volcanic products related to subduction.

2. High strain schist or gneiss belts where there are no selective channelways for fluid focussing. Such terranes may, however, contain placer gold deposits (e.g. Adola, Ethiopia).
3. Simple lithostratigraphy with lack of competency contrasts
4. Simple structural geometry with linear faults.
5. Belts which are consistently amphibolite to granulite facies; these can be prospective, but, on average, are less-well endowed than greenschist-facies belts.

2. What is Geodynamic History of (World-Class/Giant) Orogenic Gold Systems?

2.1 Constraints

- The distribution of orogenic gold deposits in time is episodic, or punctuated. Peaks occur in the late Archaean and Palaeoproterozoic and again over the last 600 m.y. whereas other time intervals lack major concentrations of these deposits. Temporal distribution reflects a tectonic control on the formation and preservation of these deposits. Goldfarb et al. (2001) present a model of evolution of tectonics from plume-modified plate tectonics to modern-day plate-tectonics to explain this distribution.
- Deposits occur especially in accreted parts of Orogenic Belts, such as the fore arcs, and as a result are commonly associated with Volcanogenic Massive Sulphide (VMS) deposits (e.g., southern Abitibi; Alaska), particularly in belts formed on oceanic lithosphere.
- Mesozoic orogenic gold deposits are associated with anomalous thermal events in a subduction/accretion setting. These include ridge subduction and delamination of “hanging slabs” following subduction (e.g., Alpine systems) and may include slab window subduction related to changes in relative plate motions during subduction. There is some evidence for such anomalous thermal events in the Abitibi Belt (Wyman et al., 2000). Direct evidence of plume activity (e.g. extensive komatiites) appears to be important in Archaean and Palaeoproterozoic terranes.
- Deposit formation is often temporally linked to a change in subduction direction and a switch from compression to transpression.
- Larger deposits and richer districts tend to occur in Orogenic Belts that represent one major pulse of crustal growth and accretion (e.g., ~ 50 m.y. age span of Abitibi volcanic rocks; Ashanti). See comments on oceanic lithosphere in Section 1.1.2 above.
- Anomalous amounts of granitoids occur in almost all orogenic gold provinces, and linear batholiths are associated with younger orogenic gold provinces. The granitoids are a signal of very high heat flux in the crust (and lithosphere).
- Based on placer deposit occurrence, ~100 m.y. are required to fully expose the deposits: the observation reflects the predominantly deep setting of orogenic gold deposits in an Orogenic Belt.
- World Class Districts exhibit structural reactivation within the orogenic tectonic setting, and commonly contain multiple generations of orogenic gold (e.g., deformed placers at Tarkwa and syn-deformational Ashanti deposits; two generations of gold in the southern Abitibi; three events (Golden Mile, Oroya, Mt. Charlotte) at Kalgoorlie). The reactivations may be linked to tectonic complexities such as multiple terrane accretions, subduction flipping, hotspot/plateau accretion, etc. (e.g. Wyman et al., 2000).

2.2 Interpretation

- Field mapping, plate movement reconstructions, geophysical data, etc. incontrovertibly constrain the setting of Phanerozoic orogenic gold provinces to convergent-margin orogenic settings (e.g., Goldfarb et al., 1998). Archaean and Palaeoproterozoic provinces share numerous common features with the younger provinces and are also generated in an orogenic setting associated with subduction. Lithoprobe deep seismic images from the Abitibi reveal the presence of a subducted slab at the northern margin of the belt and Archaean subduction can reasonably account for the present relationship of the underthrust Pontiac subprovince beneath the gold-rich southern margin of the Abitibi belt. The geochemistry of felsic volcanic rocks in many Archaean belts also supports a subduction setting.

- Any convergent margin associated with accretion appears capable of hosting orogenic lode-gold deposits. However, the peaks in the temporal distribution of this deposit class, and the sporadic occurrence of World-Class or Giant Deposits, indicates that special conditions are required to generate, and preserve, the largest examples of this class. A key source factor appears to be lithospheric-scale thermal anomalies acting on the host orogen. This anomaly may result from ridge subduction or other disturbances acting on lithosphere geotherms established by subduction processes. Changes from compressive to transpressive plate interactions enhance the capacity of an orogen to host World-Class Deposits by providing localised regions of crustal extension, coincident with lithospheric (lower crust/upper mantle) thermal anomalies resulting from slab disruption, slab window formation, etc. The occurrence of orogeny following accretion of plume material and (or) interaction of mantle plumes with subduction zones may act to enhance the capacity of an orogen to host world-class deposits, based on:
 - i) the world-wide occurrence of orogenic gold deposits following a ~2.7 Ga global plume event, and
 - ii) the specific spatial association of World-Class and Giant Orogenic Deposits with thick sequences of 2.7 Ga komatiites in the Eastern Goldfields and southern Abitibi Belt. Circumstantial evidence in the form of associations of komatiites and siliceous high-magnesium basalts with arc-type volcanic rocks in the Birimian of West Africa (and possibly north-eastern South America) supports this link between “special” orogens and large gold deposits.
- The occurrence of multiple generations of orogenic gold in World-Class Provinces suggests:
 - i) enhancement or multiplication of deep gold sources during complex orogenies,
 - ii) efficient removal of gold from deep sources by multiple extraction events, or
 - iii) a combination of both processes.
- The recurring temporal overlap between gold deposit formation and orogenic-type events at the lithospheric scale reflects the fact that the deposit type is an integral part of the orogenic tectonic setting. Broadly, the key *geodynamic* features of the metallogenic processes are interpreted to be:
 - i) formation of a gold reservoir via subcretion of carbonate- and S-rich oceanic lithosphere and sediments and (or) metasomatism of the sub-arc lithosphere during subduction-related lowering of the mantle geotherm; asthenospheric heating of the lithosphere;
 - ii) subsequent orogenic disturbance of subduction-related geotherms,
 - iii) release of gold and transport in fluids via major trans-lithospheric structures to mid-crustal depths, and;
 - iv) mid-crustal transport and deposition of gold, at or above the brittle-ductile transition, in major crustal shear networks.

An alternative model (the metamorphic model) is that ore fluid and gold are released during prograde metamorphism of the hosting volcanosedimentary pile due to thermal disturbances deep in the lithosphere.

2.3 Outstanding Questions

Do the changes between early Precambrian and Phanerozoic orogenic gold provinces mainly reflect changes in tectonic style (e.g. plume vs plate) or preservation, or both? See Goldfarb et al. (2001) for an in-depth discussion.

2.4 Exploration Criteria

2.4.1 Positive Criteria

1. Orogenic belts that are Late Archaean (particularly 2.7 Ga), Palaeoproterozoic (2.1 – 2.0 Ga; 1.9 – 1.8 Ga) or post 600 Ma but pre- 50 Ma (deep deposits not uplifted until that time).
2. Accreted terranes or upper segments of collisional belts (some with VMS deposits), preferably formed in one tectonic cycle (≤ 100 m.y.), or with lateral rather than vertical accretion which may tectonically (rather than stratigraphically) juxtapose older and younger supracrustal sequences.
3. Anomalous subduction environments recognised by:
 - Petrogenetic associations (e.g. calc-alkaline volcanic rocks) and plume (e.g. komatiites) lithologies.
 - Complex or stacked sequences related to multiple, closely timed orogenies.
 - Rock types associated with slab disruption/detachment or arc/orogen extension (e.g., Nb-enriched basalts, shoshonites, other alkalic rock types)
4. Reactivation of compressional structures, particularly early thrust duplexes, in oblique-slip (or extensional) regimes.
5. Multiple reactivation of specific segments of reactivated structures with overprinting gold mineralisation events over relatively short time periods (i.e., approximately 20 ± 10 m.y.).

2.4.2 Negative Criteria

1. Orogenic belts that are Mesoproterozoic to early Neoproterozoic (1.7 – 0.6 Ga). These appear to be linear plate-related orogenic belts that have experienced too much uplift (e.g. Goldfarb et al., 2001).
2. The deep roots of collisional belts where metamorphic grade is high.
3. Normal (or simple) subduction environments recognised by:
 - petrogenetic associations of arc-type rocks lacking extension-related volcanic rock types or plume-type lithologies
 - arc sequences and orogens with no evidence of significant rifting, plate re-arrangement, subduction “flipping”, etc.
4. Limited reactivation of pre-existing structures.

3. What is the Nature of the Fluid Reservoirs?

3.1 Constraints

3.1.1 Fluid

- Fluid inclusion studies show that the main components of the fluids which formed orogenic lode-gold deposits are H₂O, CO₂, CH₄, and H₂S generally with low dissolved salts ± N₂ ± complex hydrocarbons. Individual fluid inclusion studies define H₂O-rich, CO₂-rich and CH₄-rich inclusions and (or) combinations of these.
- Theoretical studies and vein studies indicate that pressures in these systems are lithostatic to supralithostatic. Fault-valving is widely accepted from individual deposit studies. Therefore, pressure variations and phase separation are expected phenomena or requirements.
- Some detailed fluid inclusion studies based on high-quality field constraints have met the requirements of Ramboz et al. (1982) for fluid immiscibility, which produces H₂O (+ salt)-rich and CO₂- and(or) CH₄-rich fluids. This is particularly true for early Precambrian examples. Other studies, particularly of Phanerozoic examples, show no evidence of immiscibility. Immiscibility is more common in fluids with higher CO₂ and CH₄ contents, which are preferentially developed in the Archaean and Palaeoproterozoic examples.
- To date, no study has demonstrated fluid-mixing unequivocally on the basis of fluid inclusion data. However, stable isotope studies suggest mixing of deep fluid with meteoric water in comparatively shallow-level deposits (e.g., Wiluna; Race Track), although even this possibility is dependant upon the temperatures used in modelling. High fluid pressures and strong upward advective flow probably inhibit fluid mixing at the ore-forming stage. However, it must be noted that mineralogical assemblages and zoning emphasised by John Walshe from some deposits can be best explained by some form of fluid mixing.
- In an orogenic setting, the “seafloor” geochemical signatures identified in Yilgarn gold environments by Ian Campbell and co-workers at ANU must represent interaction of deep fluids with seafloor-altered host rock not a genuine seawater contribution, as the orogenic belts were uplifting, and hence above sea level, at the time of gold mineralisation. It is very unlikely that sea water would directly infiltrate the hydrothermal system if current timing constraints on gold formation (e.g. Groves et al., 2000) are accepted. If the gold deposits were formed earlier, prior to the major compressional/transpresional D₂–D₄ events, as suggested by Bateman et al. (2001) for Kalgoorlie, it would be possible.

3.1.2 Reservoirs

- The gold and fluid reservoir is normally associated with subduction processes and subsequent orogeny. It may be associated with local lithosphere delamination (e.g. Jiadong Peninsular, China).
- Some orogenic gold provinces are not associated with contemporaneous granitoid magmatism (e.g., Otago, NZ; NW Alps, Italy; Klondike, Yukon).
- Granitoid abundance does not correlate positively with the gold potential of greenstone belts (the Abitibi has the lowest proportion of granitoids in greenstone belts of the Superior Province).
- Fluids associated with the San Andreas and companion faults display mantle He isotopic values, and the Sb-Hg occurrences on the San Andreas Fault are considered the surface expression of orogenic gold deposits at depth. Interestingly, there is limited evidence for

mixing in this system, even though sampled fluids have reached the surface and are depositing sinters.

- Orogenic gold deposits may occur in crustal sequences formed and metamorphosed 100s of m.y. before the orogenic event associated with mineralisation (e.g., Jiadong Peninsular, China).
- Radiogenic isotope characteristics of the gold-associated fluids reflect the influence of differences in composition of the crust both within and beneath host greenstone sequences. For example, in the Eastern Goldfields Province, Pb isotopes have been interpreted to reflect a granitic source (these are the most enriched in Pb), Sr isotopes have been interpreted to reflect a dominant basaltic source (these are most enriched in Sr) and Nd isotopes suggest a komatiite source (REE only mobilized in ultramafic rocks by H₂O-CO₂ fluids). The strong evidence for long crustal pathways for the fluid is elegantly presented by Ridley and Diamond (2000).
- Recently, Rob Kerrich and co-workers have suggested that N isotopes firmly establish a metamorphic, rather than magmatic, fluid reservoir.

3.2 Interpretation

Three sources (or a combination of them) are commonly postulated for gold and its associated fluids:

1. Magmatic fluids derived from penecontemporaneous granitoids.
2. Metamorphic devolatilisation of a volcanic-sedimentary.
3. Devolatilisation of the lower crustal and (or) subcreted/subducted oceanic crust and marine sediments.

1. Evidence against a granitoid source in general includes:

- Gold-associated fluids have uniform low salinity, at least ruling out a high-level source.
- Granitoids, and particularly cotemporal granitoids, do not occur in all orogenic gold provinces.
- Broadly coeval granitoids vary from monzogranites to diorites and from oxidised (magnetite-type) to reduced (ilmenite-type).
- The presence of pyrite+arsenopyrite ± pyrrhotite in some deposits constrains fluid Eh to conditions at or below the QFM buffer, so that oxidised magma models cannot be universally applied unless there are strong host-rock buffers.
- The lack of any isotopic data that convincingly ties the gold mineralisation to granitoids.

2 An upper-crustal metamorphic gold source is much more plausible, and cannot be discounted, but evidence against it includes:

- The barren nature of many syn-metamorphic quartz veins.
- Fluid inclusion studies of syn-metamorphic veins in the Pine Creek Inlier indicate decrepitation at ~ 600° C versus ~ 300° C for later gold-associated veins: this implies low CO₂ ± CH₄ in the metamorphic fluids there. However, this is not valid worldwide, as CO₂-rich metamorphic fluids are known from fluid inclusion studies of metamorphic terranes
- Syn-folding saddle reef veins are commonly barren quartz: gold is normally introduced during a later event.
- The preservation of asbestos in metamorphosed komatiites of regional greenstone sequences (not predicted by pervasive flow of local carbonate-bearing metamorphic fluids).

- The presence of orogenic gold deposits in previously metamorphosed, substantially older (e.g., 2 G.y. in China), crustal sequences.
 - Sources in upper crustal volcanic-sedimentary piles, at least in Archean examples, which do not account for regional variations in radiogenic isotope compositions of gold-related fluids.
 - The occurrence of some deposits near the base of greenstone piles in upper-amphibolite to lower-granulite facies domains, despite the fact that most metamorphic devolatilisation models invoke upward flow of released fluid.
 - The presence of multiple generations of orogenic gold, separated by ~10 - 15 m.y., which occur in the Abitibi Belt in spatially overlapping fields, and must have occurred in SW Ghana to account for metamorphosed placer deposits in the same terrane as broadly syn-metamorphic gold lodes. These are difficult to reconcile with most proposed mechanisms for upper crustal, metamorphic devolatilisation and fluid generation which are broadly one-pass processes at any crustal level.
3. This source for fluids and gold is favoured as a general source for the following reasons:
- Gold-associated fluids are distinctive in terms of their major components (high $\text{CO}_2 \pm \text{CH}_4 \pm \text{N}_2$) and dissolved salts (low salinity), irrespective of variations in the makeup of crustal sequences or the style and proportions of granitoid types that occur in the individual terranes.
 - The distinctive, but consistent, nature of the fluids:
 - i) precludes mixing of two dissimilar fluids as a common feature of orogenic gold deposit formation and
 - ii) argues against the presence of a volumetrically significant, second fluid reservoir as a fundamental requirement for formation of these deposits.
 - The only common factor among approximately 75 provinces is the link with subduction and orogeny. Therefore, the most logical source region for gold and fluids should be one directly related to the subduction process.
 - Carbonated and hydrated basalts and oceanic crust, overlain by organic and S-rich sediments, represents a potential gold source that is consistent with the known fluid characteristics of the deposit type. Even the contrast in CO_2 content of the fluids between Archean/Palaeoproterozoic (high CO_2) and Phanerozoic (lower CO_2) deposits could be explained in terms of hotter Precambrian lithosphere, more mid-ocean ridge convection and alteration, more MgO rich basalts and no CO_2 – fixing organisms, all of which would produce higher CO_2 contents in Precambrian oceanic sequences.
 - Young orogenic gold deposits are known to be associated with mantle thermal anomalies associated with slab detachment, etc. There is evidence for re-heating of subduction-“refrigerated” lower crust.
 - Slab-derived veins, containing water-rich fluid inclusions, are known from upper mantle xenoliths above subduction zones (e.g., Lihir). They illustrate a mechanism for metasomatism of the lower crust and provide evidence of water advection in vein systems at mantle depths.
 - The timing of lower-crust thermal anomalies can account for the post-peak metamorphic age of greenschist-hosted gold deposits.
 - Variations in fluid radiogenic isotope compositions can be accounted for by interaction with a combination of greenstone belt /slate belt lithologies and lower crustal components.

- Temporally distinct, but spatially overlapping, orogenic gold events can be accounted for by complex orogenies that have the potential to re-charge the system in terms of fluid and gold.
- Long-lived structures hosting broadly contemporaneous lamprophyres porphyries and syenites, and much younger generations of lamprophyres, kimberlites and syenites, imply that major channelways to the base of the lithosphere occur in orogenic gold provinces, making the ascent of deeply derived fluids plausible.
- Helium isotope data on the San Andreas system provides evidence of mantle components in fluids associated with major faults which may currently be precipitating Hg- and Sb-rich sinters above the sites of orogenic lode-gold deposit formation.

3.3 Outstanding Problems

- Why doesn't the crust undergo (large-scale) melting during fluid advection?
- Why does fluid advection (devolatilisation?) occur in pulses that are often associated with a change in the stress field?
- If real, these apparent pulse events may represent a synergy between mantle thermal pulses and shallow crustal motions; for example:
 - Slab detachment or window formation coincident with a change to transpressive tectonics.
 - Fluid driven ahead of a melting front.

3.4 Exploration Criteria

3.4.1. Positive Criteria

1. Uplift segments of terranes that promote phase separation in fluids and enhance rock failure.
2. Evidence of prior widespread alteration around major structures (normally carbonated) and/or granitoid (normally having haematite alteration). These identify long-lived structures and the alteration may act as "ground preparation", for example changing the physical (e.g. competency) or chemical (e.g. Fe/Fe+Mg ratio) characteristics of the rocks, which can then localise gold mineralization during a subsequent hydrothermal event (e.g. Sheba-Fairview, Barberton Mountain Land).

4. What is the Method of Fluid Advection/Convection?

4.1 Constraints

- The shape of gold provinces, together with evidence for thermal anomalies in the upper mantle associated with young gold deposits, suggests a first-order association with linear zones of anomalous heat flow (100s to 1000s of km long and 10s to 100s of km wide) in the lithosphere, which transfers to the lower crust.
- Hydrous vein systems in upper-mantle xenoliths indicate that vein-related advection of deep fluids is possible. Studies of exhumed eclogites confirm the presence of hydrous fluids in banded eclogites at depths corresponding to 2 GPa (~ 60-70 km).
- There is an association with structures containing primitive and mantle-derived dyke rocks, which indicates that fluid flow from the lowest crust to mid-crustal levels may occur along major structures that can focus magma flow at lithospheric scale.
- There is a preferred siting of world-class gold deposits in greenschist-facies domains, suggesting that the ductile-brittle transition is an important constraint on effective fluid flux and generation of selective structural permeability in rock sequences which show large competency contrasts at the crustal level.
- Seismic and “Worming” evidence from the Yilgarn Block indicates that crust similar to that of the Southern Cross Province may occur below the Eastern Goldfields Province.
- There is a common association of gold camps in both greenstone belts and slate belts with structural highs and (or) anticlinal hinges: ie., uplift zones where lithostatic pressure may be lower and caps or seals more effective.
- Ribbon quartz, flat and steep extensional veins, and hydraulic breccias in the many deposits (e.g. Sigma) all indicate that fluid pressure is the driving force at mid- to shallow-crustal depths, and that deposits occur as a result of the local interplay between supralithostatic and near-hydrostatic pressure regimes.
- Upper sedimentary sequences may cap the hydrothermal systems in orogenic gold districts: this is most clearly shown in greenstone belts.

4.2 Interpretation

- There are fault valve analogies with San Andreas micro seismic events (e.g., inferred magnitude 3 to 4 events for the Sigma Mine, Quebec).
- “Fault meshes” and transient components in fault networks account for the preferred (but not exclusive) occurrence of gold deposits in 2nd and 3rd order structures because of more focussed fluid flow along lesser structures and high fluid pressures at terminations of these structures.
- High competency-contrast contacts are likely to be zones of enhanced permeability.
- Fluid behaviour along large ductile structures may be different. Deposits form despite the absence of a cap to the system, but little space is generated and hence selectively large fluid fluxes in specific parts of the system are rare. Under ductile conditions at deeper crustal levels, competency contrasts are reduced and fluid focussing may be less rock-specific.

4.3 Outstanding Problems

- Link to thermal anomalies at depth is clear, and mid-crustal fluid pumping mechanisms are relatively well constrained, but there is a gap in our knowledge of fluid advection processes between lower crustal depths and mid-crustal depths.
- Relationships between 1st and 2nd or 3rd order structures require clarification in terms of controls on connectivity between fault systems at different scales.

4.4 Exploration Criteria

4.4.1 Positive Criteria

1. Second- or third-order structures containing lamprophyres and porphyries (\pm syenites) indicating connectivity to crustal-scale faults that tap the mantle.
2. Gravity “Worms” that may indicate the deeper structural channels
3. Greenschist facies domains with brittle-ductile deformation (although amphibolite facies domains are still respective).
4. Anticlinal hinges or uplift zones where lithostatic pressures may be relatively low.
5. Clockwise terrane P-T-t paths.
6. Thick upper sedimentary sequences that act as caps on hydrothermal systems.

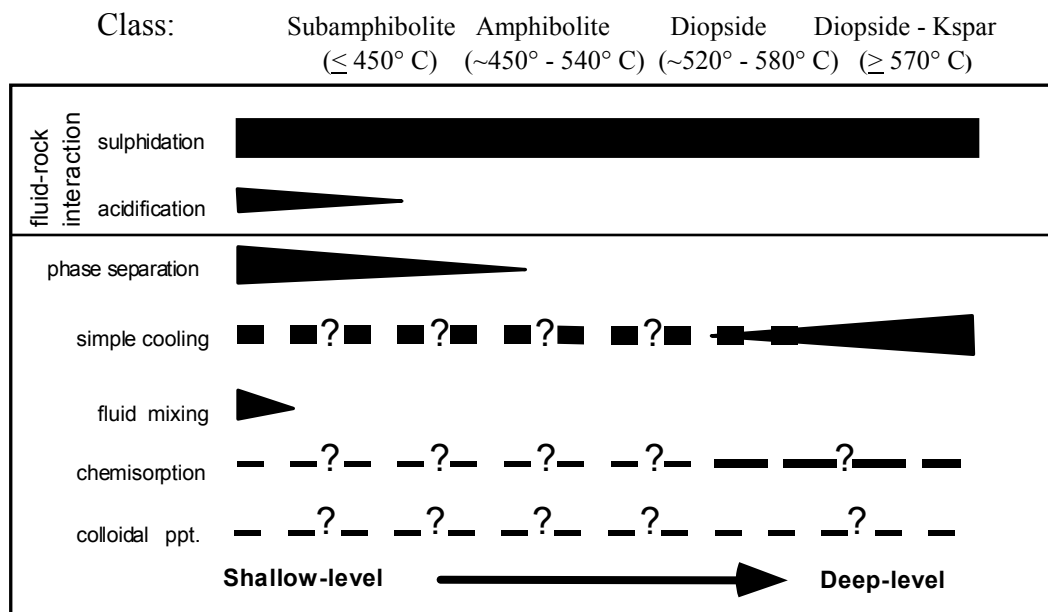
4.4.2 Negative Criteria

1. A lack of lamprophyres and (or) porphyries in known structures.
2. Synclinal structures or homoclinal sequences.
3. Blueschist facies terranes.

5. Mechanisms of Metal Transport and Deposition

5.1 Constraints

- There are low base-metal contents in the deposits.
- Non-magmatic elemental ratios or correlations typify the deposits (e.g., S/Se, Al/Ga, K/Tl, K/Li, etc are unlike porphyry deposit systematics).
- Spectacular breccia ores are present in both the Golden Mile and Timmins, among many other deposits, and sulphidation of rocks with high Fe contents and/or Fe (Fe+Mg+Ca) ratios is clear in deposits of many orogenic gold provinces. Several gold deposition mechanisms are possible, but most reviews papers (e.g., Hagemann and Cassidy, 2000) cite phase separation and wall rock interaction as the dominant mechanisms of metal deposition. Such syntheses are typified by the following figure from Mickuki (1998):



- Back-mixing of ‘spent’ fluid with an influx of normal deeply-sourced fluid may be a viable mechanism in some deposits. At Ashanti, for example, maturation of carbonaceous shales could have generated methane-rich fluids that back-reacted with fresh deeply-sourced fluid to precipitate gold (also Wattle Gully deposit, Victoria).
- Apart from deposits associated with carbonaceous host rocks, direct oxygen and hydrogen evidence for fluid mixing is largely restricted to shallow-level deposits where draw-down of meteoric fluids may occur. There is little recorded evidence from fluid inclusions.
- The broad consistency of quartz oxygen-isotope values (e.g., metamorphic versus magmatic versus basinal versus surface fluids) in orogenic gold deposits suggests that mixing of fluids generated from vastly different sources is not a common process.
- Anomalously negative sulphur-isotope ratios, and large variations in such ratios, suggest the involvement of oxidised fluid. This is covered by John Walshe and Paul Hodkiewicz for Yilgarn examples, particularly the Golden Mile.
- There is debate about whether these oxidised fluids result from a component of magmatic fluid (from a source not yet conclusively identified) or from modification of the same deep ‘metamorphic’ fluid that produced the deposits that do not show the sulphur-isotope variation.

- The involvement of oxidised fluid cannot be the controlling factor, with the majority of giant to world-class deposits having reduced ore assemblages (e.g. Homestake, Mother Lode, Kolar, Ashanti, Geita, Sheba-Fairview).

5.2 Interpretation

Effective gold deposition is controlled by chemical gradients but the exact nature of these gradients is not unequivocally defined in most cases, and may vary from goldfield to goldfield or from deposit to deposit. Chemical gradients can be related to variations in rock reactivity caused by contrast in Fe/ (Fe+Mg+Ca) ratios or reactive C contents, to redox boundaries due to fluid mixing, fluid “backmixing”, fluid reactions with oxidised or reduced mineral assemblages, or, in younger deposits, perhaps fluid infiltration into hydrocarbon concentrations (Carlin?). Phase separation can cause variations in pH, fO_2 , fluid salinity and fS_2 , which may all cause gold precipitation.

As most giant orogenic gold deposits are sited in rocks with high Fe contents and/or high Fe/ (Fe+Mg+Ca) ratios (e.g. Golden Mile, Timmins, Homestake, Geita) or rocks with high C contents (e.g. Muruntau, Ashanti, Ballarat-Bendigo), rock reaction or fluid “backmixing” are the most likely cause of large-tonnage deposits. However, the high gold grades are more likely to be related to phase-separation or some form of fluid mixing, whether internally generated in a single deeply-sourced generic fluid, or involving an external (exotic) source. Mixing with an oxidised magmatic fluid has become a popular model for the Golden Mile during AMIRA 511, but cannot be a universal model for giants of this deposit class. At the Golden Mile, and elsewhere in the Yilgarn, the identification of potential magmatic source rocks that are synchronous with the proposed magmatic-fluid event poses a problem. In other magmatic systems, such source rocks are evident in, or adjacent to, the ore environment, but most intrusive rocks in the orogenic-gold ore environment are demonstrably pre-ore intrusions. This is a major problem to be addressed by AMIRA P680. There are also few demonstrably oxidised intrusions in the region, although magmatic-deuteric magnetite alteration around some intrusions (e.g. Wallaby, Binduli) can host gold deposits: whether the magnetite alteration and gold deposition are related to the same hydrothermal event or separated by 10 to 30 m.y. is currently hotly debated.

5.3 Exploration Criteria

5.3.1 Positive Criteria

1. Competent Fe-rich rocks and/or rocks with high Fe/ (Fe+Mg+Ca) ratios in stratigraphic sequences. These may be original components of the supracrustal belts, with differentiated dolerites, BIFs and tholeiitic basalts being particularly prospective, or pre-existing alteration zones, for example magnetite alteration zones around syenites or porphyries or regions of magnetite alteration of sulphidic shales (e.g. Kapai Slate – mineralised at Victory).
2. Carbonaceous shales in stratigraphic sequences (to provide redox gradients or CH_4 for fluid mixing and (or) increased vapour pressure and more phase separation).
3. Complex stratigraphy to promote disequilibrium between fluids and specific potential host rocks, or alteration zones in fault channelways that may change the redox state of fluid reservoirs.
4. Evidence of anomalously oxidised (e.g., haematite, magnetite, negative S isotope values) or anomalously reduced fluids (e.g., pyrrhotite-arsenopyrite-loellinite). Anomalous fluid composition *may* be important but are not diagnostic of Giant deposits.

6. SUMMARY OF POSITIVE GEOLOGICAL EXPLORATION CRITERIA FOR GIANT TO WORLD-CLASS DEPOSITS: LISTED IN ORDER OF DECREASING SCALE: (REGOLITH GEOCHEMISTRY AND GEOPHYSICAL TARGETTING EXCLUDED)

6.1 Terrane or Province Selection Scale

- Orogenic belts with supercrustal back arc, arc and/or fore-arc rocks, particularly those that formed on oceanic lithosphere or anomalously thinned continental lithosphere and have an orogenic history of about 100 m.y. or less.
- Accreted terranes, preferably formed in one tectonic cycle (≤ 100 m.y.), with dominantly lateral docking.
- These terranes preferably 2.7-2.6, 2.1-2.0, 1.9-1.8 Ga or post-600 Ma and pre-50 Ma.
- Anomalous subduction environments recognized by: a) petrogenetic associations of arc and plume (komatiite) volcanic products, b) complex or stacked sequences related to multiple, closely-timed, orogenies, which may fluctuate between compressional and extensional regimes, and c) rock types associated with slab disruption/detachment or arc/orogen extension (e.g. Nb-enriched basalts, shoshonites, alkaline rocks).
- Anomalous volumes of granitoids, irrespective of petrogenesis.
- Regional-scale deformation of complex lithostratigraphic sequences involving the generation of limited ($<10\%$) high-strain zones in an overall low-strain environment with preservation of the majority of volcanic and sedimentary structures and textures.
- Numerous crustal-scale deformation zones, containing anomalous concentrations of lamprophyres, porphyries and/or syenites, with evidence of reactivation and reworking during changes in far-field stresses, plus evidence of early regional-scale alteration.
- Complex structural geometries associated with the crustal-scale deformation zones, including reactivated thrust duplexes and flower structures.
- Belts typified by a significant percentage of greenschist-facies rocks, although amphibolite-facies terranes should not be discarded.
- Presence of elongate structural basins of late, conglomeratic sedimentary sequences that potentially mark zones of most extensive vertical uplift.

6.2 Goldfield or Camp Selection Scale

- In lithostratigraphic sequences with diverse rock types of contrasting chemistry and competency, and particularly those with Fe-rich or C-rich lithologies, and potential cap rocks (e.g. sedimentary sequences overlying volcanic basement), preferably at greenschist facies to lower-amphibolite facies.
- Adjacent to zones where crustal-scale deformation zones are oblique to their regional trend (i.e. where simple rather than pure shear may dominate), particularly where corridors of regional-scale shear/fault zones cross-cut at a high angle and/or there is evidence for thrust duplexes, flower structures or curvilinear structures at a high angle to the crustal-scale deformation zone: i.e. geometrical complexity and abundance of contacts and faults.
- Adjacent to 500m $<$ 5km length, rigid, porphyry, granitoid or gabbro bodies (“larrikins” of Roberto Weinberg) which can produce zones of heterogeneous stress and/or magnetite alteration haloes.
- Adjacent to linear structural basins of late conglomeratic sequences.
- Adjacent to zones showing evidence of early, regional-scale wallrock alteration.

6.3 Target-Scale Geological Guides (Not Necessarily Exclusive to Large Deposits)

- Evidence of overprinting alteration and/or veining events.
- Quartz veins with CO₂ (± CH₄) –rich inclusions that decrepitate at 300 ± 50°C (barren H₂O-rich inclusions normally decrepitate at >500°C)
- Mineralogical evidence for anomalously oxidised (hematite, anhydrite, V-rich micas) or anomalously reduced (pyrrhotite-arsenopyrite-loellingite, carbon) systems.
- Anomalously negative sulphur isotope ratios and/or large ranges of those ratios in Fe-sulphides.
- Anomalous bedrock topography (base of regolith) in RAB drilling: reflects contrasts due to weak, altered shear zones, chemically-reactive sulphide-bearing zones and/or carbonate-bearing zones, and resistant quartz veins and/or silicification (compare Mt Charlotte to Golden Mile at Kalgoorlie).

7. References

- Bateman, R.J., Hagemann, S.G., McCuaig, T.C. and Swager, C.P., 2001. Protracted gold mineralization throughout Archaean orogenesis in the Kalgoorlie camp, Yilgarn Craton, Western Australia: structural, mineralogical, and geochemical evolution. *Geological Survey of Western Australia Record* 2001/17: 63-98.
- Goldfarb, R.J., Groves, D.I. and Gardoll, S., 2001. Orogenic gold and geologic time: a global synthesis. *Ore Geology Reviews*, 18: 1-75.
- Goldfarb, R.J., Phillips, G.N. and Nockleberg, W.J., 1998. Tectonic setting of synorogenic gold deposits of the Pacific Rim. *Ore Geology Reviews*, 13: 185-218.
- Groves, D.I., Goldfarb, R.J., Gebre-Mariam, M., Hagemann, S.G. and Robert, F., 1998. Orogenic gold deposits – a proposed classification in the context of their crustal distribution and relationship to other deposit types. *Ore Geology Reviews*, 13: 7-27.
- Groves, D.I., Goldfarb, R.J., Knox-Robinson, C.M., Ojala, J., Gardoll, S., Yun, G.Y. and Holyland, P., 2000. Late-kinematic timing of orogenic gold deposits and significance for computer-based exploration techniques with emphasis on the Yilgarn Block, Western Australia. *Ore Geology Reviews*, 17: 1-38.
- Hagemann, S.G. and Cassidy, K.F., 2000. Archean orogenic lode gold deposits. *Ore Geology Reviews*, 13: 9-68.
- Mikucki, E.J., 1998. Hydrothermal transport and depositional processes in Archaean lode-gold systems. A review. *Ore Geology Reviews*, 13: 307-321.
- Ridley, J.R. and Diamond, L.W., 2000. Fluid chemistry of orogenic lode-gold deposits and implications for genetic models. *Reviews in Economic Geology*, 13: 141-162.
- Wyman, D.A., Kerrich, R. and Groves, D.I., 2000. Lode gold deposits and Archean mantle plume-island arc interaction, Abitibi subprovince, *Canada Journal of Geology*, 107: 715-725.